

Doctoral Thesis

**Role of lipids in HIV-1 pathogenesis.
Implications in viral infectivity and
development of antiretroviral drugs**

Jon Ander Nieto Garai

May 2019

Supervisor

Maier Lorizate Nogales

eman ta zabal zazu



Universidad
del País Vasco

Euskal Herriko
Unibertsitatea

Department of Biochemistry and Molecular Biology (UPV/EHU)

Instituto Biofisika (UPV/EHU, CSIC)

ACTA DE GRADO DE DOCTOR O DOCTORA
ACTA DE DEFENSA DE TESIS DOCTORAL

DOCTORANDO/A DON/DÑA. _____

TITULO DE LA TESIS: _____

El Tribunal designado por la Comisión de Postgrado de la UPV/EHU para calificar la Tesis Doctoral arriba indicada y reunido en el día de la fecha, una vez efectuada la defensa por el/la doctorando/a y contestadas las objeciones y/o sugerencias que se le han formulado, ha otorgado por _____ la calificación de:
unanimidad ó mayoría

--

SOBRESALIENTE / NOTABLE / APROBADO / NO APTO

Idioma/s de defensa (en caso de más de un idioma, especificar porcentaje defendido en cada idioma):

Castellano _____

Euskera _____

Otros Idiomas (especificar cuál/cuales y porcentaje) _____

En _____ a _____ de _____ de _____

EL/LA PRESIDENTE/A,

EL/LA SECRETARIO/A,

Fdo.:

Fdo.:

Dr/a: _____

Dr/a: _____

VOCAL 1º,

VOCAL 2º,

VOCAL 3º,

Fdo.:

Fdo.:

Fdo.:

Dr/a: _____ Dr/a: _____ Dr/a: _____

EL/LA DOCTORANDO/A,

Fdo.: _____

"It's the questions we can't answer that teach us the most. They teach us how to think. If you give someone an answer, all they gain is a little fact. But give them a question and they'll look for their own answer."

Patrick Rothfuss

Para vosotros, Ama, Aita, Luka.

Declaration

I, Jon Ander Nieto Garai, declare that this thesis has been composed solely by myself and that it has not been submitted, in whole or in part, in any previous application for a degree. The work presented is entirely my own, if not stated otherwise by reference or acknowledgment, with the following exceptions:

- The lipidomic analysis of chapter 3 was carried out by Gemma Fabriàs and Josefina Casas. The proteomic analysis of chapter 3 was carried out by Kerman Aloria.
- Unlabeled photocholesterol in chapter 3 was synthesized by F-Xabier Contreras.
- Infectivity data acquisition on chapter 4 was performed by Bärbel Glass, Cornelia Schroeder and Maier Lorizate.
- Lipidomimetic compounds in chapter 4 were designed, synthesized, screened and analyzed by Sameer Agarwal, Hans-Joachim Knölker, Kai Simons, Cornelia Schroeder, Claudia Zankl, Carmen Bunn, Matthias Giese, Beate Brankatschk and Gary Jennings.
- AAV particle purification and infectivity experiments were performed by Kathleen Börner.
- Molecular modeling analyses and phosphatidylserine exposure experiments in chapter 4 were carried out by F-Xabier Contreras.
- In chapter 5, nanoparticle capture by mDC, transfer to J-lat, and J-lat reactivation data were acquired by FACS by Susana Benet, Itziar Erkizia, Patricia Resa, and Nuria Izquierdo-Useros.
- Nanoparticle characterization by transmission electron cryomicroscopy, and PLGA core generation in chapter 5 was performed by Mary Cano.

Financial support and acknowledgments

The author of this work has been a recipient of a predoctoral fellowship and a mobility fellowship from the Basque Government, and further supported by Fundación Biofísica Bizkaia.

This work has been supported by the Basque Government, grant IT838-13; amfAR AIDS Research, grant 108676-55-RKRL; and Ministerio de Ciencia, Innovación y Universidades, grant SAF2017-91767-EXP.

This work has been performed at Instituto Biofísica (UPV/EHU, CSIC) and Department of Biochemistry and Molecular Biology of the University of the Basque Country (UPV/EHU) under the supervision of Maier Lorzate. I thank her for the opportunity she has given me and her supervision and invaluable help throughout these years.

Contributions

Journal publications

- Nieto-Garai JA, Glass B, Bunn C, Giese M, Jennings G, Brankatschk B, Agarwal S, Börner K, Contreras FX, Knölker HJ, Zankl C, Simons K, Schroeder C, Lorizate M, Kräusslich HG (2018). Lipidomimetic Compounds Act as HIV-1 Entry Inhibitors by Altering Viral Membrane Structure. *Frontiers in Immunology*, 9: 1983.
- Molinos-Albert LM, Bilbao E, Agulló L, Marfil S, García E, Rodríguez de la Concepción ML, Izquierdo-Useros N, Vilaplana C, Nieto-Garai JA, Contreras FX, Cardona PJ, Martínez-Picado J, Clotet B, Villà-Freixa J, Lorizate M, Carrillo J, Blanco J (2017). Proteoliposomal formulations of an HIV-1 gp41-based miniprotein elicit a lipid-dependent immunodominant response overlapping the 2F5 binding motif. *Scientific Reports*, 7: 40800.
- Huarte N, Carravilla P, Cruz A, Lorizate M, Nieto-Garai JA, Kräusslich HG, Pérez-Gil J, Requejo-Isidro J, Nieva JL (2016). Functional organization of the HIV lipid envelope. *Scientific Reports*, 6: 34190.

Congress contributions

- Nieto-Garai JA, Arboleya A, Lopez S, Contreras FX, Lorizate M (Santander, Spain, 10-13/09/2018). HIV envelope protein-cholesterol interaction in the viral membrane: a promising requirement for cell entry. 41 Congreso de la Sociedad Española de Bioquímica y Biología Molecular.
- Arboleya A, Nieto-Garai JA, Contreras FX, Lorizate M (Santander, Spain, 10-13/09/2018). The role of HIV-1 Env CT in cellular lipid interaction and the relationship with the recruitment of Env into virions. 41 Congreso de la Sociedad Española de Bioquímica y Biología Molecular.
- Nieto-Garai JA, Bilbao E, Contreras FX, Lorizate M (Barcelona, Spain, 23-26/10/2017). Correlation between distinct HIV-1 envelope protein domains mutants in cholesterol interaction and its effect in virus entry and infectivity. XL Congreso de la Sociedad Española de Bioquímica y Biología Molecular.
- Benet S, Nieto-Garai JA, Erkizia I, Prado JG, Martínez-Picado J, Lorizate M, Izquierdo-Useros N (Madrid, Spain, 27-28/03/2017). Bryostatins action on mature dendritic cells promotes HIV-1 reactivation of latently infected cells. Madrid Meeting on Dendritic Cells and Macrophages 2017.

- Benet S, Nieto-Garai JA, Erkizia I, Prado JG, Martínez-Picado J, Lorizate M, Izquierdo-Useros N (San Sebastian, Spain, 29/11/2016-02/12/2016). Bryostatatin-1 action on mature dendritic cells promotes HIV-1 reactivation of latently infected cells. VIII Congreso Nacional GeSIDA.
- Nieto-Garai JA, Benet S, Bilbao E, Erkizia I, Prado JG, Martínez-Picado J, Izquierdo-Useros N, Lorizate M (Barcelona, Spain, 22-24/11/2016). Nanoliposomes targeting myeloid cells to deliver HIV-1 reactivation compounds. NanoBio&Med2016 International Conference.
- Nieto-Garai JA, Bilbao E, Contreras FX, Lorizate M (Salamanca, Spain, 05/09/2016). The role of HIV-1 gp41's Lentivirus Lytic peptides in the interaction of the envelope protein with viral membrane cholesterol. XXXIX Congreso de la Sociedad Española de Bioquímica y Biología Molecular.
- Benet S, Nieto-Garai JA, Pino M, Bilbao E, Erkizia I, Pérez Zsolt D, Prado JG, Martínez-Picado J, Lorizate M, Izquierdo-Useros N (Killarney, Ireland, 10-14/04/2016). A dendritic cell nanocarrier system to reactivate latent HIV-1. Keystone Symposia on Molecular and Cellular Biology. Myeloid Cells.
- Nieto-Garai JA, Bilbao E, Contreras FX, Lorizate M (Berlin, Germany, 04/07/2015). Studying HIV-1 envelope lipid environment using photoactivatable lipids. 40th FEBS Congress.
- Izquierdo-Useros N, Nieto-Garai JA, Benet S, Pino M, Bilbao E, Erkizia I, Fernandez Figueras M, Prado JG, Martínez-Picado J, Lorizate M (Boston, United States of America, 26/04/2015). Nanocarrier system to efficiently deliver small therapeutic molecules to lymphoid tissues. Keystone Symposia on Molecular and Cellular Biology. Mechanism of HIV persistence: Implications for a cure.
- Nieto-Garai JA, Benet S, Pino M, Bilbao E, Erkizia I, Prado JG, Martínez-Picado J, Izquierdo-Useros N, Lorizate M (09-13/09/2014). Targeting myeloid cells with liposomal nanocarriers for therapeutic purposes. XXXVII Congreso de la Sociedad Española de Bioquímica y Biología Molecular.
- Izquierdo-Useros N, Nieto-Garai JA, Benet S, Pino M, Erkizia I, Prado JG, Lorizate M, Martínez-Picado J (09-15/03/2014). Specific targeting of nanoliposomes to myeloid cells for therapeutic purposes. Keystone Symposia on Molecular and Cellular Biology. HIV Vaccines: Adaptive Immunity and Beyond.

Resumen

El Virus de la Inmunodeficiencia Humana 1 (VIH-1) es el agente causante del Síndrome de Inmunodeficiencia Adquirida (SIDA). El VIH-1 es un retrovirus perteneciente al género *Lentivirus* y, como tal, está rodeado por una membrana lipídica que obtiene a partir de la membrana plasmática de la célula huésped en el proceso de gemación. En esta membrana se encuentra embebida la proteína de envuelta (Env) responsable del reconocimiento y la fusión con la células huésped.

La membrana del virus es rica en varios lípidos cuando se la compara con la membrana plasmática de la que procede. De entre esos lípidos son de especial interés el colesterol, la fosfatidilserina, la esfingomielina, y especies saturadas de fosfatidilcolina, todos ellos ricos también en los microdominios lipídicos tipo *raft*. Además, estudios realizados con la sonda fluorescente Laurdan, sensible al estado de fase de los lípidos, demostraron que la membrana lipídica del VIH-1 muestra una estructura de membrana de lípido ordenado (fase l_o), similar también a lo que ha sido descrito para microdominios tipo *raft*. Esto demuestra un parecido no solo a nivel de composición, sino también de estructura entre la membrana lipídica del virus y los microdominios tipo *raft*.

Las propiedades estructurales de la membrana viral y la presencia de ciertos lípidos han sido descritas como requisitos indispensables de la capacidad infectiva del virus. Se sabe por ejemplo que el tratamiento del virus con agentes secuestrantes de colesterol deriva en una enorme disminución de la capacidad infectiva de la partícula viral, lo que apunta a un papel importante de este lípido en el proceso de fusión entre el virus y la célula huésped. Interesantemente, los dominios *raft* que igual que el virus también son ricos en colesterol, son capaces de incluir o excluir ciertas proteínas de regiones específicas de la membrana. De igual manera, este fenómeno podría estar presente en el virus, lo que conllevaría un mecanismo por el cual la eliminación del colesterol de la membrana lipídica supondría una redistribución de Env y una inhibición de su capacidad fusogénica. Cambios en la estructura de la membrana que alteren microdominios *raft*, por lo tanto, también podrían ser factores contribuyentes en la inhibición de la infectividad viral.

Env es una glicoproteína formada por dos subunidades, gp120 o glicoproteína de superficie, y gp41 o glicoproteína transmembrana. Ambas subunidades se encuentran unidas de manera no covalente formando un heterodímero, que a su vez se asocia para formar un homotrímero (Ilustración 1). En el virus maduro, los trímeros de Env se asocian en una sola espícula, lo que se ha descrito como requisito indispensable para que se dé la fusión de manera eficiente entre el virus y la célula huésped.

La subunidad transmembrana gp41 ancla el heterodímero de Env a la membrana viral. En los últimos años se ha planteado que gp41 interacciona con microdominios de membrana tipo *raft*, o incluso directamente con el colesterol, lo que ayudaría a explicar la dependencia de la infectividad viral con respecto a este lípido. Si la eliminación del colesterol induce una disrupción de dominios tipo *raft*, o si gp41

interacciona directamente con el lípido, la pérdida de infectividad observada podría deberse a la imposibilidad de Env de asociarse en una espícula. Por ello, estudiar el entorno lipídico de gp41 y específicamente su interacción con colesterol podría dar información sobre el mecanismo mediante el cual el colesterol está relacionado con la capacidad infectiva del VIH-1.

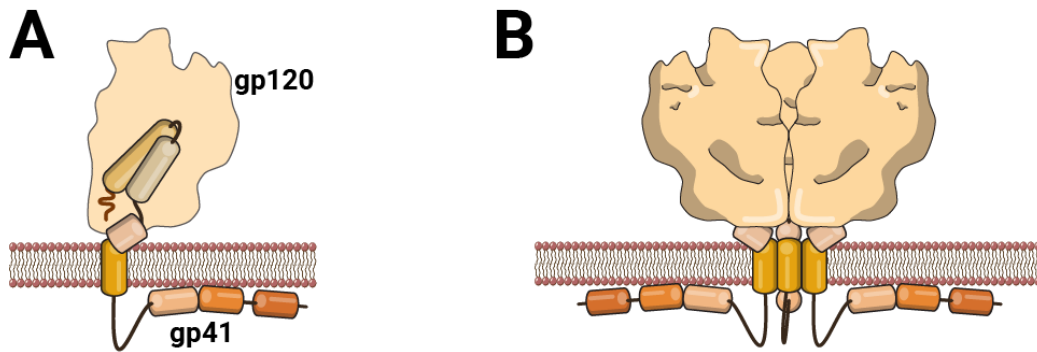


Ilustración 1 - Estructura de Env. A) Heterodímero de Env compuesto por las subunidades gp41 and gp120. El área ocupada por gp120 aparece marcada transparentemente para revelar la subunidad gp41 que se encuentra debajo. gp120 está orientada hacia el exterior del virus, y reconoce el receptor y co-receptor celulares. gp41 ancla el heterodímero a la membrana, e induce la fusión de las membranas viral y celular. B) Tres heterodímeros de gp41-gp120 oligomerizan para formar un trímero de heterodímeros.

Aunque la terapia antirretroviral de gran actividad (TARGA) disponible hoy en día es capaz de disminuir la presencia de partículas virales en sangre (viremia) hasta niveles indetectables, lo que disminuye notablemente las probabilidades de contagio y el avance de la infección, a día de hoy no existe una cura completa para el VIH-1. Cuando se interrumpe la TARGA la carga viral en sangre aumenta en cuestión de semanas, lo que implica que pacientes infectados con VIH-1 tengan que recibir tratamiento el resto de sus vidas. Esta reaparición del virus tras interrumpir el tratamiento se debe a la presencia de reservorios virales, tejidos anatómicos en los que residen células latentemente infectadas. Estas células son infectadas en las primeras etapas del ciclo de infección del virus, antes de la aparición de los primeros síntomas. Por ello, aunque al paciente se le administre la TARGA y el tratamiento sea capaz de inhibir la replicación de nuevas partículas virales, no es capaz de eliminar el material genético viral integrado en estas células, que permanece sin ser expresado. Esto hace que el sistema inmune no pueda encontrar y eliminar estas células latentemente infectadas que se mantienen como reservorios virales. Si el tratamiento es interrumpido, el material genético latente se expresa, y la carga viral reaparece en el organismo. Hasta que se desarrolle una vacuna profiláctica que impida toda infección inicial de células por parte del VIH-1, y por lo tanto impida también la generación de reservorios virales, es necesario diseñar estrategias para purgar estas células latentemente infectadas. Hoy en día la mayoría de estas estrategias se basan en la reactivación de las células latentemente infectadas, forzando la expresión del material genético del virus para así poder ser reconocidas por el sistema inmune y eliminadas, en una estrategia conocida como "shock and kill".

Objetivos

Los objetivos de esta tesis son los siguientes:

- Estudiar la interacción de la subunidad gp41 de la proteína de envuelta con colesterol, además de la región implicada en esta interacción, para encontrar los factores determinantes de la relación entre el colesterol y la infectividad viral.
- Estudiar el uso de compuestos lipídomiméticos raftofílicos como herramienta antirretroviral contra varios patógenos con envuelta lipídica.
- Desarrollar nuevas terapias antirretrovirales basadas en la purga de los reservorios virales mediante el uso de nanopartículas que transportan agentes diseñados para reactivar las células latentemente infectadas y potenciar la respuesta inmune innata del organismo contra ellas.

Interacción de gp41 con colesterol

Gracias al uso de lípidos fotoactivables, capaces de formar un enlace covalente con cualquier molécula a menos de 3 Å de distancia, el estudio del entorno lipídico de gp41 realizado en esta tesis ha demostrado que gp41 interacciona con moléculas de colesterol tanto en la membrana plasmática de células productoras de proteínas virales como en partículas virales libres. Esto constituye la primera prueba directa de la interacción de gp41 con colesterol hasta la fecha. Además, se descubrió que una proteína identificada como la cola citoplasmática de gp41 truncada, derivada de la proteína salvaje (Tr-Env-CT), interaccionaba con colesterol al mismo nivel que la proteína completa, indicando que este dominio citoplasmático podría estar involucrado en la interacción. Además, se ha determinado que las secuencias LLP (del inglés *Lentiviral Lytic Peptide*, o péptidos líticos lentivirales) 2 y 3, pero no la secuencia LLP1, están involucradas en la interacción de gp41 con el colesterol (Ilustración 2).

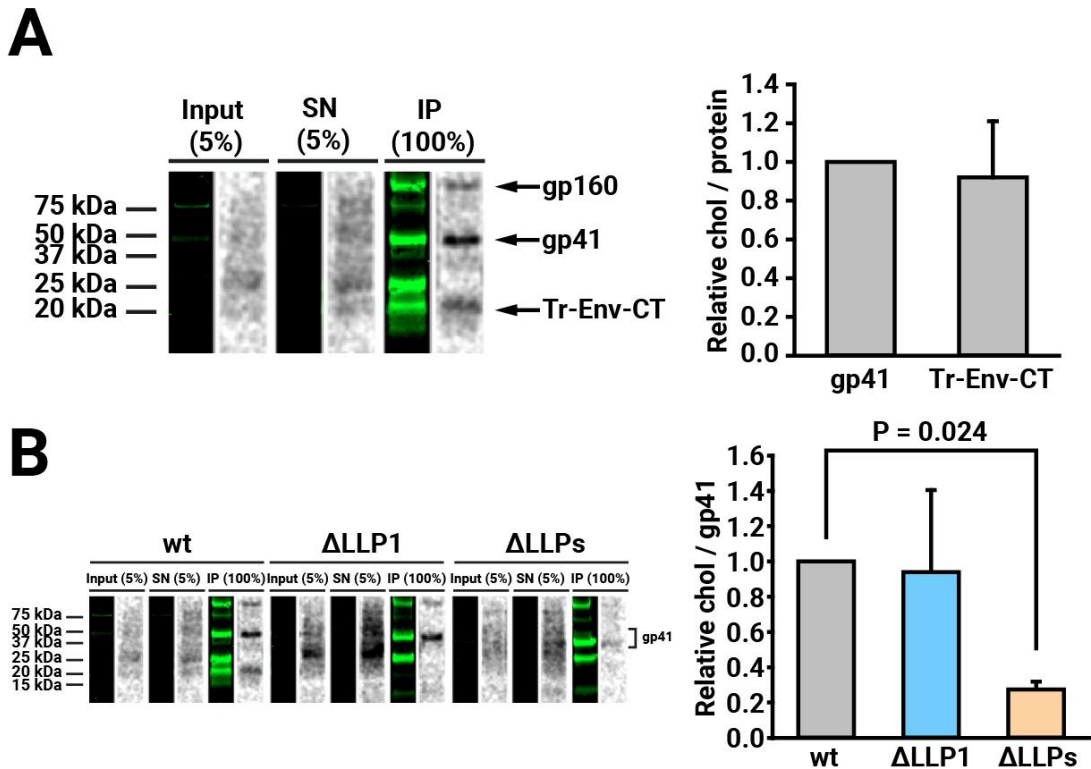


Ilustración 2 - Efecto de la eliminación del dominio citoplasmático en la interacción de gp41 con colesterol en partículas virales. SN = sobrenadante no inmunoprecipitado; IP = muestra inmunoprecipitada. **A** A la izquierda, imagen representativa del Western blot (verde) de la inmunoprecipitación de gp41 completa y el dominio citoplasmático truncado (Tr-Env-CT) y su interacción con colesterol (gris). A la derecha, cuantificación de la interacción con colesterol de Tr-Env-CT y la proteína completa. **B** A la izquierda, imagen representativa del Western blot (verde) de la proteína gp41 salvaje, y mutantes de eliminación del dominio citoplasmático, y su interacción con colesterol (gris). A la derecha, cuantificación de la interacción con colesterol de las tres variantes de gp41. Las barras representan la media de tres experimentos independientes.

Se proponen varios modelos para explicar la dependencia de la interacción de gp41 con colesterol con las secuencias LLP2-3: modelos directos en los que los dominios LLP2-3 se insertan parcialmente en la membrana e interaccionan con colesterol de manera directa (Ilustración 3A); o modelos indirectos en los que los dominios LLP2-3 determinan la estructura conformacional de la proteína, o en la que seleccionan el entorno lipídico de la proteína, permitiendo la interacción con colesterol de otra región de gp41 (Ilustración 3B).

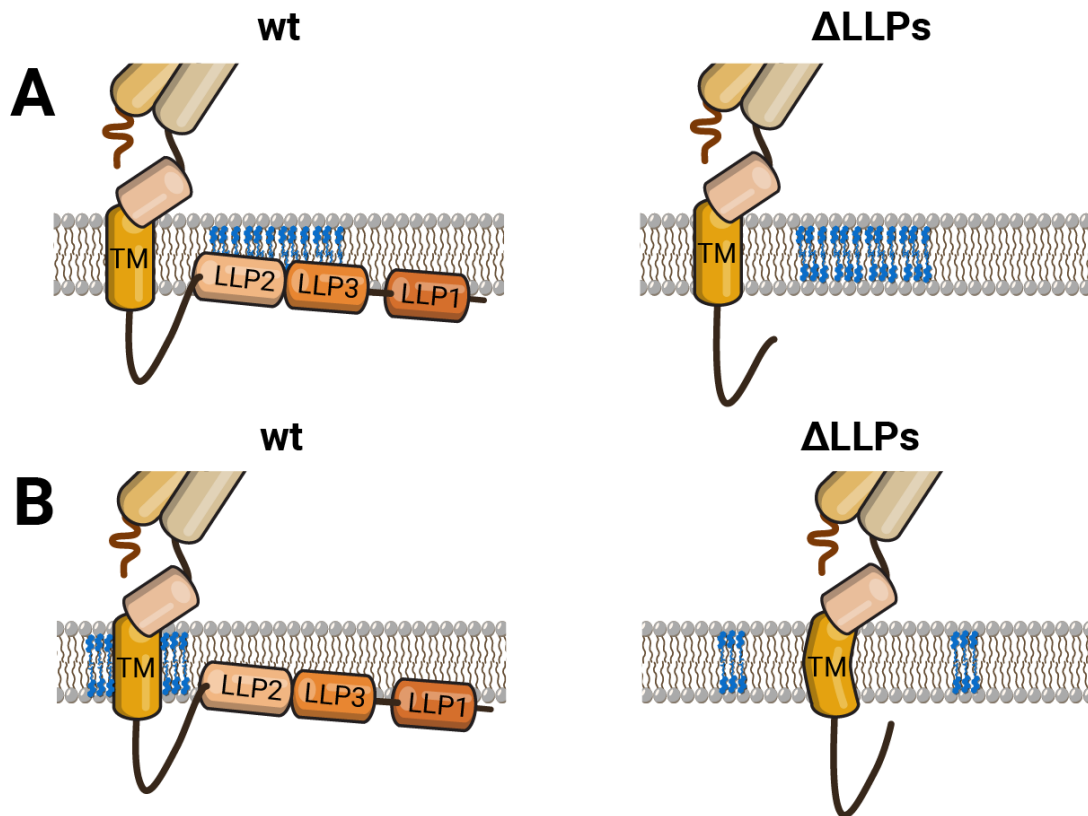


Ilustración 3 – Modelos de interacción gp41-colesterol. **A)** Las secuencias LLP2-3, parcialmente insertadas en la membrana, interaccionan directamente con colesterol. Tras su eliminación, la interacción directa de gp41 con el lípido es inhibida. **B)** Otra región de gp41 interacciona con colesterol (en la imagen el dominio transmembrana se muestra como ejemplo). La eliminación de las secuencias LLP induce un cambio conformacional, o la exclusión de gp41 de regiones específicas de la membrana (no mostrado en la imagen), inhibiendo la interacción de dicho dominio con colesterol.

Para determinar si otra región de gp41 interacciona con colesterol se estudió el papel de varias regiones de gp41 de interés en la interacción con colesterol: secuencias de interacción con colesterol CRAC (del inglés *Cholesterol Recognition Aminoacid Consensus*) en el dominio pre-transmembrana MPER; el dominio transmembrana y varias secuencias en él; y dos argininas altamente conservadas en el dominio LLP2. Los resultados obtenidos demuestran que ninguna de las regiones estudiadas está involucrada en la interacción de gp41 con colesterol. Aunque no se puede descartar que otra región no estudiada esté involucrada en la interacción, estos resultados parecen sugerir que son los dominios LLP2-3 los que interaccionan de manera directa con el lípido. Teniendo en cuenta que la cola citoplasmática de gp41, donde se encuentran los dominios LLP, está involucrada en la asociación de Env en las espículas y que esta asociación es necesaria para la entrada del virus en la célula huésped, los resultados de esta tesis proponen un modelo mediante el cual la interacción con colesterol de gp41, vía LLP2-3, permite a la proteína asociarse en una espícula y llevar a cabo una correcta fusión con la células huésped (Ilustración 4).

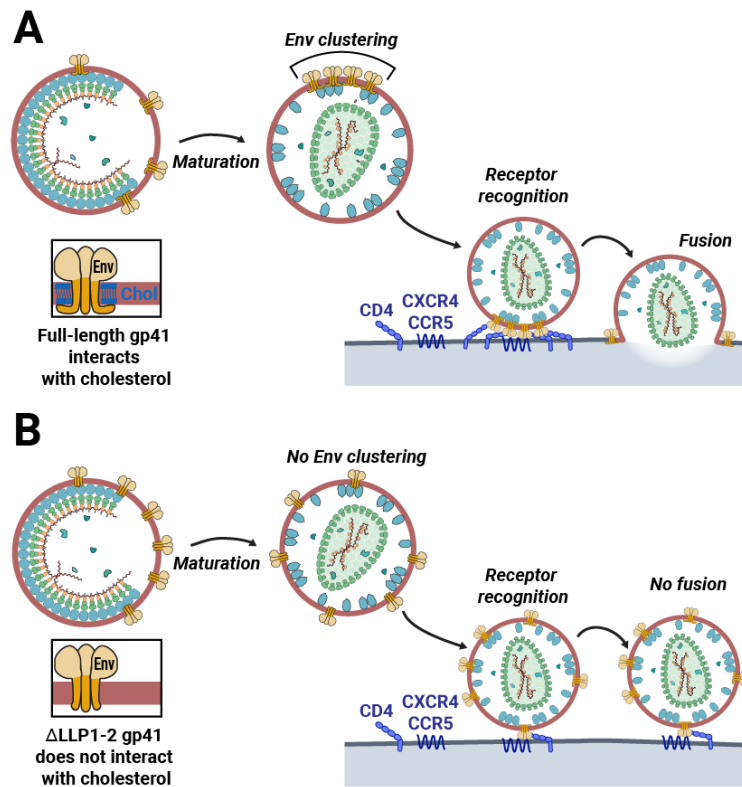


Ilustración 4 - Modelo de relación entre la interacción con colesterol dependiente de los dominios LLP2-3 de gp41 y la acumulación de Env en una sola espícula necesaria para la fusión viral.

Lipidomiméticos como inhibidores de entrada

Para cumplir el segundo objetivo de la tesis se estudió el efecto antirretroviral de una serie de compuestos lipidomiméticos raftofílicos y sus mecanismos de acción. Estos compuestos, de estructura similar a lípidos naturales (Ilustración 5), demostraron tener funciones antirretrovirales inhibiendo la fusión de las membranas viral y celular impidiendo la entrada del virus y la infección de la célula huésped. Una vez descartado un efecto directo de los lipidomiméticos en las proteínas virales, se estudió el mecanismo de acción de los compuestos lipidomiméticos demostrando que estos compuestos alteran la estructura de la membrana del virus induciendo cambios en el empaquetamiento de los lípidos. De especial interés fue el descubrimiento de que distintos compuestos lipidomiméticos tienen efectos opuestos en la estructura de la membrana del virus, induciendo algunos un cambio de los lípidos hacia fases ordenadas, y otros cambios hacia fases desordenadas. A pesar de estas diferencias, todos los lipidomiméticos estudiados inhibieron notablemente la fusión del virus con la célula. Además, se descubrió que el compuesto derivado de colesterol J391B requería la presencia de fosfatidilserina en la membrana del virus para llevar a cabo su acción reestructuradora. Estos resultados demuestran que, además de su composición, la estructura específica de la membrana del virus tiene un gran impacto en la capacidad infectiva del virus.

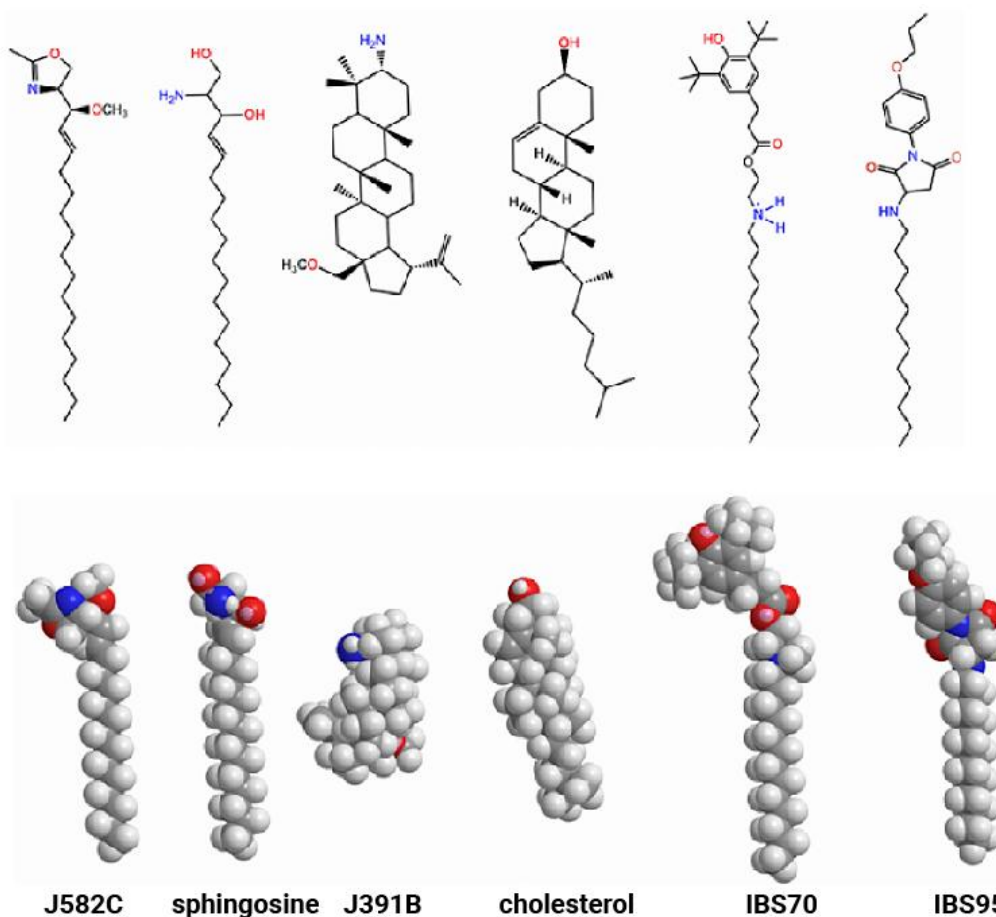


Ilustración 5 – Modelos moleculares de las estructuras 3D de los compuestos lipodimiméticos en comparación con lípidos naturales.

Nanopartículas transportadoras de agentes reactivadores de latencia

Cumpliendo con el tercer objetivo de la tesis se desarrollaron una serie de nanotransportadores cargados de agentes reactivadores de latencia para inducir la reactivación de células latentemente infectadas. La focalización de estos nanotransportadores hacia las células latentemente infectadas se llevó a cabo aprovechando el proceso natural de *trans*-infección del VIH-1. El virus, gracias a la presencia de gangliósidos en su membrana, es reconocido por el receptor Siglec-1 en las células dendríticas maduras (mDCs). Las mDCs capturan y acumulan el virus y cuando en su ciclo natural migran hasta tejidos linfoides e interactúan con células T los virus son liberados e infectan a las células CD4+. Funcionalizando nanotransportadores con gangliósidos que son reconocidos por Siglec-1, se diseñó un sistema que utiliza a las mDCs como “caballos de Troya” para focalizar los nanotransportadores hacia las células latentemente infectadas. Con ello se consigue aumentar la potencia de las drogas encapsuladas al evitar su difusión por todo el organismo, permitiendo llegar a tejidos anatómicos de difícil acceso. Además, péptidos virales cargados en nanopartículas también fueron focalizados por la misma

vía a células T CD8+ para inducir una activación del sistema inmune contra el VIH (Ilustración 6).

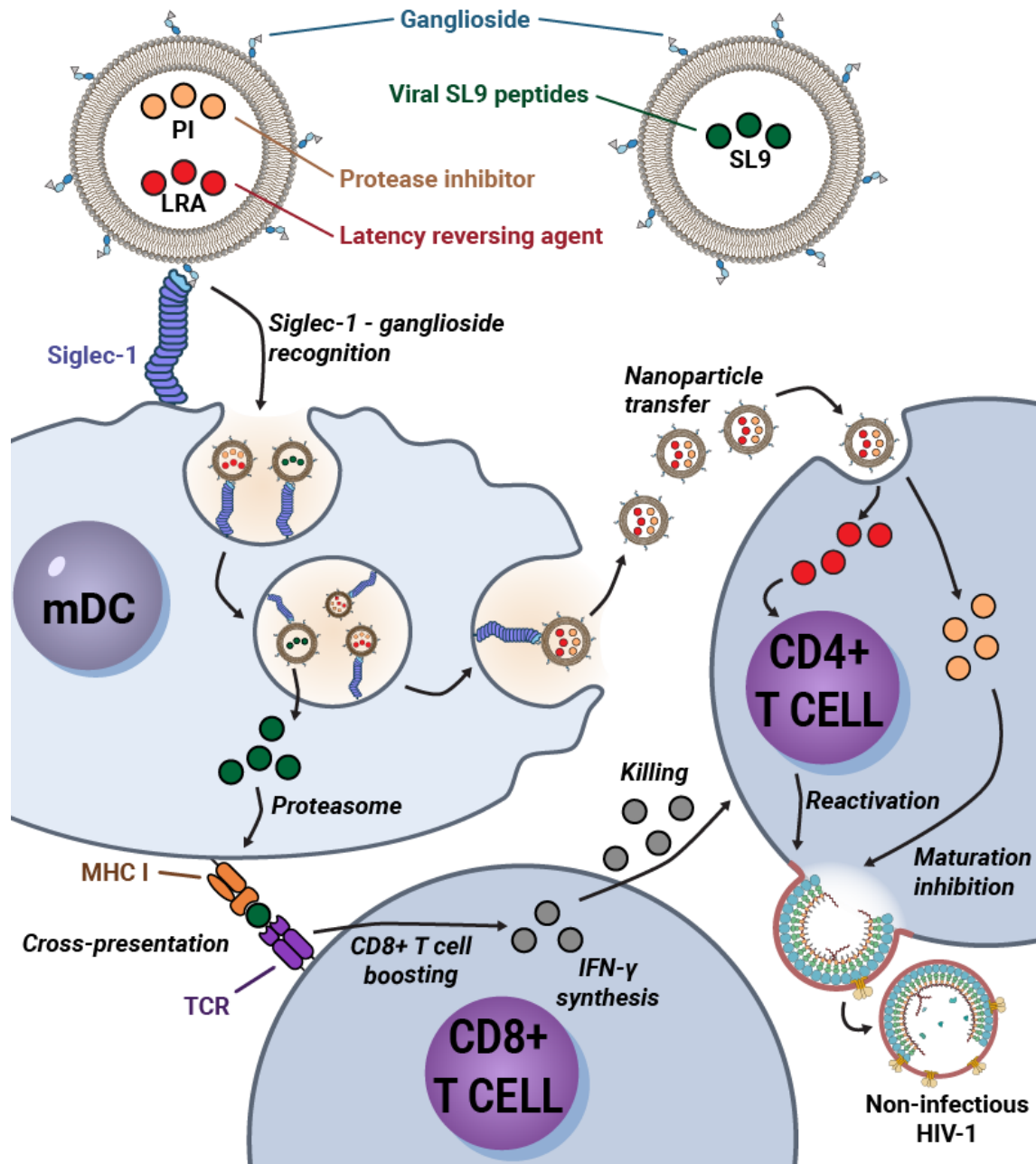


Ilustración 6 - Uso de la vía gangliósido/Siglec-1 para el transporte de agentes reactivadores de latencia y péptidos activadores del sistema inmune por parte de nanopartículas.

Resultados obtenidos con liposomas que contenían el gangliósido GM1 demostraron que las partículas son específicamente capturadas por mDCs por la vía gangliósido/Siglec-1 y que las partículas son posteriormente transferidas a células latentemente infectadas. Sin embargo, la reactivación de las células se observó

incluso en ausencia de captura, lo que parece indicar una fuga no deseada de la droga encapsulada al entrar en contacto las nanopartículas con las mDCs. Para evitar la fuga inespecífica de las drogas se desarrolló un segundo tipo de nanotransportadores, las partículas SLN (del inglés *Solid Lipid Nanoparticles*). Estas partículas están compuestas por un núcleo lipídico que encapsula con mayor eficacia las drogas hidrofóbicas, como lo son las drogas reactivadoras de latencia bryostatina y romidepsina utilizadas en esta tesis. Sin embargo, aun con estos SLNs se observó el mismo efecto de reactivación independiente de captura.

Para intentar entender el mecanismo que gobierna esta reactivación inespecífica se estudió el efecto de las drogas en las mDCs. Se descubrió que la bryostatina, al entrar en contacto con las células mieloides, inducía en ellas la síntesis de la citocina TNF α . El TNF α por su parte provocaba la reactivación de células latentemente infectadas. Aunque las nanopartículas no fueran capturadas específicamente, al entrar en contacto los liposomas o SLN con las mDCs, una mínima liberación de la bryostatina parecía suficiente para inducir la secreción de TNF α y la reactivación indirecta de células modelo J-lat. Este descubrimiento llevó al diseño de una nueva vía de reactivación en la que la administración de bryostatina a mDCs induciría una reactivación indirecta de células latentes mediante la secreción de TNF α por parte de las células mieloides. Sin embargo, para asegurar la especificidad de la focalización de los nanotransportadores la fuga inespecífica de la droga reactivadora debía ser eliminada.

Se desarrolló entonces un tercer tipo de partículas para el reparto específico de drogas reactivadoras de latencia. Estas partículas se basan en núcleos poliméricos de PLGA recubiertos de lípidos para su funcionalización. La principal ventaja que presentan es que la encapsulación de la droga reactivadora hidrofóbica en las partículas de PLGA se realiza en un paso separado del recubrimiento con membranas lipídicas por lo que se asegura que la droga quede encapsulada en el núcleo de PLGA y no se difunda a la bicapa lipídica que lo recubre. Los primeros experimentos realizados con este nuevo enfoque generaron resultados esperanzadores en los que se consiguió un recubrimiento óptimo de partículas de PLGA con vesículas lipídicas funcionalizadas con gangliósidos, los cuales eran específicamente capturados por mDCs. Es más, la captura específica de nanopartículas de PLGA cargadas con bryostatina y cubiertas de lípidos que contenían gangliósidos conllevó la síntesis específica de TNF α por parte de las mDCs. Además, se iniciaron experimentos de recubrimiento de partículas de PLGA con vesículas derivadas de plaquetas (Ilustración 7), las cuales presentan un gran número de ventajas frente al uso de vesículas lipídicas de origen sintético, al estar las vesículas derivadas de plaquetas aprobadas por la FDA para su uso clínico y al presentar una mayor biocompatibilidad en comparación con lípidos de origen sintético cuando se administran a pacientes en experimentos *in vivo*.

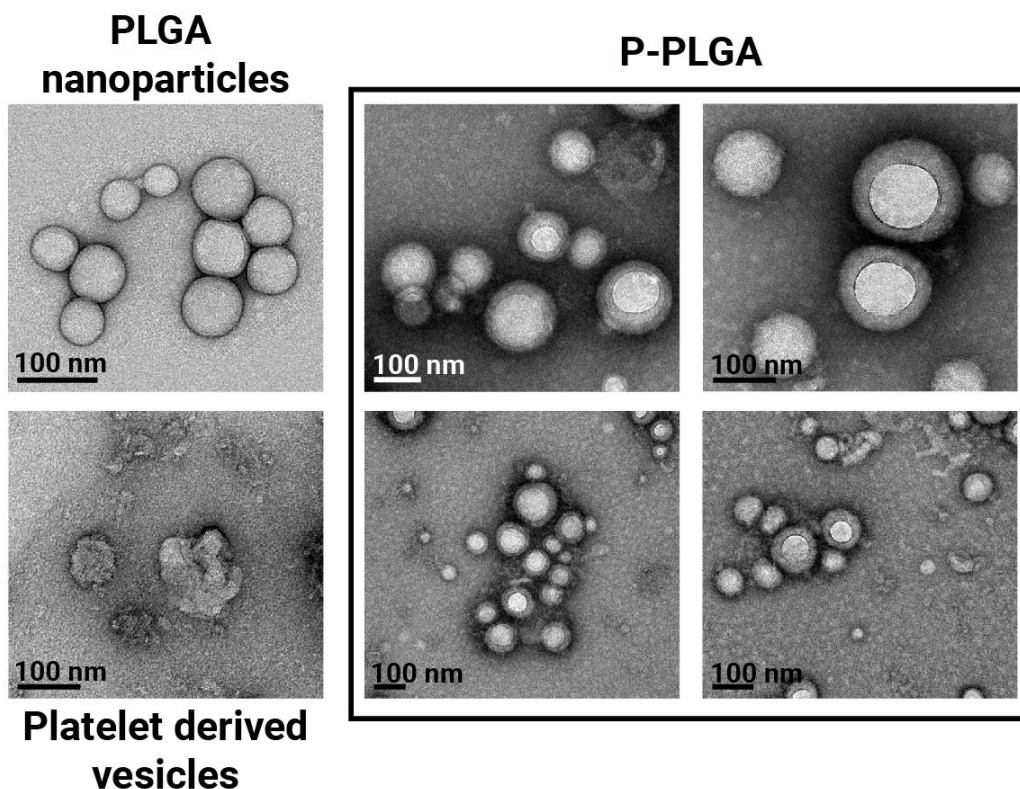


Ilustración 7 – Imágenes TEM de partículas de PLGA cubiertas de vesículas derivadas de plaquetas. Partículas de PLGA (arriba izquierda), vesículas derivadas de plaquetas (abajo izquierda), y partículas de PLGA cubiertas de vesículas derivadas de plaquetas (derecha) fueron analizadas por cryomicroscopía electrónica de transmisión.

Conclusiones

Las conclusiones de esta tesis son:

- La subunidad gp41 de la proteína de envuelta del VIH-1 interacciona con el colesterol en las membranas celular y viral, y las secuencias LLP2 y LLP3, pero no LLP1, de la cola citoplasmática de gp41 son necesarias para la interacción. El estado de maduración de la partícula viral no influye en la interacción de gp41 con colesterol. La capacidad de entrada del virus es inhibida cuando se impide la interacción de gp41 con colesterol.
- Compuestos lipodomiméticos sintéticos alteran la estructura de la membrana viral inhibiendo la infectividad del virus en el paso de entrada. La presencia de fosfatidilserina en la membrana viral es necesaria para los efectos producidos por el compuesto J391B en la estructura de la membrana viral. El uso combinado de los compuestos J391B y J582C resulta en un efecto antirretroviral sinérgico, aunque individualmente los compuestos tengan efectos opuestos en el grado de ordenamiento de la membrana.
- Nanopartículas con gangliósidos pueden ser específicamente focalizadas a mDCs y transferidas a células latentemente infectadas mediante la ruta

gangliósido/Siglec-1. Péptidos derivados del VIH-1 pueden ser empaquetados en liposomas y dirigidos a células T CD8+ mediante captura por parte de las mDCs para potenciar la respuesta del sistema inmune y generar respuestas citotóxicas específicas contra el VIH-1. Una liberación inespecífica de los compuestos reactivadores de latencia tras el contacto entre nanopartículas y mDCs resultó en una reactivación de las células J-lat espectadoras, mediada por la secreción de TNF α por parte de las mDCs. Además, núcleos poliméricos de PLGA pueden ser recubiertos con vesículas lipídicas funcionalizadas para su focalización específica y captura por parte de las mDCs.

Summary

The Human Immunodeficiency Virus 1 (HIV-1) is the causative agent of the Acquired Immunodeficiency Syndrome (AIDS). HIV-1 is a retrovirus from the *Lentivirus* genera surrounded by a lipid envelope which it obtains from the plasma membrane of the host cell in the budding process. The envelope protein (Env) responsible for the recognition of the host cell receptor and co-receptor and fusion is embedded in the viral membrane.

The HIV-1 lipid envelope is enriched in several lipids when compared to the plasma membrane from which it comes. Of special interest are lipids such as cholesterol, phosphatidylserine, sphingomyelin and saturated species of phosphatidylcholine, all of them enriched also in raft-like lipid nanodomains. Additionally, studies using the fluorescent dye Laurdan, sensitive to the phase state of lipids, demonstrated that the HIV-1 membrane has a liquid ordered (L_o phase) membrane structure, similar to what has been described for raft nanodomains. This demonstrates that the structure of the membrane, and not only the composition, is also similar between the HIV-1 lipid membrane and raft nanodomains.

The structural properties of the membrane and the presence of certain lipids have been described to be necessary for the infective capacity of the virus. For example, treatment of the virus with cholesterol-depleting or binding agents derives in a marked decrease of the infective capacity of the viral particle, which suggests an important role of this lipid in the fusion between the virus and the host cell. Interestingly, raft-like domains, also enriched in cholesterol, are capable of including or excluding certain proteins from specific regions of the membrane. Similarly, this phenomenon could also exist in the HIV-1 lipid membrane, which would suggest a mechanism by which depletion of cholesterol from the viral membrane results in a redistribution of the viral envelope protein, resulting in a decreased fusion capacity. Additionally, changes in the structure of the membrane that alter raft nanodomains could also derive in the inhibition of viral infective capacity.

Env is a glycoprotein composed of two subunits, gp120 or surface glycoprotein, and gp41 or transmembrane glycoprotein. The two subunits are non-covalently bound forming a heterodimer, three of which associate to generate a homotrimer of heterodimers (Illustration 1). In the mature virus Env trimers associate into a single spike or cluster, which has been described to be necessary for efficient fusion between the virus and the host cell.

The gp41 transmembrane subunit, which anchors Env to the viral membrane, seems to interact with raft-like membrane nanodomains and even directly with cholesterol, which could help explain the dependence in cholesterol of the virus infectivity. Thus, studying the lipid environment of gp41 and, specifically, its interaction with cholesterol, could shed some light about the mechanism by which viral infectivity depends on viral membrane cholesterol.

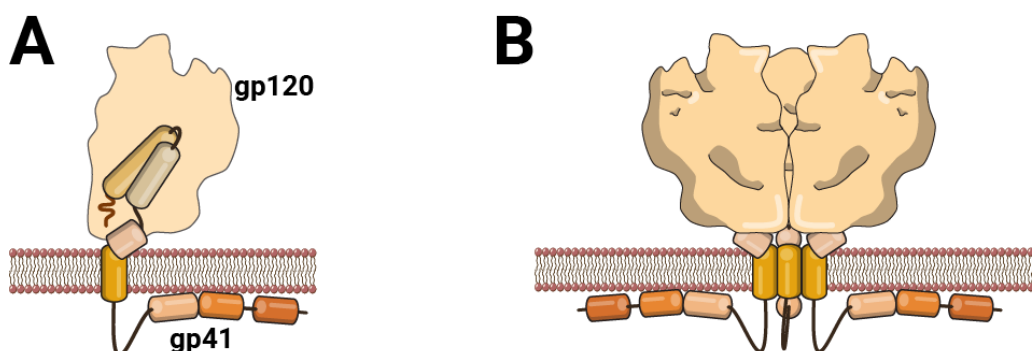


Illustration 1 - Env structure. A| Env heterodimer composed of the gp41 and gp120 subunits. Area occupied by gp120 is shown shaded to reveal the gp41 subunit underneath. gp120 is oriented towards the surface of the virion, and recognizes the cellular CD4 and CXCR4 or CCR5 co-receptors. gp41 anchors Env to the viral lipid envelope, and induces the fusion between viral and cellular membranes. B| Three gp41-gp120 heterodimers oligomerize to generate a trimer of heterodimers.

Although the High Activity Antiretroviral Therapy (HAART) available nowadays is capable of suppressing viral presence in the blood (viremia) to undetectable levels lowering the transmission rates and infection spread, no complete cure for HIV-1 exists yet. When patients under HAART get their treatment interrupted, their viremia spikes in as short as two weeks, which implies that HIV-1 infected patients must be under treatment for the rest of their lives. This virus surge after treatment interruption is caused by the existence of viral reservoirs, anatomical sites in which latently infected cells reside. These cells are infected in the first stages of the viral infection cycle, before the first symptoms appear and when no antiretroviral drugs have been administered yet. When antiretroviral drugs are given to the patient, replication of new viral particles is inhibited, but the viral genetic material remains latently integrated in these cells, without being expressed, so the immune system cannot find and purge these latently infected cells. If treatment is interrupted, the latent genetic material is expressed, and the viral levels in the organism spike again. Until a prophylactic vaccine is developed which inhibits initial infection of any cell with HIV-1, and thus the establishment of viral reservoirs, the development of an HIV-1 cure requires strategies designed to purge the latently infected cells. The majority of these strategies are based in the concept of “shock and kill”, consisting on the reactivation of latently infected cells forcing expression of viral proteins so that the immune system can recognize and eliminate the viral reservoirs.

Objectives

The main objectives of this thesis are:

1. Study the interaction with cholesterol of the gp41 subunit of HIV-1 envelope protein, and look for the protein region involved in the interaction, to find determinant factors involved in the relationship between cholesterol and viral infectivity.
2. To study raftophylic lipidomimetic compounds as antiretroviral tools for their use in various enveloped pathogens.
3. Develop new antiretroviral therapies based on the purge of viral reservoirs by the use of nanoparticles transporting agents designed to reactivate latently infected cells and boost the innate immune response of the organism, a system which can induce a functional cure of the HIV-1 infection.

gp41 interaction with cholesterol

Thanks to the use of photoactivatable lipids, capable of covalently binding to any molecule closer than 3 Å, the study of the lipid environment of gp41 carried out in this thesis have demonstrated that gp41 interacts with cholesterol molecules both in the cellular and viral membranes. This constitutes the first direct and *in vivo* prove of the interaction of gp41 with cholesterol to date. Additionally, a protein consisting of the truncated cytoplasmic domain of gp41 derived from the full-length protein (Tr-Env-CT) was found to interact with cholesterol at the same level as the full-length version, indicating that the cytoplasmic domain may be involved in the interaction (Illustration 2A). Indeed, the Lentiviral Lytic Peptide (LLP) sequences 2 and 3 in the cytoplasmic domain, but not LLP1, were demonstrated to be necessary for the interaction of gp41 with cholesterol (Illustration 2B).

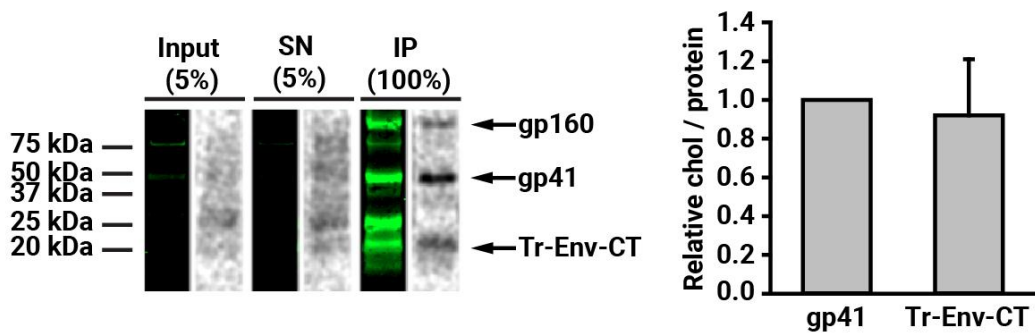
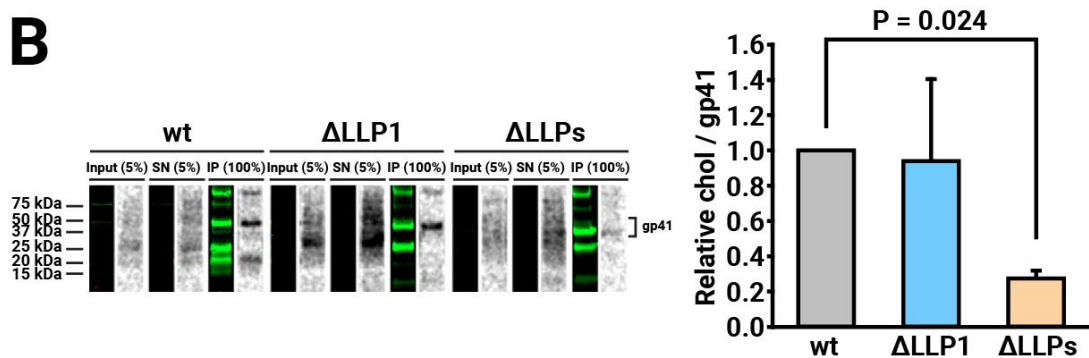
A**B**

Illustration 2 - Effect of CT truncation in gp41-cholesterol interaction in purified viral particles. SN = non-immunoprecipitated supernatant; IP = immunoprecipitated sample. **A** In the left, representative image of the Western blot (green) of the immunoprecipitated full-length gp41 and truncated gp41 cytoplasmic domain (Tr-Env-CT) and cross-linked [3 H]-photo-cholesterol autoradiography (grey) signals obtained from a purified virus amount equivalent to 1 μ g of CA. In the right, quantification of the relative cholesterol interaction of the full-length gp41 and Tr-Env-CT. **B** In the left, representative image of the Western blot (green) of the immunoprecipitated wild-type and CT truncation variants of gp41 and cross-linked [3 H]photocholesterol autoradiography (grey) signals obtained from a purified virus amount equivalent to 1 μ g of CA. In the right, quantification of the relative cholesterol interaction of the wild-type gp41 and truncation variants.

Several models are proposed for this LLP2-3 dependent interaction of gp41 with cholesterol: direct models in which the LLP2-3 domains partially insert in the membrane and interact with cholesterol directly (Illustration 3A); or indirect models in which the LLP2-3 determine the conformational structure of the protein, and/or select a specific lipid environment, allowing another region of gp41 to interact with cholesterol (Illustration 3B).

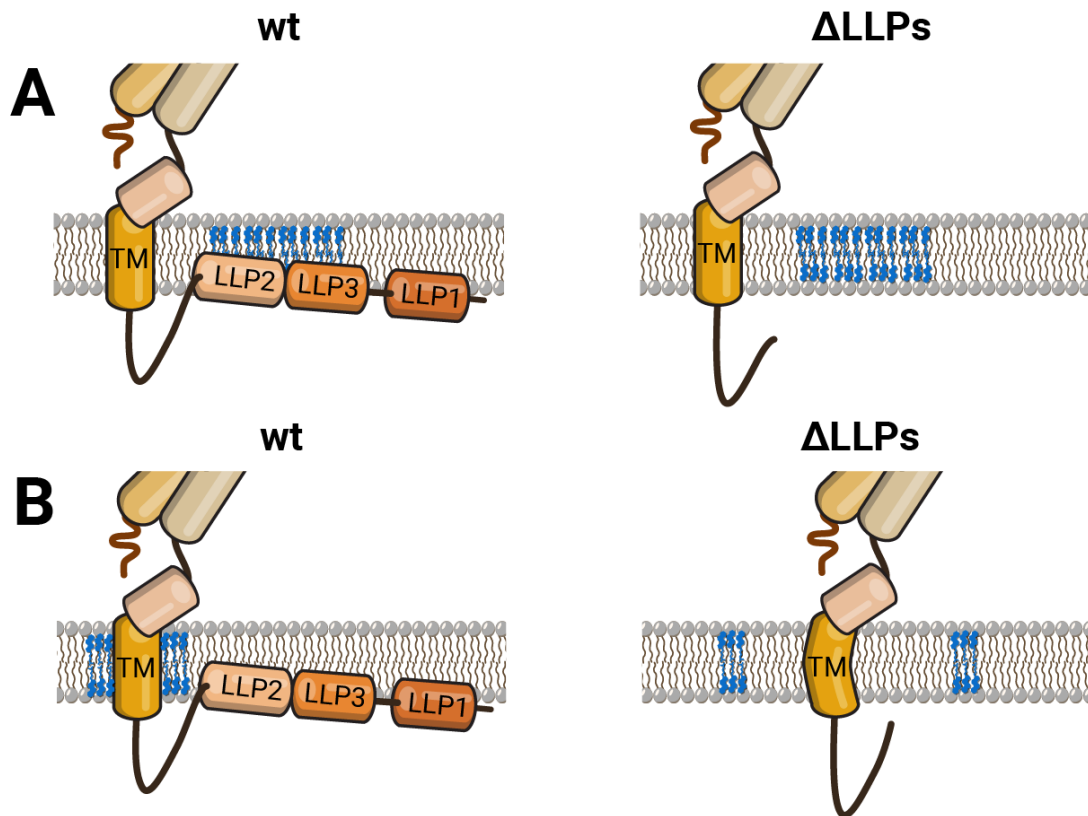


Illustration 3 - gp41-cholesterol interaction models. **A**] The LLP2-3 sequences, partially embedded in the membrane, directly interact with cholesterol. After their truncation, direct interaction of gp41 with cholesterol is hampered. **B**] Another region of the protein interacts with cholesterol (in the image, the transmembrane domain is shown as an example). Truncation of the LLP sequences induces a conformational change, or exclusion of gp41 from a certain lipid domain (not shown in the image), inhibiting the interaction of said region with cholesterol.

To determine the possible involvement of another region of the protein in the interaction with cholesterol, several domains previously described as lipid-interacting domains were studied: a Cholesterol Recognition Aminoacid Consensus (CRAC) sequence in the ectodomain conserved in several proteins and that have been described to interact with cholesterol *in vitro*; the transmembrane domain and two specific sequences (GxxxG-motif, which interacts with cholesterol in other proteins; and an arginine residue which may lay spatially close to membrane cholesterol) in it; and two highly conserved arginines in the LLP2 sequence, involved in the targeting of gp41 to the plasma membrane. The results obtained demonstrate that none of the studied regions is involved in the interaction with cholesterol, which points towards the fact that the LLP2-3 sequences are directly involved in the interaction of gp41 with cholesterol. Taking into account that the cytoplasmic domain of gp41, which harbors the LLP sequences, is involved in the association of Env in spikes or clusters, a process necessary for fusion, the results in this thesis suggest a model by which the interaction of gp41 with cholesterol, mediated by LLP2-3, allows the association of the protein into a single cluster and consequently the efficient fusion between the virus and the host cell (Illustration 4).

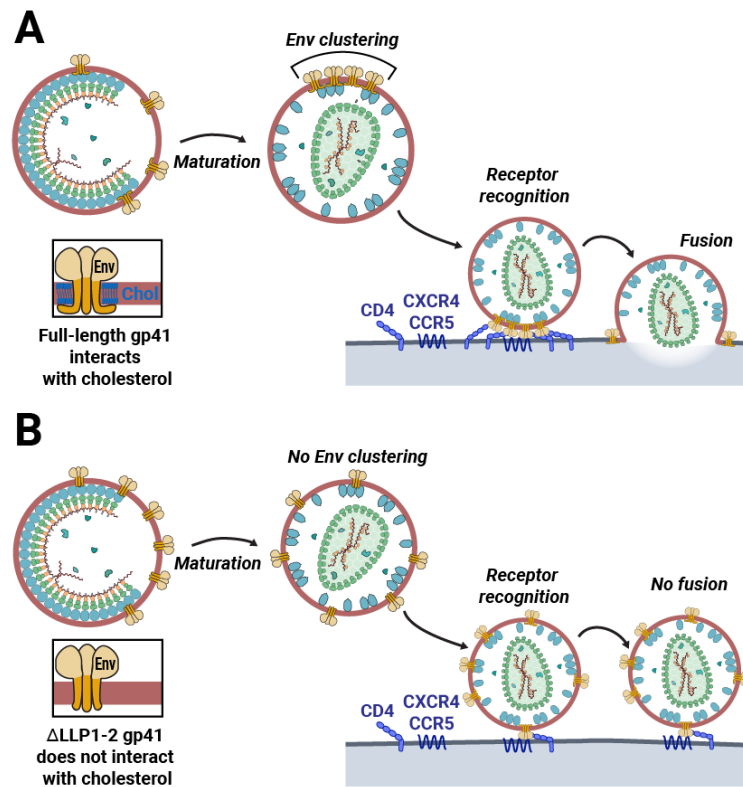


Illustration 4 - Model for cholesterol-dependent fusion. Interaction with cholesterol mediated by the LLP2-3 sequences permits an efficient clustering of Env into a single spike upon maturation, and consequent fusion between the viral and cellular membranes.

Lipidomimetics as entry inhibitors

The second objective of this thesis entailed the study of the antiretroviral properties and its mechanism of action of a series of lipidomimetic compounds. These compounds, with a structural reminiscent of natural lipids (Illustration 5), were demonstrated to have antiretroviral properties by inhibit viral and cellular membrane fusion, and consequent infection. A direct effect of the compounds in the viral proteins was discarded, and when the exact mechanism of fusion inhibition was studied, lipidomimetics were found to act in the viral membrane by altering its structure and changing the packing degree of the lipids. Interestingly, different lipidomimetic compounds had opposing effects in the structure of the membrane, either increasing or decreasing the fluidity of the membrane. Even so, all of the studied lipidomimetic compounds inhibited fusion between the virus and the host cell. These results demonstrate that, in addition to its composition, the specific structure of the viral membrane and the lipid packing have a great impact in the viral infective capacity, and constitutes a new type of drug which can be used in different membrane enveloped pathogens.

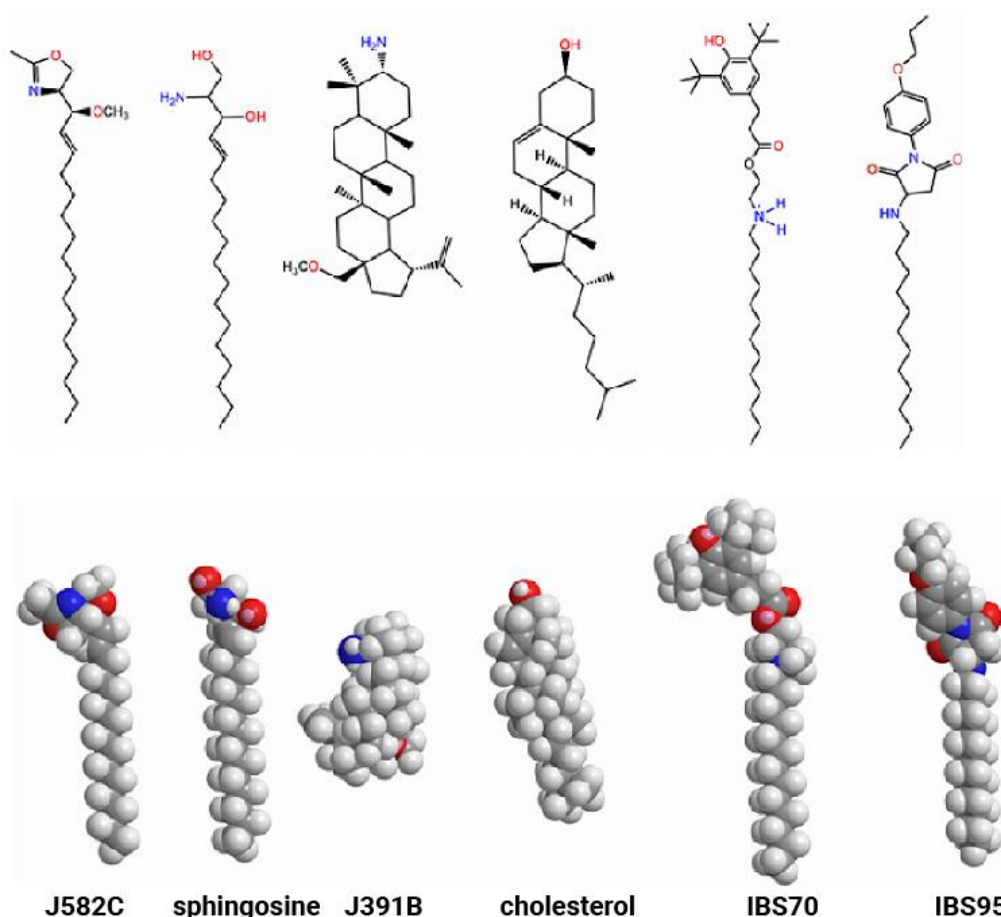


Illustration 5 - Molecular modeling of the 3D structures of lipidomimetic compounds in comparison to natural lipids.

Nanoparticles for delivery of latency reversing agents

Finally, in the pursuit of the third objective, different nanocarriers were developed for the delivery of latency reactivating agents. The targeting of these nanocarriers to latently infected cells was carried out by exploiting the natural *trans*-infection pathway followed by HIV-1. Siglec-1 receptors in mature dendritic cells recognize sialyllactose-containing gangliosides in the HIV-1 envelope, inducing a capture and accumulation of the virus inside the myeloid cells. When the mDCs migrate to peripheral tissues as part of their natural function they interact with T cells, and the accumulated virus is released and infects CD4+ cells. By functionalizing nanocarriers with gangliosides recognized by Siglec-1, a system which uses mDCs as “Trojan horses” was developed to target nanocarriers to latently infected cells, increasing the potency of the encapsulated drug by avoiding its spread through all the organism and enhancing its partition to difficultly accessible anatomical sites. Additionally, viral peptides loaded into nanoparticles were also carried by the same pathway to CD8+ T cells to boost the specific anti-HIV immune response and purge the latently infected cells (Illustration 6).

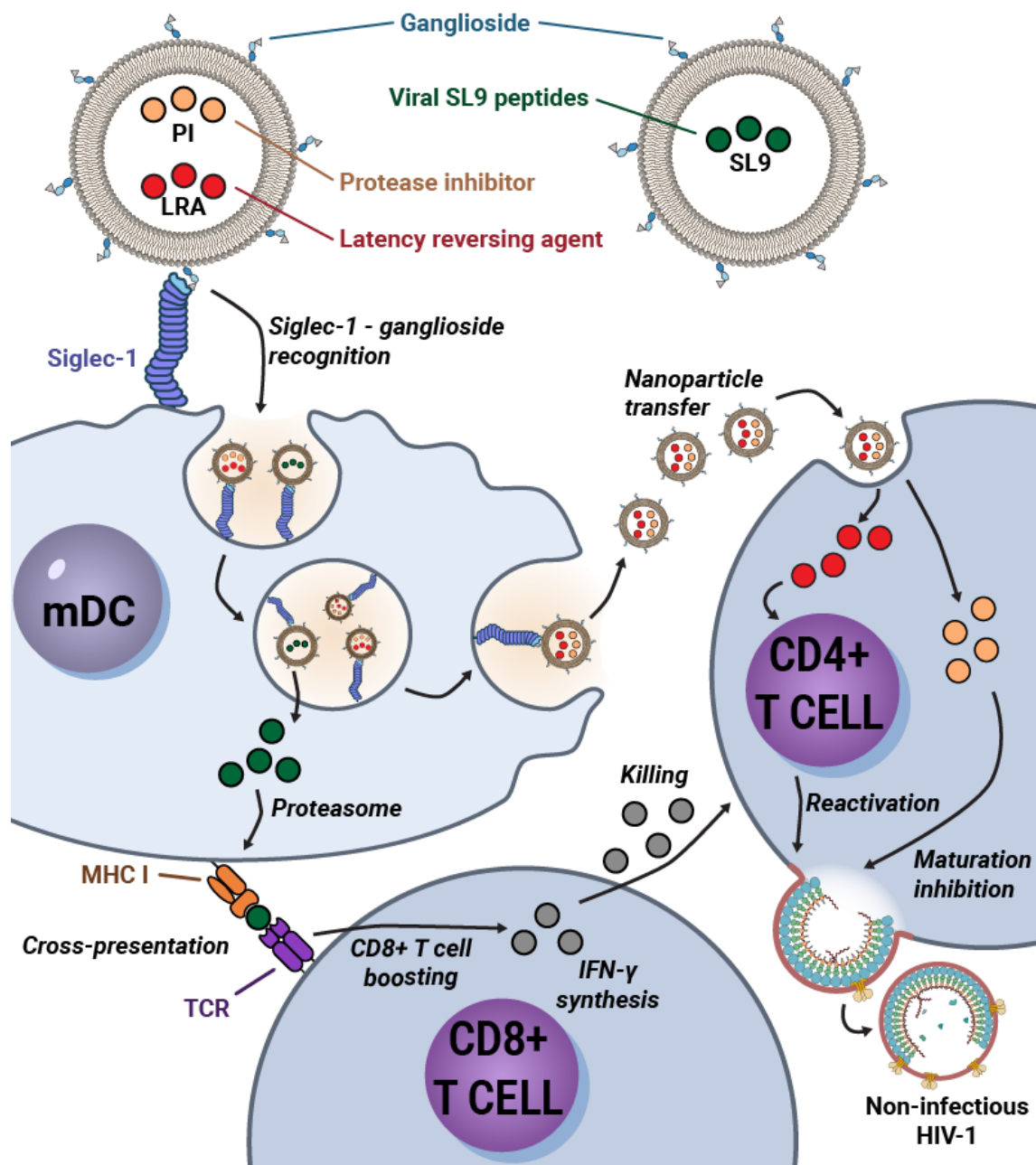


Illustration 6 - Use of ganglioside/Siglec-1 mediated pathway for delivery of latency reversing drugs and immune boosting peptides by nanoparticles.

Results observed with GM1-containing liposomes demonstrated that nanoparticles are specifically captured by mDCs by the ganglioside/Siglec-1 pathway, and that the particles are then transferred to latently infected cells. Nevertheless, latently infected cell reactivation occurred even in the absence of capture, which seemed to indicate that a non-desired drug leakage occurred when nanoparticles contacted with mDCs, even if they were not captured. To try to overcome this eventuality, a second type of nanoparticles were developed, Solid Lipid Nanoparticles (SLN). These particles contain a solid lipid core which more efficiently packages hydrophobic drugs, such as the latency reactivator agents used in this thesis. This new nanoparticles were designed to

try to overcome the undesired drug leakage, but upon testing unspecific reactivation was also observed, similar to the results obtained for liposomes.

To try to elucidate the mechanism governing the unspecific reactivation, the effect of the drugs in mDCs was studied. Bryostatin was found to induce TNF α secretion by mDCs, which in turn reactivated bystander J-lat cells. A minimal bryostatin leakage upon contact of liposomes or SLN with mDCs, even if nanoparticles were not captured, seemed to be sufficient for induction of TNF α secretion and indirect reactivation of J-lat cells. This discovery resulted in the development of a new type of latently infected cell reactivation approach, in which delivery of bryostatin to mDCs would induce an indirect reactivation of bystander J-lat cells by secretion of TNF α . Nevertheless, to ensure the specificity of the targeting of the nanoparticles, the unspecific drug leakage had to be eliminated.

For this purpose a third type of nanoparticles were developed, based in polymeric PLGA nanoparticles coated with a functionalized lipid bilayer for targeting capabilities. The main advantage of these nanoparticles is that the encapsulation of the hydrophobic drug and the lipid coating occur in two separated discrete steps, so the partitioning of the drug to the lipid bilayer and the consequent drug leakage upon contact with the cells is expected to be minimized. The first experiments carried out with this new type of nanoparticles generated promising results in which PLGA cores were successfully coated with lipid bilayers functionalized with gangliosides, which resulted in ganglioside/Siglec-1 specific capture of the nanoparticles by mDCs. Indeed, bryostatin loaded PLGA cores covered by lipids containing gangliosides resulted in specific secretion of TNF α by the mDCs after nanoparticles capture. Additionally, PLGA core coating with platelet derived vesicles was successfully carried out (Illustration 7). The use of platelet derived vesicles results in several advantages over synthetic lipid bilayers, as they are approved by the FDA for their clinical use, and results in a higher biocompatibility of the nanoparticles when administered to patients *in vivo*.

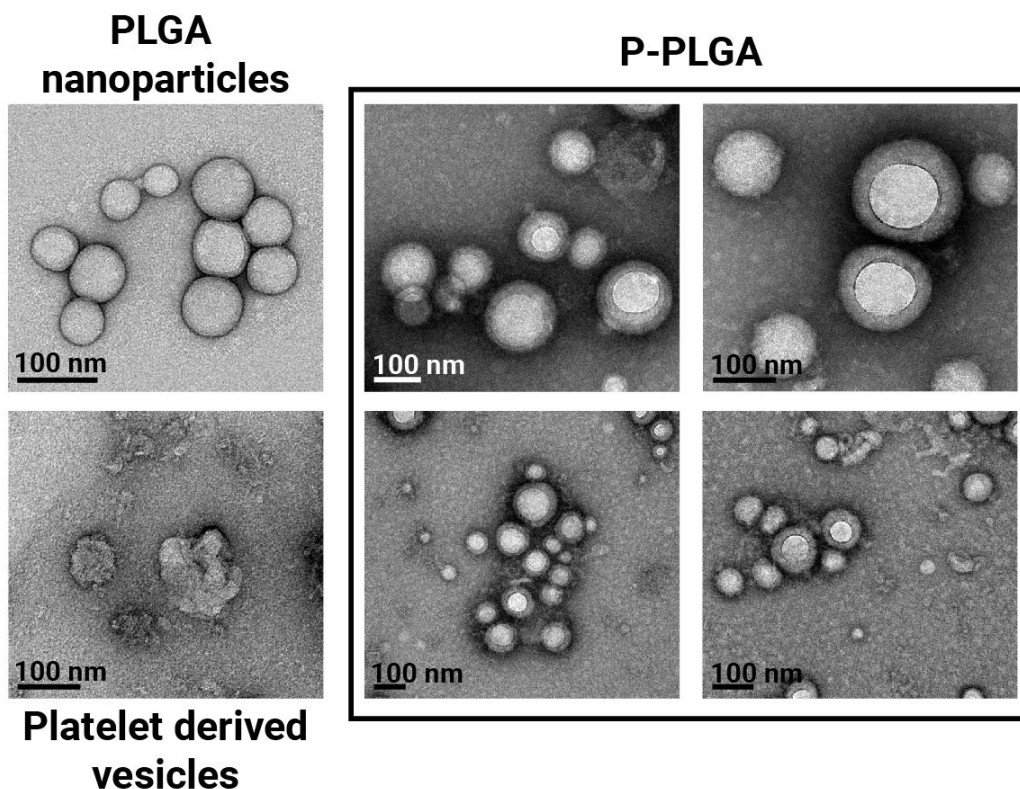


Illustration 7 - TEM images of PLGA coated with platelet derived vesicles. PLGA nanoparticles (upper left), platelet derived vesicles (lower left), and PLGA cores coated with platelet derived vesicles (right) were imaged with transmission electron cryomicroscopy.

Conclusions

The conclusions rised in this thesis are:

- The gp41 subunit of HIV-1 envelope protein interacts with cholesterol in the cellular and viral membranes, independently of the presence of Gag in the cells or the maturation state of the virus, and the LLP2 and LLP3 sequences, but not LLP1, in the gp41 cytoplasmic domain are necessary for such interaction. Loss of gp41-cholesterol interaction inhibits viral entry capacity.
- Synthetic raft lipid-like lipidomimetic compounds alter viral membrane structure, both increasing or decreasing fluidity, and inhibit viral infectivity at the entry step in a low micromolar range. Phosphatidylserine in the viral membrane is necessary for the membrane structure altering effect of the J391B compound. The combined use of antagonistic J391B and J582C compounds results in a synergistic antiretroviral effect, even if they have opposed effects in membrane order.
- Ganglioside containing nanoparticles can be specifically targeted to mDCs and transferred to latently infected cells via the ganglioside/Siglec-1 pathway. HIV-1 derived peptides can be packaged in liposomes and delivered to CD8+ T cells via mDC capture for immune boosting and generation of HIV-specific cytotoxic responses. Unspecific leakage of

latency reversing agents from liposomes and SLN upon contact with mDCs result in a bystander reactivation of J-lat cells mediated by secretion of TNF α by mDCs. Drug-loaded PLGA cores can be coated with functionalized lipid vesicles for specific targeting to and capture by mDCs. Drug-loaded PLGA cores functionalized by ganglioside containing lipids result in specific secretion of TNF α by dendritic cells after nanoparticles capture.

Abbreviations

6-HB	6-helix bundle
AAV	Adeno-Associated Virus
AIDS	Acquired Immunodeficiency Syndrome
All Geo MFI	All Geometric Mean Fluorescent Intensity
AME	Amphotericin B Methyl Ester
ANTS	8-Aminonaphthalene-1,3,6-Trisulfonic Acid
BlaM	Beta-Lactamase enzyme
bnAb	Broadly Neutralizing Antibody
CA	Capsid (HIV-1 protein)
Cav-1	Caveolin-1
CCR5	C-C chemokine receptor type 5
CD4	Cluster of differentiation 4
Chol	Cholesterol
CHR	C-terminal heptad repeat (gp41 domain)
CPM	Counts Per Minute
CRAC	Cholesterol Recognition Aminoacid Consensus
CryoTEM	Transmission Electron Cryomicroscopy
CT	gp41 Cytoplasmic Tail, or Cytoplasmic domain
CVP	Concentrated Viral Particles
CXCR4	C-X-C chemokine receptor type 4
DHPE	1,2-dihexadecanoyl-sn-glycero-3-phosphoethanolamine
DMEM	Dulbecco's Modified Eagle's Medium
DMSO	Dimethyl sulfoxide
DNA	Deoxyribonucleic acid
DOPA	1,2-dioleoyl-sn-glycero-3-phosphate
DOPE	1,2-dioleoyl-sn-glycero-3-phosphoethanolamine
DOPG	1,2-dioleoyl-sn-glycero-3-phosphoglycerol
DOPS	1,2-dioleoyl-sn-glycero-3-phospho-L-serine
DOTAP	N-[1-(2,3-Dioleoyloxy)propyl]-N,N,N-trimethylammonium chloride
DPM	Disintegrations Per Minute
DPPE	1,2-dipalmitoyl-sn-glycero-3-phosph
DPX	p-Xylene-Bis-Pyridinium Bromide
DRM	Detergent Resistant Membrane
DSPE-PEG2000	1,2-distearoyl-sn-glycero-3-phosphoethanolamine-N-[methoxy(polyethylene glycol)-2000]
ELISA	Enzyme-Linked Immunosorbent Assay
ELISpot	Enzyme-Linked Immunosorbent Spot
Env	Envelope glycoproteins (HIV-1 protein)
FACS	Fluorescence-activated cell sorting
FBS	See "FCS"
FCS	Fetal Calf Serum
FP	Fusion peptide (gp41 domain)
FSC	Forward Scattering

GFP	Green Fluorescent Protein
GP	Generalized Polarization
gp120	Glycoprotein 120, Surface glycoprotein (HIV-1 protein)
gp160	See " <i>Env</i> "
gp41	Glycoprotein 41, Transmembrane glycoprotein (HIV-1 protein)
HAART	Highly Active Antiretroviral Therapy
HBR	Highly Basic Region (MA domain)
HEPES	4-(2-hydroxyethyl)-1-piperazineethanesulfonic acid
HIV-1	Human Immunodeficiency Virus Type 1
HPLC	High-Performance Liquid Chromatography
iDC	Immature Dendritic Cell
IFN γ	Interferon gamma
IgG	Immunoglobulin G
IL	Interleukin
IN	Integrase (HIV-1 protein)
InSTI	Integrase Strand Transfer Inhibitor
LLP	Lentiviral Lytic Peptide
LPC	1-palmitoyl-2-hydroxy-sn-glycero-3-phosphocholine
L-PLGA	Lipid coated PLGA
LRA	Latency Reversing Agent
LUV	Large Unilamellar Vesicle
MA	Matrix (HIV-1 protein)
mAb	Monoclonal Antibody
mDC	Mature Dendritic Cell
MLVs	Multilamellar Vesicles
MLV	Murine Leukemia Virus
MPER	Membrane Proximal External Region
MTT	3-(4,5-dimethylthiazol-2-yl)-2,5-diphenyltetrazolium bromide
NC	Nucleocapsid (HIV-1 protein)
Nef	Negative factor (HIV-1 protein)
NHR	N-terminal heptad repeat (gp41 domain)
N-NBD-PE	L- α -phosphatidylethanolamine-N-(7-nitro-2-1,3-benzoxadiazol-4-yl)
N-Rho-PE	L- α -phosphatidylethanolamine-N-(lissamine rhodamine B sulfonyl)
NRTI	Nucleoside Reverse Transcriptase Inhibitor
nt	Nucleotide
PBMC	Peripheral Blood Mononuclear Cells
PC	Phosphatidylcholine
PCR	Polymerase Chain Reaction
PEG	Polyethylene Glycol
PI	Protease Inhibitor
PI(4,5)P2	Phosphatidylinositol (4,5) biphosphate
PLGA	Poly(lactic-co-glycolic acid)
POPC	1-Palmitoyl-2-oleoyl-sn-glycero-3-phosphocholine
P-PLGA	Platelet membrane coated PLGA
PR	Protease (HIV-1 protein)
PS	Phosphatidylserine

PVP	Purified Viral Particles
RAFI	Rigid Amphipathic Fusion Inhibitors
Rev	Regulator of Expression of Virion proteins (HIV-1 protein)
RLU	Relative Light Units
RNA	Ribonucleic acid
rpm	Revolution Per Minute
RT	Reverse Transcriptase (HIV-1 protein)
SD	Standard Deviation
SFC	Spot forming cells
SLN	Solid Lipid Nanoparticle
SM	Sphingomyelin
SSC	Side Scattering
Tat	Trans-Activator of Transcription (HIV-1 protein)
TfR	Transferrin Receptor
TLC	Thin Layer Chromatography
TMD	Trans-membrane domain
TNF α	Tumor necrosis factor alpha
UV	Ultraviolet
V3 loop	Third Variable Loop
VLPs	Viral Like Particles
Vpr	Viral Protein R (HIV-1 protein)
Vpu	Viral Protein U (HIV-1 protein)
VSV	Vesicular Stomatitis Virus
VSV-G	VSV G protein
WT	Wild type
β -gal	β -galactosidase

Contents

Chapter 1. Introduction	1
1.1. HIV and AIDS	3
1.1.1. HIV-1.....	5
1.2. Study of protein-lipid interactions.....	17
1.3. Therapeutic approaches.....	19
1.3.1. Inhibition of HIV-1 replication cycle.....	20
1.3.2. Purge of viral reservoirs.....	24
1.4. General objectives	25
1.4.1. Main objective	25
1.4.2. Specific objectives	26
Chapter 2. Experimental Techniques	27
2.1. Cells and cell culture.....	29
2.2. Constructs	30
2.2.1. gp41 variants design and cloning.....	32
2.2.2. Plasmid production.....	36
2.3. Chessie-8 antibody	38
2.3.1. Chessie-8 hybridoma	39
2.3.2. Chessie-8 IgG1 purification	39
2.4. Western blot	40
2.5. Viral particle purification	41
2.5.1. Cell transfection	42
2.5.2. Sucrose cushion concentration	44

2.5.3. Velocity gradient purification	45
2.6. Characterization of purified viral particles	47
2.6.1. Silver Stain	47
2.6.2. Purification yield quantification by anti-CA Western blot	48
2.7. Viral entry capacity	49
2.7.1. BlaM-Vpr viral particle production	50
2.7.2. BlaM-Vpr entry assay	51
2.8. Viral infective capacity	53
2.8.1. Infective viral particle production	54
2.8.2. Single round infectivity assay	54
2.9. Lipid extraction.....	55
2.10. Liposome generation.....	56
2.10.1. Lipid phosphorus concentration assay	57
2.11. Flow cytometry.....	58
2.12. Statistics.....	59
Chapter 3. Gp41-cholesterol Interaction Domain and Its Functional Implications.....	61
3.1. Introduction	63
3.2. Experimental techniques	70
3.2.1. Chessie-8 coupling to beads	70
3.2.2. Viral particle purification	72
3.2.3. Protein-lipid interaction studies	73
3.2.4. gp41 protein quantification	79
3.2.5. Proteomic studies	81
3.2.6. Lipidomic studies.....	82

3.2.7. Env localization studies	82
3.3. Results	84
3.3.1. Experimental parameters setting.....	84
3.3.2. gp41-cholesterol interaction in cells	88
3.3.3. gp41-cholesterol interaction in virus	91
3.3.4. Truncation of three LLPs but not LLP1 hampers interaction with cholesterol	95
3.3.5. Role of other protein domains in interaction with cholesterol	101
3.3.6. Truncation of LLPs hampers virus entry capacity	108
3.3.7. Maturation state does not affect gp41-cholesterol interaction	111
3.4. Discussion	118
Chapter 4. Lipidomimetic Compounds as HIV-1 Entry Inhibitors.....	131
4.1. Introduction	133
4.2. Experimental techniques	135
4.2.1. Cell culture and virus purification	135
4.2.2. Chemistry.....	136
4.2.3. Screening	136
4.2.4. Compound treatment of virus particles and cells	137
4.2.5. Infectivity and luciferase reporter assay	137
4.2.6. Entry assays	138
4.2.7. Sucrose-density equilibrium gradient centrifugation and Western blot analysis	138
4.2.8. HIV-1 laurdan staining and analysis of labeled particles.....	139
4.2.9. Lipid extraction, production of lipid vesicles and intervesicular MPER lipid mixing assay.....	140
4.3. Results	142

4.3.1. Compound screening.....	142
4.3.2. Lipidomimetics inhibit HIV-1 infection	143
4.3.3. Lipidomimetics target the virion membrane.....	145
4.3.4. Lipidomimetics inhibit HIV-1 entry at the fusion step.....	147
4.3.5. Effects of lipidomimetics on HIV-1 stability and virion density.....	150
4.3.6. Effect of lipidomimetics on HIV-1 membrane order	152
4.3.7. Phosphatidylserine-specific enhancement of membrane order by steroidal amine J391B.....	154
4.3.8. J391B and J582C exhibit synergistic effects on HIV-1 infectivity	156
4.4. Discussion	159
4.5. Annexes	163

Chapter 5. Development of Nanoparticles for Specific Delivery of Latency Reactivation Agents 167

5.1. Introduction	169
5.1.1. Latent viral reservoirs	169
5.1.2. <i>Trans</i> -infection	170
5.1.3. mDC mediated viral reservoir targeting.....	171
5.1.4. Nanoparticles for drug delivery.....	173
5.2. Experimental techniques.....	176
5.2.1. Reagents.....	176
5.2.2. Cells and cell culture.....	176
5.2.3. Liposome preparation.....	177
5.2.4. ANTS/DPX leakage assay	178
5.2.5. Solid lipid nanoparticles preparation.....	179
5.2.6. Lipid covered PLGA particle preparation.....	180
5.2.7. Nanoparticle capture and latency reactivation quantification	182

5.2.8. Flow cytometry	183
5.2.9. Cytotoxic response quantification	184
5.2.10. Cytokine secretion quantification.....	184
5.2.11. Confocal microscopy.....	184
5.3. Results	185
5.3.1. Ganglioside-dependent liposome capture	185
5.3.2. Effect of PEG in liposome capture.....	186
5.3.3. Liposomes for drug delivery.....	188
5.3.4. Solid lipid nanoparticles for drug delivery	193
5.3.5. Bystander reactivation.....	195
5.3.6. Lipid covered PLGA nanocarriers for drug delivery.....	198
5.4. Discussion	203
Chapter 6. General conclusions	209
Chapter 7. References	215

Chapter 1. Introduction

1.1. HIV and AIDS

The acquired immunodeficiency syndrome (AIDS) pandemic is caused by the human immunodeficiency virus (HIV). Although the oldest confirmed case of HIV infection was documented in a sample of stored serum obtained from a patient in 1959 in Kinshasa (Democratic Republic of Congo) (Zhu et al., 1998), the HIV infection was not observed until 1981, and the isolation of the virus first occurred two years later (Barre-Sinoussi et al., 1983; Gallo et al., 1983).

Two main types of HIV exist: type 1 and 2. Based on phylogenetic studies, the HIV type 1 (HIV-1) seems to have been brought to humans by chimpanzees (*Pan troglodytes*), which population harbors the related simian immunodeficiency virus (SIVcpz) (Gao et al., 1999). Studies based in genetic clock analysis indicate that the main (M) group of HIV-1 strains appeared in humans for the first time around 1931 in central Africa, where nonhuman primates are used for food consumption and kept as pets (Weiss and Wrangham, 1999). HIV type 2 (HIV-2) seems to have originated from the SIVsm of the sooty mangabey (*Cercocebus atys*) monkeys in coastal West Africa a decade later (Lemey et al., 2003).

Although both types of HIV are known to cause AIDS HIV-1 is the most common and virulent of the two, and the focus of this thesis. As of 2017, the Joint United Nations Programme on HIV/AIDS (UNAIDS) estimates that 36.9 million people are living with the virus, of which 69% live in Africa. Since the start of the pandemic almost 30 years ago, 35 million people have died because of the virus, and nowadays 1.8 million people are newly infected each year. The AIDS-related yearly death toll reached its maximum in 2005 with 1.9 million people, but hopefully the number of AIDS-related deaths and new HIV infections has declined and continues declining considerably since then (Figure 1.1).

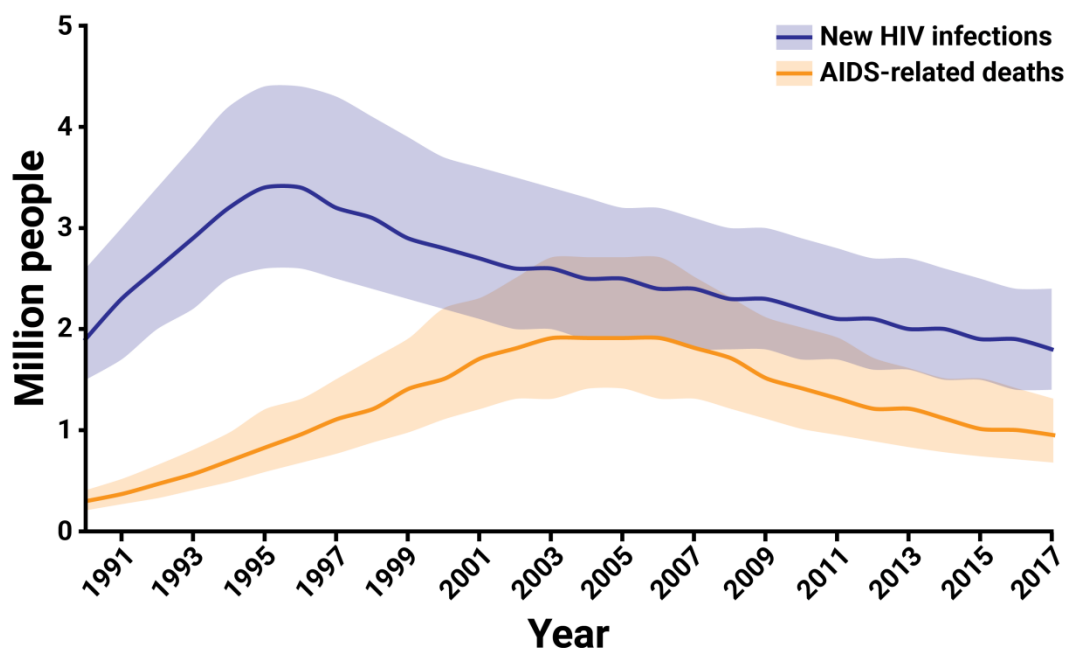


Figure 1.1 – Number of new HIV infections and AIDS-related deaths since 1990. The shaded area represents the upper and lower limits of the 2018 estimations published by UNAIDS.

This decline in new infections and deaths is mainly the result of advances in antiretroviral therapy. With the introduction of the highly active antiretroviral therapy (HAART) approach almost 30 years ago, the control of the infection spread and the quality of life of the infected individuals have improved considerably (Saag et al., 2018), but it nowadays requires the administration of daily treatment in the best of cases. The absence of a prophylactic vaccine or a complete cure for HIV-1 entails that in regions where daily treatment is not accessible and affordable for the patients, control of the pandemic is complicated, which nowadays results in 5,000 new HIV infections occurring each day. Of note, although the prevalence of the virus in Europe is lower than in sub-Saharan Africa, in the Basque Country the number of new HIV infections each year has not declined considerably in the past 20 years according to the Basque Health Agency (Osakidetza), which indicates that even in regions where antiretroviral therapy is available control of new infections can be complicated. Thus, generating new knowledge that helps understand the molecular mechanisms that govern HIV-1 infection to help develop new antiretroviral therapies is of utmost importance for the complete eradication of the pandemic.

1.1.1. HIV-1

HIV-1 is part of the *Retroviridae* family, and *Lentivirus* genera, a category that encompasses non oncogenic exogenous enveloped retroviruses. They generally are the causative agents of chronic infections of the immune and central nervous system, characterized by long incubation periods.

The HIV-1 genome contains three main genes: i) *pol*, which codifies for viral enzymes protease (PR), reverse transcriptase (RT), and integrase (IN); ii) *gag*, codifying for the Gag precursor polyprotein, which will generate matrix (MA), capsid (CA), nucleocapsid (NC), and p6, and is responsible for virus morphogenesis and budding; and iii) *env*, which codifies for the envelope protein precursor or gp160, which upon cleavage by cellular furins generates two subunits: gp120 and gp41, proteins responsible for cellular receptor recognition and posterior viral entry. A number of accessory genes also exist that codify for the rest of the viral proteins: *vif*, *vpr*, *vpu*, *tat*, *rev*, and *nef*. Although the *gag* gene can be expressed by itself to generate the Gag polyprotein, *pol* is always expressed in tandem with *gag*, generating the GagPol polyprotein.

HIV-1 is delimited by a lipid membrane envelope with a size of around 120 nm in diameter. Inside the lipid envelope, a cone shaped viral capsid surrounds two copies of positive-sense RNA, packaged as viral genetic material, together with enzymes necessary for the viral replication cycle: PR, RT, and IN. Associated to the viral lipid envelope two main proteins can be found: underneath the viral membrane the MA protein; and embedded in the membrane and protruding to the outside, the envelope protein (Env) (Figure 1.2).

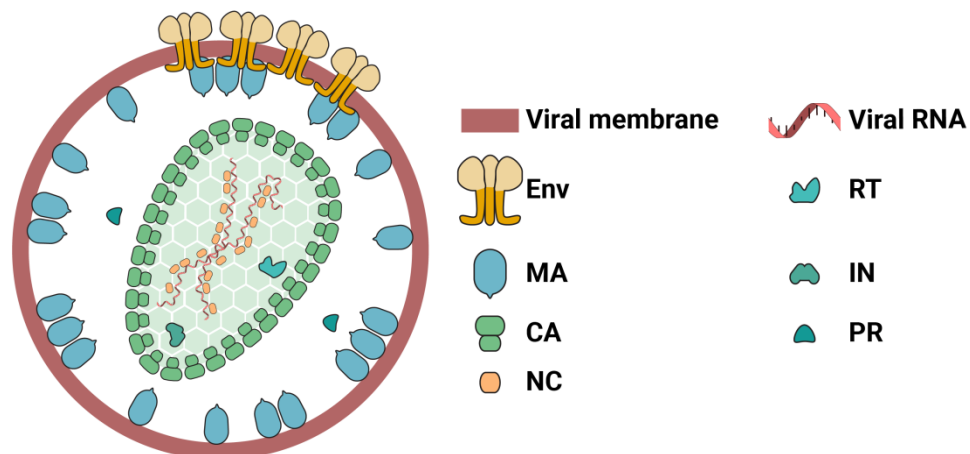


Figure 1.2 – Schematic structure of a mature HIV-1 viral particle. HIV-1 is delimited by a lipid membrane, in which the Env proteins are embedded and protrude to the outside. Underneath the viral membrane MA remains associated with it, and CA generates a cone shaped capsid that surrounds the viral RNA, which is packed thanks to NC. The viral enzymes RT, IN and PR are also packed inside the virus.

CHAPTER 1

Based on calculations on HIV-1 particle content from different groups, and adjustments later made by (Carlson et al., 2008), a HIV-1 particle of 120 nm in diameter has been described to contain ~160,000 molecules of lipids (Brugger et al., 2006); ~2500 molecules of Gag (or, after maturation, ~2500 of each of its constituents, MA, CA, NC and p6) (Briggs et al., 2004); ~550 molecules of Vpr (Muller et al., 2000); ~120 molecules each of PR, RT, and IN (Welker et al., 1996); ~20-45 molecules (~7-15 trimers) of Env (Chertova et al., 2002); and 2 molecules of viral RNA.

1.1.1.1. HIV-1 replication cycle

During the canonical HIV-1 replication cycle (Figure 1.3), a free HIV-1 mature particle initiates entry to its main host cell, a CD4+ T cell, by recognition of the cellular CD4 receptor and CXCR4 or CCR5 co-receptors by the gp120 subunit of Env. After receptor and co-receptor recognition, gp41 induces the fusion between the viral and cellular membrane, and the viral capsid enters the cell. While the viral capsid is slowly uncoated and is transported towards the cell nucleus by what evidence suggests is the microtubule network (Malikov et al., 2015), double stranded DNA copies of the viral RNA are created by the RT. This enzyme lacks proofreading activity and is responsible for the high mutation rate of HIV-1 (Roberts et al., 1988). After introduction of the viral DNA to the nucleus, the viral IN enzyme integrates the HIV-1 genetic material into the cellular genome.

The integrated viral genetic material may lay dormant for a variable period of time. This is probably one of the main problems in current antiretroviral therapy, which in most cases can effectively hamper spread of the virus and reduce viral load in the blood (viremia) of HIV-1 infected patients to undetectable levels, but is not capable of purging the dormant HIV-1 which latently infects cells (Siliciano et al., 2003). The factors that regulate HIV-1 latency and later expression are not completely understood, and constitute one of the most important milestones for HIV-1 cure nowadays.

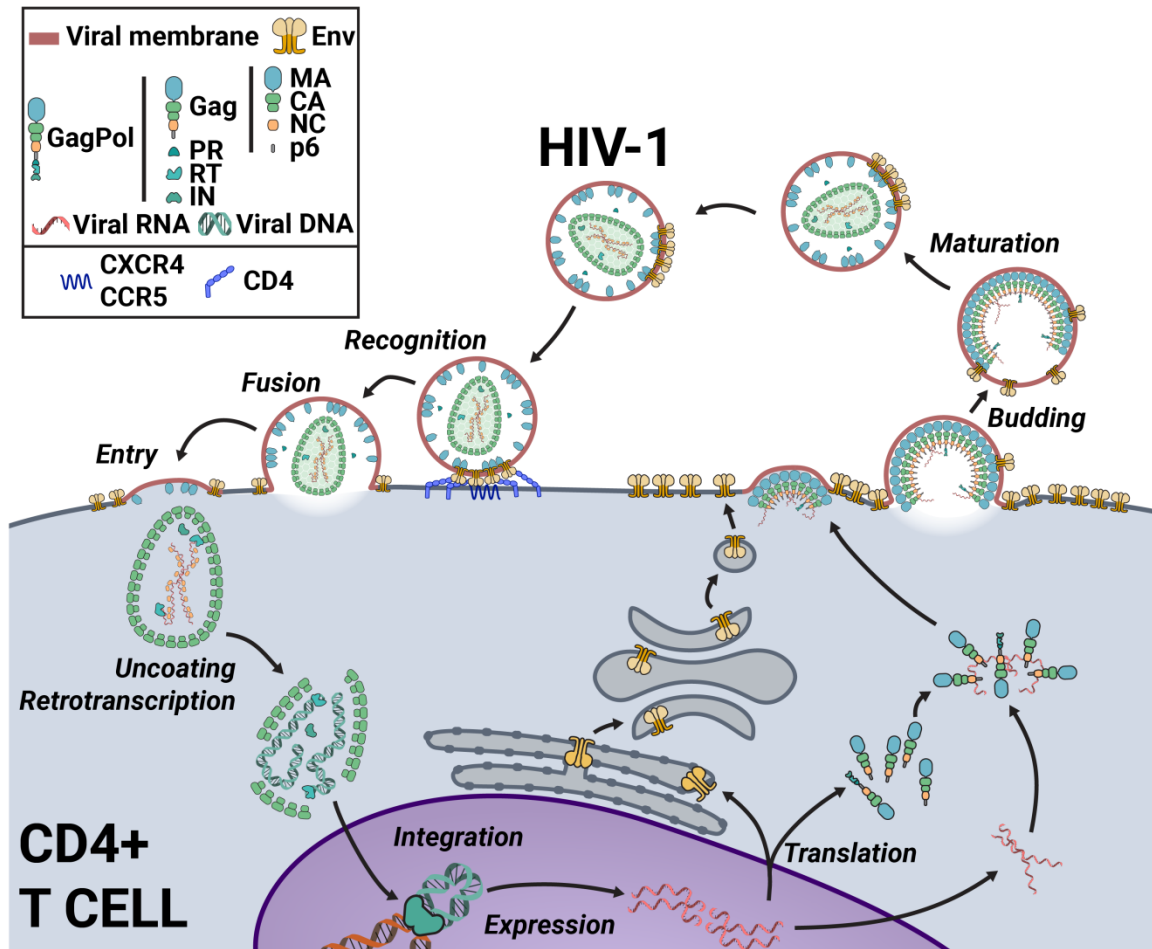


Figure 1.3 – Schematic representation of the HIV-1 replication cycle. After Env mediated cell receptor and co-receptor recognition and viral and cellular membrane fusion, the HIV-1 capsid enters the host cell. The viral capsid uncoats while it is transported towards the nucleus, concomitant with the retrotranscription of the HIV-1 RNA to DNA. Viral DNA enters the nucleus and is integrated in the cellular chromosomes until its transcription to new RNA molecules. The RNA molecules are in part translated into viral proteins. Gag and GagPol are synthesized in the cytosol, while Env is produced in the rough endoplasmic reticulum and finally targeted to the plasma membrane. Two RNA molecules per virus dimerize and associate with the recently synthesized Gag and GagPol proteins, and also associate to the plasma membrane, initiating the budding of a new viral particle. The viral particle is released and, concomitantly or shortly after, the PR in GagPol separates the constituents of the polyprotein in a process known as maturation.

When the integrated HIV-1 genetic material is expressed, transcribed viral RNA copies are created, most of which are translated into the viral proteins. The MA, CA, NC and p6 components of HIV-1 are produced as a 55 kDa Gag polyprotein, which is involved in the assembly and morphogenesis of the virus. In parallel and at 5% the level of the *gag*, the *gag* and *pol* genes are expressed in tandem to generate the GagPol polyprotein precursor. GagPol contains the constituents of Gag (MA, CA, NC and p6) and the constituents of Pol, namely PR, RT, and IN.

For each viral particle, two copies of non-translated positive-sense viral RNA dimerize and bind to several Gag precursor proteins (Moore and Hu, 2011), and the Gag-RNA complex is targeted to the plasma membrane and accumulates in Gag assembly sites.

CHAPTER 1

Three main mechanisms are involved in the targeting of Gag to the plasma membrane: a highly basic region in MA; a myristoyl anchor; and specific interactions with plasma membrane phosphatidylinositol (4,5) biphosphate (PI(4,5)P₂). During synthesis of the Gag polyprotein, the N-terminal domain of the MA protein is modified by the attachment of a myristic acid, a 14-carbon fatty acid that can switch between being sequestered in the protein or anchored in the membrane. After Gag binding to the membrane by ionic interactions of the highly basic region (HBR) of MA with negatively charged lipids in the inner leaflet of the plasma membrane, this myristoyl switch may further stabilize this association between Gag and the membrane (Freed, 2015; Lorizate and Krausslich, 2011). Interestingly, the ionic interactions and myristoyl anchor do not seem to be sufficient to completely anchor Gag lattices in the plasma membrane, and the presence of PI(4,5)P₂ has been shown to also be necessary. Recent studies have demonstrated that interaction between MA and PI(4,5)P₂ play a role beyond initial targeting of Gag to the plasma membrane, as depletion of the lipid results in complete loss of already assembled Gag lattices, indicating that Gag association with the membrane is a highly dynamic process dependent on specific protein-lipid interactions (Mücksch et al., 2017).

Independently of Gag production, the Env protein is synthesized in the rough endoplasmic reticulum as the gp160 precursor. When gp160 reaches the Golgi complex through the secretory pathway, it is proteolytically cleaved by cellular furins, to yield the gp41 and gp120 subunits which are kept non-covalently bound. When Env reaches the plasma membrane, it gets targeted by a yet unknown mechanism to Gag assembly sites, so that when the recruitment of new Gag molecules induces plasma membrane budding and new viral particle release, the envelope proteins in the plasma membrane get recruited to the nascent virion.

Release of the budding virus requires a highly energetically demanding fission between the viral and plasma membrane. Because the HIV-1 genome does not codify for fission machinery, it must recruit cellular proteins for the process. The p6 protein of the Gag polyprotein contains several highly conserved sequences, known as "late domains", which interact with the cellular ESCRT machinery and similar proteins. When ESCRT-III proteins are recruited to the budding site by their interaction with p6, they assemble into circular arrays in the thin connection between the viral and plasma membrane, which constricts the membrane and induces fission and liberation of the new virus (Freed, 2015).

Concomitant or shortly after budding the viral PR, still as a part of the GagPol polyprotein, dimerizes and cleaves the GagPol and Gag polyproteins to release MA, CA, NC, p6, RT, IN and the PR itself in a process known as maturation. MA remains attached to the viral membrane, while CA coalesces to form the viral capsid surrounding the RNA molecules, packed thanks to NC (Freed, 2015). During this maturation process, Env trimers redistribute in the membrane and usually form a single Env cluster (Chojnacki et al., 2012). This mature free viral particle can infect new cells and initiate another round of replication.

1.1.1.2. Viral membrane

HIV-1 obtains its lipid envelope from the infected cellular plasma membrane through the budding process. In this process, the virus acquires plasma membrane embedded Env protein, together with a number of cellular host proteins present in the same lipid bilayer (Burnie and Guzzo, 2019). HIV-1, like all retroviruses, does not encode for lipid-synthesizing or metabolizing enzymes so the lipid composition of the viral membrane depends on the host cellular membrane from which they bud. For the HIV-1, it could then be expected for the viral lipid composition to be the same as the cellular plasma membrane but, on the contrary, the composition of the HIV-1 lipid membrane shows significant differences compared to the host cell membranes (Aloia et al., 1988, 1993; Brugger et al., 2006), including the plasma membrane (Chan et al., 2008; Lorizate et al., 2013).

The HIV-1 lipidome has been a subject of several studies, and it has been found to be enriched in phosphatidylserine (PS), sphingomyelin, hexosylceramide, saturated species of phosphatidylcholine (PC) (Brugger et al., 2006; Lorizate et al., 2013), and phosphatidylinositol (4,5) biphosphate (PI(4,5)P₂) (Chan et al., 2008) when compared to the host cell plasma membrane. Additionally, although not necessarily enriched, cholesterol (Chol) constitutes up to 50 % of the total lipid molecules in the viral membrane (Brugger et al., 2006; Lorizate et al., 2009). The high amount of saturated phosphoglycerolipids, sphingomyelin and cholesterol in the HIV-1 lipid envelope has led to its comparison to raft-like nanodomains (Brugger et al., 2006). Moreover, the similarities between the viral membrane and raft domains also extend to its structure, and studies using the phase-sensitive stain Laurdan found that the HIV-1 lipid envelope displays an ordered lateral membrane structure (*L_o* phase), similar to what is presumed for raft-like nanodomains (Lorizate et al., 2009).

The differences between the viral and cellular membranes and the enrichment of certain lipids imply that in the budding of new viral particles a selection of a specific lipid domain or an active enrichment of certain lipids occurs. Virus morphogenesis starts with the targeting of Gag to the plasma membrane and its coalescence in viral assembly sites, and recent studies have demonstrated that PI(4,5)P₂ is highly involved in this process. The lipid is necessary not only for the initial anchoring of Gag to the plasma membrane, but also for the maintenance of stable Gag assemblies, suggesting a dynamic equilibrium highly dependent on Gag-lipid interactions (Mücksch et al., 2017). This dependence in PI(4,5)P₂ for Gag assembly helps to explain its enrichment in the virus, and although no clear mechanism has been demonstrated for the selection of other lipids, they have been described to play several roles in the HIV-1 replication cycle (Lorizate and Krausslich, 2011).

Cholesterol, specifically, has been shown to be of key importance in HIV-1. Cholesterol constitutes almost half of the total lipid molecules in the HIV-1, and the two viral proteins associated with the viral membrane, MA and Env, have been postulated to be associated with this lipid. Studies have described interactions of MA and Env with detergent resistant membranes (DRM) (Bhattacharya et al., 2006; Ono and Freed, 2001;

Yang et al., 2010), and although these studies do not constitute absolute proof of an interaction of a protein with cholesterol (Thiele et al., 2000), these membrane structures are commonly associated with the lipid.

Additionally, cholesterol has been found to be necessary for several steps of the viral replication cycle. Cholesterol-depleting agents such as β -cyclodextrin and statins strongly reduce HIV-1 infectivity at entry level (Campbell et al., 2002; Liao et al., 2001, 2003; Mañes et al., 2000), an effect that has also been observed for cholesterol binding compounds like amphotericin B methyl ester (Waheed et al., 2006). Being Env the protein responsible for the initiation of the viral replication cycle by inducing the fusion between the viral and cellular membrane, the cholesterol-dependent infectivity of the HIV-1 could point towards a relationship between the lipid and the Env protein. Indeed, the lipid environment of certain proteins has long been known to regulate their function, both in a direct and indirect way. Several cellular receptors, for example, have been described to generate or coalesce lipid nanodomains, or lipid rafts, after ligand binding, indicative of a link between lipid nanodomains and the active form of the protein (Gahbauer and Böckmann, 2016; Smart et al., 1999). Similarly, due to the physicochemical properties of a protein this can be excluded or included in certain regions of the membrane (Simons and Toomre, 2000), and taking into account that Env clustering and mobility are necessary for effective fusion activity (Chojnacki et al., 2012, 2017), the inclusion or exclusion of the protein from a specific lipid domain may play a key role in its function.

1.1.1.3. Envelope protein

The Env protein of HIV-1 is composed of two subunits: gp120 or surface glycoprotein, and gp41 or transmembrane glycoprotein. In the HIV-1 viral particle these two subunits remain non-covalently bound as a heterodimer (Figure 1.4A), three of which oligomerize to generate a homotrimer of gp120-gp41 heterodimers, or Env (Figure 1.4B).

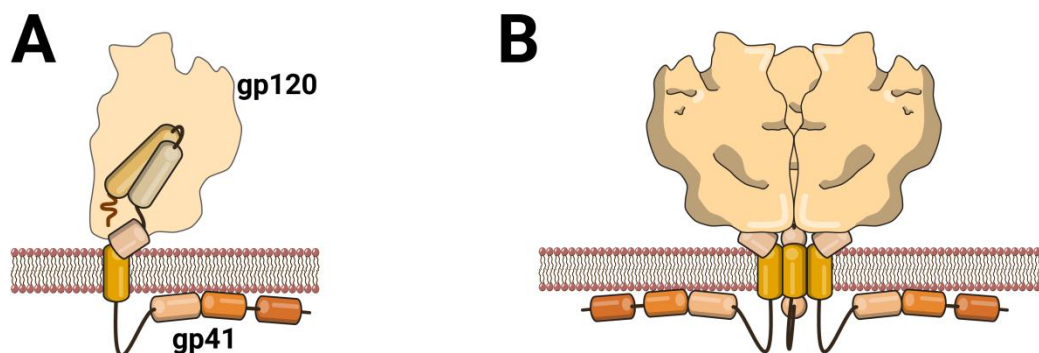


Figure 1.4 – Env structure. **A|** Env heterodimer composed of the gp41 and gp120 subunits. Area occupied by gp120 is shown shaded to reveal the gp41 subunit underneath. gp120 is oriented towards the surface of the virion, and recognizes the cellular CD4 and CXCR4 or CCR5 co-receptors. Gp41 anchors Env to the lipid envelope, and induces the fusion between membranes. **B|** Three gp41-gp120 heterodimers oligomerize to generate a homotrimer of heterodimers.

Recognition of the cellular receptor CD4 and co-receptors CXCR4 or CCR5 is carried out by gp120, a heavily glycosylated protein. Exposed in the outside of the viral particle, it is non-covalently bound to gp41 and covers it. Upon receptor and co-receptor recognition, gp120 changes its conformation, permitting gp41 to interact with the cellular membrane and induce virus and cell fusion. In the case of cell-to-cell infection, the gp120 subunit of Env expressed in infected cells recognizes receptors and co-receptors of adjacent cells, and starts the fusion process in a similar manner (Durham and Chen, 2015).

1.1.1.3.1. Gp41 subunit

Gp41 anchors Env to the viral membrane, but is also responsible for the fusion activity of the protein. It can be divided in three main topological domains: ectodomain, transmembrane domain (TMD), and cytoplasmic domain, and at least nine structural regions (Figure 1.5). The most N-terminal sequence of the ectodomain of gp41 is the fusion peptide (FP). Next, the N-terminal and C-terminal heptad repeat (NHR and CHR, respectively) sequences are connected by a flexible loop, and involved in the conformational changes necessary for fusion. The most C-terminal region of the ectodomain is the Membrane Proximal External Region, or MPER, which harbours epitopes for some broadly neutralizing antibodies (Huang et al., 2012; Stiegler et al., 2001), and has been described to be able to associate with membranes, possibly playing a role in the fusion process (Lorizate et al., 2008; Molinos-Albert et al., 2017; Saez-Cirion et al., 2002a). Indeed, MPER contains a highly conserved sequence named Cholesterol Recognition Aminoacid Consensus (CRAC), which have been shown to interact with cholesterol and cholesterol derivatives *in vitro* (Chen et al., 2009; Vincent et al., 2002; Vishwanathan et al., 2008).

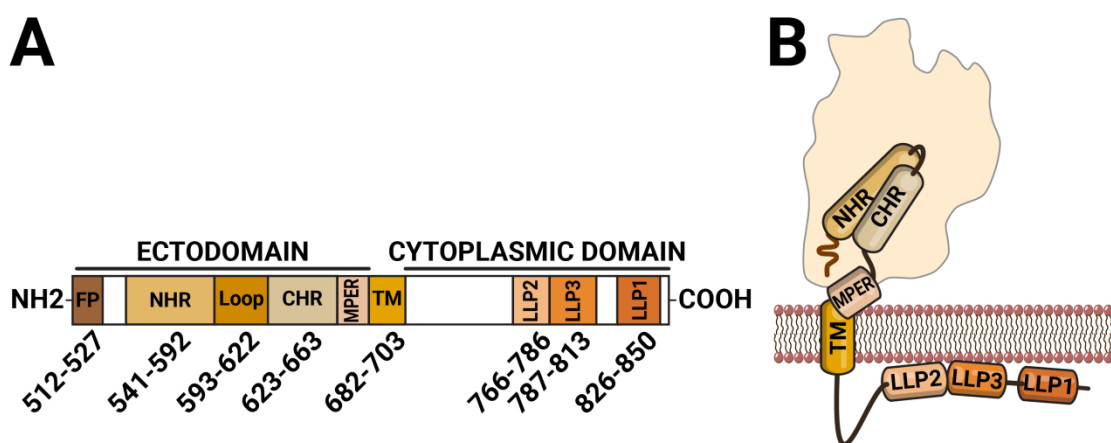


Figure 1.5 – gp41 structure. **A** | gp41 can be divided in three main topological domains (ectodomain, transmembrane domain (TM), and cytoplasmic domain) and at least nine distinct structural regions. Numbers represent the aminoacid residues spanning each region, using the residue numbering of the gp160 precursor of the HIV-1 NL4-3 strain. **B** | Proposed approximate disposition of the regions of gp41. The approximate space occupied by gp120 is shaded in yellow. Fusion peptide (FP); N-terminal Heptad Repeat (NHR); C-terminal Heptad Repeat (CHR); Membrane Proximal External Region (MPER); Transmembrane Domain (TM); Lentiviral Lytic Peptide (LLP).

The TMD spans the viral membrane and anchors the protein to it, also having been described to be involved in the trimerization of Env (Baker, 2014) and intracellular sorting of the protein. Interestingly, it contains a highly conserved charged arginine residue and, although this arginine residue would be expected to induce localization of the protein in the endoplasmic reticulum during synthesis (Perrin et al., 2018), it has been shown to be important for Env localization to the plasma membrane and incorporation (Yue et al., 2009), and cholesterol has been described to be necessary for its salvation (Baker, 2014; Baker et al., 2014).

Finally, the unusually long cytoplasmic domain of gp41 of HIV-1 accounts for more than a third of the total length of the protein. Although its structure has not been completely solved, it contains three α -helices known as Lentiviral Lytic Peptides (LLP) 1, 2 and 3. These LLP domains have been described to be amphipathic (Abad et al., 2009), and play a key role in protein expression (Bultmann et al., 2001), incorporation into the virion (Murakami and Freed, 2000; Piller et al., 2000), and function (Durham and Chen, 2015; Kalia et al., 2003). Interestingly, they have been described to be partially embedded in the membrane and perturb its structure in studies carried out with peptides (Kliger and Shai, 1997; Srinivas et al., 1992), a fact that gave rise to their name.

The gp41 protein is responsible for the fusion between membranes. In the most accepted fusion model, in its native state the FP is oriented towards the viral membrane and center of the trimer, since the N-terminal and C-terminal heptad repeat (NHR and CHR, respectively) sequences are oriented antiparallel to each other thanks to the flexible loop that connects them (Lee et al., 2016; Ozorowski et al., 2017) (Figure 1.6A). Upon cellular receptor and co-receptor recognition and engagement by gp120, NHR and CHR sequences unfold and extend, pointing the FP towards the cellular membrane and inducing its insertion (Figure 1.6B). Once the FP has inserted into the cellular plasma membrane, the NHR and CHR fold among each other, bringing the membranes closer together inducing hemifusion (Figure 1.6C). The NHR and CHR sequences of the three heterodimers interact and form a structure known as 6-helix bundle (6-HB), the only solved crystal structure related to post fusion events. This generates complete fusion between viral and cellular membranes and allows entry of the viral capsid to the cell (Figure 1.6D).

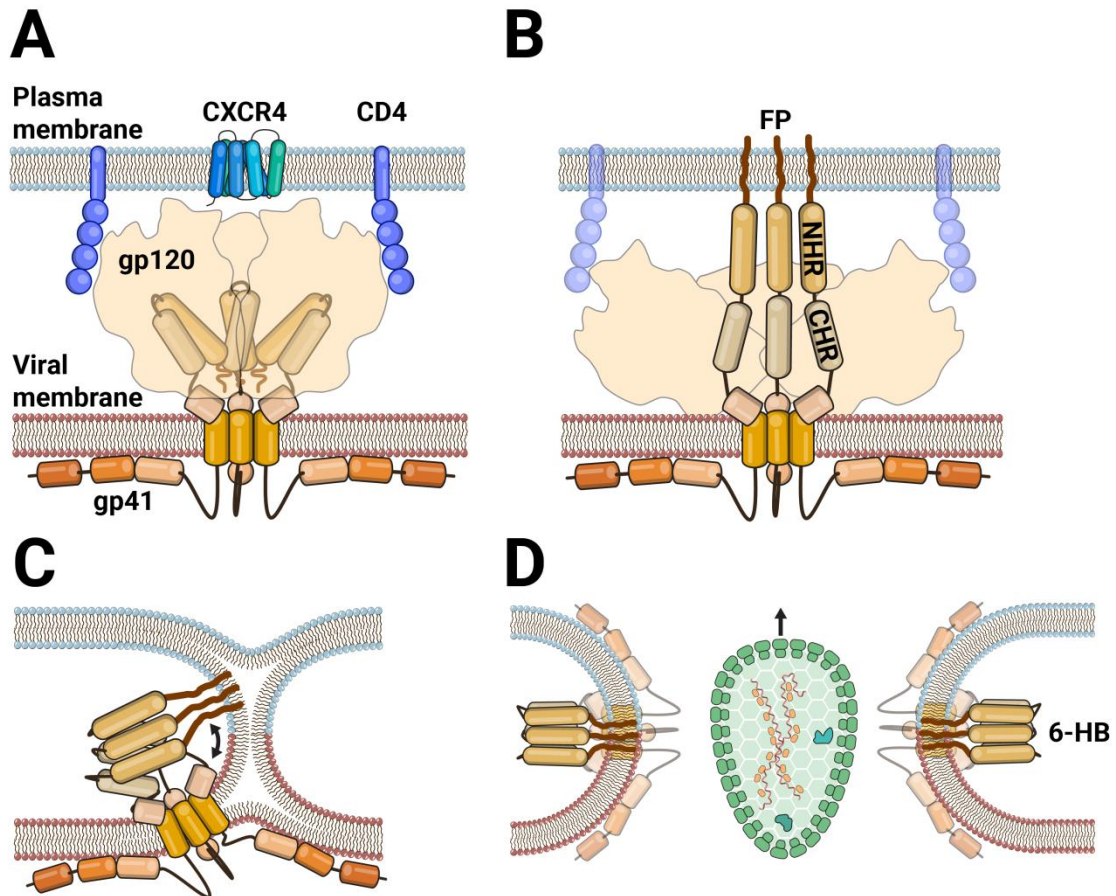


Figure 1.6 – Sequential steps of Env mediated viral and cellular membrane fusion. A| gp120 recognizes and binds to cellular CD4 receptor and CXCR4 (or CCR5) co-receptors. **B|** Conformational changes in gp120 after receptor recognition translate to unfolding of NHR and CHR sequences of gp41 into the “pre-hairpin conformation” and insertion of the FP into the cellular plasma membrane. **C|** NHR and CHR sequences of gp41 fold, bringing the two membranes closer and inducing hemifusion state. **D|** The NHR and CHR sequences associate between trimers to generate a 6-helix bundle (6-HB), which generates fusion between viral and cellular membranes and allows entry of the viral capsid (not drawn to scale).

1.1.1.3.2. Env incorporation and clustering

Upon virus maturation, most of the trimers rearrange in a single focus, or cluster (Figure 1.7). Although individual Env trimers can recognize and interact with the cellular receptor and co-receptor, clustering of Env is necessary for the efficient fusion between the viral and cellular membrane (Chojnacki et al., 2012), suggesting that one trimer is not enough to overcome the energetic barrier of membrane fusion. Indeed, although the exact number of Env trimers necessary for entry, or stoichiometry of entry, differs between viral strains, for the majority of them the coordinated action of 2 to 7 Env trimers seem to be necessary for fusion (Brandenberg et al., 2015). Interestingly, even considering this dependence in several Env trimers for fusion, only in the order of 7-15 of them are present in the viral particles, significantly less than in the related SIV which contains 75 to 150 trimers (Chertova et al., 2002) (Figure 1.7). The low number of Env trimers in the HIV-1 is suggested to be an evolutionary response from the virus to avoid

detection by the immune system. The incorporation of Env into the virion is thus a key factor in HIV-1 infectivity: a minimum amount of Env trimers have to be incorporated so their coordinated action can induce viral and cellular membrane fusion, but their number must stay relatively low to presumably avoid the immune system.

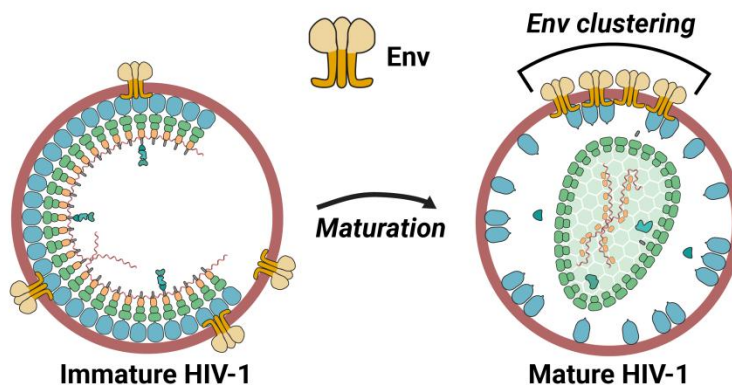


Figure 1.7 – Env redistribution to a single cluster upon maturation. Note the low number of Env trimers in the viral particle (7-15 for most strains), and their distribution into a single cluster upon maturation.

The targeting of Env to Gag assembly sites and posterior incorporation into the virion is a complex mechanism yet to be elucidated. Interestingly, in cells expressing viral proteins, Env has been shown to accumulate surrounding Gag assembly sites, but seems to be partially excluded from the actual budding site, since only a low number of trimers co-localize with the center of the Gag assembly (Buttler et al., 2018; Muranyi et al., 2013), which comes in agreement with the low number of trimers observed in the released viral particle. The exact mechanism that regulates this process has not yet been elucidated, but these findings suggest that Env recruitment is regulated by a combination of selection and exclusion processes: Env is selectively localized around Gag assembly sites, but partially excluded from the center of the budding region. Nowadays, several Env incorporation models exist, which are based either in direct Gag-Env interactions; in co-targeting of Gag and Env to a specific lipid nanodomain; or in indirect Gag-Env interactions mediated by accessory cellular proteins or specific lipids (Checkley et al., 2011).

While the exact molecular mechanism for Env incorporation is yet to be described, the cytoplasmic domain of gp41 have been demonstrated to be heavily involved in the process. Truncation of gp41 CT results in Env randomly distributing in the plasma membrane and not accumulating around Gag assemblies (Muranyi et al., 2013). Interestingly, exclusion of Env from the center of budding sites also seems to be regulated by the gp41 long cytoplasmic tail, since deletion of CT results in a loss of incorporation regulation. In the wild-type protein, Env incorporation into the virion reaches a plateau independently of the number of Env expressed in the plasma membrane, but when the gp41 CT is truncated, higher protein expression leads to a linear increase in Env incorporation (Qi et al., 2013). The cytoplasmic tail of gp41 is then

involved in both the recruitment of Env to the Gag assembly sites, and in the regulation of its incorporation into the virion. In the viral particle the gp41 CT has also been shown to be necessary for the clustering of Env trimers, and its deletion leads to a random distribution of Env even after particle maturation, which results in a loss of infective capacity of the virus (Chojnacki et al., 2012).

The gp41 long cytoplasmic domains is thus a very important region that regulates not only targeting of Env to Gag assembly sites and its posterior incorporation into the virion, but also clustering of Env and, consequently, the fusion capacity of the virus.

1.1.1.3.3. Interaction of gp41 with cholesterol

The interaction of Env with lipid nanodomains or lipids commonly related with them has long been postulated. As explained above, cholesterol has been shown to be a crucial component of HIV-1 infectivity (Campbell et al., 2002; Liao et al., 2001, 2003; Mañes et al., 2000; Waheed et al., 2006), and several studies have demonstrated that Env interacts with lipid rafts and DRMs in cells (Bhattacharya et al., 2006; Rousso et al., 2000; Yang et al., 1995) even in the absence of other viral proteins, suggesting that Env itself contains the properties necessary for interaction with lipid nanodomains. Interestingly, this association of Env with raft nanodomains or DRMs seems to be dependent on the presence of cholesterol in the membrane, since treatment with cholesterol depleting agents induces a decrease in Env localization in DRMs in a dose-dependent manner (Yang et al., 2010). Consequently, being Env the protein responsible for viral and cellular membrane fusion, an interaction between gp41 and cholesterol could constitute the mechanism by which HIV-1 infectivity depends on the presence of the lipid in the viral membrane. Removal of cholesterol from the virus could alter the function of the envelope protein, hampering viral and cellular membrane fusion and posterior entry and infectivity.

All of the three main topological domains of gp41 have been described to interact with lipid bilayers, a fact that was recently reviewed in a publication by Klug *et al.* (Klug et al., 2017). Starting with the N-terminal ectodomain, the FP is believed to be the sequence by which gp41 anchors to the host cell plasma membrane, starting the fusion process (Figure 1.8, brown). Therefore, it is not considered to be responsible for the anchoring of gp41 in the viral lipid bilayer and consequently it is not expected to be related with envelope trimerization, mobility in the membrane, or clustering. Thus, although specific interactions of FP with lipids may be important for fusion, they do not help explain the dependence in cholesterol of HIV-1 infectivity. Next, the NHR and CHR sequences (Figure 1.8, blue and grey, respectively) have been described to show membrane interacting properties in their 6-HB conformation, which, although not being the primary force behind viral and cellular membrane fusion, could provide additional destabilization and assist on it, although this results are based in studies carried out with liposomes and peptides derived from the 6-HB bundle, and not *in vivo* studies (Lev et al., 2009).

CHAPTER 1

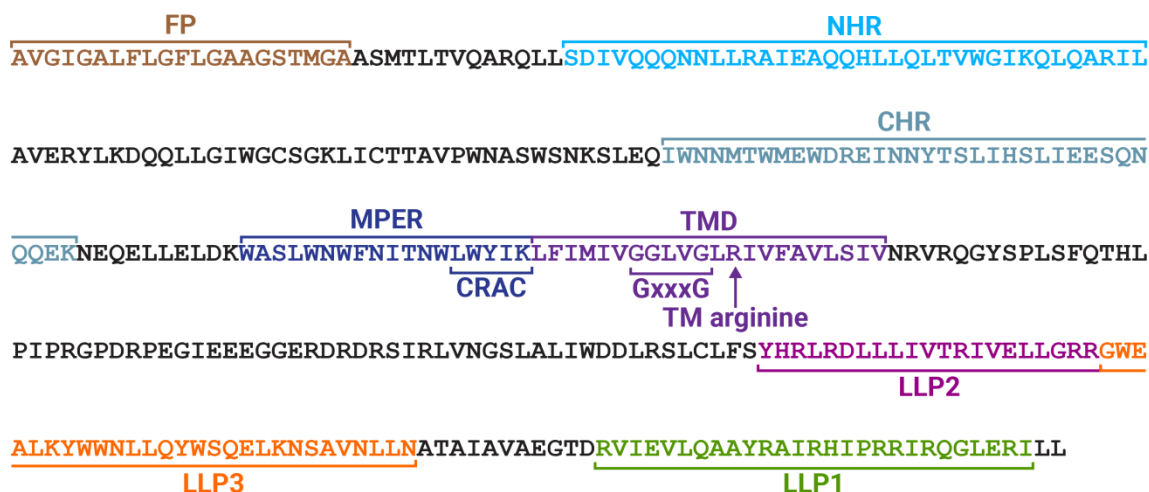


Figure 1.8 – gp41 aminoacid sequence with lipid-interacting domains.

The most C-terminal region of the ectodomain is composed by the highly conserved Membrane Proximal External Region (MPER) sequence (Figure 1.8, dark blue). MPER has been shown time and again to strongly interact with lipid bilayers in *in vitro* experiments and has been found to destabilize membranes (Lorzate et al., 2008; Saez-Cirion et al., 2002b; Suarez et al., 2000b, 2000a). Accordingly, MPER seems to acquire an α -helix conformation and partially embed in the viral membrane, burying its aromatic residues in the lipid bilayer interface (Schibli et al., 2001). Interestingly, the last 5 aminoacid residues of MPER (₆₇₇LWYIK₆₈₁) constitute a highly conserved sequence known as Cholesterol Recognition Aminoacid Consensus (CRAC). This CRAC has been described to interact with cholesterol or cholesterol derivatives (Vincent et al., 2002) or target the gp41 protein to DRMs (Chen et al., 2009) which, although these results were obtained using *in vitro* or predictive studies, defines this sequence as a great candidate for the interaction of Env with lipid nanodomains associated with cholesterol.

The transmembrane domain of the protein is composed of 22 aminoacid residues believed to be structured as an α -helix (Figure 1.8, purple). It anchors the gp41 subunit in the viral membrane, and is responsible for the trimerization of Env. It contains, among others, two regions of special interest: a positively charged arginine residue in the middle of the sequence; and a GxxxG sequence apparently involved in the trimerization of the protein. On the one hand, the presence of the arginine residue in the transmembrane domain has long tried to be explained, and although several models exist that suggest that the residue snorkels towards the more hydrophilic lipid bilayer interface (Baker et al., 2014; Gangupomu and Abrams, 2010), no definitive mechanism has been found yet. Additionally, molecular dynamic simulations have suggested that this arginine might be involved in the interaction of gp41 with cholesterol (Baker, 2014). On the other hand, the GxxxG sequence in the gp41 TMD has been described to be involved in the trimerization of the protein, and has been described to be important for the infectivity of HIV-1 (Abad et al., 2009). Interestingly, the GxxxG sequence is common to several transmembrane proteins, and it was suggested to be responsible for the binding of cholesterol in the

amyloid precursor protein (Barrett et al., 2012). This cholesterol-binding property of GxxxG could also exist in the gp41 subunit, and thus be related with the selection of the lipid environment of the protein.

Lastly, the unusually long cytoplasmic domain of gp41 is also involved in the interaction of the protein with lipid membranes. The cytoplasmic domain contains three sequences of special interest in this regard: the so-called Lentiviral Lytic Peptides. LLP1 was first described in 1991, and was found to consist of a toxic strongly amphipathic α -helix (Miller et al., 1991), and was later confirmed to alter membrane permeability by total or partial insertion into the lipid bilayer (Miller et al., 1993) (Figure 1.8, green). In parallel, a second LLP domain, LLP2, was also discovered and found to be helicoidal in structure and to contain membrane-perturbing characteristics, and its conservation suggested that a strong selective pressure exists to conserve the amphipathic helicoidality of the sequence (Srinivas et al., 1992) (Figure 1.8, pink). Later, a third domain with the same properties as the other two was found and dubbed LLP3 (Kliger and Shai, 1997) (Figure 1.8, orange). The LLP domains have been described to be involved in several processes regarding Env, from expression of the protein to the cell surface and incorporation into the virion, to protein stability, multimerization and HIV-1 infectivity. Perhaps more interestingly, all of the LLP domains have been described to partially embed in the membrane (Moreno et al., 2008) and a peptide consisting of the last two-thirds of the cytoplasmic domain, which contains the three LLP sequences, was found to strongly interact with DRMs (Yang et al., 2010). Taking into account their amphipathic nature, partial insertion in the membrane, and their partitioning to lipid nanodomains, the LLP domains are strong candidates for interaction of gp41 with these membrane structures or lipids commonly associated with them.

1.2. Study of protein-lipid interactions

The study of the lipid environment of Env may then be of key importance to help understand the factors that govern the function of the protein. Up until now, one of the most widely used approaches to fulfill this goal relies in the use of DRMs. DRMs are obtained from cellular or other membranes after treatment with non-ionic detergents at low temperatures (around 4°C). DRMs are composed of specific lipids and proteins that presumably resemble raft-like nanodomains (Brown and Rose, 1992). The presence of a protein in DRMs thus may point towards its interaction with lipid nanodomains and lipid species commonly associated with them, such as sphingomyelin and cholesterol (Simons and Ikonen, 1997). Using this approach, several authors have described an association of HIV-1 Env with DRMs and, consequently, lipid rafts. Bhattacharya *et al.* described that the viral polyprotein Gag associates with DRMs in the plasma membrane, and Env is then recruited to these membrane structures, proposing thus an Env incorporation mechanism based on targeting of the protein to specific regions of the membrane. These studies are based in the treatment with detergents of cells expressing only Env or all the viral proteins, and posterior analysis of the presence of the protein in

CHAPTER 1

DRMs by flotation analysis, which found that when Gag was present Env localized in DRMs, while Env expressed alone was not (Bhattacharya et al., 2006). Following a similar strategy, Yang *et al.* studied the association with DRMs of Env expressed in the plasma membrane, and found that the cytoplasmic tail, and specifically the LLP sequences, were involved in this association (Yang et al., 2010).

Nonetheless, these works studied the association of the protein with lipid nanodomains only in the cellular plasma membrane, and not in the virus, and no direct interaction of the protein with cholesterol or other specific lipids was studied. An additional consideration is the fact that the study of protein-lipid interactions by DRMs relies on the use of low temperatures and detergents, which could potentially alter the natural structure of membranes. Indeed, DRMs have been suggested to be generated after detergent-induced bilayer partial solubilization and reassembly, thus not necessarily corresponding with structures existing in the membrane (Sot et al., 2002). As a result, the detection of a certain protein in a DRM does not constitute absolute prove of its association with raft or raft-like nanodomains *in vivo*, nor its interaction with lipids such as cholesterol or sphingomyelin. Similarly, the absence of a protein in a DRM does not necessarily correlate with its exclusion from lipid nanodomains, since the detergents used for DRMs studies, although weak, can disrupt hydrophobic protein-lipid interactions (Thiele et al., 2000).

In the last decade a new approach for directly studying the interaction *in vivo* between a protein and certain lipids has been developed, which is based in the use of photoactivatable lipids. Photoactivatable lipids are a set of molecules with the same properties as their natural counterparts, but containing a photoactivatable diazirine ring. When irradiated with ultraviolet (UV) light at 360 nm, the diazirine ring generates a highly reactive carbene group, which covalently binds to any molecule closer than 3 Å (Thiele et al., 2000). The use of this tool have permitted to identify sphingomyelin binding domains in several proteins through a specific detection of *in vivo* interactions between proteins and single lipid species in cells (Contreras et al., 2012), validating them as a great tool for the direct study of specific protein-lipid interactions.

Taking into account the role that cholesterol plays in the HIV-1 replication cycle, the interaction between Env and cholesterol will be studied in this work using the photoactivatable cholesterol analogue [³H]photocholesterol. This lipid contains a diazirine group in the B ring, attached to the sixth carbon, which is generally buried in the hydrophobic region of the lipid bilayer, thus avoiding nonspecific cross-linking with superficial solvent molecules (Thiele et al., 2000). Additionally, this photoactivatable lipid can be radioactively labeled with tritium in the A ring, permitting easy detection and quantification of the [³H]photocholesterol (Figure 1.9).

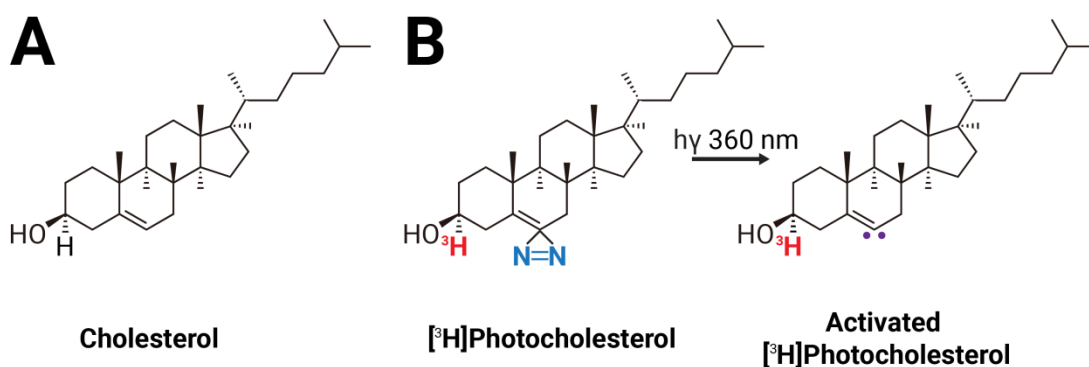


Figure 1.9 – Photoactivatable cholesterol. A| Structure of natural cholesterol. B| Structure of tritium-labeled photoactivatable cholesterol analogue [³H]photocholesterol. After irradiation with ultraviolet light (360 nm) the diazirine group (blue) of [³H]photocholesterol generates a highly reactive carbene group (purple) in the activated [³H]photocholesterol molecule, which covalently binds to any molecule closer than 3 Å. The tritium labeling (red) permits detection and quantification of the lipid.

1.3. Therapeutic approaches

Since the start of the pandemic almost 30 years ago, a global effort has been put forward to eradicate HIV-1 and cure the related AIDS. Unfortunately, no prophylactic vaccine exists yet, and the antiretroviral drugs available nowadays are not capable of completely eliminating HIV-1 from infected patients. As a matter of fact, since the discovery of the virus, a single truly confirmed case of a person being cured of HIV-1 exists, known as the Berlin Patient, and it comprises a very specific circumstance. The Berlin Patient, infected with CCR5-tropic HIV-1, was diagnosed with leukaemia. After chemotherapy treatment for his leukaemia failed, he received two haematopoietic stem-cell transplantation procedures from a donor that had a mutation in the CCR5 co-receptor that rendered target cells resistant to CCR5-tropic HIV-1, so the HIV-1 in the organism of the Berlin Patient could no longer replicate and spread (Hütter et al., 2009). Interestingly, just recently, a second similar case have been reporter, dubbed the London Patient, who also received a transplant from a donor with the same mutation. Although no virus have been detected in the organism of the London patient since interruption of antiretroviral therapy only 18 months have passed, and the authors admit that confirming this case as a complete cure is yet premature (Gupta et al., 2019). Nevertheless, these two cases are not enough to assure that this strategy would work as a global cure, and the special circumstances in which they occurred imply that it cannot be feasibly followed in a large scale. Additionally, this approach does not constitute a cure for patients infected with a CXCR4-tropic HIV-1 strain.

Thus, new therapeutic strategies keep being devised to try to overcome some of the key properties of HIV-1 that result in the persistent infection existing nowadays. Current antiretroviral strategies can be divided into two main approaches: those looking to inhibit

the HIV-1 replication cycle to avoid initial infection or spread of the virus; and those designed to purge the HIV-1 viral reservoirs that establish a latent infection.

1.3.1. Inhibition of HIV-1 replication cycle

1.3.1.1. Entry inhibition

1.3.1.1.1. Inhibition of Env recognition of cellular receptor and co-receptors

Among the therapeutic approaches looking to inhibit the HIV-1 replication cycle, targeting the recognition of the CD4 receptor and CXCR4 or CCR co-receptors by Env is probably one the most desired ones. By hampering initial binding of the virus to the host cell, and posterior viral and cellular membrane fusion and thus entry and infectivity, the initial spread of the virus and the establishment of viral reservoirs could be avoided from the start. The inhibitors of Env recognition of cellular receptor and co-receptors are composed of antibodies against Env, soluble CD4 receptors, negatively charged molecules binding gp120, and antibodies targeting the CXCR4 or CCR5 co-receptors.

In patients infected by HIV-1 several antibodies against the envelope protein can be found in their blood, as part of a natural immune response from the host to the virus. In 10-15% of the patients the combination of several of these antibodies is capable of developing a potent inhibition of HIV-1 infectivity. Interestingly, in an even smaller number of cases, inhibition of HIV-1 infectivity is obtained with a single antibody, known as broadly neutralizing antibody (bnAb). Unfortunately, although the existence of bnAbs have attracted great interest due to their infectivity-hampering properties, they are normally not capable of completely inhibiting infection and viral spread in patients, since HIV-1 has evolved a wide variety of immune evasion mechanisms that overcome the neutralizing capacity of this antibodies. Because of the lack of proof-reading ability of the HIV-1 reverse transcriptase enzyme (Roberts et al., 1988), a high number of mutations occur in each viral replication, quickly giving rise to a pool of different HIV-1 clades in each patient (Gaschen, 2002). Consequently, bnAbs that recognize and block the envelope protein of a viral clade are frequently incapable of exercising their effect in newly mutated viral subtypes. This Env variability is also patent in the glycosilation pattern of the protein, which contains more than 20 possible glycosilation sites that sterically hamper accessibility of the antibody to the protein epitopes.

Several other alternative approaches have been developed to hamper Env/receptor recognition, including the use of soluble CD4 receptors to compete with Env binding; negatively charged molecules (*i.e.* dextran sulfate and heparin sulfate) that bind the positively charged V3 loop of gp120 and hamper viral entry; and antibodies and molecules targeting the CXCR4 or CCR5 co-receptors. Unfortunately, none of these approaches have been demonstrated to completely block HIV-1 binding to receptors and co-receptors (Haqqani and Tilton, 2013).

1.3.1.1.2. Inhibition of HIV-1 fusion

A complementary set of approaches are designed to inhibit the fusion between the viral and cellular membranes and posterior entry of the viral capsid and genetic material the host cell.

1.3.1.1.2.1. Targeting gp41

As explained above, after receptor and co-receptor recognition by gp120, fusion of the membranes requires gp41 FP insertion into the cellular membrane and formation of the 6-HB that puts both membranes in close proximity. This 6-HB formation involves the interaction between NHR and CHR sequences of neighboring gp41 subunits. Because the formation of the 6-HB structure is necessary for membrane fusion, several peptides have been designed to bind to the NHR or CHR sequences in their extended conformation and inhibit the formation of the 6-HB and consequent membrane fusion. A good example of promising molecules developed following this approach is T20, a 36 aminoacid peptide that potently inhibits membrane fusion by competitively binding to the NHR sequences in the extended conformation, which inhibits bundle formation and membrane fusion (Kliger and Shai, 2000) (Figure 1.10). T20 is the base of antiretroviral therapies such as enfurvirtide, but the high cost of their development and the appearance of resistant strains and clades have rendered the application of this therapy limited (Haqqani and Tilton, 2013). A new drug based on the same concept, known as sifuvirtide, was also developed and has reached phase III clinical trials, and although it showed some promise since it blocked membrane fusion in strains resistant to enfurvirtide, new HIV-1 strains have already developed resistance to it (Yu et al., 2018).

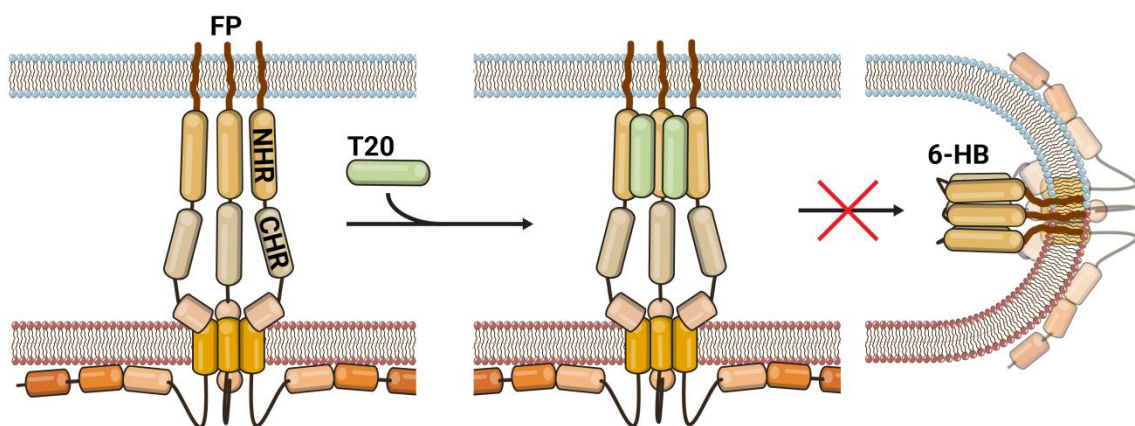


Figure 1.10 – T20 mediated inhibition of fusion of enfurvirtide. The T20 peptide binds to NHR sequences, competing with the CHR sequences and inhibit formation of the 6-helix bundle necessary for viral and cellular membrane fusion, sequestering gp41 in a pre-hairpin conformation.

1.3.1.1.2.2. Targeting the viral lipid envelope

Viral and cellular membrane fusion is also highly dependent on membrane composition and structure. The integrity of lipid nanodomains in the viral membrane is key for an effective virus entry, and dissociation of these structures by modulating cholesterol (Campbell et al., 2002; Liao et al., 2001, 2003; Mañes et al., 2000) or sphingomyelin levels (Brugger et al., 2006; Mizrachi et al., 1996; Tamma et al., 1996) greatly hamper viral infectivity. The mechanism by which depletion of these lipids inhibits viral entry is not yet completely understood, but it may be related to the interaction of Env with raft nanodomains (Bhattacharya et al., 2006; Rousso et al., 2000; Yang et al., 1995, 2010). Interestingly, an increase of ceramide levels in the viral lipid bilayer also resulted in a similar inhibitory effect (Finnegan et al., 2004), which may be explained by the fact that ceramide displaces cholesterol from ordered lipid domains composed of sphingomyelin and cholesterol (Megha and London, 2004). Indeed, Domanska et al. found that deletion of cholesterol in the influenza virus, which also contains ~50% in its lipid bilayer, also results in an inhibition of fusion. This work proposed a mechanism in which lipid domains in the viral lipid envelope regulate the distribution of the fusion-inducing hemagglutinin protein. This specific distribution of hemagglutinin was proposed to be necessary for fusion, and the significant alteration of the organization of membrane nanodomains induced by depletion of cholesterol was thought to be the cause of the inhibition of infectivity (Domanska et al., 2015). A similar effect could exist in the HIV-1, which would help explain the cholesterol-dependent Env-mediated fusion.

Targeting of cholesterol is then in principle an interesting candidate for development of antiretroviral drugs, and has already been demonstrated to reduce HIV-1 infectivity. Indeed, in addition to cholesterol extracting compounds such as β -cyclodextrin or statins (Campbell et al., 2002; Liao et al., 2001, 2003; Mañes et al., 2000), an antifungal antibiotic known to bind cholesterol, Amphotericin B and its derivative Amphotericin B methyl ester (AME), have been shown to inhibit HIV infection (Schaffner et al., 1986; Waheed et al., 2006). The antiretroviral effect of AME was found to be based in its disruption of membrane morphology (Waheed et al., 2008) and, interestingly, HIV-1 strains have been found to develop resistance to AME by developing mutations that result in truncation of the cytoplasmic domain of gp41 (Waheed et al., 2007). This suggests that a specific structure of the membrane and existence of lipid nanodomains is necessary for Env-mediated fusion and that, interestingly, targeting of Env to lipid nanodomains may be mediated by the gp41 CT.

Unfortunately, as shown above, targeting of a single lipid species is vulnerable to development of new resistance strategies by HIV-1, as well as having potential undesired cytotoxic effects. An alternative approach to targeting the viral lipid envelope is altering its structure and properties, without necessarily depleting a specific lipid species. One of such strategies is based in the use of synthetic rigid amphipathic fusion inhibitors (RAFIs), small wedge-shaped compounds that insert into the viral membrane and induce positive curvature, increasing the energy barrier necessary for membrane fusion (St. Vincent et al., 2010). The synthetic nature of these compounds presents a considerable advantage over natural lipids with the same properties, as they are not as

cytotoxic or rapidly metabolized or degraded by the organism. Additionally, a number of other compounds have also been found to exert their antiretroviral activity through modification of the viral membrane, its fluidity, or alteration of lipid nanodomains (Dumas and Haanappel, 2017). Natural compounds such as glycyrrhizin (Harada, 2005) and fattiviracin FV-8 (Harada et al., 2007), for example, have been demonstrated to lower or increase membrane fluidity, respectively, and suppress HIV-1 infectivity. Targeting the structure and properties of the viral lipid envelope is, in summary, a viable approach for the development of new antiretroviral drugs, and could potentially be applied for several retroviruses, not only HIV-1.

1.3.1.2. Inhibition of HIV-1 reverse transcription, integration, and maturation

Although development of therapeutic approaches that inhibit HIV-1 entry to the cells (via blocking of Env mediated fusion, or alteration of lipid properties) is nowadays one of the main milestones for obtention of an HIV-1 cure, until initial HIV-1 infection can be completely inhibited, a set of alternative therapies must be used to stop viral spread and its effects and reduce virus levels in the organism. This is the basis of the current clinical approach known as Highly Active Anti Retroviral Therapy (HAART). HAART is based in the use of several combined antiretroviral drugs in order to inhibit different steps of the HIV-1 replication cycle, and thus try to overcome possible resistances developed by the virus. Nowadays, recommended initial regimens are based in the combination of three antiretroviral drugs that inhibit two different steps: the reverse transcription of viral RNA, and the integration of viral DNA into the host cell. Alternatively, when recommended regimens are not available or are not an option, combination of antiretroviral drugs targeting reverse transcription and the viral protease are administered.

The initially recommended HAART regimen consist in the administration of two nucleoside reverse transcriptase inhibitors (NRTIs), combined with a single integrase strand transfer inhibitor (InSTI) (Saag et al., 2018). NRTIs are part of the first generation of antiretroviral drugs used for HIV-1, and are composed of analogs of endogenous nucleosides that compete with their corresponding endogenous nucleosides for incorporation by the HIV-1 reverse transcriptase. Once incorporated, they serve as terminators of the transcripts, inhibiting the generation of proviral DNA and thus the incorporation and expression of the viral genetic material (Cihlar and Ray, 2010). InSTI drugs are a novel class of anti-HIV agents showing high HIV-1 replication inhibition capacity by blocking the function of the integrase enzyme. Current InSTIs are active against HIV-1 strains resistant to NRTIs, so its administration in combination with the two NRTI agents normally ensures a competent inhibition of the HIV-1 replication cycle (Zolopa et al., 2010). When the regimen above is not an option because of concomitant diseases and conditions, potential for future pregnancy, or financial reasons, an alternative therapy based in protease inhibitors (PI) and NRTIs is recommended (Saag et al., 2018). Protease inhibitor drugs bind to the viral protease active site and inhibit its

activity, hampering maturation and sequestering the viral particle in an immature, inactive state, hampering virus spread (Wang et al., 2015).

Thanks to the combination of several antiretroviral drugs targeting different steps of the HIV-1 replication cycle in most of the cases a correctly administered HAART can suppress viremia to undetectable levels. This, in addition to leading to a considerable increase in quality of life (Lee et al., 2018), results in a dramatic decrease of HIV-1 transmission rates. Namely, the PARTNER and PARTNER-2 studies have reported no cases of HIV-1 transmission in thousands of male-female and male-male serodiscordant couples (where one partner is infected by HIV and the other is not) when the infected individual was under HAART, even when no condom was used in the sexual activities (Rodger et al., 2018, 2016).

1.3.2. Purge of viral reservoirs

Although the HAART reduces viremia to undetectable levels and dramatically lowers the rate of transmission, it does not completely remove HIV-1 from the organism. During the HIV-1 replication cycle, the viral genetic material is integrated in the host cell, and may lay dormant for long periods of time even with the administration of antiretroviral drugs. When HAART is suspended (voluntarily or by accident), the HIV-1 genes are expressed and viral replication starts again. Several case reports have been put forward in which HAART interruption has led to rapid viral rebound, where a patient that had been under HAART for up to 10 years and showed no detectable levels of HIV-1 DNA in their organism suffered viral rebound only 50 days after HAART interruption (Chun et al., 2010). Even in ideal cases of extremely early HIV-1 diagnoses and start of HAART, where no detectable HIV-1 was observed in blood, cerebrospinal fluid, bone marrow or several other tissues, interruption of treatment led to viral rebound in only 225 days (Henrich et al., 2017). These cases highlight that even in the absence of detectable HIV-1 in the organism viral reservoirs established early in the infection phase are sufficient to initiate a new spread of the infection once the antiretroviral therapy is interrupted, entailing that infected patients under HAART cannot stop their treatment and must be administered medication for the rest of their lives.

As stated, the viral rebound after treatment interruption is facilitated by the existence of cells non-productively infected by HIV, called latently infected cells. These cells contain the viral genetic material integrated in their genome and retain the capacity to produce infectious particles, but while in their latent state, do not express viral transcripts. Because no expression of viral proteins occurs, the immune system cannot recognize the infected cells and is unable to purge them. These latently infected cells constitute one of the biggest handicaps in the finding of a cure for HIV-1.

Latently infected cells may accumulate in specific anatomical sites known as viral reservoirs or sanctuaries, and several cell types exist which have been described to be latently infected with HIV. The main type of latently infected cells are CD4+ T cells,

specially the long-lived memory subtype (Barton et al., 2016; Kulpa and Chomont, 2015), which normally reside in lymphoid tissues such as spleen, thymus and lymph nodes. Additionally and in lower levels, HIV-1 has also been suggested to be able to latently infect macrophages, epithelial cells, fibrocytes and astrocytes (Churchill et al., 2009; Siliciano et al., 2003; Stebbing et al., 2004). Because these cell types reside in varied anatomical sites, such as the brain, lungs, kidneys, liver, adipose tissue, gastrointestinal tract, genitourinary systems and bone marrow, together with the lymphoid tissues they constitute a wide variety of viral reservoirs scattered throughout the organism, making their specific targeting and delivery of a potential drug a challenging barrier to overcome (Vanhamel et al., 2019).

The main strategies for the purge of viral reservoirs being developed nowadays are based on the concept of “shock and kill”. This concept is based in the reactivation of latent virus with the use of latency reversing agents (LRA), which restart replication and induce the expression of viral proteins and production of viral particles. Massive production of virions should lead to the death of the infected cell, through a viral cytopathic effect. In parallel, HIV-1 derived viral peptides or drugs designed to boost the immune system would be administered to ensure the death of the reactivated cells expressing the viral proteins through immune-mediated killing. Although the concept of “shock and kill” presents a robust basis for the development of therapies looking to purge viral reservoirs, no successful treatment has been developed yet (Thorlund et al., 2017; Vanhamel et al., 2019). One of the main handicaps of this approach relies on the wide variety of anatomical sites in which latently infected cells reside. Individual targeting of each latently infected cell type with LRAs is, although theoretically possible, not a viable option, and some of the viral reservoir organs or tissues are significantly difficult to reach, which may lead to the necessity of using high concentrations of LRA with severe cytotoxic effects. Thus, the development of a LRA administration route that greatly enhances specific delivery to several key anatomical sites to induce latently infected cell reactivation seems to be a necessary requisite for the purge of viral reservoirs and the development of a so-called “sterilizing cure” (Chun et al., 2015).

1.4. General objectives

1.4.1. Main objective

The main objective of the present work is to study the involvement of lipids in the HIV-1 replication cycle, studying the lipid environment of the HIV-1 envelope protein and determining its relationship to protein entry capacity; developing therapeutic antiretroviral tools that target the viral membrane; and making use of specific lipid-based targeting as new therapeutic approaches for latency reactivation for a future functional cure.

1.4.2. Specific objectives

1. To study the interaction of HIV-1 envelope protein with cholesterol in the cellular and viral membranes, and to determine the region(s) of the gp41 protein involved in the interaction with cholesterol.
2. To characterize the relation between gp41 interaction with cholesterol and protein function.
3. To study raftophilic lipidomimetic compounds as antiretroviral tools.
4. To engineer nanoparticles with specific targeting ability exploiting the HIV-1 *trans*-infection route for delivery of latency reactivation agents to latently infected cells, and for boosting of specific anti-HIV-1 immune responses.

Chapter 2. Experimental Techniques

In this chapter a general overview of the reagents and experimental techniques performed during this thesis is shown. Generally, experimental techniques used in more than one chapter are included, while techniques used exclusively in a specific chapter, and more specific details of each experiment are detailed in the *Experimental techniques* section of each chapter.

2.1. Cells and cell culture

For this work several cells types were used: HEK 293T, HeLa TZM-bl, and Chessie-8 Hybridoma cells were obtained through the NIH AIDS Reagent Program, Division of AIDS, NIAID, NIH, and Jurkat E6-1, MT-4, and DFJ8 cells were kindly donated by Hans-Georg Kräusslich (University Hospital of Heidelberg, Germany).

HEK 293T are a highly transfectable derivative of human embryonic kidney 293 cells commonly used for obtaining large amounts of viral particles. HeLa TZM-bl reporter cells were used for entry and infectivity assays. They constitute an indicator cell line that enables a quantitative analysis of HIV infection, as the HIV-1 Tat protein induces the expression of the firefly luciferase (*luc*) reporter gene in the cell after a single round of infection. Virus entry assays were also carried out in physiologically more relevant Jurkat E6-1 cells, a CD4+ and CXCR4+ T-lymphocyte cell line (Weiss et al., 1984). Viral infectivity was also tested in MT-4 cells, a cell line commonly used for infectivity assays (Harada et al., 1985). For obtention of the anti-gp41 antibody Chessie-8, Chessie-8 Hybridoma Balb/c mouse splenocyte cells were used. The monoclonal IgG1 antibody of the same name they express is specific for gp41 and reacts with gp160 (Abacioglu et al., 1994).

HEK 293T, HeLa TZM-bl and DFJ8 cells were maintained at 37°C and 5% CO₂ in DMEM GlutaMAX™ High glucose culture medium supplemented with 10% FBS, and 100 U/ml Penicillin-Streptomycin. Cells were usually splitted at a 1:10 ratio every two or three days. Jurkat E6-1, MT-4 and Chessie-8 Hybridoma cells were maintained at 37°C and 5% CO₂ in RPMI 1640 GlutaMAX™ culture medium supplemented with 10% FBS and 100 U/ml Penicillin-Streptomycin. Cells density was always maintained between 0.3·10⁶ and 1·10⁶ cells/ml.

DMEM GlutaMAX™ High Glucose, RPMI 1640 GlutaMAX™, Fetal Bovine Serum (FBS), Trypsin-EDTA and Penicillin-Streptomycin were purchased from Thermo Fisher Scientific. Cell culture flasks, dish and plates were purchased from Sigma-Aldrich. Phosphate Saline Buffer or PBS (100 mM phosphate buffer, 2.7 mM potassium chloride, 137 mM sodium chloride, pH 7.4) from Sigma-Aldrich was also used for cell culture.

2.2. Constructs

In this chapter several infectious and non-infectious proviral (Table 2.1) and Env only expressing (Table 2.2) plasmids has been used. For each of the plasmids several variants expressing different gp41 protein mutants have been used. Additionally, a few other plasmids have been used for different purposes, such as the generation of BlaM-Vpr viral particles for entry assays, or pseudotyping of HIV-1 with VSV-G and MLV envelope protein expressing plasmids (Table 2.3). All of the constructs contain a resistance to ampicillin gene for selection of transformed clones.

Table 2.1 – Proviral plasmids.

Infectious capacity	Denomination	gp41 mutation	Description
Non-infectious (SL2)	pCHIV	wt	Non-infectious plasmid expressing all HIV-1 _{NL4-3} proteins except Nef, but cannot replicate because of the lack of the viral long-terminal repeat sequences (Muller et al., 2004). The plasmid was kindly provided by Barbara Müller.
	pCHIV L677I	p.L677I	pCHIV derivative expressing a gp41 protein variant where the CRAC segment Leu677 has been exchanged by Ile.
	pCHIV G688L G692L	p.G688L p.G692L	pCHIV derivative expressing a gp41 protein variant where the Gly688 and Gly692 of the GxxxG motif have been exchanged by Leu.
	pCHIV R696I	p.R696I	pCHIV derivative expressing a gp41 protein variant where the transmembrane Arg696 has been exchanged by Ile.
	pCHIV CD22 TMD	Entire TMD	pCHIV derivative expressing a chimeric gp41 protein with a substitution of its membrane spanning domain by the TMD of the cellular receptor CD22.
	pCHIV R770K R778K	p.R770K p.R778K	pCHIV derivative expressing a gp41 protein variant where the Arg770 and Arg778 has been exchanged by Lys.
	pCHIV TR751	p.L751*	pCHIV derivative expressing a gp41 protein variant with a 104 amino-acid truncation on its CT, lacking the three LLP domains.
	pCHIV TR812	p.L812*	pCHIV derivative expressing a gp41 protein variant with 43 amino-acid truncation on its CT, lacking the LLP1 domain.
	pCHIV Env(-)	-	pCHIV derivative with a frameshift in the beginning of the <i>env</i> gene (nt 6401), thus not expressing the Env protein (Lampe et al., 2007).

			The plasmid was kindly provided by Barbara Müller.
	pCHIV PR(-)	wt	pCHIV derivative containing a mutation in the HIV-1 protease active site (p.D25N), rendering the enzyme non-functional, and sequestering the viral particle in a immature state.
	pCHIV PR(-) TR751	p.L751*	pCHIV PR(-) derivative expressing a gp41 protein variant with a 104 amino-acid truncation on its CT, lacking the three LLP domains.
Infectious (SL3)	pNL4-3	wt	Infectious plasmid expressing all HIV-1 _{NL4-3} proteins (Adachi et al., 1986).
	pNL4-3 Env(-)	-	pNL4-3 derivative with a frameshift in the beginning of the <i>env</i> gene (nt 6351), thus not expressing the Env protein (Henriksson and Bosch, 1998).

Table 2.2 – Env expressing plasmids.

Denomination	gp41 mutation	Description
pCAGGS.NL4-3	wt	Plasmid expressing the HIV-1 _{NL4-3} Env protein.
pCAGGS L677I	p.L677I	pCAGGS derivative expressing a gp41 protein variant where the CRAC segment Leu677 has been exchanged by Ile.
pCAGGS G688L G692L	p.G688L p.G692L	pCAGGS derivative expressing a gp41 protein variant where the Gly688 and Gly692 of the GxxxG motif have been exchanged by Leu.
pCAGGS R696I	p.R696I	pCAGGS derivative expressing a gp41 protein variant where the transmembrane Arg696 has been exchanged by Ile.
pCAGGS CD22 TMD	Entire TMD	pCAGGS derivative expressing a chimeric gp41 protein with a substitution of its membrane spanning domain by the TMD of the cellular receptor CD22 (Wilk et al., 1996).
pCAGGS R770K R778K	p.R770K p.R778K	pCAGGS derivative expressing a gp41 protein variant where the Arg770 and Arg778 has been exchanged by Lys.
pCAGGS TR751	p.L751*	pCAGGS.NL4-3 derivative expressing a gp41 protein variant with a 104 amino-acid truncation on its CT, lacking the three LLP domains.
pCAGGS TR812	p.L812*	pCAGGS.NL4-3 derivative expressing a gp41 protein variant with 43 amino-acid truncation on its CT, lacking the LLP1 domain.

Table 2.3 – Other plasmids.

Denomination	Description
pMM310	Plasmid expressing a β -lactamase-Vpr chimeric protein (BlaM-Vpr) readily incorporated into the virions upon co-transfection with a proviral plasmid (Munk et al., 2002).
MLV-Env	Plasmid expressing the Friend ecotropic Murine Leukemia Virus glycoprotein (Sherer et al., 2003).
VSV-G	Plasmid expressing the G glycoprotein of Vesicular Stomatitis Virus (Emi et al., 1991).
AAV2	Plasmid expressing the Adeno-Associated Virus 2 proteins (Grimm, 2002).

2.2.1. gp41 variants design and cloning

To determine the role of the different regions and domains of gp41 in the interaction of the protein with lipids, its incorporation into the virion, the lipid content of the particle, and the entry and infective capacity, several variants of the protein were designed and cloned in a non-infectious plasmid (Table 2.1). Broadly, two main regions of interest were the aim of these mutagenesis experiments: the transmembrane domain (TMD) and adjacent regions (MPER), and the LLP (Lentiviral Lytic Peptide) domains in the cytoplasmic domain (CT). Two main approaches were used to obtain the gp41 variants: cloning and mutagenesis experiments.

2.2.1.1. Cloning

Plasmids expressing the gp41 variants CD22 TMD, TR812, and TR751 were kindly provided by Valerie Bosch. These provided variant *env* genes were cloned in a variety of vectors, different to the pCAGGS.NL4-3 vector expressing the wt Env protein. As such, the variant *env* genes had to be cloned in the pCAGGS vector to allow a proper comparison of the samples.

The vectors expressing the CD22 TMD, TR812 and TR751 gp41 variants were each digested with Acc65I and XhoI, separating part of the *env* gene insert from the rest of the plasmid. The samples were then loaded into a 1% agarose preparative gel, run in an electrophoresis, and the band corresponding to the insert (2.5 kb) was cut and purified from the gel. The same procedure was carried out for the wild type protein expressing

pCAGGS.NL4-3 plasmid, but in this case the insert was discarded and the band corresponding to the vector (4.8 kb) was purified.

The pCAGGS vector and the mutant *env* gene inserts were then ligated and used to transform chemocompetent DH5a bacteria. Several clones of each transformation were selected, grown in LB medium, and their plasmidic content was purified using a Midi-Prep Kit (Macherey Nagel). The resulting plasmids (pCAGGS CD22 TMD, pCAGGS TR751, pCAGGS TR812) were sequenced to verify that they contained the desired gp41 insert.

2.2.1.2. Mutagenesis

The rest of the pCAGGS variants shown in Table 2.2 (pCAGGS L677I, pCAGGS G688L G692L, pCAGGS R696I, pCAGGS R770K R778K) were produced by site-directed mutagenesis using the “Gibson Assembly” method, commercially available as a kit by New England BioLabs. The Gibson Assembly is designed to ligate two DNA inserts with overlapping ends to a digested DNA vector. In this work, these DNA inserts were obtained by amplifying by PCR two halves of the *env* gene insert: a pair of oligonucleotides amplifies the 5' region of the gene, from the start of the gene to the mutation point; while a second pair of oligonucleotides amplifies the 3' region, from the mutation point to the end of the gene. By using oligonucleotides containing the desired mutation, mutated PCR products are obtained. These amplified inserts were ligated to the DNA vector by the Gibson Assembly, which employs three enzymatic activities in a single-tube reaction: a 5' exonuclease chews back the 5' end sequences and exposes the complementary sequences of the overlapping DNA inserts for annealing; a polymerase then fills in the gaps of the annealed regions; and finally a DNA ligase seals the nick and covalently links the DNA fragment together (Figure 2.1).

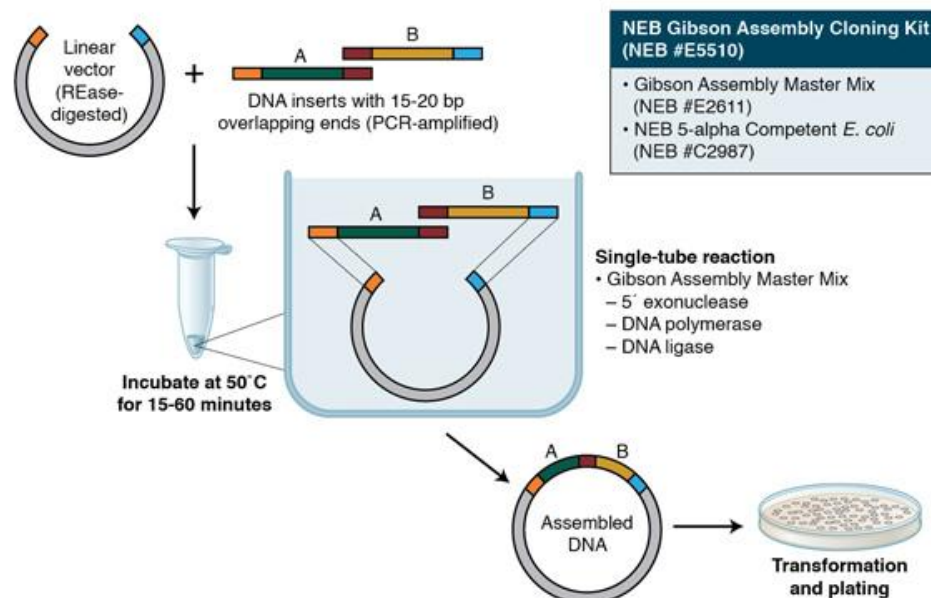


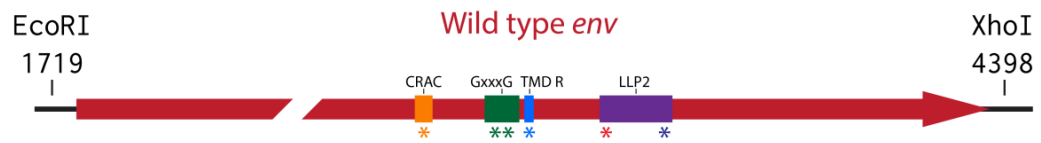
Figure 2.1 – Schematic representation of the Gibson Assembly. This image was obtained from the New England BioLabs website¹.

For the amplification of the mutated DNA inserts the following primer pairs design rationale was used (Table 2.4, Figure 2.2):

Table 2.4 – Oligonucleotides used for the mutant DNA insert amplification. In red, the codons differing from the wild type sequence, with which the desired mutations were introduced. The overlapping sequence between the two mutated primers is highlighted in grey.

Mutation	Primer pairs			
	5' fragment		3' fragment	
	Forward	Reverse	Forward	Reverse
G688L G692L	5'-TTGTTGT GCTGTCTCA TCATTTTG-3'	5'-CTATTCT TAA AAG TACCA AGCC CAG TAC-3'	5'-GATAGTACT GTG GGCTTGGTACT TTT TTAAGAATAG-3'	5'-GGCAGAG GGAAAAAGA TCTGCTAG-3'
R696I	5'-TTGTTGT GCTGTCTCA TCATTTTG-3'	5'-TACAGCAAAA ACTAT TATT AA ACCTACCAAG-3'	5'-GGCTTGGTAG GTTT ATA AATAG TTTTTGCTGTAC-3'	5'-GGCAGAG GGAAAAAGA TCTGCTAG-3'
L677I	5'-TTGTTGT GCTGTCTCA TCATTTTG-3'	5'-GAATAATTT TATATACCA GAT CCAATTTGTTA TGTTAAACC-3'	5'-GTGGAATT GGTTTAAACATAA CAAATTGG ATCT GGTATATAA AATTATTG-3'	5'-GGCAGAG GGAAAAAGA TCTGCTAG-3'
R770K R778K	5'-TTGTTGT GCTGTCTCA TCATTTTG-3'	5'-CGTTACAAT CAAGAGTAAGT CTT CAAGC-3'	5'-GACTTACT CTTGATTGTA ACG AAA AATT GTGGAAC-3'	5'-GGCAGAG GGAAAAAGA TCTGCTAG-3'

¹ www.neb.com



Mutation	Oligonucleotide	
	5' fragment	3' fragment
G688L G692L		
R696I		
L677I		
R770K R778K		

Figure 2.2 – Oligonucleotide design rationale. For each mutant, the DNA insert is amplified in two overlapping fragments (i.e. 5' and 3' fragments) using two pairs of oligonucleotides, one pair for each fragment. The mutation points in the oligonucleotides are marked by (*). The grey shaded box marks the overlapping region of the two fragments.

Note that the 5' fragment forward and 3' fragment reverse oligonucleotides are the same for all of the variants, as they recognize the same region in the vector just outside the *env* gene. The other two oligonucleotides of each variant contain the desired changes needed to introduce the mutation.

These primers were mixed an appropriate amount of wild type pCAGGS.NL4-3 DNA template, and using the Q5 PCR Mix provided by the NEBuilder commercial kit, each of the fragments was amplified separately. The PCR products were then treated with DpnI to remove the template DNA, and the fragments were purified using a commercial PCR clean-up kit (Macherey Nagel). In parallel, the wild type pCAGGS.NL4-3 DNA was digested with EcoRI and XhoI and loaded into a 1% agarose preparative gel. The band corresponding to the vector (4.9 kb) was cut and purified from the gel, then mixed with appropriate amounts of each of the mutated fragments, and ligated using the Master Mix provided by the NEBuilder Assembly kit (Figure 2.1). The ligation product was used to transform chemocompetent bacteria, and after growth several clones of each variant were selected for plasmid extraction and sequencing.

2.2.2. Plasmid production

The plasmids used for the different experiments in this chapter were produced in large quantities by transformation of DH5α *Escherichia coli* competent cells, followed by clone selection and growth in liquid LB medium, and plasmid extraction and purification by a commercial kit. Plasmid verification was performed by enzymatic digestion or sequencing.

2.2.2.1. Generation of competent bacteria

Generation of competent *Escherichia coli* DH5α bacteria for plasmid transformation was carried out using SOB medium (20 g/l Tryptone, 5 g/l yeast extract, 0.5 g/l NaCl, 2.5 mM KCl), TFB I buffer (3 g/l potassium acetate, 10 g/l MnCl₂, 16 mM CaCl₂, 15% (v/v) glycerol pH = 5.8), TFB II buffer (2 g/l MOPS, 76 mM CaCl₂, 10 mM KCl, 15% (v/v) glycerol pH = 7.0), and Lysogeny Broth or LB (Laboratorios Conda) (Cohen et al., 1972).

1. 50 µl of the stock DH5α bacteria was spread in a LB agar petri dish and grown overnight at 37 °C.
2. Next day a colony was picked and grown overnight in 5 ml of liquid LB medium (20 g/l lysogeny broth) at 37 °C and constant shaking.
3. Next day the liquid medium containing bacteria was diluted 1:200 in liquid SOB medium, and grown for 3-4 h at 37 °C, until the optical density at 600 nm (OD_{600}) of the growth medium was $OD_{600} = 0.5$.
4. The SOB medium containing bacteria was kept in ice for 10 min, separated in 50 ml aliquots, pelleted by centrifugation at 32,000 rpm for 12 min at 4°C, and each aliquot was carefully resuspended in 10 ml cold TFB I buffer.
5. After incubation for 10 min at 4°C with TFB I buffer, the bacteria aliquots were pelleted and carefully resuspended in 2.5 ml of cold TFB II buffer each.
6. After the samples were incubated for 10 min, the aliquots were pelleted and carefully resuspended in 5 ml of cold TFB II each. 50 µl aliquots of competent DH5α bacteria were then frozen in liquid nitrogen and stored at -80 °C until their use.

2.2.2.2. Transformation and clone selection

The following protocol was used for bacteria transformation (Cohen et al., 1972):

1. A 50 μL aliquot of frozen DH5a competent bacteria were thawed in ice and mixed with 0.5 μg of the desired construct.
2. The bacteria were kept in ice for 15 min and then subjected to a heat shock by incubation at 42 $^{\circ}\text{C}$ for 90 s followed by incubation in ice for 2 min. In this heat shock the added plasmidic DNA enters the bacteria by zone of adhesion channels.
3. After transformation the bacteria were seeded in a LB agar petri dish supplemented with 100 $\mu\text{g}/\text{ml}$ ampicillin to induce a selective growth of transformed bacteria. The petri dishes were incubated overnight at 37 $^{\circ}\text{C}$ to induce bacterial growth.
4. Clearly isolated clones from the petri dish were selected and seeded to 500 mL of liquid LB medium (20 g/L lysogeny broth) supplemented with 100 $\mu\text{g}/\text{ml}$ ampicillin, and the bacterial culture was grown overnight at 37 $^{\circ}\text{C}$ for no more than 12 h.

Once grown, the bacterial culture was used for plasmid extraction and purification.

2.2.2.3. Plasmid preparation

The plasmid extraction and purification from the bacterial culture was carried out with a commercial NucleoBond® PC 500 kit (Macherey-Nagel) following the manufacturer's instructions with some modifications. Briefly:

1. The plasmid-containing bacterial culture was centrifuged at 5,000 g for 15 min at 4 $^{\circ}\text{C}$ to pellet the bacterial cells and separate them from the medium.
2. Bacterial culture supernatant was removed, and bacteria were resuspended in 12 ml of S1 resuspension buffer supplemented with RNase A.
3. 12 ml of lysis buffer S2 was added to the resuspended cells, the samples were mixed by inverting the tube, and incubated at room temperature for 3 min. This step induces the lysis of the bacteria under alkaline conditions and the liberation of plasmidic and chromosomic DNA.
4. 12 ml of cold (4 $^{\circ}\text{C}$) neutralization buffer S3 was added to the samples, mixed by inverting the tubes, and incubated on ice for 5 minutes. The neutralization buffer contains acetate which precipitates the proteins bound to the chromosomic DNA, while the protein-free plasmidic DNA remains in solution.

CHAPTER 2

5. In parallel, NucleoBond® columns were equilibrated with 6 ml of N2 equilibration buffer.
6. The lysed bacterial samples were cleared through a paper filter to avoid loading of the precipitated chromosomal DNA to the column, while the plasmidic DNA in solution passes through the filter and is allowed to enter the column.
7. The cleared lysate was loaded into the column and passed through by gravity flow. The plasmidic DNA remains bound to the column.
8. The column was washed with 32 ml of N3 washing buffer, and bound plasmidic DNA was eluted with 15 ml of N5 elution buffer.
9. 11 ml of room-temperature isopropanol was added to the eluted DNA to induce precipitation. The samples were mixed and centrifuged at 5,000 *g* for 30 min.
10. The supernatant was carefully discarded and 1 ml of 70% (v/v) ethanol was added to the precipitated DNA pellet to remove isopropanol. The pellet was transferred into a microcentrifuge tube and centrifuged at 5,000 *g* for 10 min at room temperature.
11. The ethanol supernatant was removed and plasmidic DNA was allowed to dry for 20 min. The DNA was resuspended in 100 µl of ultrapure water and its concentration was measured with a NanoDrop Microvolume Spectrophotometer (ThermoFisher). The plasmidic DNA concentration was adjusted to 1 mg/ml.

0.5 µg of the purified plasmidic DNA was digested with 1 µl of Hind III for 1 h at 37 °C loaded into a 1% (w/v) agarose in TAE gel stained with 0.01% (v/v) of SYBR Safe (ThermoFisher), and subjected to electrophoresis. Digested plasmidic DNA bands were visualized by an UV transilluminator (Scie-Plas) and number of bands and their size was corroborated to be as expected. When necessary, plasmid identification was corroborated by sequencing.

2.3. Chessie-8 antibody

The anti-gp41 Chessie-8 antibody has been widely used in this work. It is a monoclonal antibody of isotype IgG1, which reacts with gp160 and is specific for gp41 (Abacioglu et al., 1994), produced from Chessie-8 anti-HIV-1 gp41 hybridoma cells. This antibody is used for recognition of gp41 in Western blot experiments and for the immunoprecipitation of the protein throughout this work.

2.3.1. Chessie-8 hybridoma

Chessie-8 anti-HIV-1 gp41 hybridoma cells are a type of Balb/c mouse splenocyte. For antibody production, cells were overgrown until they died, generating an approximate yield of 10-20 µg of antibody per mL of culture medium. After overgrowth and cell death, the culture medium was centrifuged at 500 *g* for 5 minutes followed by filtering through 0.45 µm syringe filters. This clarified culture medium supernatant was stored at -80 °C until the antibody purification was carried out.

2.3.2. Chessie-8 IgG1 purification

For chessie-8 antibody purification HiTrap Protein G High Performance 1 mL column were used (Sigma-Aldrich). Disodium phosphate (Na_2HPO_4) and sodium phosphate (NaH_2PO_4) from Merck, Glycine from VWR International and Tris from Apollo Scientific were used for the antibody purification in the HiTrap Protein G columns. Purified antibody concentration was determined using a BCA assay kit from ThermoFisher.

The Chessie-8 IgG1 monoclonal antibody was purified using a HiTrap protein G 1 mL column from clarified Chessie-8 hybridoma cell culture supernatant. The buffers used for the purification are detailed in Table 2.5. The following protocol was used for isolation and purification of the Chessie-8 IgG1 antibody:

1. The HiTrap protein G 1 mL column was equilibrated with 10 mL equilibration buffer at a 1 mL/minute flux at room temperature.
2. The clarified cell culture supernatant was fed to the column in a closed cycle for 3 hours, so the total volume of the supernatant (45 mL) could circulate the column at least three times, so as to ensure a high antibody binding to the column.
3. The column was washed with 10 mL of equilibration buffer.
4. The antibody was eluted by using 5 mL of elution buffer. Fractions of 250 µL were collected, and to each fraction 10 µL of neutralization buffer were added to obtain a final pH value of around 7.0.
5. The protein concentration of the fractions was determined by a BCA assay and the fractions containing a high amount of protein were collected, combined and dialyzed overnight against 2 liters of PBS at 4°C.

The following day the purified and dialyzed antibody solution was collected and the IgG1 concentration was determined using a BCA assay following the manufacturer's recommendations.

Table 2.5 – Chessie-8 IgG1 antibody purification buffers.

Buffer	Composition	pH
Equilibration buffer	15.6 mM NaH ₂ PO ₄ 24.4 mM Na ₂ HPO ₄	7.0
Elution buffer	0.1 M Glycine-HCl	2.7
Neutralization buffer	1 M Tris-HCl	9.0

2.4. Western blot

The Western blot technique was used for several purposes during this work. For membrane blocking and primary and secondary antibody incubation, Odyssey Blocking Buffer (LiCOR), and for membrane washing, TBST buffer (150 mM NaCl, 10 mM Tris-HCl, 0.2% (w/v) Tween 20, pH 8) were used. In general, the following protocol was used:

1. The samples were dissolved in SDS-PAGE sample buffer and heated to 95°C for 5 minutes.
2. Samples were loaded into a 12.5% polyacrylamide gel containing SDS and subjected to electrophoresis for ca. 1 h at 120 V.
3. Proteins were transferred to Immobilon®-FL transfer membrane (Merck) using a semi-dry blotting technique for 1 h at 15V.
4. The membranes were blocked for 1 hour at room temperature with Blocking Buffer (Odyssey).
5. The blots were probed with the appropriate primary antibody diluted in Odyssey Blocking buffer with 0.1% (w/v) Tween 20, washed three times with TBST, incubated with the appropriate secondary antibody diluted in Odyssey Blocking buffer with 0.1% (w/v) Tween 20, and washed again three times with TBST.
6. Detection of the proteins was carried out by the use of infrared dye-conjugated secondary antibodies using the LI-COR Odyssey imaging system.

The antibodies used in this work for Western blot experiments are shown in Table 2.6 (primary antibodies) and Table 2.7 (secondary antibodies).

Table 2.6 – Primary antibodies used for Western Blot experiments.

Antigen	Host	Dilution	Incubation conditions	Manufacturer
gp41 (Chessie-8)	Mouse	1:2,000	Overnight at 4°C	Produced in the lab
CA	Sheep	1:2,000	1 h at room temperature	Kindly donated by Professor Hans-Georg Kräusslich
MA	Rabbit	1:5,000	1 h at room temperature	Kindly donated by Professor Hans-Georg Kräusslich
Caveolin-1	Rabbit	1:1,000	1 h at room temperature	Abcam (# ab2910)
Transferrin receptor	Mouse	1:1,000	1 h at room temperature	Abcam (# ab1086)

Table 2.7 – Secondary antibodies used for Western Blot experiments.

Antigen	Host	Detection	Dilution	Incubation conditions	Manufacturer
Mouse IgG	Donkey	Near infrared fluorescence: IRDye800	1:15,000	45 min at room temperature	LI-COR (#926-32212)
Sheep IgG	Donkey	Near infrared fluorescence: IRDye800	1:15,000	45 min at room temperature	Rockland (613-732-168)
Rabbit IgG	Donkey	Near infrared fluorescence: IRDye680	1:15,000	45 min at room temperature	LI-COR (926-68073)

2.5. Viral particle purification

Viral particles have been used in this work for several different experiments; namely for entry and infectivity assays, gp41-lipid interaction experiments, quantification of viral gp41 protein, viral lipidomic studies and for liposome formation from HIV-1 extracted lipids. The viral particle obtention starts with the transfection of HEK 293T with proviral plasmids and, depending on the type of experiment, the viral particle obtention was stopped in the sucrose cushion concentration (entry and infectivity assays), or in the velocity gradient purification (gp41-lipid interaction experiments, quantification of gp41 protein, lipidomic measurements and liposome preparation). The general workflow for viral particle purification is shown in Figure 2.3.

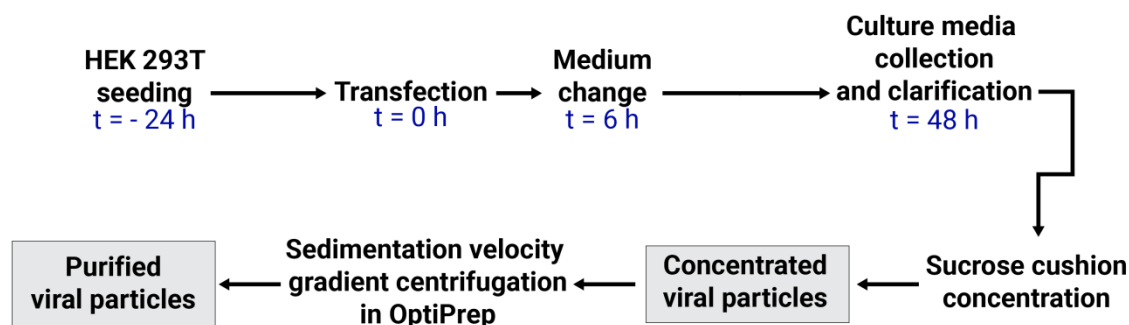


Figure 2.3 – General workflow of viral particle purification.

For cell transfection by the Calcium Phosphate method CellPure® Calcium chloride (CaCl_2) from Carl Roth and CellPure® HEPES from Carl Roth, and Disodium phosphate (Na_2HPO_4) from Sigma-Aldrich were used. The different reagents for transfection were dissolved in UltraPure water from Sigma-Aldrich. The cell culture supernatant is clarified by a filtration through 0.45 μm CME filters purchased from Carl-Roth. The virus particle concentration and purification were carried out by centrifugation in TLA-110, SW 28.1 and SW 60Ti rotors and ultracentrifuge tubes and Optima MAX-TL and Optima L-100 XP ultracentrifuges from Beckman Coulter. Ultrapure Sucrose from Thermo Fisher Scientific and OptiPrep from Axis-Shield were used for concentration and purification, respectively. The concentrated and purified viral particles were resuspended in HeNa buffer (10 mM HEPES, 150 mM NaCl, pH 7.4). This same buffer was used to dissolve the sucrose for the sucrose cushion and to prepare the different dilutions of the OptiPrep solution for the velocity gradient centrifugation.

2.5.1. Cell transfection

Viral particles containing different gp41 variants were produced by transfection with the calcium phosphate method of HEK 293T cells with pCHIV proviral plasmids. This pCHIV proviral plasmid contains all of viral proteins needed for viral particle assembly and budding. For pseudotyping, pCHIV Env(-) plasmids were cotransfected with VSV-G and MLV Envelope expressing plasmids. For the calcium phosphate transfection protocol the following reagents were used (Table 2.8):

Table 2.8 – Reagents used for the calcium phosphate transfection method.

Reagent	Composition
Calcium chloride	2.5 M CaCl ₂
2x HBS	280 mM NaCl 50 mM HEPES 1.5 mM Na ₂ HPO ₄ ·2H ₂ O pH 7.10

In this work two types of culture surfaces were used for virus purification: 35 mm and 10 cm dishes. The amount of seeded cells and reagents used for transfection in each one of the culture surfaces is detailed in Table 2.9. 24 hours prior to transfection the appropriate amount of HEK 293T cells were seeded in the selected dish. The next day the cells were transfected with the selected plasmidic DNA:

1. The appropriate amount of plasmidic DNA was added to a 0.25 M calcium chloride solution and vortexed to ensure a complete mixture.
2. Then, the 2xHBS solution was added drop wise while vortexing at low speed, to ensure a homogeneous mixture.
3. This resulting transfection reagent was incubated at 37°C for 15 minutes for a complete conjugation of the DNA to the calcium phosphate precipitate.
4. The aggregates were then added drop wise to the cell culture ensuring a complete spread through the entire culture surface.
5. Cells were incubated in normal culture conditions for 6 hours, after which the medium was substituted with fresh culture medium.

Table 2.9 – Seeded cell density and transfection reagents amount used in the different culture surfaces.

	35 mm dish	10 cm dish
Seeded cells	0.5·10 ⁶	4·10 ⁶
Proviral DNA	2 µg	10 µg
<i>--OR--</i>		
Env(-) proviral DNA	2 µg	10 µg
VSV-G or MLV Env expressing DNA	0.8 µg	4 µg
CaCl₂ 0.25 M	250 µL	1 mL
2x HBS	250 µL	1 mL

2.5.2. Sucrose cushion concentration

48 hours after transfection the culture medium supernatant was collected and cell debris was eliminated by a clarification process, consisting in a centrifugation at 500 *g* for 5 minutes followed by a filtration through 0.45 μm filters. Viral particles were concentrated from this clarified medium by centrifugation through a cushion of 20% (wt/wt) sucrose (Welker et al., 2000). For this, an appropriate amount of 20% sucrose was added to the bottom of an ultracentrifuge tube and the clarified culture media was carefully added on top and the samples were centrifuged at 4°C. For the different experiments in this chapter viral purifications of different scales were carried out. Depending on the sample volume to be purified different ultracentrifuge tubes, 20% sucrose solution volume, and centrifugation speeds and time were used (Table 2.10).

Table 2.10 – Ultracentrifugation conditions for different sample volumes.

	Sample volume		
	1 – 2 mL	4 – 8 mL	>30 mL
Tubes and rotor	TLA-110	SW 60Ti	SW 28.1
Ultracentrifuge	Optima MAX-TL	Optima L-100 XP	Optima L-100 XP
20% sucrose volume/tube (mL)	0.1	0.5	6
Sample volume/tube (mL)	1	4	30
Rotor speed (rpm)	44,000	31,000	25,000
Avg. G-force (g)	80,000	96,000	85,000
Time (minutes)	45	120	120

After centrifugation, the culture medium and sucrose supernatant were removed, and the pelleted virus was resuspended in HeNa buffer (Figure 2.4), obtaining concentrated viral particles (CVP). For entry and infectivity assays viral particles concentrated by sucrose cushion were stored at -20°C until their use. However, for gp41-lipid interaction, gp41 quantification and lipidomic studies the concentrated viral particles were further purified using a velocity gradient purification (section 2.5.3).

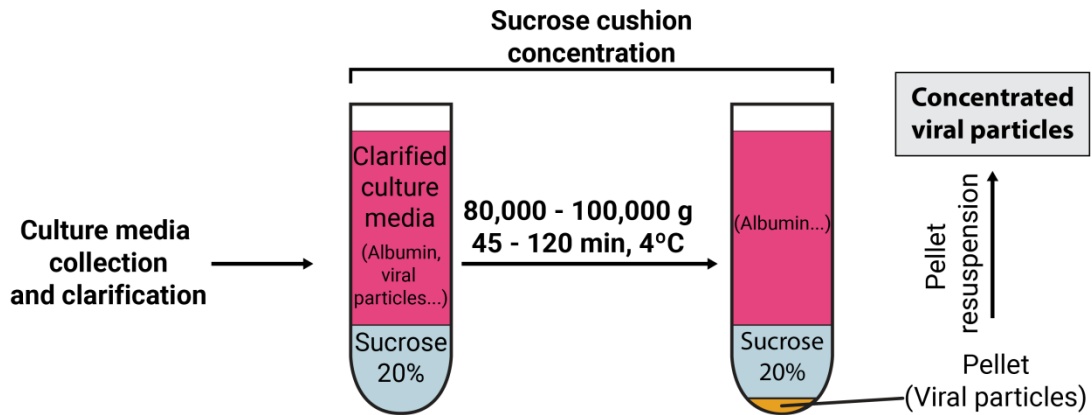


Figure 2.4 – Schematic representation of viral particle concentration in a sucrose cushion.

2.5.3. Velocity gradient purification

In some of the experiments concentrated HIV-1 was further purified by a sedimentation velocity gradient using OptiPrep (Brugger et al., 2006; Dettenhofer and Yu, 1999; Lorizate et al., 2009). A discontinued gradient was prepared in a SW 60Ti ultracentrifuge tube with decreasing OptiPrep concentrations (Table 2.11), which were prepared by diluting the commercially available OptiPrep in HeNa buffer.

Table 2.11 – Concentration of the different layers of the discontinuous OptiPrep gradient, from bottom to top.

OptiPrep concentration (% wt/wt)	Volume (µL)
35.0	420
18.0	300
16.8	300
15.6	300
14.4	300
13.2	300
12.0	300
10.8	300
9.6	300
8.4	300
7.2	300
6.0	430

CHAPTER 2

The concentrated virus sample was added on top of this discontinued gradient using the protocol below, for which a schematic overview is shown in Figure 2.5:

1. 150 μL of the resuspended concentrated virus were added on top of the 6.0% layer.
2. The samples were centrifuged at 32,000 rpm (100,000 g avg.) for 90 minutes at 4 $^{\circ}\text{C}$ in a SW 60Ti rotor.
3. Fractions of 270 μL were collected and those containing the visible virus band (fractions 11-13) were combined and diluted 1:8 (v/v) with HeNa buffer.
4. The purified diluted virus was then pelleted by ultracentrifugation in a SW 60Ti rotor at 44,000 rpm (200,000 g avg.) for 45 minutes at 4 $^{\circ}\text{C}$.
5. The supernatant was removed and the pelleted purified virus was resuspended in HeNa buffer, obtaining purified viral particles (PVP). The samples were stored at -20 $^{\circ}\text{C}$ until their characterization and use.

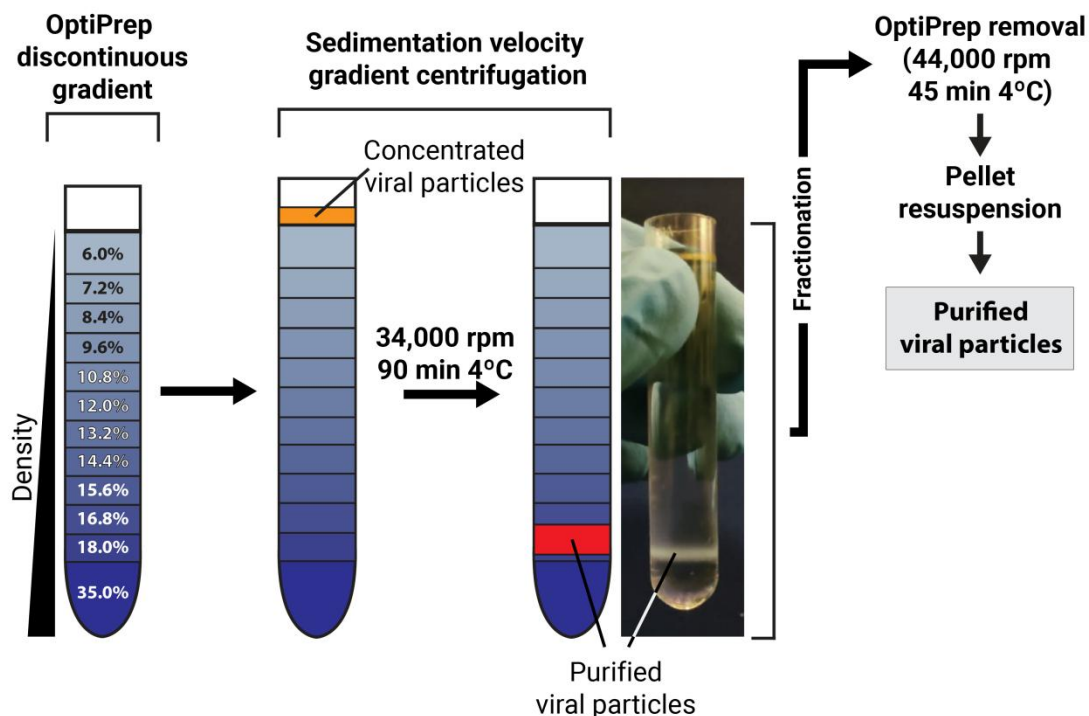


Figure 2.5 – Schematic representation of the concentrated virus particle purification by a centrifugation in a discontinuous OptiPrep gradient.

2.6. Characterization of purified viral particles

2.6.1. Silver Stain

To characterize the concentrated or purified viral particles an appropriate amount of each sample was loaded into a SDS-PAGE, and the gel was then silver-stained. In this protocol all of the proteins in the samples are stained, which allows both to confirm that the samples contain the expected viral protein pattern, and to determine if contamination from albumin or other proteins from the cell culture or cell debris exists. For the silver stain of the samples 100 mL/gel of different solutions are prepared fresh using MiliQ ultrapure water (Table 2.12).

Table 2.12 – Composition of the solutions used for the silver-stain of SDS-PAGE gels.

Solution	Composition
Fixation	50% methanol (v/v) 12% CH ₃ COOH (v/v) 0.02% (wt/v) formaldehyde
Solution I	50% ethanol (v/v)
Solution II	0.9 mM Na ₂ SO ₄
Solution III	11.7 mM AgNO ₃ 0.03% (wt/v) formaldehyde
Solution IV	0.56M NaCO ₃ 0.02% (wt/v) formaldehyde 30 μM Na ₂ SO ₄

Depending on the viral concentration, undiluted or diluted samples were used for Silver stain following the next protocol (Chevallet et al., 2006):

1. The samples were dissolved in SDS-PAGE sample buffer and heated to 95°C for 5 minutes.
2. Samples were loaded into a 12.5% polyacrylamide gel containing SDS and subjected to electrophoresis.
3. The gels were recovered and incubated with 100 mL/gel of fixation solution for 1h at room temperature.

4. After fixation, each gel was washed three times for 5 minutes/wash with solution I, and then three more times with ultrapure water for 20 seconds/wash.
5. The gels were then incubated with solution II for 1 minute at room temperature for signal enhancing, and washed with ultrapure water three times.
6. The samples were stained with solution III for 20 minutes at room temperature.
7. Before developing, a single washing step with ultrapure water was carried out, after which the gels were developed with solution IV for the necessary time.

If a sufficient virus amount has been loaded into the SDS-PAGE a visible CA protein band at ~25 kDa and MA protein band at ~15 kDa can be observed. The gp41 band at ~41 kDa is usually too faint to be clearly observed, due to the low copy of Env protein trimers present in each viral particle (Chertova et al., 2002).

2.6.2. Purification yield quantification by anti-CA Western blot

The yield of the viral particle purification was determined either by a quantitative Western blot analysis probed against CA. To quantify the viral CA amount, a solution of purified CA of known concentration was used as a standard, which was kindly donated by Professor Hans-Georg Kräusslich (University Hospital of Heidelberg, Germany).

Several amounts of the CA standard and a titration of purified virus were dissolved in SDS-PAGE sample buffer, and a SDS-PAGE was performed following the protocol in section 2.4. The blots were probed with a sheep antibody to CA (Table 2.6) as a primary antibody, and anti-sheep IRDye800 (Table 2.7) as a secondary antibody. Protein bands were visualized using the Odyssey infrared imaging system (LI-COR) and quantified using the instrument software.

The integrated intensity signal of the bands corresponding to the CA standard and the purified virus CA were determined. A calibration curve was established with the CA standard and the CA amount of the viral samples was calculated using said calibration curve.

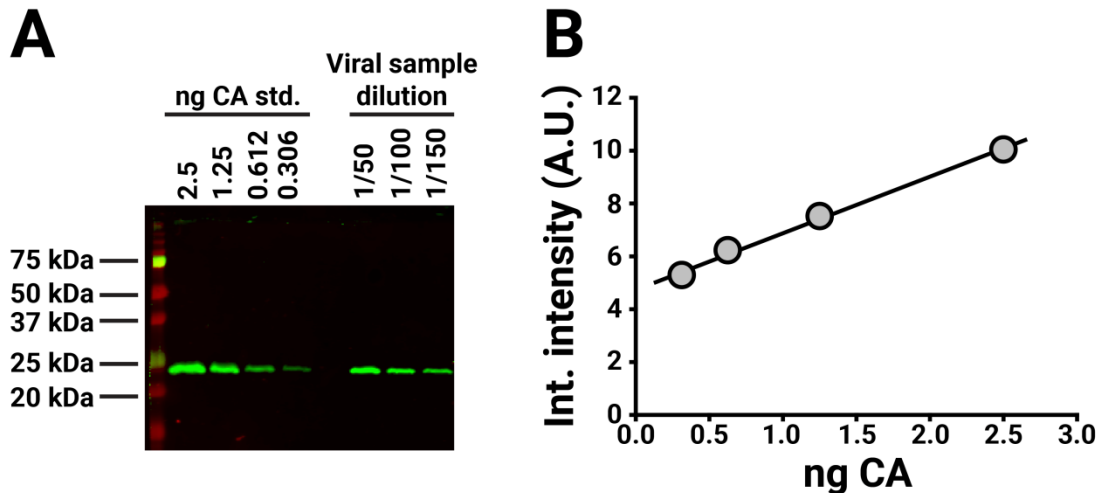


Figure 2.6 – Example of CA quantification by Western blot. A| A known amount of CA protein is loaded as a standard to generate a calibration curve. In the same Western blot, several dilutions of the viral sample are loaded. The Western blot is developed against CA as indicated. B| The integrated intensity of the samples in panel A is measured in the LI-COR Odyssey imaging system. The values of the CA standard are used to build a calibration curve, from which a regression curve is extracted to calculate the amount of CA in the viral sample dilutions.

2.7. Viral entry capacity

The entry capacity of the viral particles was determined by a BlaM Assay using the LiveBLAzer FRET-B/G Loading Kit with CCF2-AM from Thermo Fisher Scientific. For substrate incubation with the cells CO₂-Independent medium (Thermo Fisher Scientific) was used. Sample fluorescence was determined using a Synergy HT microplate fluorimeter (BIO-TEK).

Viral entry capacity was tested using infectious and non-infectious viral particles. This type of virus lacks the viral long-terminal repeat sequences, rendering the HIV-1 integrase unable of binding the viral cDNA, thus preventing integration. As a consequence, no virus replication occurs upon virus entry. These viral particles cannot be used to determine viral infective capacity, as infection requires the integration of the viral genome and its expression, but they constitute a great tool to study virus entry to the host cell as they contain Env, the protein mediating the host cell recognition and fusion of viral and cellular membranes. The main advantage of non-infectious viral particles is that they can be manipulated in a biosafety level 2 laboratory, unlike the infectious virions, whose manipulation require a biosafety level 3 laboratory.

In order to quantify virus entry to the host cell a fluorescence assay based on the β -lactamase enzyme (BlaM) is used (Cavrois et al., 2002). This method is based on the incorporation of β -lactamase-Vpr chimeric proteins (BlaM-Vpr) into the HIV-1 virions due to the Vpr accessory protein, and their delivery into the cytoplasm of target cells as a

result of virion entry. This transfer of BlaM-Vpr is then detected by enzymatic cleavage of the CCF2 dye, a fluorescent substrate of β -lactamase, loaded in the target cells. BlaM cleaves the β -lactam ring in CCF2, changing its fluorescence emission spectrum from green (520 nm) to blue (447 nm) and thereby allowing fusion to be detected by a fluorimetric measurement. A schematic overview of the process is shown in Figure 2.7.

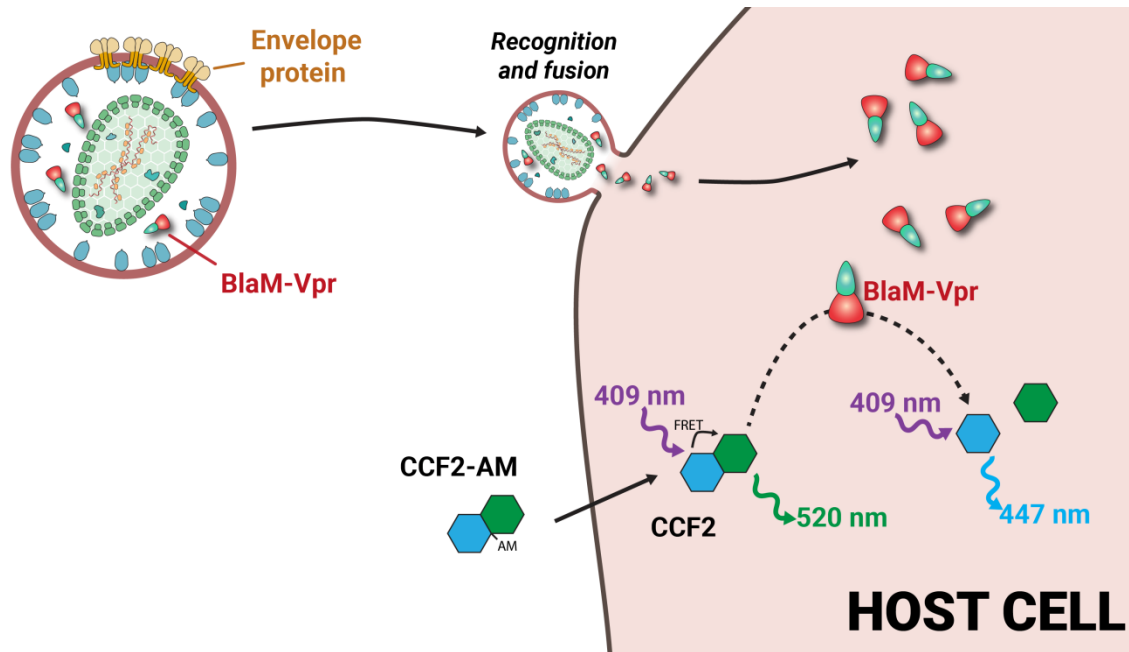


Figure 2.7 – Schematic representation of the basis of the BlaM-Vpr assay.

2.7.1. BlaM-Vpr viral particle production

To obtain virus containing BlaM-Vpr, for each of the gp41 variants one 10 cm dish of HEK 293T cells was cotransfected with infectious or non-infectious proviral DNA and the BlaM-Vpr expressing plasmid (pMM310) (Table 2.13). The BlaM-Vpr virions were concentrated with a sucrose cushion following the protocol showed in section 2.5.2.

Table 2.13 – Transfection conditions for the production of BlaM-Vpr containing non-infectious viral particles.

	10 cm dish / gp41 variant
Seeded cells	4·10 ⁶
Proviral DNA	10 µg
<i>--OR--</i>	
pCHIV Env(-) proviral DNA VSV-G or MLV Envelope expressing DNA	10 µg 2 µg
pMM310 BlaM-Vpr DNA	1 µg
CaCl₂ 0.25 M	1 mL
2x HBS	1 mL

After concentration the viral particles were resuspended in HeNa buffer and quantified by anti-CA Western blot.

2.7.2. BlaM-Vpr entry assay

The entry capacity of the viral particles containing the different gp41 variants was tested in HeLa TZM-bl and Jurkat E6-1 cells for particles expressing HIV-1 Env, and DJF8 cells for particles pseudotyped with MLV envelope. As a negative control of entry capacity AMD3100 was added to wt gp41 viral particles. AMD3100 functions by blocking the CXCR4 co-receptor engage essential for HIV-1 entry and has a very potent effect (Donzella et al., 1998), which can help to establish a background level of entry.

Once the BlaM-Vpr viral particles are purified and their CA concentration was determined, for each gp41 variant a BlaM-Vpr entry assay was set up:

1. A viral particle amount corresponding to the same CA quantity was added to a culture of either HeLa TZM-bl ($2 \cdot 10^4$ cells/well) or Jurkat E6-1 (10^5 cells/well) cells in a 96 well plate. AMD3100 was added to half of the wt gp41 viral particle assays as a negative control.
2. After a 15 minute centrifugation at 2,500 rpm the cells were incubated for 2.5 h in normal culture conditions to allow virus entry to the host cell.

In the meantime the loading solution for the BlaM-Vpr fluorescent substrate (CCF2) was prepared. To allow the entry of the probe to the host cell the commercial kit provides an esterified form of the CCF2, CCF2-AM. This lipophilic form of the substrate allows it to readily enter cells and, upon entry, cleavage by endogenous cytoplasmic

CHAPTER 2

esterases rapidly converts CCF2-AM into its negatively charged form, CCF2, which is retained in the cytosol:

1. According to the manufacturer's recommendations, for each 96 well plate 1 mL of 6x substrate loading solution is prepared (Table 2.14).

Table 2.14 – 6x Substrate loading solution.

Reagent	Description	Volume (µL)
Solution A	CCF2-AM	6
Solution B	Pluronic® -F127 surfactant	60
Solution C	PEG400, TR-40	934

2. The 6x Substrate loading solution was diluted to the final working concentration (1x) with CO₂-independent medium and kept from light until its use.
3. After incubation with the BlaM-Vpr viral particles the cells were washed with PBS and 60 µL/well of the 1x Substrate loading solution was added. At least six wells not seeded with cells were used as a control of the background emission from the loading solution.
4. Following incubation in the dark at room temperature for 15 h the relative fluorescence intensities of the samples was measured in a plate reader using the settings shown below (Table 2.15).
5. After subtraction of the background from the loading solution not incubated with cells, the ratio of emission intensities at 460/528 nm was calculated.

Table 2.15 – Fluorescence measurement conditions for the BlaM-Vpr entry assay.

Setting	Value
Sensitivity	75
Excitation	400(±30) nm
Emission	528(±20)/460(±40) nm

2.8. Viral infective capacity

The infective capacity of viral particles was studied by either single round infectivity assay based in the expression of luciferase as a reporter gene in the infected HeLa TZM-bl host cell, or by immunofluorescence against internal CA derived from production of viral progeny in MT-4 cells. For the luciferase reporter assay, HeLa TZM-bl reporter cells were infected with infectious viral particles containing different gp41 variants. This cell line contains a firefly luciferase gene (*luc*) whose expression is activated by the HIV-1 Tat protein. Upon virus entry, integration of genetic material and expression of viral genes in the reporter host cell, the synthesis of the HIV-1 Tat protein induces an expression of the *luc* gene and synthesis of the luciferase. The cells are then incubated with luciferin, a substrate of the luciferase and, when this luciferin is oxygenated by the enzyme to oxyluciferin, light is generated as a byproduct (Figure 2.8). By measuring the luminescence of the sample a relative luciferase activity can be determined, which is directly correlated with the amount of enzyme present in the cell and, thus, also correlated with the HIV-1 Tat protein amount in the host cell (Derdeyn et al., 2000).

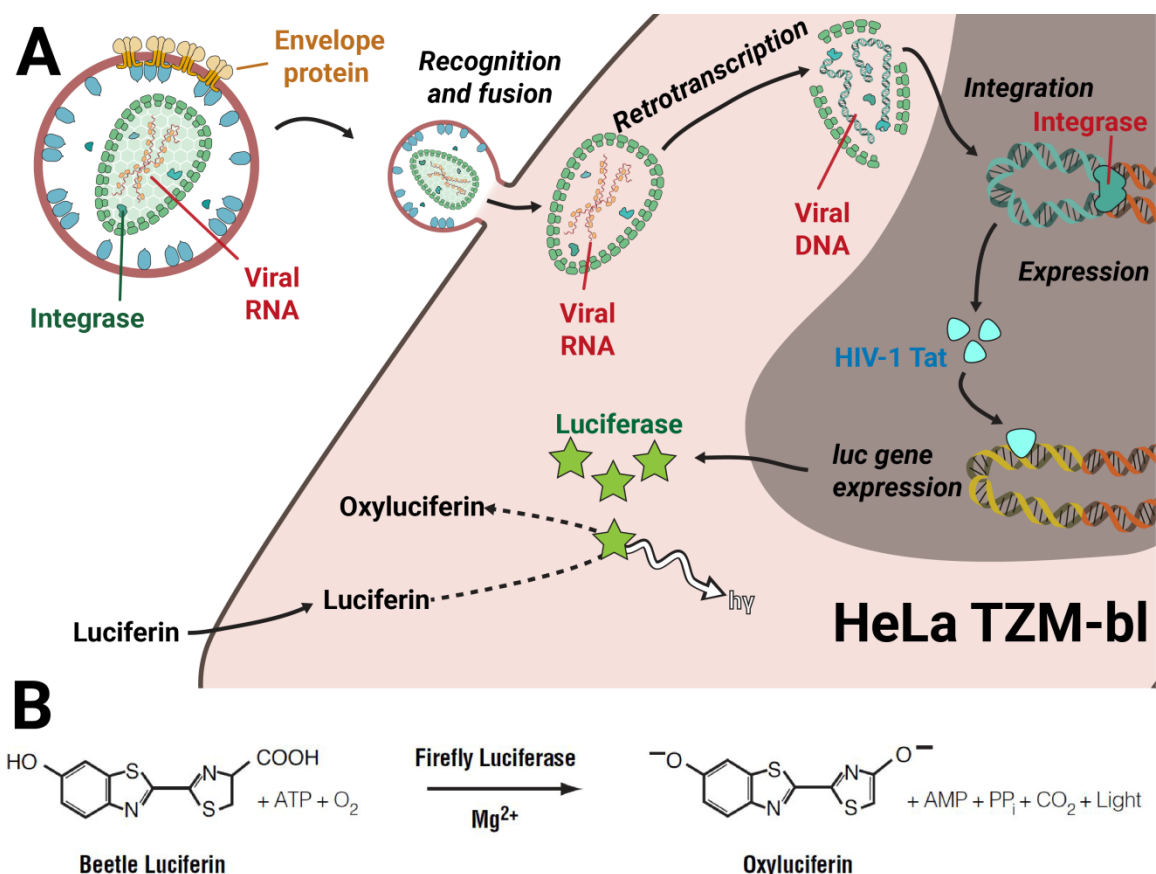


Figure 2.8 – Single round infectivity assay. **A** Schematic representation of the single round infectivity assay using luciferase as a reporter. **B** Mono-oxygenation of luciferin is catalyzed by luciferase in the presence of Mg²⁺, ATP and molecular oxygen, generating light.

2.8.1. Infective viral particle production

For this purpose infective viral particles were produced by cotransfection of HEK 293T cells with an Env expressing plasmid and the pNL4-3 Env(-) viral plasmid, which encodes for the rest of the viral proteins necessary for a complete infection of host cells. Infectivity experiments were carried out in a biosafety level 3 laboratory during a stay in Hans-Georg Kräusslich's laboratory in the University Hospital of Heidelberg, Germany. To obtain infectious viral particles, for each of the gp41 variants one 35 mm dish of HEK 293T cells was cotransfected (Table 2.16), and the virions were concentrated following the protocol showed in section 2.5.2 (Table 2.10).

Table 2.16 – Transfection conditions for the production of infectious viral particles.

	35 mm dish / gp41 variant
Seeded cells	0.5·10 ⁶
Infectious pNL4.3 Env(-) proviral DNA	2 µg
Env expressing DNA	0.8 µg
CaCl₂ 0.25 M	250 µL
2x HBS	250 µL

After concentration and resuspension, the infective viral particle yield was quantified by an anti-CA Western blot.

2.8.2. Single round infectivity assay

For the single round infectivity assays the following protocol was used (Muller et al., 2004):

1. TZM-bl cells ($1.2 \cdot 10^4$ cells/mL) were seeded 24 hours before infection in a 96-well plate.
2. Serial fivefold dilutions of the concentrated viral samples were used to infect the TZM-bl cells.

At 48 h post-infection, cells were lysed using a Steady-Glo Luciferase Assay System (Promega) and luciferase activity was measured in the lysates using a microplate luminometer (Luminoskan Ascent; Thermo LabSystems) according to the manufacturer's recommendation.

2.9. Lipid extraction

Lipids extracted from viral particles were used for lipidomic analysis and generation of liposomes. Lipids were isolated with a double extraction method (Brugger et al., 2006) using the following extraction mixture, which was prepared fresh the day of use. Around 2 ml of extraction mixture were needed for each sample (Table 2.17):

Table 2.17 – Lipid extraction mixture.

Reagent	Volume
Chloroform	6.22 ml
Methanol	12.44 ml
HCl 37% (v/v)	93 μ l

1. The volume of the aqueous viral sample was adjusted with water to 500 μ l, and transferred to a Teflon-cap glass tube (Tube A).
2. 1875 μ l of the extraction mixture was added to Tube A, followed by vortexing for at least 5 min.
3. 500 μ l of chloroform were added to the sample, followed by vortexing for 5 min.
4. 500 μ l of water were added to the sample, followed again by vortexing for 5 min.
5. Tube A was centrifuged at 500 *g* for 5 min at 4 °C. After phase separation, the organic phase in the bottom was collected from Tube A and transferred to a second tube containing 500 μ l of water, Tube B. This is a washing step to remove undesired molecules. Tube B was vortexed for 5 min.
6. Tube A was subjected to a second extraction, to ensure a better yield. 500 μ l of chloroform were added to Tube A followed by vortexing for 5 min.
7. Tube A and B were vortexed at 500 *g* for 5 min at 4 °C.
8. The washed organic phase in the bottom of Tube B was collected and stored in a third tube, Tube C.
9. The organic phase in the bottom of Tube A, corresponding with the second lipid extraction, was transferred to Tube B for washing.
10. Tube B was vortexed for 5 min and centrifuged at 500 *g* for 5 min at 4 °C.

11. The organic phase in the bottom of Tube B was collected and combined with the first extraction in Tube C.
12. Tube C contains the organic phases of the double extraction, in which most lipids from the sample have been extracted. Tube A will contain the majority of the molecules in the aqueous phase of the sample, including some gangliosides that are not suitably extracted with this method.

2.10. Liposome generation

Two types of liposome vesicles were used in this work: multilamellar vesicles (MLVs) and large unilamellar vesicles (LUVs). In both cases, liposome preparation started with the thin layer hydration method, to obtain MLVs. In the case of LUV formation, additionally an extrusion protocol was followed (Figure 2.9).

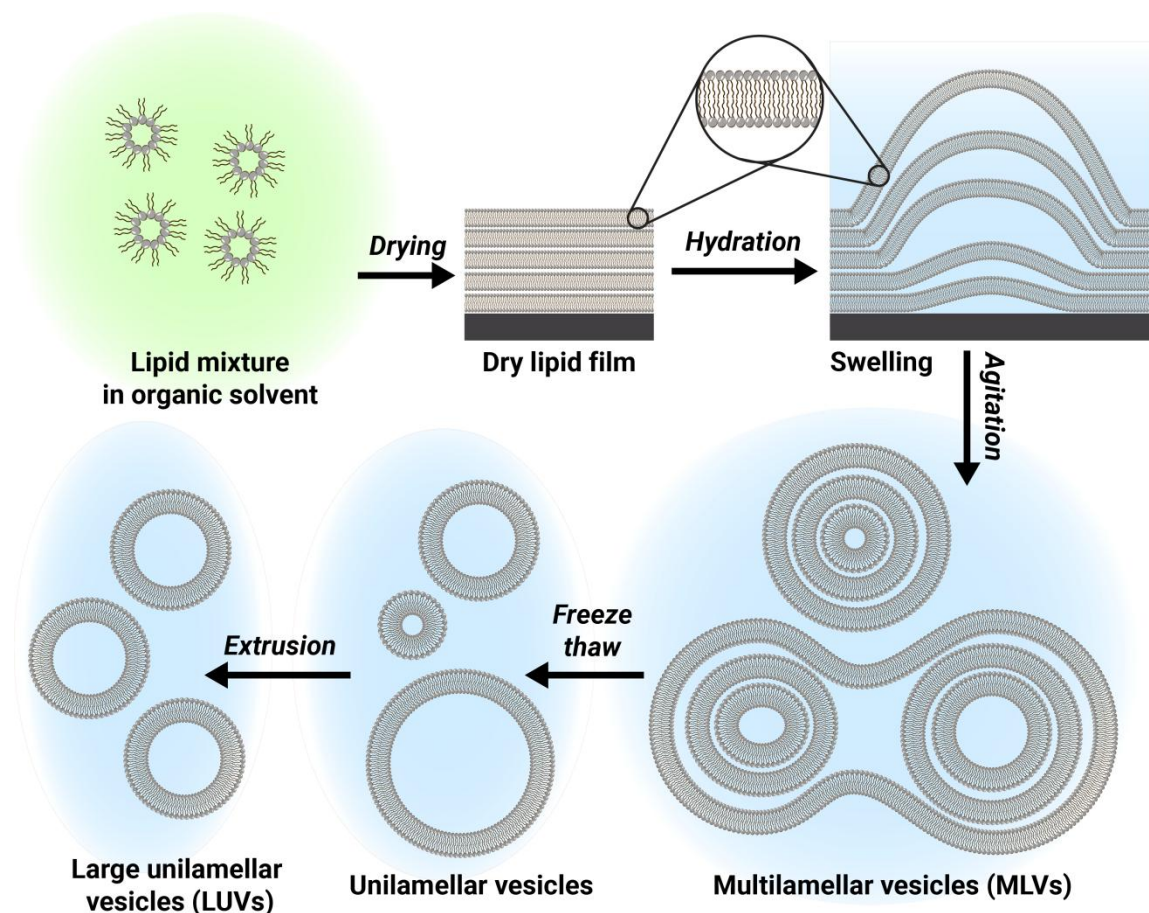


Figure 2.9 – Liposome formation by dry lipid film hydration and extrusion method.

Commercial lyophilized lipids dissolved in chloroform:methanol (2:1 vol:vol), and in the case of gangliosides in (1M NaOH):chloroform:methanol (0.15:2:1 vol:vol), were used as a lipid stock:

1. Depending on the final lipid composition of the liposome, appropriate volumes of each dissolved lipid were mixed.
2. The organic solvent was evaporated by constant gaseous nitrogen flux. During evaporation, the container was constantly rotated so that the lipid evenly distributes in its surface. The organic solvent was additionally evaporated under vacuum for 1 hour at room temperature until a thin layer of dried lipid formed in the tube.
3. The lipid layer was then resuspended in resuspension buffer (10 mM HEPES, 150 mM NaCl pH = 7.4) at a temperature 5 °C higher than the transition temperature (T_m) of the lipids in the mixture, to ensure that all of the lipids were in a liquid disordered state.
4. The hydrated mixture was then vigorously vortexed to induce the separation of the dry lipid from the tube and the formation of multilamellar vesicles (MLVs).
5. For unilamellar vesicle formation, the MLVs were subjected to repeated freeze and thaw cycles by submerging the tube in liquid nitrogen (-195 °C) for 1 minute, and thawing the sample in a water bath at 5 °C higher than the highest T_m of the lipids in the mixture, for a total of 10 cycles. After freeze and thaw cycles, unilamellar vesicles of a wide distribution of sizes were obtained.
6. For obtention of unilamellar vesicles of 100 nm of diameter, so called large unilamellar vesicles (LUVs), the extrusion based protocol was followed (Hope et al., 1985). The differently sized unilamellar vesicle samples were extruded through two polycarbonate membranes with a pore size of 100 nm (Nucleopore) at a pressure of 15 bar using an extruder, for a total of 10 cycles.

2.10.1. Lipid phosphorus concentration assay

After liposome generation, lipid concentration was calculated by quantification of phosphorus concentration in the samples, followed the rationale first developed by Fiske (Fiske and Subbarow, 1925) and later modified by Böttcher (Böttcher et al., 1961). The assay requires hydrolysis of the phosphorus in the phospholipids composing the liposomes, so it can then react with coloring agents and its concentration be measured by a colorimetry.

CHAPTER 2

1. A calibration curve is prepared using a reagent with a known concentration of phosphorus. In this case 0, 50, and 100 nmol of Na_2HPO_4 were pipetted into a glass test tube.
2. In parallel, a sample volume approximately corresponding to 50 nmol of phospholipids is also pipetted into a test tube.
3. 500 μl of 60% (v/v) HCl_4 were added to each tube, after which the samples are vortexed and heated to 200 °C for 45 minutes. Perchloric acid hydrolyzes the phosphorus in the phospholipid headgroups, releasing free inorganic phosphate.
4. The samples are cooled down to room temperature, and 4 ml of ammonium heptamolybdate solution (22 g $[(\text{NH}_4)_6\text{Mo}_7\text{O}_{24}\cdot 4\text{H}_2\text{O}]$, 143 ml H_2SO_4 , 857 ml H_2O) were added to each tube, followed by addition of 500 μl of 10% (v/v) ascorbic acid and vortexing. The molybdate reacts with the inorganic phosphate, and the complex reacts with ascorbic acid generating a yellow colored solution.
5. The tubes are heated to 100 °C for 7 min in a boiling water bath. The color of the solution shifts to blue in a phosphate-concentration dependent manner.
6. The samples are cooled down and the phosphate concentration is measured by absorbance at 812 nm in an Ultrospec 500 pro (Amersham Biosciences) spectrophotometer.
7. The absorbance of the standard solution was used to generate a calibration curve. The linear regression of the calibration curve was extracted and used to calculate the concentrate of phosphate of the samples.

Lipid molecules not containing phosphate, such as cholesterol or gangliosides, cannot be quantified by this method. In the case of liposomes composed by a combination of phospholipids and these lipids, phospholipid content of the liposomes was quantified by this method and cholesterol or gangliosides concentration was assumed to be proportional to the theoretical one.

2.11. Flow cytometry

Env localization studies in *Chapter 3*, and nanoparticle capture, J-lat reactivation, and platelet derived vesicle labeling in *Chapter 5* were analyzed by flow cytometry. Flow cytometry allows studying characteristics of individual cells or vesicles, giving information about their size, complexity, or fluorescent signal, by shining a light to the cells and recovering the transmitted, dispersed, or emitted light from the sample.

1. Forward Scattering (FSC). The detector is localized in front of the incident light, so it captures transmitted photons. It gives information about the size/volume relation of the cell or vesicle.
2. Side Scattering (SSC). The detector is localized perpendicular (at 90 °) from the incident light, so it captures dispersed photons.

Each type of cell or vesicle has a unique range of FCS and SSC values, so by blotting the FCS and SSC values of each individual cell or vesicle, different populations can be distinguished.

Quantification of Env signal in cells expressing viral proteins, and of nanoparticles capture by mDCs, transfer to J-lat, reactivation of J-lat cells, and labeling of platelet derived vesicles was carried out by measuring the fluorescent signal of the samples, which are detected by detectors perpendicular (at 90 °C) to the incident light. Depending on the measurement type, a different set of excitation lasers and emission detectors were used, which are detailed in each chapter.

2.12. Statistics

Experimental groups were compared and significance determined by analysis of variance and Tukey test, when more than two samples were compared, and by Student's t-test, when two samples were compared, using SigmaPlot. Data are represented as means with standard deviation (\pm SD) unless otherwise stated.

Chapter 3. Gp41-cholesterol Interaction Domain and Its Functional Implications

3.1. Introduction

The enrichment in the viral membrane of sphingomyelin and saturated species of phospholipids, together with the high concentration of cholesterol which constitutes up to 50% of the total lipid molecules in HIV-1 (Brugger et al., 2006; Lorizate et al., 2013), has led to its comparison with lipid nanodomains. This resemblance has also been observed in the structure of the viral lipid envelope which, similar to what is assumed for lipid rafts, displays an ordered lateral membrane structure (L_o phase) (Lorizate et al., 2009). These raft-like nanodomains which may exist in the virus have been described to be able to include or exclude certain proteins from specific regions of the membrane (Simons and Toomre, 2000) suggesting that these membrane structures may be regulators of the function of certain proteins in which a specific localization or association with other proteins is necessary.

Interestingly, the envelope glycoprotein of HIV-1 has been suggested to be associated with lipid rafts or related structures in both producer cells and budded virions in a cholesterol dependent manner (Bhattacharya et al., 2006; Yang et al., 2010). Although this conclusion is based in studies with DRMs, and this tool does not constitute an absolute probe for the partitioning of a protein to lipid rafts *in vivo*, or for the interaction of the protein with cholesterol (Thiele et al., 2000), they point towards an important role of cholesterol and lipid rafts in the function of the virus. Accordingly, depletion of cholesterol from the viral membrane (Campbell et al., 2002; Liao et al., 2001, 2003; Mañes et al., 2000) or cholesterol binding agents (Waheed et al., 2006, 2008) have been shown to result in a marked inhibition of the entry capacity of HIV-1 viral particles. Because cholesterol is one of the constituents of lipid raft nanodomains (Simons and Sampaio, 2011), the loss of entry capacity derived from depletion of the lipid could be related to a loss of nanodomain generation, which is analyzed in *Chapter 4* and the related published work (Nieto-Garai et al., 2018), or to an exclusion of Env from lipid raft nanodomains. It is important to note that the accumulation of Env into a single cluster is a necessary prerequisite for an efficient fusion between the viral and cellular membranes, as the loss of clustering capacity results in an inhibition of entry of the viral particles (Chojnacki et al., 2012). No clear mechanism has yet been proposed for the clustering of Env, but considering that it is suggested to be associated with lipid rafts in a cholesterol-dependent manner, and that lipid rafts have been described to be able to include or exclude certain proteins from regions of the membrane, interaction of Env with cholesterol, and by consequence with lipid nanodomains, may constitute the main mechanism by which clustering occurs.

The envelope glycoprotein is composed of two subunits, gp160 or surface glycoprotein, and gp41 or transmembrane glycoprotein. The transmembrane subunit anchors the protein to the viral membrane, so it follows that the interaction of Env with viral lipids involves gp41. This protein is divided into three main domains: ectodomain, transmembrane domain, and cytoplasmic domain, all of which have been described to have membrane interacting capacity. More specifically, a number of specific sequences

or regions in the three domains are suggested to be directly involved in the interaction of the protein with the lipid environment in the viral membrane.

Traditionally, the interaction of different domains of gp41 with specific lipids or membrane nanodomains has been carried out by the use of peptides derived from the full-length protein, or by the use of DRMs or liposome based systems. DRMs are thought to come from *in vivo* occurring lipid raft nanodomains after treatment of cellular membranes with non-ionic detergents and cold temperatures. They are enriched in certain lipids such as cholesterol and proteins commonly associated with it (Magee and Parmryd, 2003), and the presence of a protein in DRMs may constitute a first suggestion of its partitioning to lipid rafts or its interaction with cholesterol.

Some of the studies reporting an association between Env and DRMs found a specific region of the cytoplasmic domain to be involved. The cytoplasmic domain of gp41 harbors three amphipathic helicoidal sequences known as Lentiviral Lytic Peptides (LLP). The C-terminal LLP, dubbed LLP1, was first described in 1991 and was found to be highly conserved between strains and contain cytopathic properties (Miller et al., 1991). Later studies found that the LLP1 sequence was able to associate with membranes, and that this association was dependent in the highly conserved amphipathic nature of the peptide (Miller et al., 1993). A second highly conserved LLP sequence, LLP2, was also found in the cytoplasmic domain of gp41, and was also described to be helicoidal in nature and perturb membranes. Similarly to LLP1, comparison between strains suggested a strong selective pressure to conserve the amphipathic helical segment of the sequence (Srinivas et al., 1992). Finally, a third LLP sequence (LLP3) was found to be located between the other two in the sequence, and was again found to perturb lipid membranes by its association with them and to contain an amphipathic α -helix secondary structure (Kliger and Shai, 1997). Recent structural studies of the cytoplasmic tail of gp41 have confirmed that the three LLP domains acquire an α -helix structure and penetrate the membrane to varying degrees (Murphy et al., 2017) (Figure 3.1).

These LLP sequences play a very important role in the expression of Env to the cell surface (Bultmann et al., 2001) and its posterior incorporation into the virion (Murakami and Freed, 2000; Piller et al., 2000). Additionally, they have also been described to be important for Env stability (Lee et al., 2002) and multimerization (Lee et al., 2000), and perhaps more interestingly, to be key determinants of cell-to-cell and cell-free viral infectivity (Durham and Chen, 2015; Kalia et al., 2003). Of note, studies approaching the interaction of Env with membranes have reported that the last two thirds of the cytoplasmic domain, where the three LLP sequences are located, are capable of targeting the protein to DRMs (Yang et al., 2010), which could suggest a very important role of these LLP sequences in the selection of the lipid environment of Env. Additionally, studies with AME, which inhibits HIV-1 infection by binding viral membrane cholesterol (Waheed et al., 2006), found that HIV-1 strains evolved resistance to the compound by truncation of the cytoplasmic domain of gp41 (Waheed et al., 2007), further supporting that this domain is involved in the relation between cholesterol and infectivity.

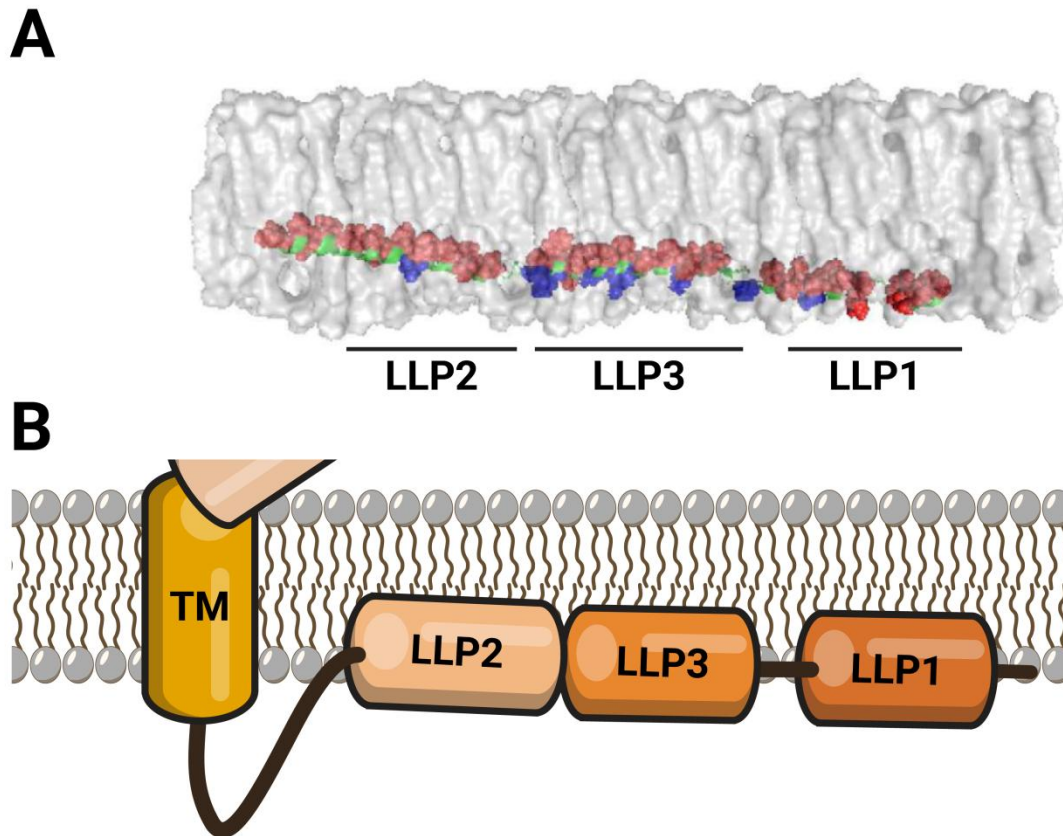


Figure 3.1 – Structure of the LLP sequences in the gp41 cytoplasmic domain. **A** Model of gp41 cytoplasmic domain bound to a lipid bilayer, with the amphipathic LLP sequences embedded in the membrane. In red, residues that interact extensively with the interior of the membrane, and in blue exposed residues that interact with the polar head. Modified from (Murphy et al., 2017). **B** Simplified representation of the three amphipathic LLP α -helices embedded into the viral membrane.

Interestingly, the interaction of gp41 cytoplasmic domain with specific lipid nanodomains could also be necessary for the efficient recruitment of the protein to nascent viral particles. During generation of new viral particles, Env molecules are synthesized in the rough endoplasmic reticulum and transported through the Golgi apparatus and the endomembrane system to the cellular plasma membrane. Because Gag clusters define the sites from which new viral particles will bud, for Env to be incorporated into the virion it must target the pre-assembled Gag lattice in the plasma membrane. The specific mechanism of this Env recruitment to nascent virions is not yet completely confirmed, but one of the proposed mechanisms relies on the targeting of Env to specific lipid nanodomains in which Gag assembly sites reside (Checkley et al., 2011). Indeed, a recent study analyzing the incorporation mechanism of proteins to HIV-1 particles demonstrated that the assembly of Gag into the plasma membrane initiates local accumulation of cholesterol in the region, and that membrane proteins sort actively into these HIV assembly sites based on their preference for localizing in ordered (L_o phase) domains enriched in cholesterol (Sengupta et al., 2019). Although the authors did not study the recruitment of HIV-1 Env specifically, other works have already shown that both Gag and Env interact with DRMs in the cellular plasma membrane (Bhattacharya et

CHAPTER 3

al., 2006; Hogue et al., 2011; Ono and Freed, 2001), heavily supporting that a lipid-based partition mechanism also exists for Env. Specifically, seeing that the gp41 cytoplasmic domain have been described to be necessary for targeting of Env to Gag assembly sites (Muranyi et al., 2013; Qi et al., 2013), and that it has been described to interact with DRMs (Yang et al., 2010), sorting of Env to domains rich in cholesterol could be regulated by the specific interaction of gp41 with the lipid.

The cytoplasmic domain of gp41 is not the only region to be proposed to interact with the viral membrane. Not surprisingly, the transmembrane domain is also an important candidate for the association of Env with lipids in the viral membrane, as it constitutes the canonically accepted membrane spanning domain, and as such it is surrounded by lipids in the viral membrane. This domain contains two sequences of special interest regarding the interaction with viral lipids: a GxxxG-motif and a highly conserved arginine residue. The GxxxG motif is a common occurrence in transmembrane proteins, and in the case of gp41 it has been described to play an important role in the dimerization and trimerization of the protein (Figure 3.2, orange). Accordingly, disruption of this GxxxG motif was described to induce a loss of infectivity of HIV-1, which is expected taking into account its role in protein oligomerization (Abad et al., 2009). Interestingly, more recently a GxxxG motif also present in the amyloid precursor protein was found to bind cholesterol (Barrett et al., 2012), and although no interaction between this motif and cholesterol has been found in gp41 up to date, it could point towards an involvement of this sequence in the interaction of the protein with membrane lipids. Another region of interest in the transmembrane domain is the highly conserved arginine residue localized in the membrane spanning domain (Figure 3.2, red). The presence of a polar amino acid in the hydrophobic core of the viral lipid bilayer has been tried to be explained by several models that propose that the residue snorkels towards the more hydrophilic interface of the lipid bilayer (Gangupomu and Abrams, 2010). Interestingly, molecular dynamic simulations have suggested that cholesterol may be involved in the solvation of the TMD arginine, which may suggest an involvement of the residue in the interaction with the lipid (Baker, 2014; Baker et al., 2014).

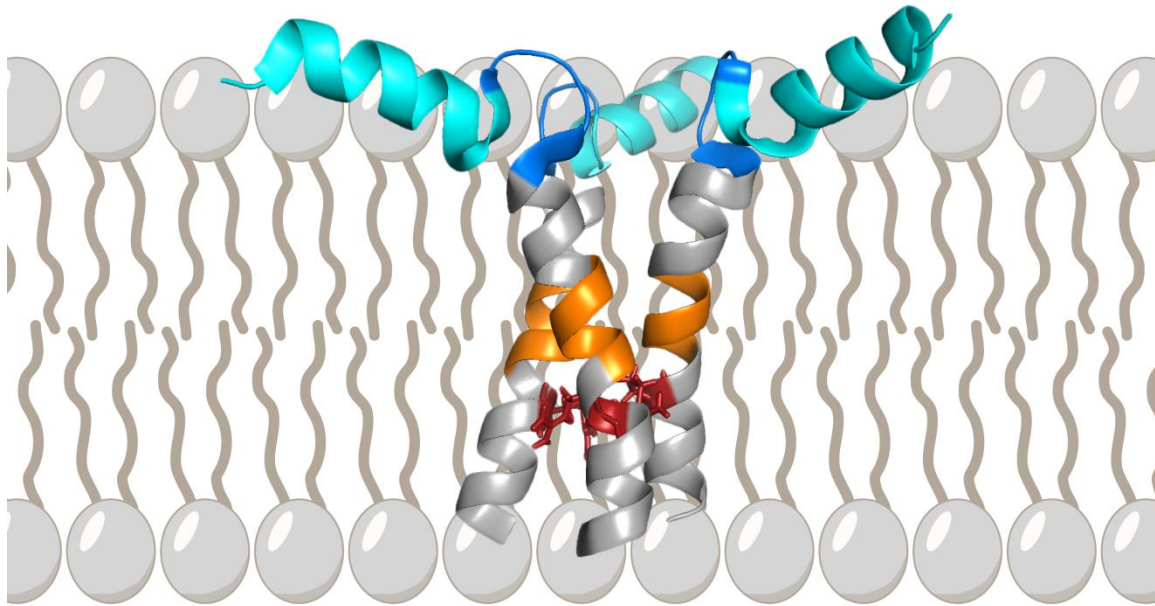


Figure 3.2 – gp41 MPER and transmembrane domain structure. Structure and localization of the gp41 MPER (cyan) and the CRAC sequence in it (blue); and the GxxxG-motif (orange) and the highly conserved arginine residue (red) in the TMD in relation to the viral membrane. Structural data was obtained from the 6DLN entry in the RCSB Protein Data Bank (Kwon et al., 2018). Viral lipid bilayer is represented in grey as a rough reference and does not constitute exact structural data.

Finally, the gp41 ectodomain harbors the MPER region flanking the membrane spanning sequence. This MPER has been described to partially insert in the membrane and to constitute a contiguous α -helix with the transmembrane domain (Apellániz et al., 2015; Nieva et al., 2011) (Figure 3.2, cyan), and harbors the epitope for several broadly neutralizing antibodies. Interestingly, these MPER-recognizing antibodies seem to bind epitopes occluded in the membrane interface, and the lipid environment of MPER have been shown to regulate this recognition (Klein et al., 2013; Molinos-Albert et al., 2017), indicating that a specific association of this sequences with viral membrane lipids may exist. Of special interest for the interaction of gp41 with lipids are the C-terminal five amino acid residues contiguous to the transmembrane domain, ${}_{677}\text{LWYIK}_{681}$, which constitute a sequence present in several proteins known as Cholesterol Interaction Aminoacid Consensus (CRAC) (Figure 3.2, blue). The CRAC sequence in the gp41 protein was found to bound cholesterol derivatives in *in vitro* experiments (Vincent et al., 2002; Vishwanathan et al., 2008), representing the first suggestion that this sequence may interact with cholesterol. Additionally, a disruption of CRAC that induced a loss of the fusion activity of the peptide (a L677I substitution) was also found to lose the cholesterol binding capacity of the sequence, suggesting a relationship between cholesterol binding and fusion capacity (Vishwanathan et al., 2008). Nevertheless, posterior studies suggested that the LWYIK sequence was not necessary for the association of gp41 with DRMs, challenging the previous data (Chen et al., 2009). It is important to note that none of the studies constitute absolute probe of the CRAC-dependent interaction of gp41 with cholesterol or lack of it, as the use of DRMs presents

some important handicaps when studying specific interactions (Thiele et al., 2000), and the *in vitro* studies of CRAC binding to cholesterol derivatives was carried out with a truncated protein lacking the transmembrane domain (Vincent et al., 2002), or small isolated peptides derived from the CRAC sequence (Vishwanathan et al., 2008), hardly resembling the *in vivo* situation.

Taking into account the importance of cholesterol in the fusion capacity of Env, and the wide variety of sequences and regions that have been described to interact with viral lipids, studying the specific interaction of Env with cholesterol could help elucidate the molecular mechanisms of the cholesterol dependence on infectivity of HIV-1, and provide new information about the lipid environment of Env laying the groundwork for the design of future therapeutic approaches. Nevertheless, as stated above most of the studies carried out in this regard are based in the use of DRMs, which do not constitute absolute probe of specific protein-lipid interactions or the *in vivo* localization of the protein in the cellular membrane (Thiele et al., 2000). Similarly, studies based in peptides derived from proteins, although giving information about the intrinsic membrane-interacting properties of the particular sequence, are not directly translatable to the interaction of that region with membrane lipids in the full-length protein.

The development of photoactivatable lipids in the last two decades has constituted a new tool for the specific study of the direct interaction between proteins and certain lipids. This wide set of cross-linking lipids developed throughout the years contain a diazirine group which, after irradiation with ultraviolet light, generates a highly reactive carbene group. The carbene group covalently binds to any molecule closer than 3 Å (2.5 times the diameter of a hydrogen atom), allowing the interaction of the photoactivatable lipid with specific molecules. Because of the high reactivity of the carbene group, the diazirine precursor in a photoactivatable lipid is usually designed to be localized in the hydrophobic interior of the lipid bilayer, since its presence in the more hydrophilic head group would result in the covalent binding of the carbene group with water molecules from the solvent, which would compete with the target protein for the photoactivatable lipid and hamper the study of the interaction. Photoactivatable cholesterol is one of the molecules available nowadays as a tool to study direct interactions of proteins with cholesterol and its properties, metabolism and distribution have been shown to be the same as the naturally occurring cholesterol counterpart (Haberkant et al., 2008; Thiele et al., 2000). This cross-linking molecule can be further functionalized by labeling it with a tritium atom, generating [³H]photocholesterol, which allows its easy detection and quantification (Figure 3.3A). Similarly, for the study of protein interaction with sphingolipids, the sphingolipid precursor analog [³H]-D-*erythro*-sphingosine is available (Figure 3.3B). Together, these two cross-linking lipids allow the specific study of the interaction of proteins with cholesterol and sphingolipids and its association with membrane domains enriched in said lipids, such as lipid rafts.

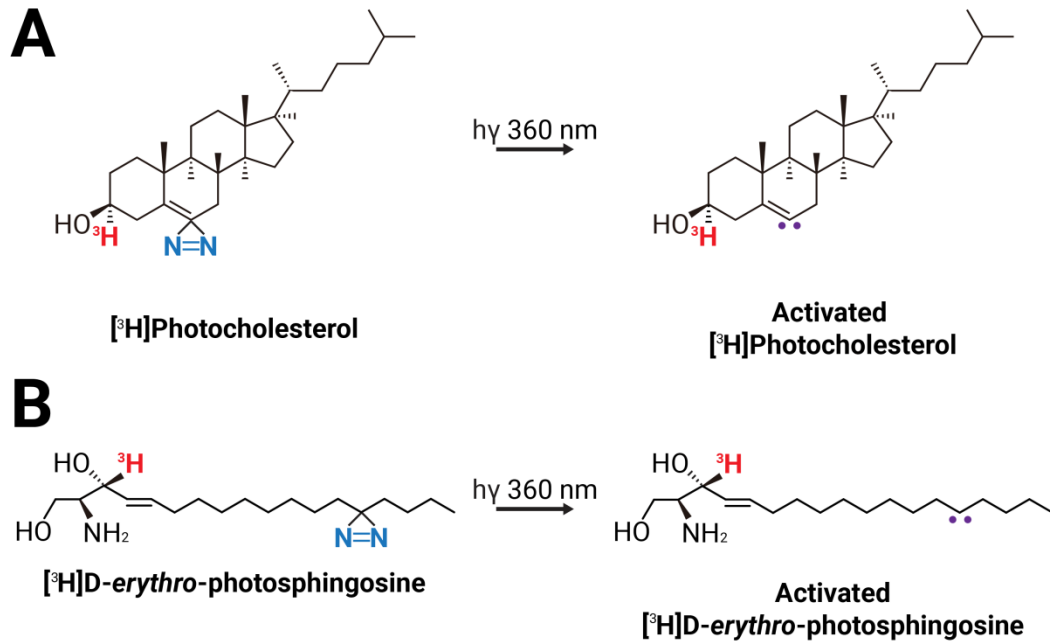


Figure 3.3 – Photoactivatable lipids. **A** Structure of tritium-labeled photoactivatable cholesterol analogue [³H]photocholesterol and **B** sphingolipid precursor [³H]D-erythro-photosphingosine. After irradiation with ultraviolet light (360 nm) the diazirine group (blue) of the photoactivatable lipids generates a highly reactive carbene group (purple) in their activated form, which covalently binds to any molecule closer than 3 Å. The tritium labeling (red) permits detection and quantification of the lipid.

In summary, although several sequences and regions of the gp41 protein have been described to interact with detergent resistant membranes and by extension with the related *in vivo* raft nanodomains, or with cholesterol specifically, no absolute probe has yet put forward in this regard. In this chapter, to elucidate the mechanism by which HIV-1 infectivity depends on viral membrane cholesterol, the interaction of gp41 with the lipid will be studied, for which photoactivatable lipids will be used as a tool to study specific protein-lipid interactions. Additionally, the specific cholesterol-interaction region of gp41 will be studied, which could generate new knowledge regarding the link between gp41 lipid environment and function, enabling generation of new targets for therapeutic approaches.

3.2. Experimental techniques

3.2.1. Chessie-8 coupling to beads

The anti-gp41 Chessie-8 antibody is used in the gp41-lipid interaction experiments for both for immunoprecipitating the protein and developing the Western blot against said protein. If the immunoprecipitation against the gp41 protein is carried out with a anti-gp41 Chessie-8 antibody non-covalently bound to the sepharose beads, when loading the immunoprecipitate in a SDS-PAGE, the antibody would also run in the gel along gp41 and, being the size of the heavy chain of the antibody (~50 kDa) very similar to that of gp41 (~41 kDa), the cross-recognition of the heavy chain by the secondary antibody used in the Western blot would interfere with the signal of the immunoprecipitated gp41 protein. As a consequence, the anti-gp41 Chessie-8 antibody was covalently bound to the sepharose beads to ensure that the heavy chain remains attached to the beads and does not run in the SDS-PAGE. The light chain of the antibody (~25 kDa) does not covalently bind to the beads with this procedure, so it runs free in the gel and get recognized by the secondary antibody, but its size is different enough from that of gp41 (~41 kDa) that it does not interfere in the immunoprecipitation result analysis.

For the covalent binding of the antibody to the beads, Protein G Sepharose 4 Fast Flow (GE Healthcare); Dymethyl pimelimidate Dyhydrochloride or DPM and ethanolamine (Fluka Biochemika); and CellPure® $\text{Na}_2\text{B}_4\text{O}_7$ and H_3BO_3 (Carl Roth) were used, with which the following buffers were prepared (Table 3.1):

Table 3.1 – Buffers used for the covalent coupling of the antibody to the beads.

Buffer	Composition
Borat buffer	0.2M $\text{Na}_2\text{B}_4\text{O}_7$ 0.2M H_3BO_3
DPM borat buffer	0.2M $\text{Na}_2\text{B}_4\text{O}_7$ 0.2M H_3BO_3 5.184 mg/mL DMP
Ethanolamine buffer	0.2M ethanolamine pH 8.0

3.2. Experimental techniques

The antibody coupled beads were prepared in batch following the protocol below:

1. 50 μL of the Protein G Sepharose beads were aliquoted and washed three times with 500 μL of 20 mM HEPES, 100 mM NaCl, 5mM EDTA, 0.5% (w/v) sodium deoxycholate, 1% (w/v) Triton X-100, adjusted to a pH of 7.4 lysis buffer by centrifugation at 13,000 rpm for 5 minutes.
2. 10 μg of the anti-gp41 chessie-8 antibody were then added to the washed beads and incubated overnight at 4°C with constant stirring to ensure a complete binding.
3. The samples were centrifuged at 13,000 rpm for 1 min to separate the beads bound to the antibody in the pellet from the free antibody in the supernatant.
4. The beads were washed two times with freshly prepared borat buffer (Table 3.1) as described above, resuspended in 1 mL of DPM borat buffer and incubated for 30 min at room temperature with continuous stirring.
5. The beads were then washed two times with freshly prepared ethanolamine buffer (Table 3.1) as before, resuspended in 1 mL of ethanolamine buffer, and incubated for 2 h at room temperature with stirring.
6. Finally, the beads were washed three times with 500 μL of lysis buffer and stored at 4°C until their use.

Two of the aliquots of the batch were used for testing and corroborating that the covalent binding was adequate. For this purpose, one of the aliquots was used to immunoprecipitate a viral sample containing wild type gp41 following the protocol in section 3.2.3.4, while the other aliquot was used as a negative control, which consisted in beads coupled to chessie-8 mixed only with sample buffer without any virus sample. Finally, beads mixed with the same amount of chessie-8 but not coupled to it were also loaded as a control of non-coupled beads. An adequate binding was considered when a clear gp41 protein band could be observed at ~41 kDa in the Western blot of the immunoprecipitated sample containing wild type gp41, while no antibody heavy chain band could be observed at ~50 kDa in the negative control. In both samples a ~25 kDa band can be observed corresponding to the antibody light chain, as the light chain is not covalently bound to the beads but it is recognized by the secondary antibody used (Figure 3.4).

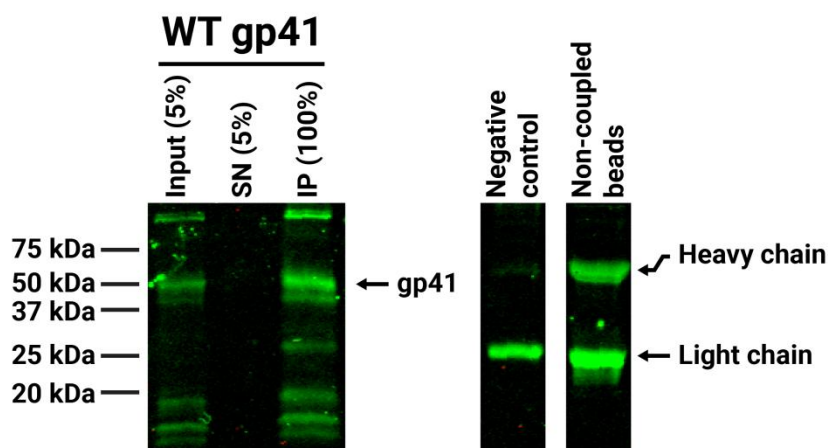


Figure 3.4 – Chessie-8 coupling to beads test. To test adequate coupling of the antibody to the sepharose beads, coupled beads were used to immunoprecipitate a viral or cellular sample containing wild type gp41. In parallel, coupled beads not mixed with any sample were used as a negative control. Beads mixed with the antibody but not coupled to it were also loaded as a control of non-coupled beads.

3.2.2. Viral particle purification

The viral particles used in this chapter for gp41-cholesterol interaction studies, lipidomic and proteomic analysis, and entry assays were purified following the general protocol in *Chapter 2*. Below, the specific transfection (Table 3.2) and viral particle concentration ultracentrifugation conditions are specified (Table 3.3). The viral particle purification by velocity gradient purification using Optiprep was carried out as described in *Chapter 2*.

Table 3.2 – Transfection conditions for each type of experiment in this chapter.

	10 cm dish
Seeded cells	$4 \cdot 10^6$
Proviral DNA	10 μ g
CaCl ₂ 0.25 M	1 mL
2x HBS	1 mL

Table 3.3 – Ultracentrifugation conditions for viral particle concentration in the experiments in this chapter.

Tubes and rotor	SW 28.1
Ultracentrifuge	Optima L-100 XP
20% sucrose volume/tube (mL)	6
Sample volume/tube (mL)	30
Rotor speed (rpm)	25,000
Avg. G-force (g)	85,000
Time (minutes)	120

3.2.3. Protein-lipid interaction studies

3.2.3.1. Photoactivatable lipid radioactive labeling

For the gp41-lipid interaction experiments radioactively labeled photoactivatable lipids were used. Photoactivatable lipids were chemically synthesized by Dr. F.-Xabier Contreras (Instituto Biofisika, Spain), and labeled with radioactive tritium to allow their detection and quantification following an established protocol (Thiele et al., 2000):

1. 2.5 mg of photocholesterol dissolved in 1 ml tetrahydrofuran was added to 25 mCi of tritiated sodium borohydride ($[^3\text{H}]\text{NaBH}_4$) (Amersham Biosciences) dissolved in 1 ml of 0.1M NaOH. The mixture was stirred at room temperature for 16 h to induce photocholesterol labeling with radioactive tritium.
2. 300 μl of 1N HCl was added to the mixture above and stirred for 15 min. The mixture containing tritiated photocholesterol was extracted twice with 1 ml ethyl acetate ($\text{CH}_3\text{-COO-CH}_2\text{-CH}_3$).
3. The combined organic phases from the double extraction were partially evaporated to reduce the volume to 250–300 μl , and subjected to a thin layer chromatography. The mobile phase was a mixture of hexane/ethyl acetate (2:1 vol:vol).
4. The TLC plate was dried and radioactive bands were visualized by phosphorimaging. Two products were detected: $[^3\text{H}]$ photocholesterol and its α -epimer with higher mobility (in a 9:1 ratio).
5. The TLC plate was sprayed with water to prevent dispersion of radioactive dust, and the bands corresponding to $[^3\text{H}]$ photocholesterol were scraped from the plate and collected.

6. [³H]photocholesterol was purified from the silica dust with four consecutive extractions using 800 µl ethanol. [³H]photocholesterol concentration was determined by a scintillation counter and stored at -20 °C.

[³H]photocholesterol allows studying specific *in vivo* interactions as it contains a photoactivatable diazirine group, producing a highly reactive carbene upon UV irradiation which covalently binds to any molecule closer than 3 Å (Contreras et al., 2012; Haberkant et al., 2008; Thiele et al., 2000) (Figure 3.3). Thus, by immunoprecipitating the studied protein, if any radioactively labeled lipid molecule has cross-linked with it, it can easily be detected by measuring the radioactivity of the sample. Radioactively labeled photoactivatable sphingolipid precursor [³H]-D-erythro-sphingosine was synthesized and radioactively labeled by Dr. F.-Xabier Contreras (Instituto Biofisika, Spain).

3.2.3.2. Photoactivatable lipid incorporation in cells

For radioactively labeled photoactivatable lipid addition to the cell culture delipidated medium was used, as to enhance photoactivatable lipid absorption by avoiding competition from other lipids in the medium. The delipidated medium was prepared using DMEM GlutaMAX™ High glucose culture medium supplemented with 10% delipidated FBS, and 100 U/mL Penicillin-Streptomycin.

Lipid incorporation quantification was carried out by extraction of cellular lipids and quantification of radioactivity in a liquid scintillation counter, and [³H]photocholesterol metabolism was determined by a thin layer chromatography. For quantification of radioactively labeled lipid incorporation into the cells, HEK 293T cells seeded in a 35 mm well were incubated with 10 µCi [³H]photocholesterol at different times, scraped and centrifuged at 5,000 rpm for 2 min. The pelleted cells were resuspended in 100 µl of methanol and 10 µl of water, and vortexed vigorously. The samples were centrifuged at 14,500 rpm for 15 min to induce separation of the aqueous and organic phases. The upper organic phase containing the extracted lipids was collected, and 10 µl of it were mixed with 2 ml of PCS liquid scintillation cocktail (Amersham Biosciences) in a scintillation counter tube. Disintegrations per minute (DPM) data of the sample was obtained in a Tri-Carb 2900TR (Perkin Elmer) liquid scintillation counter, and the radioactive signal in µCi was obtained using the following formula:

$$1 \mu Ci = 2.2 \times 10^6 \text{ DPM}$$

For lipid metabolism analysis, HEK 293T cells were treated in the same way as above with [³H]photocholesterol or [³H]D-erythro-photosphingosine. At different time points, cells were collected and their lipids extracted. A sample volume of extracted lipids corresponding to 0.025 µCi was loaded into a thin layer chromatography (TLC). A mixture of chloroform:methanol:water (65:25:4 vol:vol) was used as a mobile phase, and

3.2. Experimental techniques

the TLC was run for approximately 1 h. After the mobile phase had reached ~80% of the length of the silica-coated aluminium sheet, the TLC was dried and the radioactive bands were developed by autoradiography in a BetaIMAGER™ (Biospace Lab) for approximately 18 h or less.

For protein-lipid interaction studies in cells, HEK 293T cells seeded into a 10 cm dish were transfected with either a proviral or Env expressing plasmid as described in *Chapter 2*. 18 h post-transfection, 100 μ Ci of photoactivatable lipid was diluted in 8 ml of culture medium containing delipidated FBS and added to the transfected cells. The photoactivatable lipid was incubated with the cells for 8 h, after which the medium was removed, the cells were washed with PBS, and cold PBS supplemented with protease inhibitor cocktail was added. Cells were then irradiated for 5 min with UV light to induce lipid cross-linking. These cells were then scraped, pelleted, and resuspended in 200 μ l of lysis buffer (Figure 3.5) for posterior gp41 immunoprecipitation, which is detailed in section 3.2.3.4.

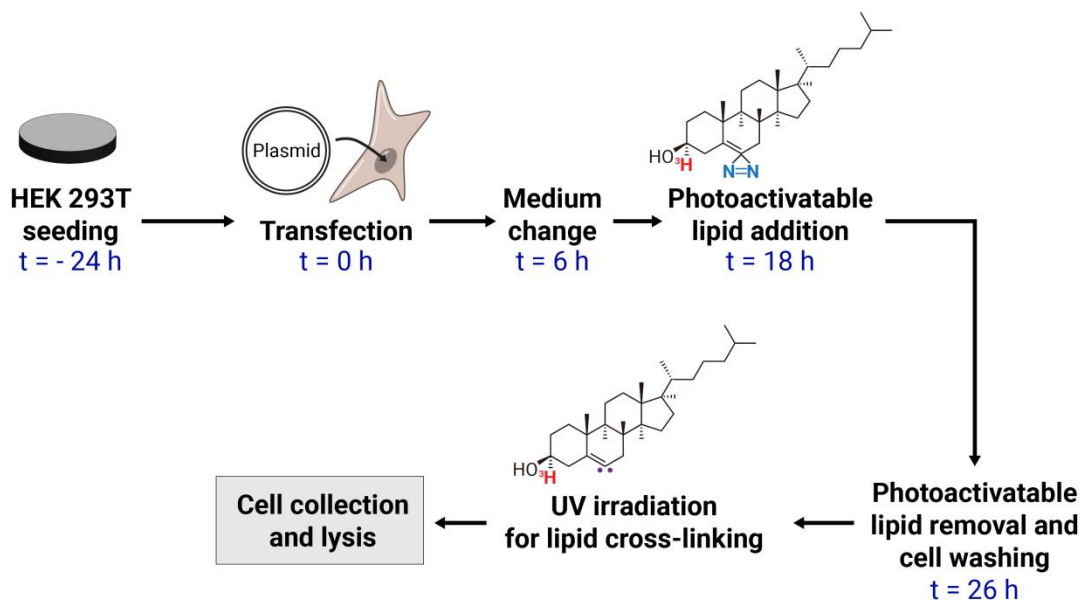


Figure 3.5 – General principle and workflow of protein-lipid interaction studies in cells.

For the study of protein interaction with [3 H]photocholesterol in cells positive and negative controls were used. As control of positive interaction with cholesterol, the caveolin-1 (Cav-1) protein was used. HEK 293T cells were seeded into a 10 cm dish and transfected with 10 μ g of Cav-1-GFP expressing plasmid with the calcium phosphate method already detailed in *Chapter 2*. 18 h post-transfection, 100 μ Ci of [3 H]photocholesterol were added to the cells in delipidated medium, and incubated for an additional 8 h. Cells were then washed, irradiated with UV light for 5 min, lysed with lysis buffer, and immunoprecipitated against the GFP tag:

CHAPTER 3

1. 50 μ l of Protein A sepharose beads were washed extensively with lysis buffer, and mixed with 5 μ g of rabbit anti-GFP ChIP Grade antibody (Abcam). The cell lysate was then added to the beads and antibody mixture and incubated overnight at 4 °C in constant mixing.
2. The sample was then immunoprecipitated by centrifugation and washed extensively. 50 μ l of sample buffer was added to the sample and incubated at 95 °C for 5 min to release the immunoprecipitated protein.

In parallel, the transferrin receptor (TfR) protein was used as a negative control, as it constitutes the archetypal non-lipid raft marker (Magee and Parmryd, 2003). In the case of the transferrin receptor endogenous protein was used, so HEK 293T cells were seeded into a 10 cm dish, and 100 μ Ci of [³H]photocholesterol were added for 8 hours. The cells were then collected, lysed as above, and immunoprecipitated against transferrin receptor:

1. 50 μ l of Protein G sepharose beads were washed extensively with lysis buffer and mixed with 5 μ g of rabbit anti-transferrin receptor antibody (Santa Cruz Biotechnologies). The cell lysate was then added to the beads and antibody mixture and incubated overnight at 4 °C and constant mixing.
2. The sample was immunoprecipitated and incubated with sample buffer following the same protocol as for Caveolin-1.

The immunoprecipitated caveolin-1 and transferring receptor were then loaded into an SDS-PAGE gel and a Western blot was carried out against the caveolin-1 and transferring receptor proteins following the general Western blot protocol.

1. For caveolin-1 detection, the membrane was incubated with a rabbit anti-caveolin-1 antibody (Abcam) at a 1:1,000 dilution for 1 h, followed by washing and incubation with anti-rabbit IRDye680 (LiCor) secondary antibody at a 1:10,000 dilution for 45 min.
2. For transferrin receptor detection, the membrane was incubated with mouse anti-transferrin receptor antibody (Abcam) at 1:1,000 dilution for 1 h, followed by washing and incubation with anti-mouse IRDye800 (LiCor) secondary antibody at a 1:10,000 dilution for 45 min.
3. Detection of the proteins was carried out using the LI-COR Odyssey imaging system.

The membrane was then dried and the radioactive lipid signal was visualized by autoradiography of the membrane as explained in section 3.2.3.5 below.

3.2.3.3. Photoactivatable lipid incorporation in virus

For protein-lipid interaction studies in virus, HEK 293T seeded 10 cm dishes were transfected with proviral plasmids as described in *Chapter 2*, and 100 μCi of [^3H]photocholesterol was added to the cells as before. The photoactivatable lipid was incubated with the cells for 24 hours to ensure lipid incorporation into the released virions. Viral particles are generated which bud from the cells acquiring the viral lipid envelope from the cellular plasma membrane, thus recruiting the photoactivatable lipids along with other cellular lipids present in said plasma membrane. As a result, the cell culture supernatant will contain viral particles with photoactivatable lipids in their lipid envelope. Before viral particle concentration and purification, the clarified cell culture supernatant containing the viral particles was irradiated in a petri dish with UV light for 5 min at 4°C, to induce cross-linking between the reactive group of the lipid and any molecule closer than 3 Å. Once irradiated, the viral particles were concentrated and purified following the protocols shown in *Chapter 2* and section 3.2.2 of this chapter. The viral particle purification yield was determined by anti-CA Western blot and their protein content characterized by Silver stain. A general overview of the workflow for obtaining purified viral particles containing photoactivatable lipids is shown in Figure 3.6.

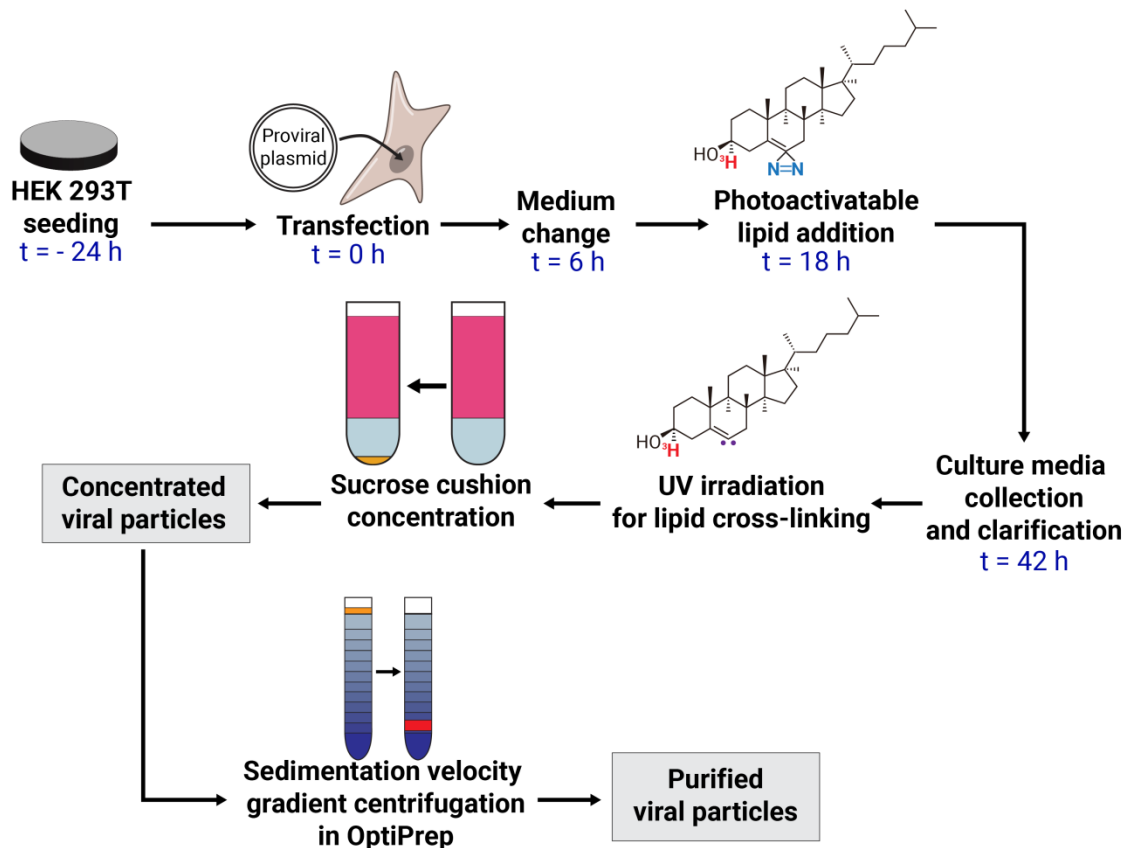


Figure 3.6 – General principle and workflow of purification of viral particles containing cross-linked photoactivatable lipids.

After viral particle characterization, the sample was mixed with 100 μ l of lysis buffer for gp41 immunoprecipitation, which is detailed below.

3.2.3.4. gp41 protein immunoprecipitation

For cell and viral particle lysis a modified RIPA buffer was used, composed of 20 mM HEPES, 100 mM NaCl, 5mM EDTA, 0.5% (w/v) sodium deoxycholate, 1% (w/v) Triton X-100, adjusted to a pH of 7.4. The lysis buffer was supplemented with cOmplete™, EDTA-free Protease Inhibitor Cocktail (Sigma-Aldrich) prior to use to avoid degradation of proteins. Cells and virus samples were resuspended in up to 200 μ l of lysis buffer supplemented with protease inhibitors and incubated for 1 h at 4°C in constant rotation.

After the obtention of cells and viral particles containing cross-linked radioactively labeled lipids, the gp41 protein was immunoprecipitated as to evaluate the presence of radioactive lipids cross-linked to the protein:

1. For viral particles, a virus amount equivalent to 1 μ g of CA was mixed with 100 μ L of lysis buffer and lysed for 1 h at 4°C in constant spinning. For cells, all of the cells from a 10 cm dish were mixed with 200 μ l of lysis buffer and lysed in the same conditions.
2. The lysed samples were centrifuged at 13,000 rpm for 5 min to pellet the non-lysed debris. An aliquot of the supernatant was stored as an input.
3. The rest of the supernatant was mixed with 50 μ L of Protein G Sepharose beads covalently coupled to 10 μ g of anti-gp41 chessie-8 antibody. The samples were incubated overnight at 4°C in constant spinning with the beads to ensure a proper recognition between the anti-gp41 chessie-8 antibody and gp41.
4. The samples were then centrifuged at 6,500 rpm for 5 min to pellet the beads and immunoprecipitate the protein, and the supernatant was stored as non-immunoprecipitated sample. The beads were washed three times with 500 μ L lysis buffer by centrifugation at 6,500 rpm for 5 min.

The input, non-immunoprecipitated and immunoprecipitated samples were loaded into an SDS-PAGE gel to detect the presence of gp41:

1. An aliquot of the input and non-immunoprecipitated samples corresponding to 5-10% of the total sample was mixed with 30 μ L of 6x SDS-PAGE sample buffer and heated to 95°C for 5 min.
2. 50 μ L of 6x SDS-PAGE sample buffer were also added to the beads and heated in the same manner to induce dissociation between the anti-gp41 antibody covalently bound to the beads and the immunoprecipitated gp41 protein.

3. After incubation with SDS-PAGE sample buffer the beads were centrifuged at 6,500 rpm for 10 min, separating the now free gp41 protein (in the supernatant) from the beads and the bound antibody (pellet).
4. The input and non-immunoprecipitated samples and the immunoprecipitated gp41 protein were then loaded into a SDS-PAGE gel as explained in *Chapter 2* and the blots were probed with the Chessie-8 mouse anti-gp41 primary antibody diluted at 1:2,000 in Odyssey Blocking Buffer overnight at 4°C.
5. gp41 protein bands were detected using the LI-COR Odyssey imaging system after probing with anti-mouse IRDye800 at 1:10,000 for 45 min at room temperature. Protein bands were visualized using the Odyssey infrared imaging system (LI-COR) and quantified using the instrument software and the integrated intensity signal of the bands corresponding to gp41 was determined.

3.2.3.5. Autoradiography and protein-lipid interaction quantification

In order to identify the presence of radioactive lipids cross-linked to the gp41 proteins in the immunoprecipitated samples, the Western blot membranes used in the previous section were dried and the radioactive lipid signal was visualized by autoradiography of the membrane in a BetaIMAGER™ (Biospace Lab) for up to 18 hours.

If a radioactive lipid signal band was detected which colocalized with the gp41 protein band shown in the Western blot, its intensity was measured as cpm/mm² using the instrument software. The protein-lipid interaction was quantified as a ratio between the colocalizing radioactive lipid signal obtained from autoradiography in the BetaIMAGER™ (in cpm/mm²) and the gp41 protein signal obtained from the anti-gp41 Western blot (in arbitrary fluorescence units). The lipid-protein signal ratios of each gp41 variant were normalized to the wild type gp41 for quantification and comparison.

3.2.4. gp41 protein quantification

The effect of the different mutations in the recruitment of Env to the nascent viral particles was analyzed by quantification via Western Blot of the gp41 protein in purified viral particles. Because no suitable envelope protein standard was available no absolute values could be obtained for the Env quantity in each variant. Instead, the relative gp41 quantity in each variant was normalized to the wild type particles. In order to achieve this, the same amount of viral particles would have to be loaded into an SDS-PAGE for each variant in order to obtain a legitimate comparison. Nevertheless, the purified viral particle method based on the anti-CA Western blot has some intrinsic variability. To ensure that the comparison was as fitting as possible, instead of loading a single

purified virus quantity for each variant and then comparing the gp41 signals obtained in a Western blot to those of wild type, several viral amounts obtained by a serial dilution were loaded for each sample (Figure 3.7A).

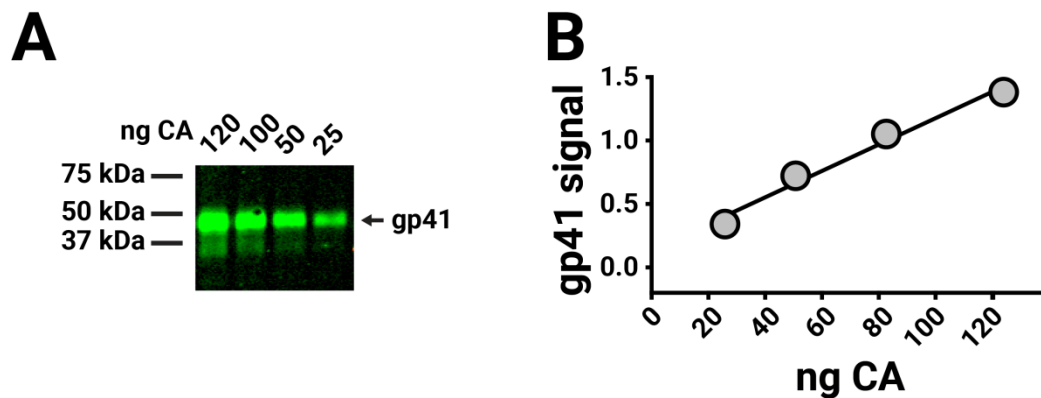


Figure 3.7 – Example of Env quantification by Western blot. **A|** Several known amounts of viral sample (expressed as ng of CA) are loaded. The Western blot is developed against Env as indicated. **B|** The integrated intensity of the samples in panel A is measured in the LI-COR Odyssey imaging system and plotted against the ng of CA loaded into each sample.

By plotting the intensity of the gp41 bands against the loaded virus amount, a linear regression curve can be obtained for each variant (Figure 3.7B), in which the equation of the line corresponds with:

$$y = ax + b$$

$$a = (y - b)/x$$

where y is the gp41 signal, x the ng of CA loaded, a the slope of the linear regression curve, and b the y-intercept of the line, so that:

$$\text{Slope } (a) = \frac{\text{gp41 signal} - b}{\text{ng CA loaded}}$$

Thus, the slope of this linear regression curve corresponds to the gp41 / CA ratio following the equation of a line. This way, even with the possibly existing variability in the viral particle quantification carried out by the anti-CA Western blot, by comparing the relative slopes of the linear regression curve of each variant a reliable relative Env quantity can be obtained. The protocol was carried out as follows:

1. Independent ultrapure viral purifications were carried out for each of the gp41 variants, and their CA concentration was analyzed by anti-CA Western blot.
2. Once the CA concentration of the samples was determined, virus amounts of each variant corresponding to different CA amounts (120, 100, 50 and 25 ng) were loaded in a SDS-PAGE following the protocol *Chapter 2*, and the blots were probed with the Chessie-8 mouse anti-gp41 primary antibody at 1:2,000 overnight at 4°C.

3. gp41 protein bands were detected using the LI-COR Odyssey imaging system after probing with anti-mouse IRDye800 secondary antibody at 1:10,000 for 45 min at room temperature. Protein bands were visualized using the Odyssey infrared imaging system (LI-COR) and quantified using the instrument software.
4. The integrated intensity signal of the bands corresponding to gp41 was determined. For each variant, a regression curve between the CA amount loaded and the gp41 band signal detected was established.
5. With the slope of said regression curve, a ratio between the gp41 band signal and the CA amount loaded was calculated. The ratios were normalized to the wild type values, thus obtaining a relative gp41 per CA protein ratio for each variant compared to the wild type viral particles.

3.2.5. Proteomic studies

The protein-lipid interaction experiments presented in this thesis require the immunoprecipitation of the gp41 protein, as described in section 3.2.3.4. To corroborate that the immunoprecipitated protein is the gp41 protein from HIV-1, and thus to confirm that the interaction experiments refer to the correct protein, a proteomic analysis of the gp41 protein immunoprecipitated from purified viral particles was carried out.

Following the protocol for viral particle purification from *Chapter 2*, HEK 293T cells seeded in 24 10 cm dishes were transfected with a proviral plasmid expressing the wild type viral proteins (pCHIV). 48 hours post-transfection, the cell culture supernatant was collected, clarified, and viral particles were concentrated and later purified. The purified viral particles were then lysed and gp41 was immunoprecipitated from the samples using Protein G Sepharose beads coupled to anti-gp41 chesie-8 antibody, as explained before.

The immunoprecipitated sample was loaded into two adjacent wells in a SDS-PAGE in order to load the entire sample, and an electrophoresis was carried out as described previously. The gel was then stained with Coomassie blue staining solution for 10 minutes at room temperature under constant agitation, and developed with destaining solution for approximately 1 hour at room temperature and agitation. The composition of the solutions is detailed in Table 3.4, for which Brilliant Blue Coomassie G-250 was obtained from Thermo Fisher Scientific.

Table 3.4 – Composition of the solutions used for the Coomassie stain of SDS-PAGE gels.

Solution	Composition
Staining	37% C ₂ H ₅ OH (v/v) 9% CH ₃ COOH (v/v) 2.45 mg/ml Brilliant Blue Coomassie G-250
Destaining	10% C ₂ H ₅ OH (v/v) 10% CH ₃ COOH (v/v)

The observable band of an apparent ~41-50 kDa of size, which is assumed to correspond with gp41, was cut from the gel and stored in a sterile microcentrifuge tube. The gel band containing the protein was then sent to the Proteomics Service of SGIKER (UPV/EHU), where the protein was extracted from the gel, digested with trypsin, and deglycosylated with Peptide-N-Glycosidase F. The deglycosylated tryptic peptides obtained from the protein extracted from the SDS-PAGE were then analyzed by a Q Exactive™ Hybrid Quadrupole-Orbitrap™ mass-spectrometer coupled to a EASY nLC1000 (ThermoFisher Scientific) liquid chromatography. The m/z ratio of the detected peptides was compared to a database containing human proteome and HIV-1 isolate BH10 protein sequences. Comparison of the extracted peptides to the database revealed a number of peptides spanning different regions of the HIV-1 gp41 protein.

3.2.6. Lipidomic studies

The composition analysis of viral membrane lipids was carried out with purified viral particles. For this purpose, HEK 293T cells were transfected with the corresponding plasmid and viral particles were purified from the cell culture supernatant as described in *Chapter 2*. After viral particle characterization and CA quantification, 500 µl of methanol (CH₃OH) was added to each sample, and vortexed vigorously before storing at -20 °C. The samples were sent to Dr. Gemma Fabriàs and Dr. Josefina Casas of the Research Unit on BioActive Molecules (RUBAM) in Instituto de Química Avanzada de Cataluña (CID-CSIC, Barcelona, Spain) for characterization of their lipid content by mass spectrometry analysis.

3.2.7. Env localization studies

gp41 localization in cells was determined by FACS analysis. HEK 293T were seeded in 24 well plates (Sarstedt), and transfected either with a proviral or Env only expressing plasmid with the calcium phosphate method. 24 hours post-transfection, the cell culture supernatant was removed, cells were washed with PBS, scraped carefully and

3.2. Experimental techniques

transferred into a microcentrifuge tube. Cells were fixed with 3% (w/v) paraformaldehyde for 10 min at room temperature, and were either permeabilized or not with 0.1% (w/v) Triton X-100 in PBS for 2 min at room temperature. Then, cells were blocked with 2% (w/v) BSA in PBS for 30 min at room temperature and, after washing with PBS, stained against envelope protein for 30 min at room temperature with 2G12 anti-g41 antibody diluted 1:400 in PBS containing 2% BSA. After washing, the samples were incubated anti-human Alexa Fluor 633 secondary antibody diluted 1:2,000 in PBS containing 2% BSA for 30 minutes at room temperature, for fluorescent labeling.

Permeabilized and non-permeabilized cells were then analyzed by flow cytometry in a FACSCalibur Flow Cytometer (BD Biosciences). Intact cells were selected based on their FSC and SSC values as explained in *Chapter 2*, and for each cell the fluorescent signal of the Env molecules labeled with Alexa Fluor 633 was measured by excitation with the 635 nm laser, and light emission detection with the FL4 emission detector.

Total envelope protein signal was determined by quantification of fluorescent signal in permeabilized cells, while the signal of envelope protein in plasma membrane was determined with non-permeabilized cells. The difference corresponded to envelope protein in the endomembrane system.

3.3. Results

3.3.1. Experimental parameters setting

The study of the interaction between gp41 and cholesterol relies on the use of radioactively labeled photoactivatable [^3H]photocholesterol. In previous works photoactivatable lipids have been fed to the cell by adding them to a delipidated cell culture medium to increase their incorporation into the cells by avoiding competing lipids in the medium (Thiele et al., 2000). Before studying the interaction between gp41 and cholesterol, the experimental parameters of the lipid incorporation were established, and the effect that the use of delipidated medium could have in virus production and processing were studied.

3.3.1.1. Lipid incorporation time and metabolism

Several experimental parameters were first set in order to establish the appropriate lipid incubation time and conditions. In one hand, the incorporation and metabolism of [^3H]photocholesterol was studied by incubating the lipid for 5 min, 1h, 6h or 24 h with HEK 293T cells. On the other hand, the effect that the presence of other lipids in the medium could have in its incorporation rate was analyzed by adding the [^3H]photocholesterol diluted in medium containing either lipidated or delipidated FBS.

HEK 293T cells seeded into a 35mm dish were incubated with 2 $\mu\text{Ci/ml}$ of [^3H]photocholesterol diluted in cell culture medium supplemented with either lipidated or delipidated FBS, and the [^3H]photocholesterol containing medium was removed at 5 min, 1 h, 6 h, or 24 h after addition. After washing with PBS the cells were collected and a small aliquot was used to measure the radioactivity of the samples using a liquid scintillation counter. The radioactivity signal in the cells at each time point was compared to the total radioactive signal added initially to calculate the percentage of incorporated lipid in both the lipidated and delipidated medium conditions (Figure 3.8A). As observed, when the culture medium is supplemented with lipidated FBS, a maximum lipid incorporation of ~25% is observed at 24 h, compared to the ~40% maximum incorporation observed when the [^3H]photocholesterol is incubated with the cells in delipidated culture medium, indicating that the absence of other competing lipids in the culture medium increases [^3H]photocholesterol incorporation into the cells. Next, the incorporation of [^3H]photocholesterol and [^3H]D-erythro-photosphingosine at different times points was compared in delipidated medium conditions (Figure 3.8B). Compared to the cholesterol derivative, [^3H]D-erythro-photosphingosine shows a maximum incorporation at 6h followed by a decrease in signal at 24 h, because of its entry into the catabolic pathway.

Next, the lipid metabolism at each incubation time point was studied in the delipidated medium condition to study the metabolism of the [^3H]photocholesterol and

$[^3\text{H}]$ D-erythro-photosphingosine fed to the cells. For each time point, the lipids from the cells were extracted and loaded into a thin layer chromatography. The radioactive signal from the $[^3\text{H}]$ photocholesterol and $[^3\text{H}]$ D-erythro-photosphingosine derivatives was observed by autoradiography (Figure 3.8C). After 24 h of incubation in delipidated medium, where a maximum incorporation of the lipid is observed, the $[^3\text{H}]$ photocholesterol is still present in the cell, and is not degraded or metabolized into any derivatives (Figure 3.8C). The $[^3\text{H}]$ D-erythro-photosphingosine, on the other hand, derivates in several sphingolipids, including ceramide, sphingosine and gangliosides, but the main sphingolipid species found after 6 and 24 h is sphingomyelin (Figure 3.8C), the canonical companion of cholesterol in lipid rafts. Thus, the use of $[^3\text{H}]$ D-erythro-photosphingosine permits the study of interaction of proteins with primarily sphingomyelin, although other sphingolipids could also be present.

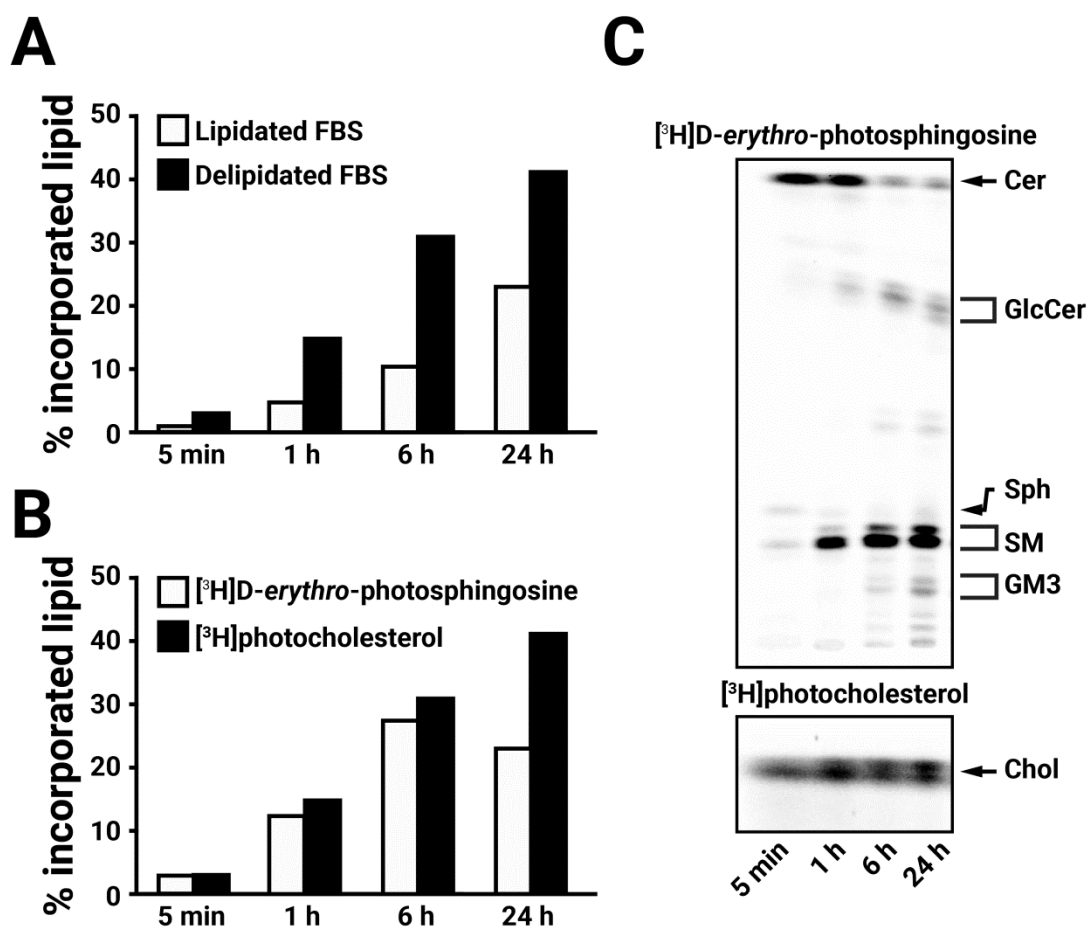


Figure 3.8 – Photoactivatable lipid incorporation and metabolism. **A** | Percentage of $[^3\text{H}]$ photocholesterol incorporated into the cells after different incubation times when the lipid was added in lipidated or delipidated FBS containing medium. **B** | Percentage of $[^3\text{H}]$ photocholesterol and $[^3\text{H}]$ D-erythro-photosphingosine incorporated into the cells after different incubation times in delipidated FBS containing medium. **C** | Autoradiography of a thin layer chromatography of lipids extracted from cells after different incubation times of treatment with $[^3\text{H}]$ photocholesterol and $[^3\text{H}]$ D-erythro-photosphingosine added in delipidated medium.

Next, to test if the use of delipidated medium had an effect in virus production and processing, HEK 293T cells were transfected with a proviral plasmid and, 24 hours post-transfection, incubated with lipidated or delipidated medium for an additional 24 hours. Then, the culture medium supernatant was collected and viral particles were first concentrated and then purified, and the virus production yield was measured by an anti-CA Western blot (Figure 3.9A). The effect of delipidated medium in the virus processing and protein content of the concentrated and purified viral particles was analyzed by loading an aliquot of each sample in an SDS-PAGE and developing with a silver and by Western blot developed against CA and MA (Figure 3.9B).

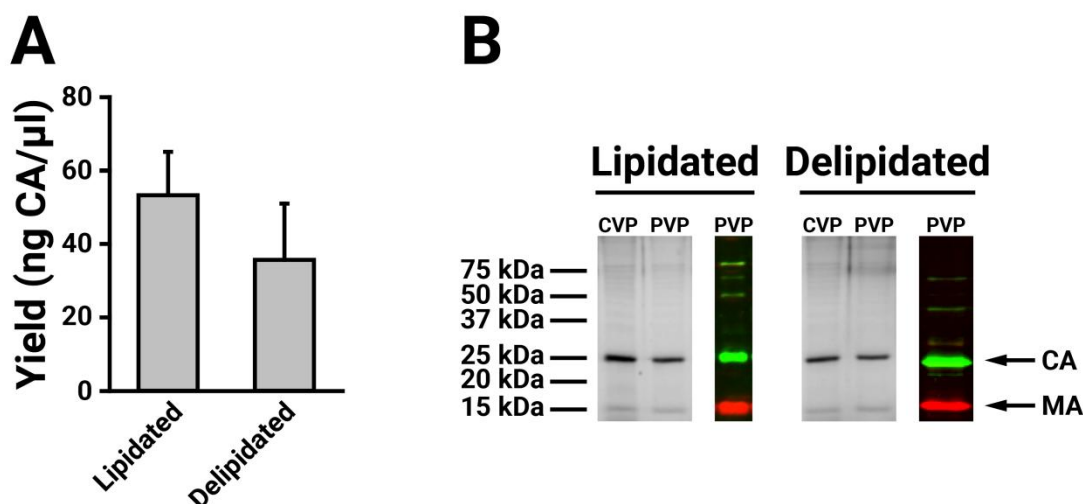


Figure 3.9 – Effect of delipidated medium in virus purification yield and processing. **A** | The production yield measured with an anti-CA Western blot of the resuspended purified viral particles obtained from cells incubated with lipidated or delipidated medium. The bars represent the mean \pm SD of three independent experiments. **B** | CVP = concentrated viral particle; PVP = purified viral particle. Silver staining of concentrated and purified viral particles and Western blot analysis of purified viral particles obtained from cells incubated with lipidated or delipidated medium. The Western blot was developed with sheep anti-CA and anti-sheep IRDye800 antibodies (green) and rabbit anti-MA and anti-rabbit IRDye680 antibodies (red).

A slight decrease can be observed in the purified viral particle production yield when delipidated medium is used compared to the use of lipidated medium, but the differences are not statistically significant (Figure 3.9A). No discernible effect was shown in the virus processing and protein content of either the concentrated or purified viral particles when using medium supplemented with delipidated FBS compared to the traditional lipidated medium when analyzing the viral particles by silver stain. Additionally, the purified viral particles obtained from both conditions present the expected CA and MA signals in the Western blot (Figure 3.9B). These results indicate that the use of delipidated medium, which increases photoactivatable lipid capture by the cells, does not significantly alter virus production, processing, or protein content.

3.3.1.2. Positive and negative controls

The photoactivatable lipids covalently bind to any molecule closer than 3 Å when irradiated with UV light. If a photoactivatable lipid is interacting with a protein and covalently binds with it after irradiation, when said protein is immunoprecipitated from a cellular or viral sample, the covalently bound lipid molecule will also precipitate with it. Thus, the study of the interaction between a protein and [³H]photocholesterol relies in the comparison of the Western blot signal of the immunoprecipitated protein and the detection of the radioactive signal of the lipid in the same Western blot membrane by autoradiography. This autoradiography is carried out in a BetaIMAGER™ system (Biospace Lab), which produces a high resolution quantitative digital autoradiography of the membrane. This digital autoradiography greatly facilitates the quantification of the radioactive signal of the lipid, and aids in the comparison of the position of the lipid signal with the position of the protein signal in the membrane, allowing for an unequivocal confirmation of interaction.

For the study of protein interaction with [³H]photocholesterol positive and negative controls were used. As control of positive interaction with cholesterol, the Cav-1 protein was used. Cav-1 have for a long time been commonly found in DRMs and are canonically considered as markers of lipid rafts or liquid-ordered domains in the membrane, and their interaction with cholesterol has long been accepted (Brown and London, 1997; Smart et al., 1999). Accordingly, Cav-1 was later demonstrated to specifically interact with cholesterol using the same cross-linking [³H]photocholesterol molecule used in this thesis (Haberkant et al., 2008), so it constitutes an adequate positive control for interaction of proteins with [³H]photocholesterol. As a negative control the TfR protein was used, as it constitutes the archetypal non-lipid raft marker (Magee and Parmryd, 2003), and as such it is not expected to specifically interact with cholesterol.

As a positive control, HEK 293T cells transfected with Cav-1-GFP were incubated with [³H]photocholesterol for 24 hours in delipidated medium, after which the cells were washed, irradiated with UV light to induce lipid cross-linking, and lysed. The sample was immunoprecipitated against GFP to isolate the Cav-1-GFP protein, and subjected to Western blot against Cav-1, and posteriorly an autoradiography was carried out (Figure 3.10A). The same rationale was followed for TfR as a negative control, although in this case endogenous TfR was used (Figure 3.10B). For both the Cav-1-GFP and the TfR the Western blot and autoradiography images were compared to determine if any radioactive lipid band corresponded with the Western blot protein bands.

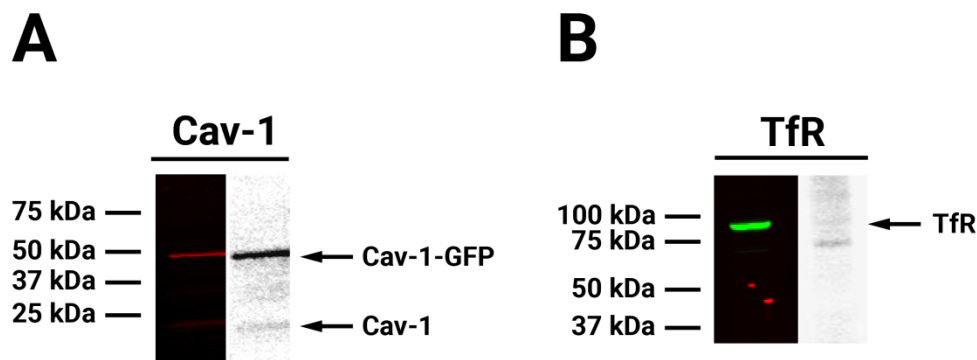


Figure 3.10 - Protein-lipid interaction of control markers. **A|** Representative image of the immunoprecipitated Cav-1-GFP Western Blot (red) and cross-linked [^3H]photocholesterol autoradiography (grey) signals obtained from HEK 293T treated with [^3H]photocholesterol for 24 hours. The Western blot was developed with a rabbit anti-Cav-1 primary antibody and anti-rabbit IRDye680 secondary antibody (red). **B|** Representative image of the immunoprecipitated TfR Western blot (green) and [^3H]photocholesterol autoradiography (grey) signals obtained from HEK 293T treated with [^3H]photocholesterol for 24 hours. The Western blot was developed with a mouse anti-TfR primary antibody and anti-mouse IRDye800 secondary antibody (green).

As observed in Figure 3.10A a clear band corresponding to the radioactively labeled lipid can be observed in the autoradiography, colocalizing with the immunoprecipitated Cav-1-GFP protein band observed in the Western blot, and with a lower size band corresponding with Cav-1, which is probably co-immunoprecipitated with Cav-1-GFP in a stable formed caveole. In comparison, in Figure 3.10B no lipid band is observed in the autoradiography at the position of the TfR band of the Western blot. These results corroborate that the radioactively labeled lipid can easily be observed by autoradiography and compared with the protein bands observed by Western blot, corroborating that the [^3H]photocholesterol covalently binds to proteins that are known to interact with cholesterol, thus confirming its use as a powerful tool for the study of specific protein-cholesterol interactions.

3.3.2. gp41-cholesterol interaction in cells

Once the experimental parameters had been set and the proof-of-concept for the radioactively labeled photoactivatable cholesterol had been corroborated, the interaction of the HIV-1 gp41 protein with membrane cholesterol was tested.

3.3.2.1. gp41 interacts with cholesterol in cells

HIV-1 obtains both the lipid envelope and the envelope protein embedded in it from the producer cell during the budding process. Thus, before testing the interaction of gp41 with viral membrane cholesterol the interaction was tested in cells.

Although no definitive mechanism for Env targeting to Gag assembly and virus budding sites have been described, one of the proposed mechanism postulates that Env localization in budding sites and posterior incorporation into the virion depends on interactions with the underlying Gag/MA lattice (Checkley et al., 2011), which could indicate that the presence of Gag/MA plays a role in the interaction of Env with membrane lipids. Thus, to determine if the interacting capacity of gp41 with cholesterol relies on other viral proteins, gp41-cholesterol interaction was compared between a proviral context, with all of the viral proteins, and when only Env was expressed in the cells.

HEK 293T cells were transfected with either the wild type (WT) proviral plasmid pCHIV, or an Env only expressing plasmid pCAGGs.NL4-3. They were then incubated with [³H]photocholesterol, irradiated with UV light to induce lipid cross-linking, lysed, and gp41 was immunoprecipitated. To test if gp41 also interacted with sphingomyelin, the canonical lipid companion of cholesterol in lipid rafts, the same experiment was carried out with [³H]D-erythro-sphingosine, a precursor of several sphingolipids (Figure 3.11).

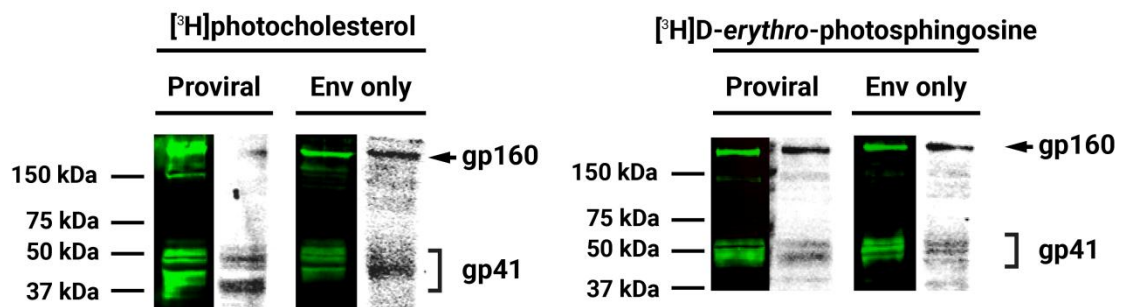


Figure 3.11 – gp41 interaction with cholesterol and sphingolipids in HEK 293T cells. Representative images of the immunoprecipitated gp41 Western blot (green) and cross-linked [³H]photocholesterol or [³H]D-erythro-photosphingosine derivatives autoradiography (grey) signals obtained from HEK 293T cells transfected with a proviral plasmid containing all viral proteins (pCHIV), or an Env only expressing plasmid (pCAGGs), and treated with [³H]photocholesterol or [³H]D-erythro-photosphingosine for 8 hours. The Western blot was developed with chesie-8 anti-gp41 primary antibody, and anti-mouse IRDye800 secondary antibody. The [³H]photocholesterol and [³H]D-erythro-photosphingosine radioactive signal was detected by autoradiography of the same membrane.

The results shown in Figure 3.11 indicate that gp41 interacts with cholesterol and sphingolipids at a cellular level, as radioactive signals can be observed in the autoradiography in the immunoprecipitated sample, corresponding to the protein bands observed in the Western blot. Bands corresponding to un-processed gp160 can also be observed both in the Western blot and autoradiography. The interaction of gp41 with the lipids is observed not only in a proviral context, when all other viral proteins are expressed in the cell, but also when the HIV-1 Env protein is expressed alone, indicating that the capacity of interaction with cholesterol or sphingolipids, and primarily sphingomyelin (Figure 3.8C) of the gp41 protein does not require the presence of other viral proteins and is probably intrinsic to the Env protein. As a result, the gp41 protein

interacts with cholesterol and probably sphingomyelin at a cellular level and, by extension, is probably associated with lipid rafts.

3.3.2.2. Env localization in cells

In the results shown in section 3.3.2.1 above the gp41 was immunoprecipitated from a cell lysate, so proteins coming both from endomembranes as well as plasma membrane would be expected to be obtained. Taking into account that most of the Env protein molecules in a producer cell have been described to be retained intracellularly in the endoplasmic reticulum and endomembranes during the trafficking of the protein to the plasma membrane (Bultmann et al., 2001), but only the proteins in the plasma membrane will be incorporated into the virion, the localization of the Env protein was analyzed in the producer cells where a positive interaction was demonstrated. To study the localization of the envelope protein HEK 293T cells transfected with either a proviral (pCHIV) or Env only expressing (pCAGGs) plasmid were immunostained against Env protein and analyzed by FACS, and the percentage of Env signal in the plasma membrane or in intracellular membranes was calculated (Figure 3.12).

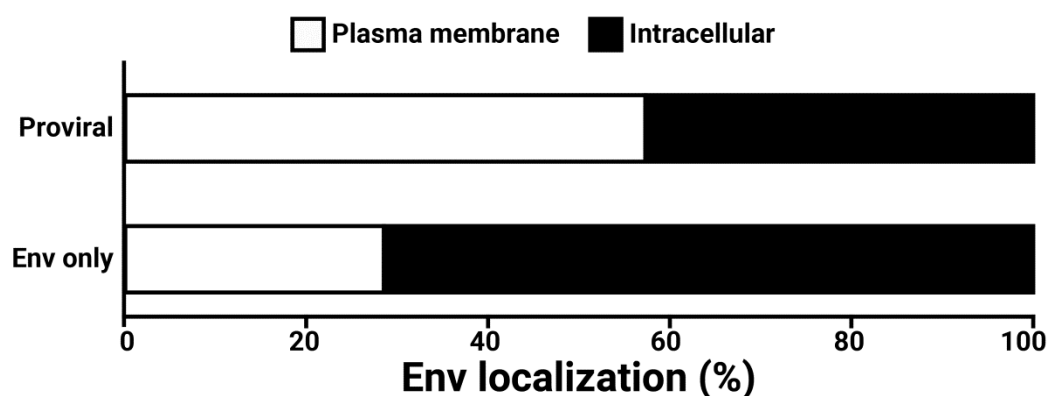


Figure 3.12 – Envelope localization in producer cells. Envprotein localization was studied by confocal microscopy in HEK 293T transfected with a proviral or Env only expressing plasmid.

In a proviral context ~55% of the Env protein is localized in the plasma membrane where, interestingly, cellular cholesterol is also mainly distributed. This could indicate that the interaction between the protein and the lipid that was observed in Figure 3.11 occurs mainly in the plasma membrane and, because viral particles are released from this membrane, the interaction could also exist in the viral particle. Interestingly, in a proviral context, the localization of Env to the plasma membrane is considerably higher than when Env is expressed alone, which would indicate that some viral protein or machinery induces either an enhanced trafficking of Env to the plasma membrane or a higher retention in it. This would explain that the interaction of gp41 with cholesterol in cellular membranes observed in Figure 3.11 is lower when Env is expressed alone, as less protein molecules are localized in the plasma membrane, where cholesterol mainly

resides. Regarding sphingolipid interaction, since these lipids are present in endomembranes and plasma membrane there is not differences in the interaction when Env is expressed alone or in combination with other viral proteins.

3.3.3. gp41-cholesterol interaction in virus

The interaction between gp41 and cholesterol in virus producing cells has been demonstrated in section 3.3.2. The next step consisted on studying if this interaction was maintained in budded and matured virions that have been released into the medium.

3.3.3.1. Gp41 immunoprecipitation in virus

Before studying the interaction of gp41 with cholesterol in purified viral particles, the immunoprecipitation of gp41 from virions was tested. Viral particles were purified from HEK 293T cells transfected with a proviral pCHIV plasmid. Once purified, gp41 was immunoprecipitated from the lysed virions, loaded into a SDS-PAGE and a Western blot was developed against gp41 (Figure 3.13A). A band corresponding to gp41 with an apparent size of ~41-50 kDa can be clearly observed in the immunoprecipitated sample. Three additional prominent protein bands can be observed in the Western blot of the immunoprecipitated sample. Of those, the one labeled *Ab LC* is thought to correspond with the light chain of the antibody (~25 kDa in size, Figure 3.4) used for immunoprecipitation, which is not covalently bound to the beads, and is expected since it is not found in the input sample. Both of the remaining protein bands relate to the Env protein: i) a band of high protein size (~160 kDa), which probably corresponds to the non-cleaved precursor gp160 or a co-immunoprecipitation of gp41 and gp120; and ii) a band of low protein size (~20 kDa), which probably corresponds to a truncated cytoplasmic domain of gp41 that has been described to derive from the full-length protein by proteolytic degradation, named Tr-Env-CT by the authors that first discovered it (Pfeiffer et al., 2013).

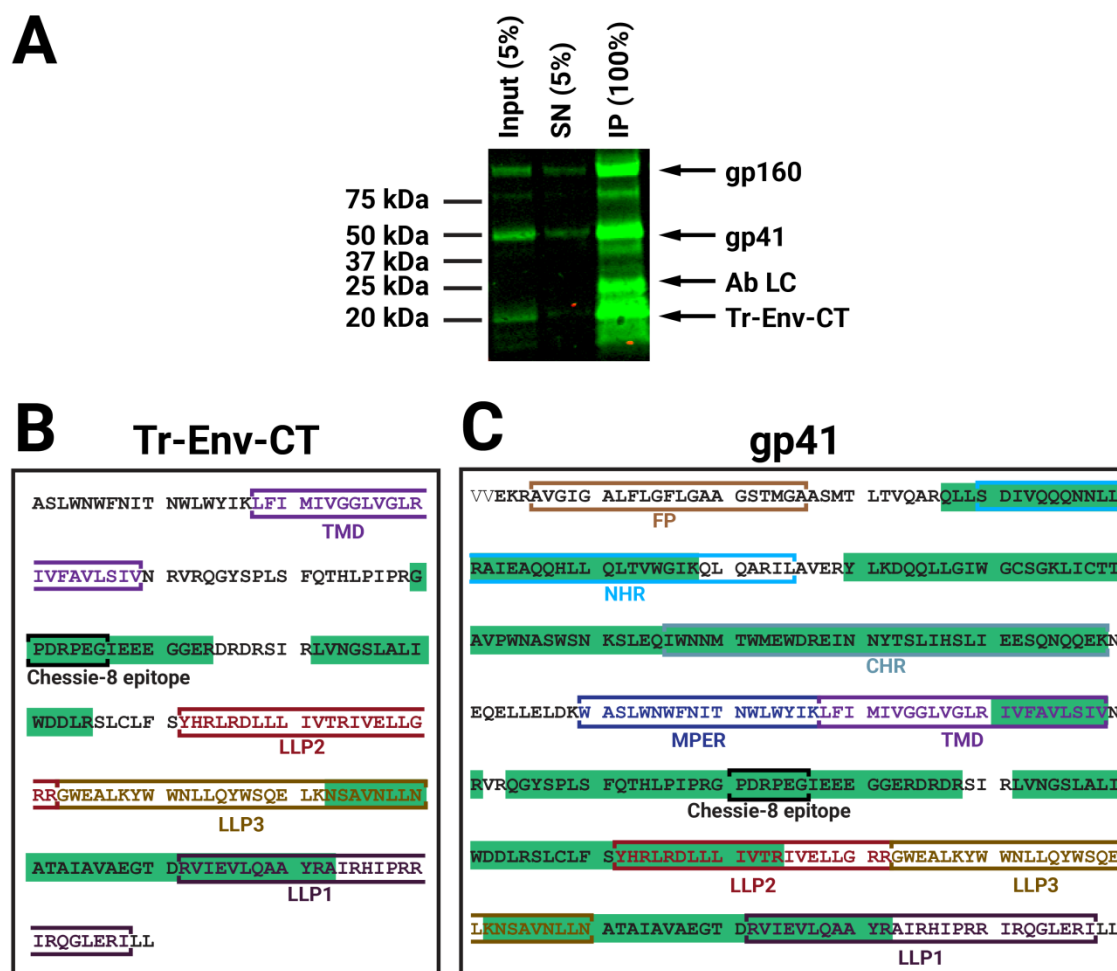


Figure 3.13 – gp41 immunoprecipitation from purified viral particles and proteomic analysis. A| SN = non-immunoprecipitated supernatant; IP = immunoprecipitated sample. Representative image of the immunoprecipitated gp41 WB (green) signal obtained from a purified virus amount equivalent to 1 μ g of CA. The Western blot was developed with chessie-8 anti-gp41 primary antibody, and anti-mouse IRDye800 secondary antibody. B| Peptides derived from the Tr-Env-CT ~20 kDa protein band were detected by proteomic analysis. Different domains are colored and marked in brackets. C| Peptides derived from the gp41 ~41kDa protein band were detected by proteomic analysis. Different domains are colored and marked in brackets.

To ensure that the ~20 kDa band corresponded with the truncated version of the gp41 CT, a proteomic analysis was carried out. Viral particles were purified and lysed, immunoprecipitated against gp41, loaded into a SDS-PAGE and stained with Coomassie blue. The band corresponding to Tr-Env-CT (~20 kDa) was cut from the gel and delivered to the Proteomics Service of SGIKER (UPV/EHU). The proteins were extracted from the gel, trypsinized and deglycosylated, and the tryptic peptides were loaded into a Q ExactiveTM Hybrid Quadruple-OrbitrapTM mass-spectrometer coupled to a EASY nLC1000 (ThermoFisher Scientific) liquid chromatograph, and their detected peptide mass compared to tryptic protein databases. Interestingly, the proteomic analysis of the ~20 kDa band immunoprecipitated by chessie-8 corroborates that this protein corresponds to a truncated form of the cytoplasmic domain of gp41 (Pfeiffer et al., 2013). In agreement

with the cited work, only peptides corresponding to the cytoplasmic domain of gp41 were found in this protein in the proteomic analysis (Figure 3.13B). Additionally, the chessie-8 epitope was confirmed to be present on this Tr-Env-CT (Figure 3.13B, black brackets), which explains by this truncated protein is immunoprecipitated by the antibody.

At the same time and following the same protocol, the rest of the bands were also subjected to proteomic analysis. The ~25 kDa band, labeled Ab LC, was confirmed by proteomic analysis to correspond to the antibody light chain of the anti-gp41 Chessie-8 mouse IgG1 used for immunoprecipitation when compared to a complete *Mus musculus* proteome (data not shown). Additionally, in the ~41-50 kDa protein band peptides spanning most of the length of the gp41 protein were detected, corroborating that the protein immunoprecipitated is indeed the full-length gp41 (Figure 3.13C).

3.3.3.2. gp41 interacts with cholesterol in virions

Once the immunoprecipitation parameters for gp41 were established for viral particles, and the nature of the immunoprecipitated proteins was elucidated, HEK 293T cells transfected with a proviral plasmid and incubated with [³H]photocholesterol were used as virion producing cells to study the interaction of gp41 with cholesterol in virions. Because the HIV-1 obtains its lipid envelope from the producer cell, the [³H]photocholesterol in the plasma membrane of the cell would be incorporated into the virion, thus enabling the study of the interaction following the same immunoprecipitation rationale as with the cells.

42 h after transfection of HEK 293T cells with the pCHIV proviral plasmid and 24 h after photoactivatable lipid addition, the culture medium supernatant containing viral particles released from the producer cells was collected, clarified, and irradiated with UV light to induce cross-linking. The viral particles were then concentrated, purified and resuspended, and after virus production yield determination by anti-CA Western blot, a viral particle preparation volume equivalent to 1 µg of CA (corresponding to approximately 2.6 nmol of viral lipids based on previously published calculations (Brugger et al., 2006; Carlson et al., 2008)) was lysed and immunoprecipitated against gp41. The input, non-immunoprecipitated supernatant, and immunoprecipitated protein were loaded into an SDS-PAGE and a Western blot against gp41 was developed. The [³H]photocholesterol covalently bound to the protein in the Western blot membrane was then detected by autoradiography.

A representative result of the gp41-cholesterol interaction in viral particles is shown in Figure 3.14A, which clearly shows three interacting bands: gp160, gp41 and Tr-Env-CT. A clear [³H]photocholesterol radioactive band can be observed in the autoradiography of the immunoprecipitated sample (Figure 3.14A IP, grey) that correlates with the gp41 signal observed in the Western blot (Figure 3.14A IP, green), similar to what was observed for cells expressing viral proteins (Figure 3.11). In addition to the gp41 protein band, gp160 and Tr-Env-CT also correlate with [³H]photocholesterol signals in the

autoradiography. Of the two, the interaction of gp160 (or the co-immunoprecipitated gp41 and gp120) with cholesterol is expected, as it probably constitutes the unprocessed Env glycoprotein precursor, which when proteolytically cleaved generates gp120 and gp41, or a co-immunoprecipitation of the two. Thus, the gp160 protein should show the same cholesterol interaction tendency as gp41, as the later forms part of the former.

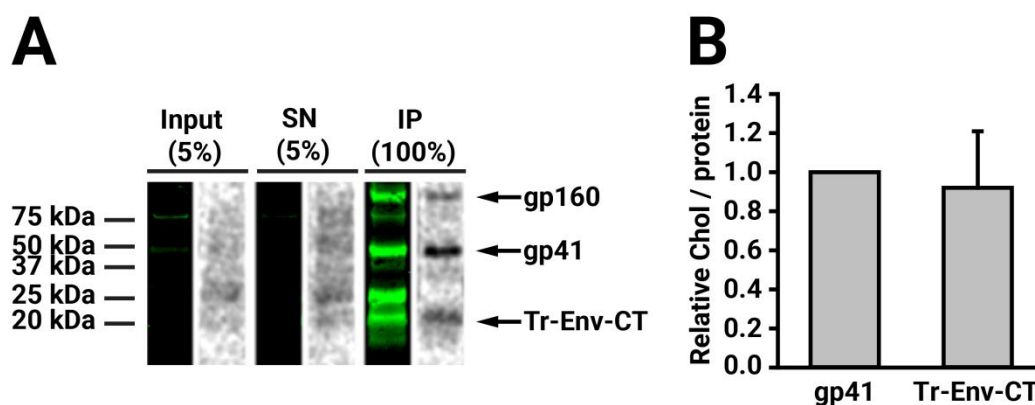


Figure 3.14 – gp41-cholesterol interaction in purified viral particles. **A** | SN = non-immunoprecipitated supernatant; IP = immunoprecipitated sample. Representative image of the immunoprecipitated gp41 Western blot (green) and cross-linked [3 H]photocholesterol autoradiography (grey) signals obtained from a purified virus amount equivalent to 1 μ g of CA. The Western blot was developed with chesnie-8 anti-gp41 primary antibody, and anti-mouse IRDye800 secondary antibody. The [3 H]photocholesterol radioactive signal was detected by autoradiography of the same membrane. **B** | Quantification of the cholesterol/protein signal ratio of the Tr-Env-CT protein band compared to the full-length gp41. The bars represent the mean \pm SD of experiments from five independent viral purifications.

The small Tr-Env-CT band of ~20 kDa of size, on the other hand, is of special interest. This band has been confirmed by proteomic analysis to consist of a truncated cytoplasmic domain of gp41 consisting of the last 139 aminoacid residues of the protein. Thus, this Tr-Env-CT protein consists only on part of the cytoplasmic domain of gp41, and lacks the canonical transmembrane domain of the full-length protein (Pfeiffer et al., 2013) (Figure 3.13B). The fact that this truncated gp41 cytoplasmic domain shows a visible interaction with cholesterol indicates a role of the cytoplasmic domain of gp41 in the interaction with the lipid. To determine if the Tr-Env-CT protein interacted with cholesterol in a level equivalent to the full-length gp41, the protein band signals in the Western blot and the lipid signals in the autoradiography (Figure 3.14A) were quantified in several independent viral purifications. For each independent experiment, the cholesterol/protein ratio of Tr-Env-CT was normalized to that of gp41 for comparison (Figure 3.14B). The quantification of the relative cholesterol/protein signals clearly shows that the interaction with cholesterol of Tr-Env-CT is equivalent to that of the full-length gp41. If a protein consisting of the truncated cytoplasmic domain, lacking any transmembrane or extracellular regions of gp41, presents an interaction with cholesterol quantitatively equivalent to the full-length protein, this result further suggests that the cytoplasmic domain of gp41 is responsible for the interaction of the protein with viral membrane cholesterol, although maybe another region could also be involved on it.

3.3.4. Truncation of three LLPs but not LLP1 hampers interaction with cholesterol

The cytoplasmic domain of HIV-1 gp41 is of special interest as it has been described to play a key role in several aspects of the proteins synthesis, translocation and function. Additionally, a fragment of gp41 consisting of only a truncated cytoplasmic domain was observed to interact with cholesterol at a level comparable to the full-length gp41 in this thesis (Figure 3.14B). To test if the cytoplasmic domain played a role in the interaction of the full-length gp41 protein with cholesterol, two gp41 truncation mutants were used for interaction experiments: Δ LLP1, lacking the last 43 amino-acids of the CT and thus the LLP1 domain; and Δ LLPs, lacking the last 104 amino-acids of the CT and thus the three LLP domains (LLP1, LLP3 and LLP2).

3.3.4.1. CT truncation does not affect Gag processing nor virus density

Prior to interaction studies several controls were carried out to corroborate that the truncation of the cytoplasmic domain of gp41 did not have an effect in virus maturation or general structure. HEK 293T cells were transfected with proviral plasmids expressing wild type, Δ LLP1 or Δ LLPs gp41 proteins (pCHIV, pCHIV TR812 and pCHIV TR751, respectively), and viral particles were purified from the cell culture supernatant.

For all three variants, in the virus purification by sedimentation velocity gradient using OptiPrep step a small aliquot of each of the collected fractions was stored, loaded into an SDS-PAGE, and stained with silver nitrate to study what fraction the viral particles were obtained in (Figure 3.15A). Additionally, a small aliquot of the concentrated and purified viral particles was also loaded to analyze the protein pattern of the virus by silver stain and Western blot against CA and MA (Figure 3.15B).

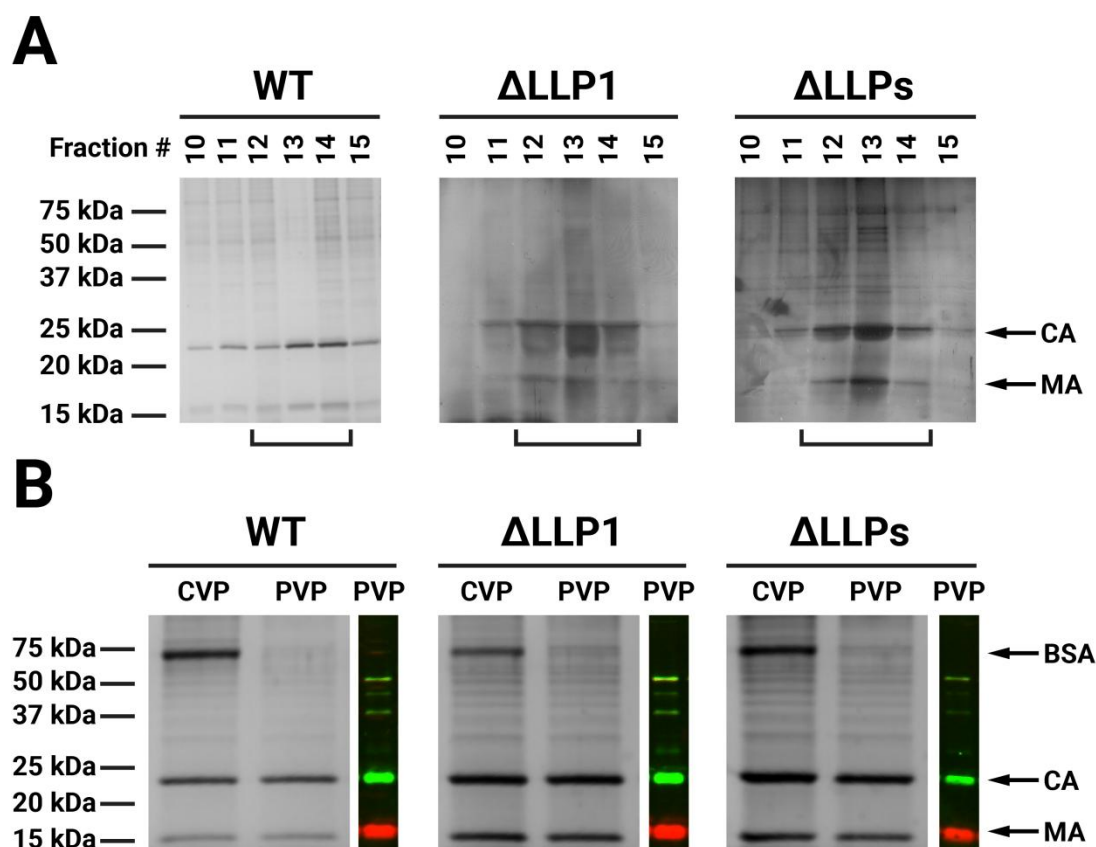


Figure 3.15 – Silver stain and Western blot analysis of fractionation and purified viral particles with wild type, Δ LLP1 or Δ LLPs gp41 variants. **A** | Silver stain of fractions 10-15 of the viral particle purification by sedimentation velocity through Optiprep gradient step. The brackets mark the fractions collected to obtain the purified viral particles. **B** | CVP = concentrated viral particle; PVP = purified viral particle. Silver stain of concentrated and purified viral particles (grey) and Western blot analysis of purified viral particles (green and red). The Western blot was developed with sheep anti-CA and anti-sheep IRDye800 antibodies (green) and rabbit anti-MA and anti-rabbit IRDye680 antibodies (red).

Truncation of gp41 CT does not seem to have an effect in virus density, as the fractionation pattern obtained for the Δ LLP1 and Δ LLPs in the sedimentation velocity purification is indiscernible from that of wild type: for the three variants prominent CA and MA protein bands are observed in fractions 12-14 (Figure 3.15A). Additionally, no differences in the viral protein pattern are observed when the CT of gp41 is truncated in neither concentrated nor purified viral particles, neither by silver stain nor Western blot (Figure 3.15B), indicating that the deletion of LLP1 or the three LLP domains has no visible effect in virus maturation or purification.

3.3.4.2. Deletion of LLPs induces a loss of interaction with cholesterol

After establishing that the truncation of the gp41 cytoplasmic domain does not alter virus maturation or purification, its effect in the gp41 interaction with cholesterol was studied. HEK 293T cells were transfected with proviral plasmids expressing wild type, Δ LLP1 or Δ LLPs gp41 proteins (pCHIV, pCHIV TR812 and pCHIV TR751, respectively), photoactivatable lipid was added 24 hours after transfection, and 48 hours after transfection the cell culture supernatant containing viral particles was clarified and irradiated with UV light to induce lipid cross-linking. The viral particles were then purified and quantified by anti-CA Western blot, and a viral amount corresponding to 1 μ g of CA was lysed, immunoprecipitated against gp41, and loaded into an SDS-PAGE which was developed against gp41 with chessie-8. Additionally, after the obtention of the Western blot against gp41, and the autoradiographical detection of the lipid, both the protein and the [3 H]photocholesterol signal were measured and a cholesterol/gp41 ratio was calculated and normalized with wild type. The interaction between the wild type and the LLP truncation variants of gp41 with cholesterol is shown in Figure 3.16.

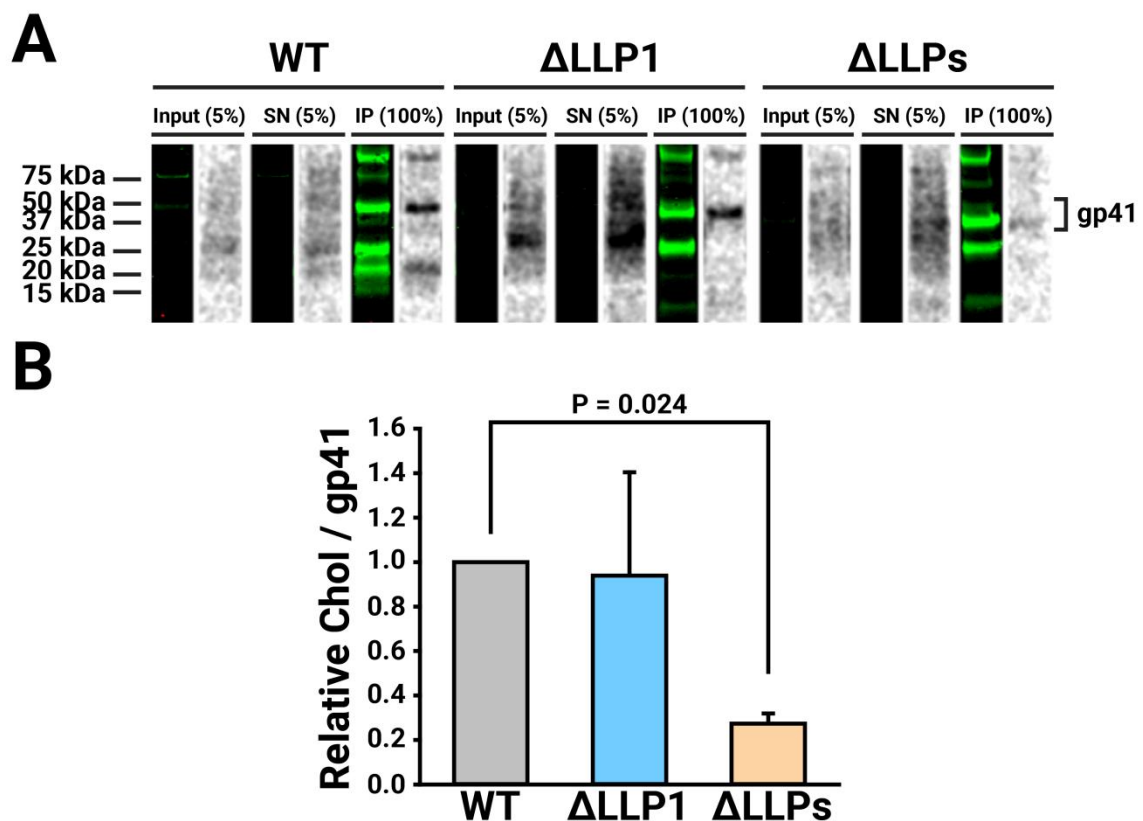


Figure 3.16 – Effect of CT truncation in gp41-cholesterol interaction in purified viral particles. **A** | SN = non-immunoprecipitated supernatant; IP = immunoprecipitated sample. Representative image of the immunoprecipitated wild type and CT truncation variants of gp41 Western blot (green) and cross-linked [3 H]photocholesterol autoradiography (grey) signals obtained from a purified virus amount equivalent to 1 μ g of CA. The Western blot was developed with chessie-8 anti-gp41 primary antibody, and anti-mouse IRDye800 secondary antibody. The [3 H]photocholesterol radioactive signal was detected by autoradiography of the same membrane. **B** | Quantification of the cholesterol/gp41 signal ratio of the CT truncation variants of gp41

CHAPTER 3

compared to the wild type protein. The bars represent the mean \pm SD of experiments from three independent viral purifications.

The results show that the deletion of the three LLP domains (Δ LLPs variant) induces a clear loss of [3 H]photocholesterol radioactive signal when compared to the wild type protein (Figure 3.16A). When the mean cholesterol/gp41 ratio of results obtained from three independent viral purifications were compared, a statistically significant 72.65% decrease in the relative cholesterol signal was observed for the Δ LLPs variant compared to wild type (Figure 3.16B). Conversely, the deletion of just the most C-terminal LLP1 domain (Δ LLP1 variant) does not have a significant effect in the interaction of gp41 with cholesterol. These results indicate that the gp41 cytoplasmic domain region spanning the three LLP sequences may play a key role in the interaction of the protein with cholesterol, and that this region may be specifically located in the LLP3-2 domains, as the deletion of just the LLP1 domain shows no effect in the interaction of the protein with cholesterol.

3.3.4.3. Deletion of LLPs does not hamper lipid or gp41 incorporation into the virion

The results in the section above show a loss of interaction between gp41 and cholesterol when the three LLP domains of the cytoplasmic domain are truncated, which could be due to this region being directly responsible for the interaction of the protein with membrane cholesterol. Admittedly, if the truncation of part of CT induces a decrease in cholesterol or protein recruitment to the virion, the lower cholesterol/gp41 ratio of the Δ LLPs variant could be caused by the alteration of the lipid or protein content in the virion, and not by a direct effect of the mutation in the interaction of gp41 with cholesterol. To address this possibility, the effect of the studied mutations in lipid and protein incorporation into the virion were corroborated, for which HEK 293T transfected with proviral plasmids containing wild type, Δ LLP1 and Δ LLPs gp41 variants (pCHIV, pCHIV TR812 and pCHIV TR751, respectively) were used to obtain purified viral particles containing the three different gp41 variants.

On the one hand, the lipids from these purified viral particles was extracted and subjected to lipidomic analysis. The quantitative results of the cholesterol, sphingomyelin (SM), and phosphatidylcholine (PC) content of the particles are shown in Figure 3.17. As observed, neither of the LLP truncation variants show a significant difference in cholesterol nor SM content in the purified virions, lipids commonly associated with lipid rafts, indicating that the truncation of part or the totality of the LLP domains does not hamper the incorporation of these lipids into the virion.

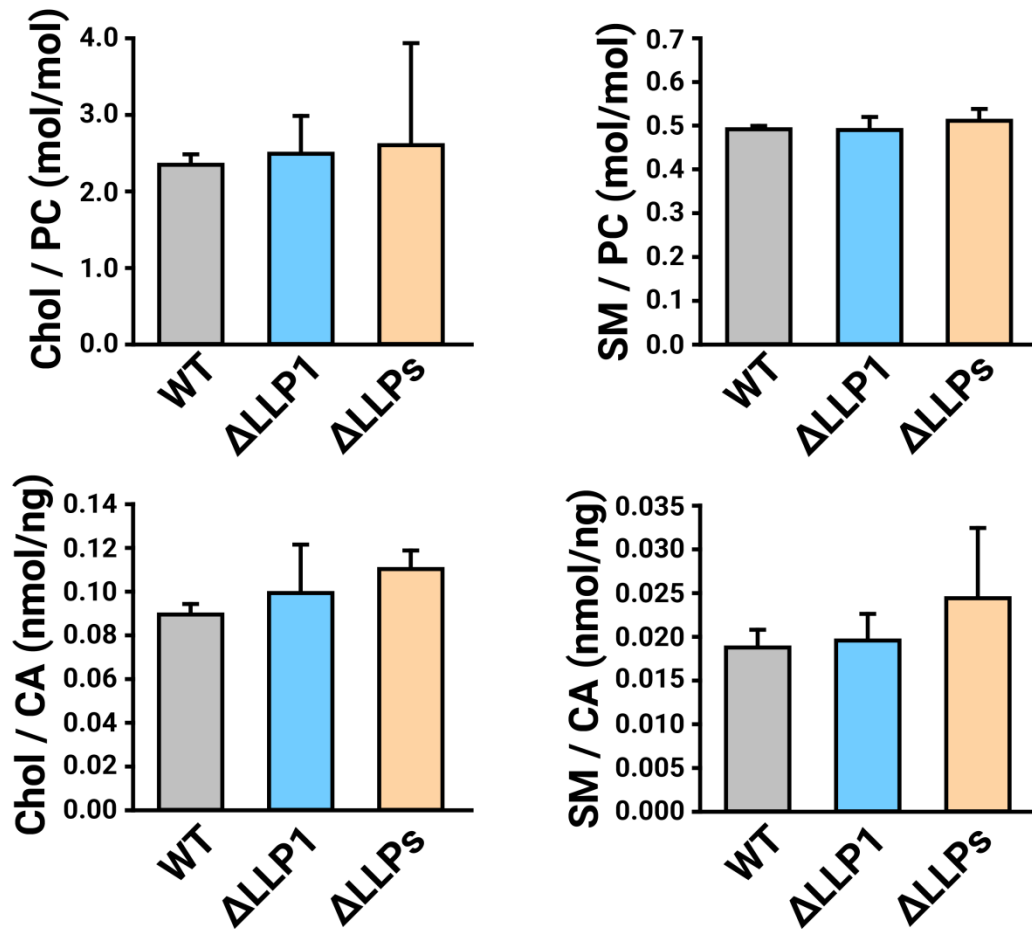


Figure 3.17 – Effect of CT truncation in cholesterol and SM recruitment into the virion. Cholesterol (left) and SM (right) content relative to PC (up) and CA (down) of lipids extracted from purified viral particles containing wild type, Δ LLP1 or Δ LLPs gp41. The bars represent the mean \pm SD of experiments from three independent viral purifications.

On the other hand, the gp41 content of the three variants was studied. A purified viral sample volume corresponding to 120, 100, 50 and 25 ng of CA was loaded into an SDS-PAGE for each variant, and a Western blot was developed against gp41 (Figure 3.18A). The integrated intensity of each gp41 band was measured and blotted against the ng of CA loaded, and for each variant a linear curve fit between the gp41 signal and loaded ng of CA was calculated, and the relative slopes of the curve fits were extracted (Figure 3.18B). The experiment was repeated with three independent viral purifications to obtain a mean gp41/CA ratio for each variant (Figure 3.18C).

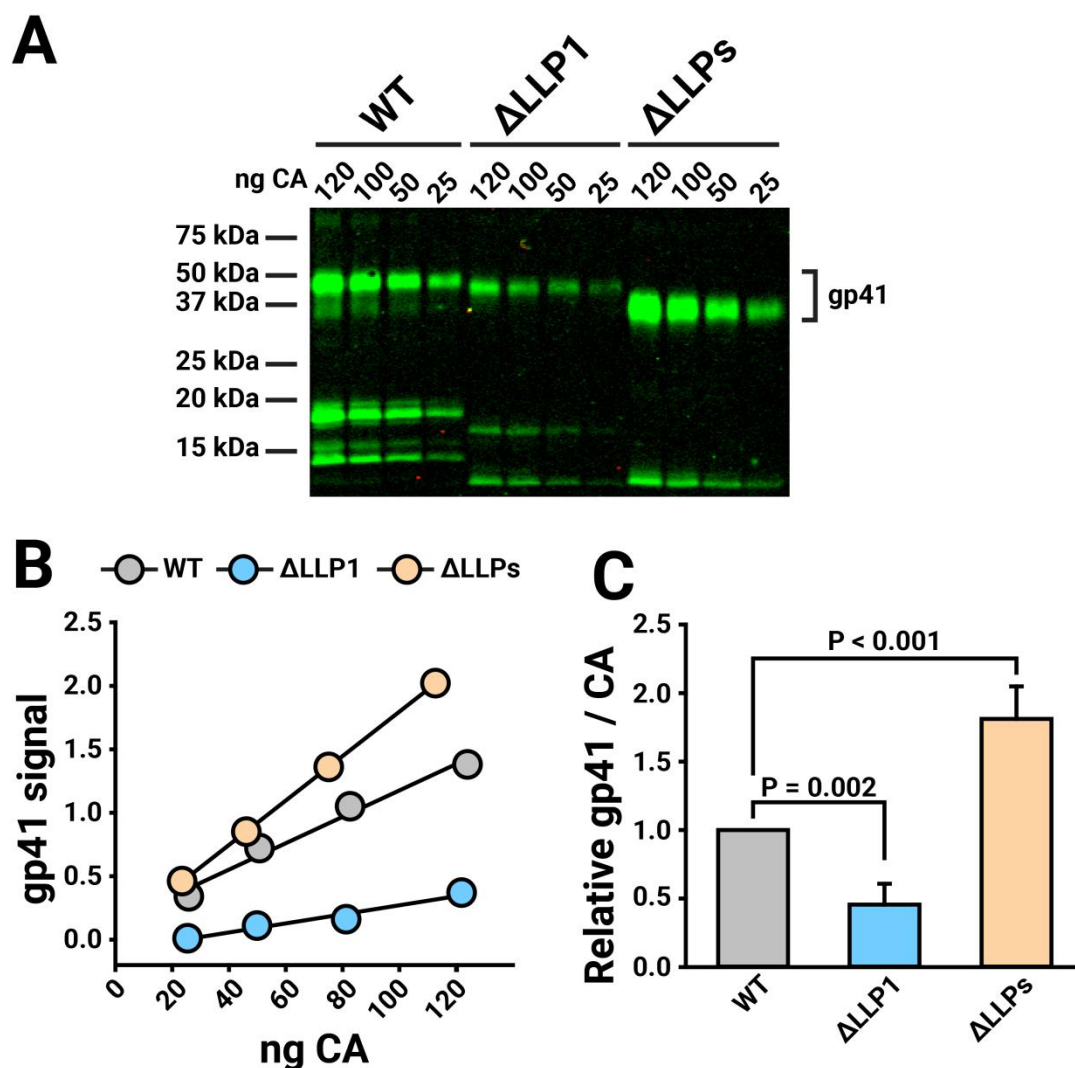


Figure 3.18 – Effect of CT truncation in gp41 recruitment into the virion. **A** Representative Western blot of gp41 quantification. A volume of purified viral particles corresponding to 120, 100, 50 and 25 ng of CA was loaded into an SDS-PAGE for each variant. The Western blot was developed with chesie-8 anti-gp41 primary antibody, and anti-mouse IRDye800 secondary antibody (green). **B** Representative blot of gp41 signal vs ng CA. The gp41 band signal of the Western blot was blotted against the loaded ng of CA, and the relative slopes of the linear curve fits of each variant were calculated. **C** The experiment was repeated three times and mean relative slopes were obtained for each variant. The bars represent the mean \pm SD of experiments from three independent viral purifications.

When the gp41 content of the variants is compared to that of wild type, the results show that, while the deletion of the LLP1 domain (Δ LLP1 variant) induces a ~50% loss of gp41 recruitment into the virion, the truncation of the three LLP domains (Δ LLPs variant) significantly increases the incorporation of the protein into the particle to ~180% that of wild type.

The results shown in Figure 3.17 and Figure 3.18 indicate that the truncation of the three LLP domains does not hamper neither lipid nor gp41 incorporation into the virion, corroborating that the loss of interaction described in section 3.3.4.2 is not due to a lower lipid or protein content, but, instead, is derived from a direct role of this region in

the interaction of the protein with membrane cholesterol. Interestingly, although the Δ LLP1 variant presents a ~55% reduction in Env content in the virion (Figure 3.18), the relative cholesterol/gp41 ratio does not show significant differences from the wild type variant (Figure 3.16), indicating that the detection of the interaction is still possible even with half the Env molecules per virion.

3.3.5. Role of other protein domains in interaction with cholesterol

In the previous sections the role of the LLP domains in the interaction of gp41 with cholesterol has been demonstrated. To determine if the LLP domains regulate the interaction with cholesterol directly or, in the contrary, another region of the protein is involved in the interaction, the role of several other regions of the Env protein that have been described to interact with cholesterol or DRMs will be studied.

Specifically, several mutations in three regions of interest were carried out. In the MPER region of the gp41 ectodomain, the CRAC sequence has been described to interact with cholesterol *in vitro*. The effect of interaction with cholesterol of a substitution of a leucine by isoleucine in CRAC that has been found to result in a loss of cholesterol-binding capacity *in vitro* (Vincent et al., 2002; Vishwanathan et al., 2008) will be studied in this work. The gp41 transmembrane domain have also been described to interact with specific membrane lipids, and to study its involvement three gp41 variants were used: a complete substitution of the gp41 TMD by the TMD of the cellular CD22 receptor, which would give information about the involvement of the complete TMD in the interaction; a disruption of the GxxxG-motif that was found to interact with cholesterol in other proteins (Barrett et al., 2012); and a substitution of the positively charged arginine residue in the TMD, described to be related to the interaction of gp41 with cholesterol by molecular dynamic simulations (Baker, 2014). Taking into account that truncation of the LLP sequences resulted in an inhibition of cholesterol interaction, two highly conserved arginines in the LLP2 region were also substituted to study the possibility of their involvement in the interaction, as they were found to have an effect in protein localization into the plasma membrane and posterior incorporation into the virion (Kuhlmann et al., 2014), a process that may be governed by a mechanism related to the interaction of Env with specific lipid structures in the plasma membrane, as stated before.

The proviral plasmids with mutations in the above mentioned regions used for the interaction experiments are summarized in Table 3.5, and detailed in *Chapter 2*.

Table 3.5 – Summary of the proviral plasmids expressing different gp41 variants.

Variant name	Mutated region	Plasmid	Description
CRAC	CRAC	pCHIV L677I	pCHIV derivative expressing a gp41 protein variant where the CRAC segment Leu677 has been exchanged by Ile.
GxxxG	GxxxG	pCHIV G688L G692L	pCHIV derivative expressing a gp41 protein variant where the Gly688 and Gly692 of the GxxxG motif have been exchanged by Leu.
R696I	Transmembrane domain arginine	pCHIV R696I	pCHIV derivative expressing a gp41 protein variant where the transmembrane Arg696 has been exchanged by Ile.
CD22 TMD	Transmembrane domain	pCHIV CD22 TMD	pCHIV derivative expressing a chimeric gp41 protein with a substitution of its membrane spanning domain by the TMD of the cellular receptor CD22.
LLP2 R	LLP2 conserved arginines	pCHIV R700K R778K	pCHIV derivative expressing a gp41 protein variant where the Arg770 and Arg778 has been exchanged by Lys.

3.3.5.1. Disruption of CRAC or transmembrane domain does not hamper gp41 interaction with cholesterol

To study the role of the different gp41 mutations in the interaction of the protein with cholesterol, following the same experimental set-up as with the LLP truncation variants in section 3.3.4, HEK 293T cells were transfected with the pCHIV plasmids containing the different gp41 variants in Table 3.5. 18 hours post-transfection, [³H]photocholesterol was added to the medium for an additional 24 hours, after which the culture medium supernatant was collected, clarified, irradiated with UV light to induce lipid-protein cross-linking, and viral particles were concentrated from the medium. After virus production yield determination by anti-CA Western blot, a viral particle preparation volume equivalent to 1 µg of CA was lysed and immunoprecipitated against gp41. The input, non-immunoprecipitated supernatant, and immunoprecipitated protein were loaded into an SDS-PAGE and a Western blot against gp41 was developed. The [³H]photocholesterol covalently bound to the protein in the Western blot membrane was then detected by autoradiography (Figure 3.19A). The protein and lipid signals were measured for each variants in experiments with three independent viral purifications, and a cholesterol/gp41 ratio was calculated and normalized to the wild type particles (Figure 3.19B).

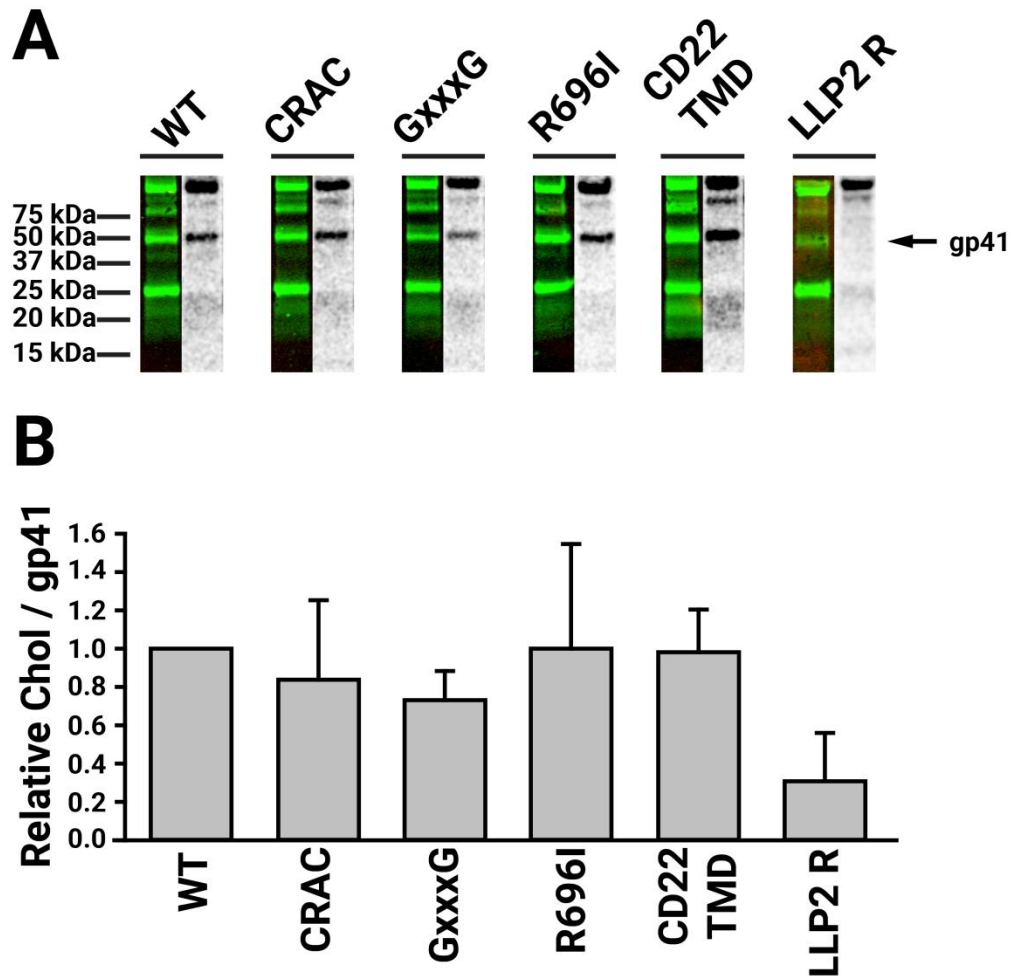


Figure 3.19 – Effect of gp41 mutations in gp41-cholesterol interaction in purified viral particles. A| Representative image of the immunoprecipitated wild type and mutated variants of gp41 Western blot (green) and cross-linked [³H]photocholesterol autoradiography (grey) signals obtained from a purified viral particle amount equivalent to 1 µg of CA. The Western blot was developed with chessie-8 anti-gp41 primary antibody, and anti-mouse IRDye800 secondary antibody. The [³H]photocholesterol radioactive signal was detected by autoradiography of the same membrane. **B|** Quantification of the cholesterol/gp41 signal ratio of the mutated variants of gp41 compared to the wild type protein. The bars represent the mean ± SD of experiments from three independent viral purifications.

The study of the gp41-cholesterol interaction of the gp41 variants generated interesting results. As observed, disruption of the CRAC sequence (L677I variant), substitution of the entire TMD (CD22 TMD variant), disruption of the GxxxG-motif (G688L G692L variant), or substitution of the TMD arginine (R696I variant) did not have an effect in the interaction of the protein with viral membrane cholesterol, as no significant differences in the cholesterol/gp41 ratio were observed when compared to the wild type protein (Figure 3.19B).

Interestingly, substitution of the highly conserved arginines in the LLP2 sequence (LLP2 R variant) resulted in a, although no statistically significant, marked reduction in the interaction of the gp41 protein with cholesterol. Nevertheless, the gp41 protein signal

in the Western blot in Figure 3.19A corresponding to this mutation is considerably less intense than for the rest of the variants. Because sensitivity of the protein detection by Western blot and lipid detection by autoradiography are not necessarily comparable, the reduced amount of gp41 in the Western blot in the LLP2 R variant may render the detection of [³H]photocholesterol difficult, even if the cholesterol/gp41 ratio is comparable to the wild type protein. To corroborate this possibility, the quantity of the gp41 variants in the viral particles was studied.

3.3.5.2. Effect of gp41 domains in protein incorporation into the virion

Some of the gp41 variants used in this section have been previously described to significantly affect envelope protein incorporation into the virion and, specially, the LLP2 R variant showed a reduced gp41 signal in the immunoprecipitated sample in Figure 3.19A, which could possibly affect quantification of the gp41-cholesterol interaction. Thus, the effect of these mutations in gp41 incorporation was analyzed by transfecting HEK 293T with proviral plasmids expressing the different gp41 variants (Table 3.5) and purifying viral particles from the cell culture supernatant. After viral particle characterization and quantification by anti-CA Western blot, a purified viral sample volume corresponding to 120, 100, 50 and 25 ng of CA was loaded into an SDS-PAGE for each variant, and a Western blot was developed against gp41 (Figure 3.20A). The integrated intensity of each gp41 band was measured and plotted against the ng of CA loaded, obtaining linear regressions between the gp41 signal and amount of CA loaded. The relative slopes of each of the linear regressions were extracted from three independent experiments to obtain a mean quantification of the effect of the different mutations in the incorporation of gp41 into the virion (Figure 3.20B).

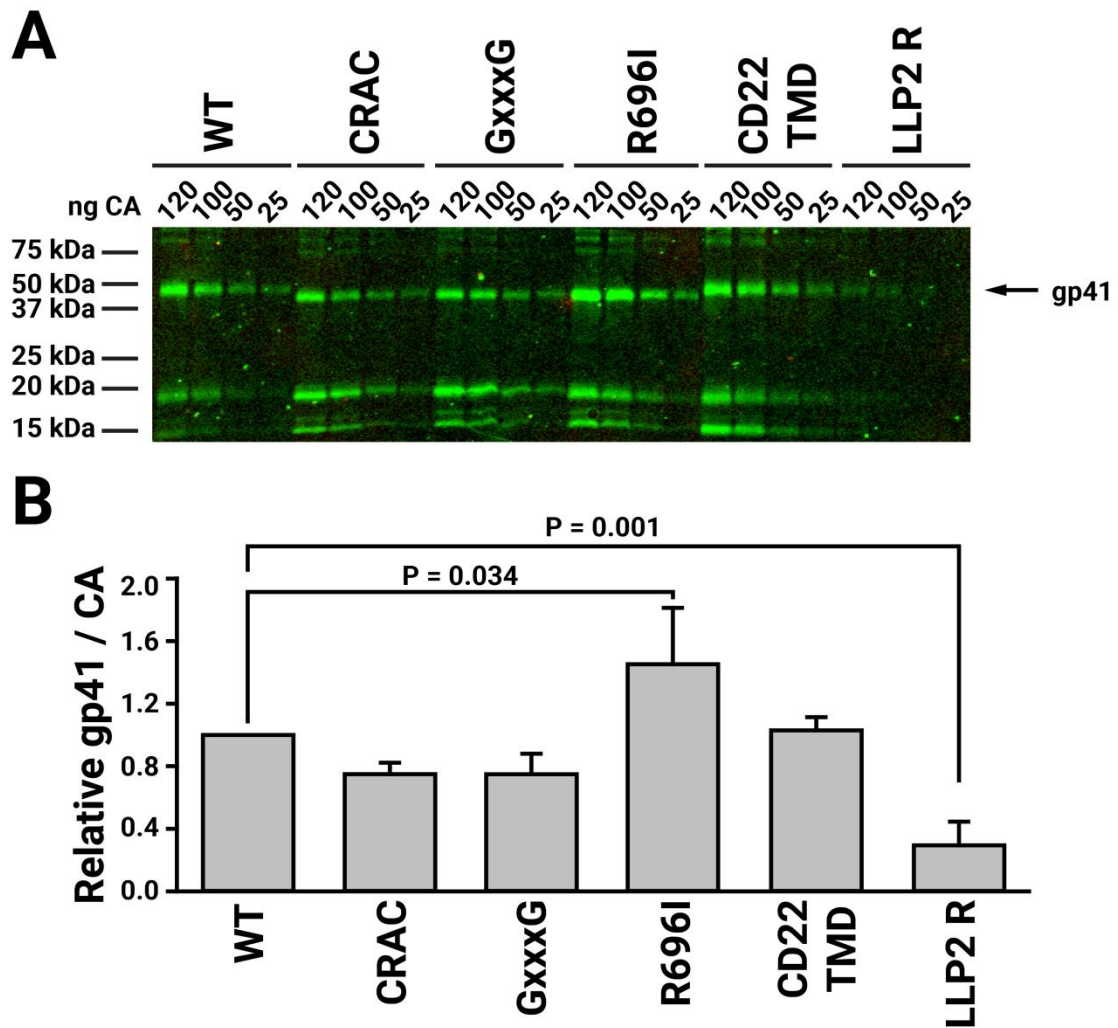


Figure 3.20 – Effect of gp41 mutations in protein recruitment into the virion. **A** Representative Western blot of gp41 quantification. A volume of purified viral particles corresponding to 120, 100, 50 and 25 ng of CA was loaded into an SDS-PAGE for each variant. The Western blot was developed with chessie-8 anti-gp41 primary antibody, and anti-mouse IRDye800 secondary antibody (green). **B** The gp41 band signal of the Western blot was blotted against the loaded ng of CA, and the relative slopes of the linear curve fits of each variant were calculated and normalized to the wild type particles. The bars represent the mean \pm SD of experiments from three independent viral purifications.

Only two of the mutations significantly altered gp41 incorporation into the virion. Substitution of the transmembrane domain arginine with an isoleucine resulted in a significant increase of gp41 incorporation to \sim 150% that of wild type. On the contrary, substitution of the two most conserved arginine residues of the LLP2 domain by lysines significantly reduced the incorporation of the protein into the virion to \sim 25%, which comes in agreement with previously published results describing a role of this arginines in the trafficking of Env to the plasma membrane (Kuhlmann et al., 2014).

The reduced incorporation of this gp41 variant into the virion explains the low gp41 signal observed in the Western blot in the gp41-cholesterol interaction experiments (Figure 3.19A), and could be the reason for the apparent loss of interaction of this variant

with cholesterol (Figure 3.19B). Even if the relative cholesterol/gp41 ratio of the variant is comparable to that of wild type, the reduced amount of protein in the sample could render the [³H]photocholesterol signal undetectable, and result in an apparent loss of interaction.

3.3.5.3. LLP2 R variant's apparent loss of interaction derives from the reduced gp41 incorporation

To further analyze if the reduced gp41 amount is responsible for the apparent reduction of gp41-cholesterol interaction, interaction experiments of the LLP2 R variant with cholesterol were repeated. To compensate for the reduction of gp41 incorporation, increasing amounts of viral sample were immunoprecipitated for the LLP2 R variant while maintaining the wild type virus amount constant. Specifically, because the LLP2 R showed a reduction of gp41 incorporation to 25% that of wild type, while the wild type sample amount was maintained at 1 µg of CA, the LLP2 R variant sample amount was increased up to 4 times that of wild type (4 µg of CA). A sample volume corresponding to 1 µg of CA for the wild type sample and 1, 2 and 4 µg of CA for the LLP2 R variant were lysed and immunoprecipitated following the same protocol as the sections above. The immunoprecipitated sample was loaded into an SDS-PAGE and subjected to Western blot. The gp41 band signals of the samples were quantified and compared to the [³H]photocholesterol signals obtained by autoradiography of the same membrane. For each sample amount, the cholesterol/gp41 ratio of the LLP2 R variant relative to wild type was calculated (Figure 3.21). The increasing amounts of sample loaded in the LLP2 R variant resulted in a recovery of the gp41-cholesterol interaction. Specifically, when 4 times more sample was loaded for the variant (4 µg of CA compared to the 1 µg of CA of the wild type sample), the cholesterol/gp41 ratio was comparable to that of the wild type samples.

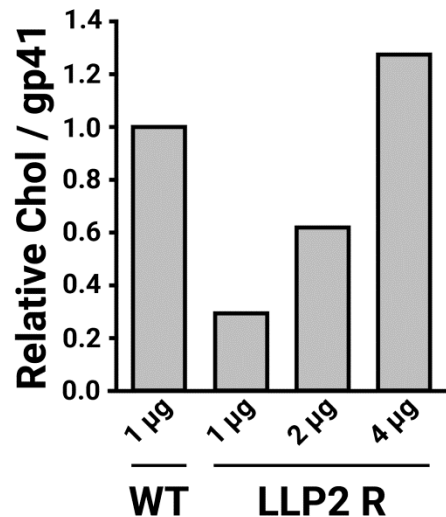


Figure 3.21 – Relative cholesterol/gp41 ratio of increasing amounts of the LLP2 R variant. Viral amounts corresponding to 1 µg, 2 µg and 4 µg of CA from the LLP2 R variant were immunoprecipitated and loaded into an SDS-PAGE. A Western blot against gp41 was developed, and the gp41 signal was measured by LiCor. The [³H]photocholesterol signal was measured by autoradiography of the same membrane. The cholesterol/gp41 ratio of each LLP2 R variant sample quantity was normalized to wild type for comparison.

Taking this into account, the interaction experiment was repeated for the LLP2 R variant with three independent viral purifications, loading 4 µg of CA for the variant to compensate for the reduced Env quantity (Figure 3.22). The results confirm that the cholesterol/gp41 ratio is recovered when the defect in gp41 incorporation into the virion is accounted for in the LLP2 R variant. The reduced gp41 amount in the virion derives in a limitation on the number of [³H]photocholesterol that can cross-link with the protein, and even if the cholesterol/gp41 ratio is comparable to that of wild type, the low amount of protein and cross-linked lipid immunoprecipitated derives in an incorrect quantification of the ratio. Thus, the apparent loss of interaction observed in Figure 3.19 is derived from the defect of Env incorporation and not from an effect in the interaction with cholesterol of the substitution of the highly conserved arginines in the LLP2 sequence.

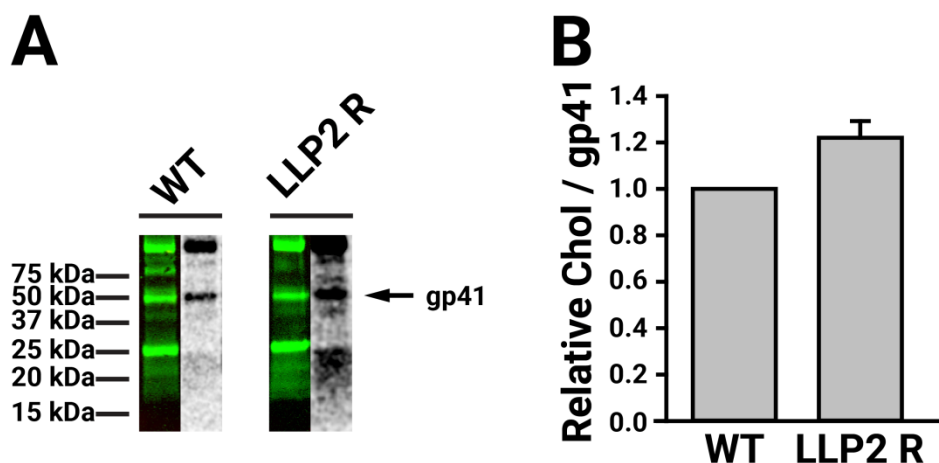


Figure 3.22 – Effect of R770K R778K mutation in the LLP2 R variant in gp41-cholesterol interaction in purified viral particles. **A** Representative image of the immunoprecipitated wild type and mutated variant of gp41 Western blot (green) and cross-linked [³H]photocholesterol autoradiography (grey) signals obtained from a purified viral particle amount equivalent to 1 μg of CA for wild type and 4 μg of CA for LLP2 R variant. The Western blot was developed with chessie-8 anti-gp41 primary antibody, and anti-mouse IRDye800 secondary antibody. The [³H]photocholesterol radioactive signal was detected by autoradiography of the same membrane. **B** Quantification of the cholesterol/gp41 signal ratio of the mutated variant of gp41 compared to the wild type protein. The bars represent the mean ± SD of experiments from three independent viral purifications.

In summary, neither the CRAC sequence, nor the transmembrane domain or the highly conserved arginines in the LLP2 sequence play a role in the interaction of gp41 with cholesterol. On the other hand, the presence of the LLP in the gp41 cytoplasmic domain, and specially the LLP2 and 3 sequences are necessary for the interaction of gp41 with viral membrane cholesterol.

3.3.6. Truncation of LLPs hampers virus entry capacity

The deletion of the LLP domains of gp41 has been shown induce a loss of interaction of the protein with viral membrane cholesterol in section 3.3.4. The lipid environment of some membrane proteins has been previously shown to modulate their function, as reviewed in (Simons and Toomre, 2000), and in the case of gp41, cholesterol has been shown to be necessary for the fusion process of the virion with the host cell (Campbell et al., 2004, 2002; Hawkes et al., 2015; Liao et al., 2003). Additionally, the CT of gp41 has been shown to regulate Env clustering, a process necessary to the efficient fusion between the virion and the host cell (Chojnacki et al., 2012). In order to study the possible relations between the interaction of gp41 with cholesterol, the clustering of Env, and the fusion capacity of the virion with the host cell, the entry capacity of purified viral particles containing wild type, ΔLLP1 and ΔLLPs gp41 variants was studied.

For these experiments concentrated viral particles containing a β -lactamase-Vpr (BlaM-Vpr) chimeric protein were obtained from HEK 293T co-transfected with pMM3100 (expressing BlaM-Vpr) and either the proviral pCHIV, pCHIV TR812 or pCHIV TR751 plasmids. After concentrated BlaM-Vpr virions were obtained, the entry capacity of the particles was tested in Jurkat E6-1 cells, a lymphoid cell line commonly used as a model for viral entry. As a negative control, AMD3100 was added to the wild type gp41 containing viral particles, a known inhibitor of gp41 mediated entry (Donzella et al., 1998). As an additional negative control viral particles lacking Env obtained from HEK 293T co-transfected with pMM3100 and pCHIV Env(-) were used. The viral particles were incubated with the cells for 2.5 h at normal culture conditions, after which the cells were washed and incubated with the β -lactamase fluorescence substrate CCF2-AM for 15 h in the dark at room temperature. The entry capacity of the viral particles is calculated as a relative fluorescence intensity ratio of the cleaved (blue) and uncleaved (green) β -lactamase fluorescence substrate. The results of the effect of truncation of the LLP1 (Δ LLP1 variant) or the three LLP (Δ LLPs) domains is shown in Figure 3.23.

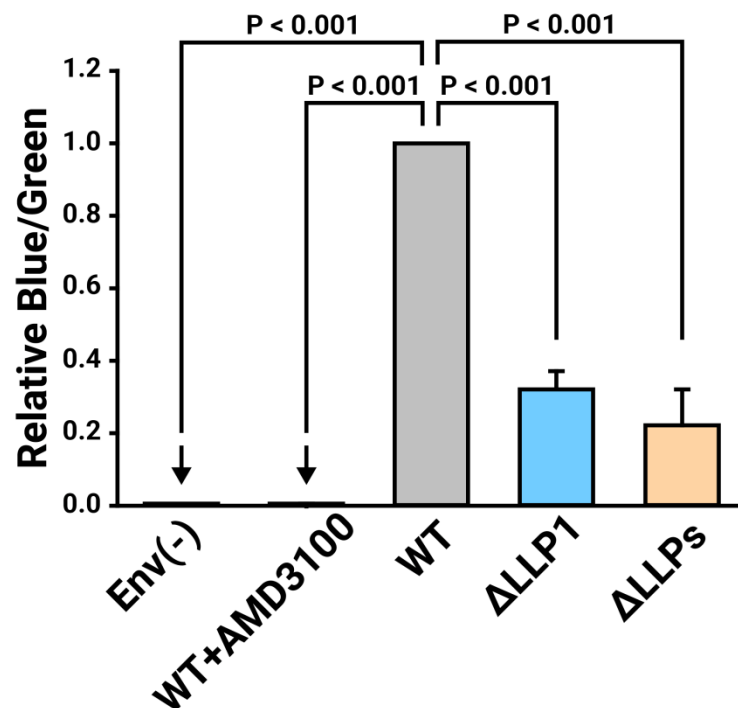


Figure 3.23 – Effect of CT truncation in entry capacity of concentrated BlaM-Vpr viral particles. For each variant, a viral amount corresponding to 30 ng of CA was incubated with Jurkat E6-1 cells for 2.5 h. The BlaM-Vpr fluorescent substrate (CCF2) was loaded into the cells for 15 h, and the relative fluorescent intensity ratios of the cleaved (blue) and uncleaved (green) CCF2A substrate was measured for each variant (ex = 400±30 nm; em = 528±20 nm (green) and 460±40 nm (blue)). The bars represent the mean±SD relative Blue/Green signal of five independent viral purifications with four replicas each.

Both of the truncation variants, Δ LLP1 and Δ LLPs, show a significant decrease in entry capacity of the virions to Jurkat E6-1 host cells, to values of ~30% and ~20% that of wild type, respectively. They both show entry levels higher than both of the negative

controls, Env(-) and wild type particles treated with AMD3100, which indicates that the entry capacity of the virions is not completely inhibited (Figure 3.23).

Admittedly, the reduced entry capacity of the Δ LLP1 may not be due to a decrease in the fusion capacity of individual gp41 molecules, but instead be caused by the decrease in Env incorporation into the virion shown previously (Figure 3.18) since a minimum number of Env trimers seems to be required to interact with host cell receptors to generate an efficient fusion between viral and cellular membranes (Brandenberg et al., 2015). Taking this into account, the decreased Env incorporation into the virion of the Δ LLP1 variant may be the cause of the inhibition of the entry capacity, instead of a loss of function of the protein. In order to test this hypothesis an entry assay was devised in which the lower gp41 incorporation of the Δ LLP1 variant was compensated by loading a higher virus amount so that the total Env quantity in the sample would be comparable to that of wild type: specifically, the Δ LLP1 variant shows a reduction of ~50% in gp41 incorporation into the virion, so the amount of viral particles loaded into the entry assay was doubled from 30 ng of CA for wild type, to 60 ng of CA for Δ LLP1 (Figure 3.24).

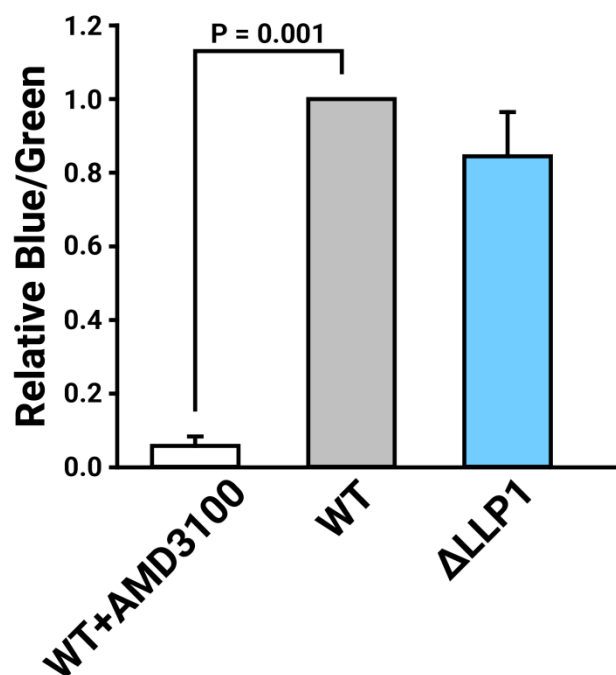


Figure 3.24 – Δ LLP1 variant recovers entry capacity when Env incorporation is accounted for. A viral amount corresponding to 30 ng of CA for wild type and 60 ng for Δ LLP1 was incubated with Jurkat E6-1 cells for 2.5 h. The BlaM-Vpr fluorescent substrate (CCF2) was loaded into the cells for 15 h, and the relative fluorescent intensity ratios of the cleaved (blue) and uncleaved (green) CCF2A substrate was measured for each variant (ex = 400 ± 30 nm; em = 528 ± 20 nm (green) and 460 ± 40 nm (blue)). The bars represent the mean \pm SD relative Blue/Green signal of three independent viral purifications with four replicas each.

The results in Figure 3.24 clearly show that when the defect in gp41 incorporation of the Δ LLP1 is compensated with an increased viral amount, the entry capacity of said virions is recovered to the level of the wild type particles, indicating that the apparent

entry defect shown in Figure 3.23 for this variant is caused by the decrease in the gp41 incorporation, and not a loss of function of the protein. The Δ LLPs variant, on the other hand, shows increased gp41 incorporation into the virion (Figure 3.18), and yet the entry capacity of virions bearing this gp41 variant is significantly inhibited compared to the wild type particles, indicating that this truncation causes a loss of function of the protein.

3.3.7. Maturation state does not affect gp41-cholesterol interaction

Several studies has described that the cytoplasmic domain of gp41 interacts in a direct or indirect manner with the underlying MA lattice of the HIV-1 virions via several possible mechanisms, reviewed in (Checkley et al., 2011). Additionally, both the gp41 cytoplasmic domain and the maturation state of Gag/MA have been described to affect Env clustering and its diffusion in the viral membrane, which indicate that a direct or indirect connection between virus maturation and Env redistribution and diffusion probably exist via the interaction of gp41 cytoplasmic domain with the underlying Gag/MA lattice.

Taking these data into consideration, it comes to reason that the interaction between Gag/MA and gp41 cytoplasmic domain, and the maturation state of the virion could also have an effect in the CT-dependant interaction between gp41 and cholesterol demonstrated in section 3.3.4. In order to deeply investigate this possibility, immature viral particles containing a wild type or truncated gp41 were used for gp41-cholesterol interaction experiments. For this purpose, a proviral pCHIV plasmid containing a mutation in the PR was used [pCHIV PR(-)]. This mutation totally inhibits the proteolytic maturation of Gag, thus generating viral particles sequestered in an immature state. Additionally, a Δ LLPs gp41 expressing variant of this plasmid was used (pCHIV PR(-) TR751).

3.3.7.1. The PR(-) variant does not process Gag

The first step was to corroborate that the pCHIV PR(-) proviral plasmids generated immature viral particles, and to study its effect in virus purification. HEK 293T cells transfected with wild type pCHIV and the immature virion generating plasmid pCHIV PR(-) were used to purify viral particles. As in section 3.3.4.1 a small aliquot of each of the fractions collected in the sedimentation velocity gradient purification was stored, loaded into an SDS-PAGE, and stained with silver nitrate to study what fraction the viral particles were obtained in (Figure 3.25A). Additionally, a small aliquot of the concentrated and purified viral particles was also loaded into a SDS-PAGE to analyze the protein pattern of the wild type and immature virions by silver stain and anti-CA and anti-MA Western blot (Figure 3.25B).

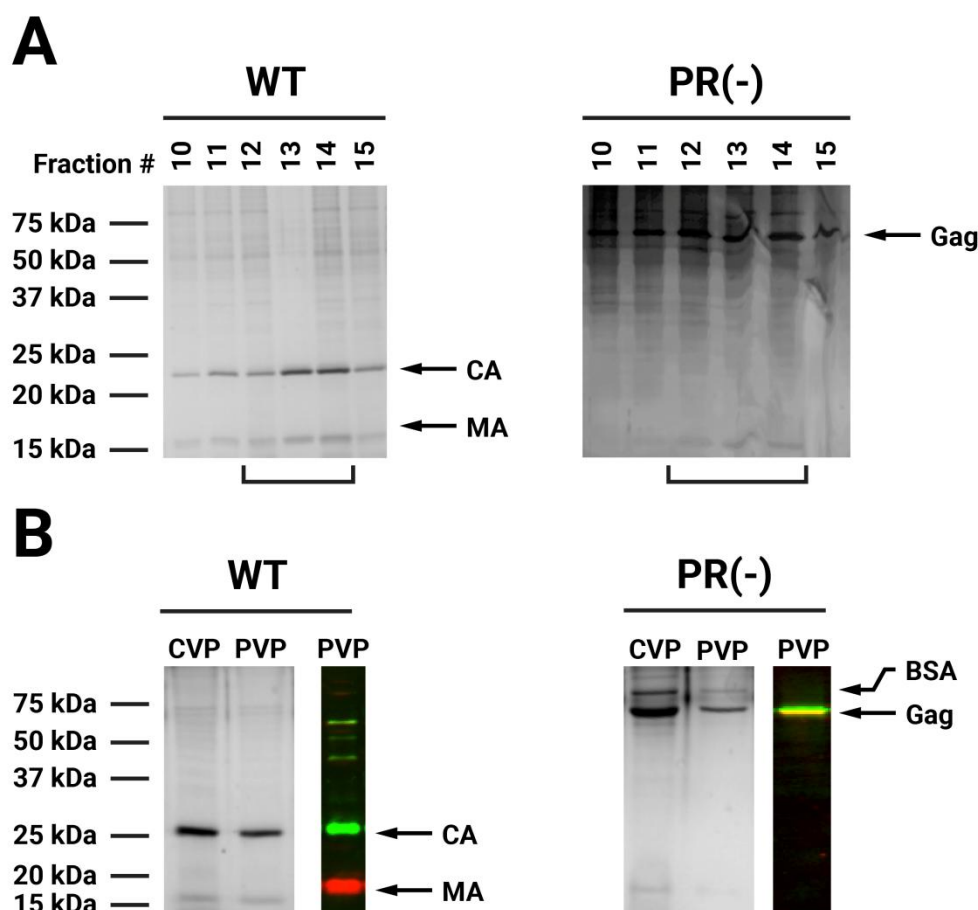


Figure 3.25 – Silver stain and Western blot analysis of fractionation and purified viral particles of mature and immature virions. **A** | Silver stain of fractions 10-15 of the viral particle purification by sedimentation velocity through Optiprep gradient step. The brackets mark the fractions collected to obtain the purified viral particles. **B** | CVP = concentrated viral particle; PVP = purified viral particle. Silver stain of concentrated and purified viral particles (grey) and Western blot analysis of purified viral particles (green and red). The Western blot was developed with sheep anti-CA and anti-sheep IRDye800 antibodies (green) and rabbit anti-MA and anti-rabbit IRDye680 antibodies (red).

The silver stain and Western blot analysis of the mature and immature viral particles demonstrate that the PR(-) variant shows a band of medium protein size (~55 kDa) which is recognized by both anti-CA and anti-MA antibodies, thus corresponding with Gag. Consequently, the PR(-) variant does not show neither the CA (~24 kDa) nor MA (~15 kDa) protein bands observed in the wild type particles. These results confirm that no free CA nor MA are present in virions obtained from the pCHIV PR(-) proviral plasmid, and that they only contain the Gag polyprotein, as expected (Figure 3.25B). Additionally, in the purification by sedimentation velocity through Optiprep gradient the most prominent CA and MA bands in the wild type virions, and Gag bands in the immature PR(-) virions, appear in both cases in fractions 12-14. In the PR(-) variant adjacent fractions present lower but still relatively high density Gag band, so a slight dispersion of the viral particles through a wider range of fractions can be observed for said variant (Figure 3.25A). Even so, these results confirm that the mutation in the PR inhibits the proteolytic maturation of Gag into its separate proteins, sequestering the virion in an

immature state, yet it does not importantly alter neither the purification process nor the density of the particles, enabling the use of the same purification protocol already established.

3.3.7.2. Maturation state does not affect interaction with cholesterol

Once the pCHIV PR(-) plasmid was confirmed to generate viral particles sequestered in an immature state, the effect of virus maturation in the LLP-dependant gp41-cholesterol interaction was studied. For that purpose, immature particles containing either wild type or Δ LLPs gp41 proteins, as well as wild type mature viral particles as a control, were purified from HEK 293T incubated with [³H]photocholesterol. The protocol followed was identical to the one described for previous experiments (sections 3.3.3.2 and 3.3.4.2). After viral particle purification, gp41 immunoprecipitation, obtention of the Western blot against gp41, and the autoradiographical detection of the lipid, both the protein and the [³H]photocholesterol signal were measured and a cholesterol/gp41 ratio was calculated and normalized with wild type samples. The interaction between the wild type and the LLP truncation variants of gp41 with cholesterol for both mature and immature viral particles is shown in Figure 3.26.

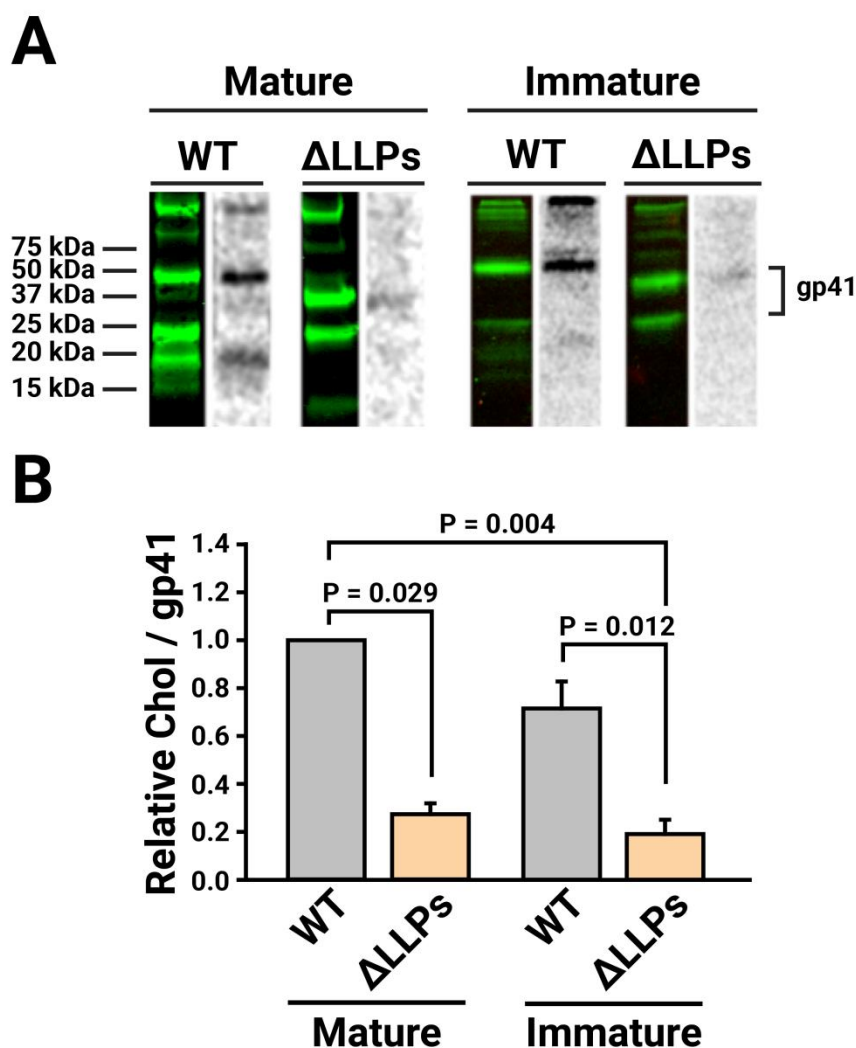


Figure 3.26 – Effect of virus maturation in the LLP-dependant gp41-cholesterol interaction in purified viral particles. **A** Representative image of the immunoprecipitated wild type and CT truncation variants of gp41 Western blot (green) and cross-linked [^3H]photocholesterol autoradiography (grey) signals obtained from a purified viral particles amount equivalent to 1 μg of CA (mature virions) or Gag (immature virions). The Western blot was developed with chessie-8 anti-gp41 primary antibody, and anti-mouse IRDye800 secondary antibody. The [^3H]photocholesterol radioactive signal was detected by autoradiography of the same membrane. **B** Quantification of the cholesterol/gp41 signal ratio of the mature and immature CT truncation variants of gp41 compared to the wild type protein. The bars represent the mean \pm SD of experiments from three independent viral purifications.

The maturation state of the viral particles does not seem to have a significant effect in gp41 interaction with cholesterol. Immature viral particles containing wild type gp41 do not show a significant difference in interaction with cholesterol when compared to mature particles with the same wild type protein. Correspondingly, the truncation of the LLP domains in the ΔLLPs variant induces a statistically significant $\sim 80\%$ reduction in the gp41-cholesterol interaction in immature particles, comparable to the reduction observed in the mature particles. Given the above, the LLP-dependant interaction of gp41 with cholesterol seems to be independent from the maturation state of the virus,

indicating that the redistribution of MA after Gag processing does not play a role in the interaction of gp41 with membrane cholesterol.

3.3.7.3. Maturation state does not affect gp41 incorporation into the virion

To corroborate if the reduction of interaction with cholesterol observed in the Δ LLPs gp41 variant in immature viral particles shown in Figure 3.26 may be caused by an alteration in gp41 recruitment into the virion derived from the immature state, the incorporation of the wild type and truncated protein were studied as in section 3.3.4.3. Viral particles obtained from HEK 293T transfected with pCHIV, pCHIV PR(-) and pCHIV PR(-) TR751 were used to quantify gp41 content in the virions.

A purified viral sample volume corresponding to 120, 100, 50 and 25 ng of CA (for mature particles) or Gag equivalent (for immature particles) was loaded into an SDS-PAGE for each variant, and a Western blot was developed against gp41 (Figure 3.27A). The integrated intensity of each gp41 band was measured and blotted against the loaded ng of CA or Gag equivalent and for each variant a linear curve fit between the gp41 signal and loaded ng of CA or Gag equivalent was calculated, and the relative slopes of the curve fits were extracted (Figure 3.27B). The experiment was repeated with three independent viral purifications to obtain a mean gp41/CA ratio for each variant (Figure 3.27C).

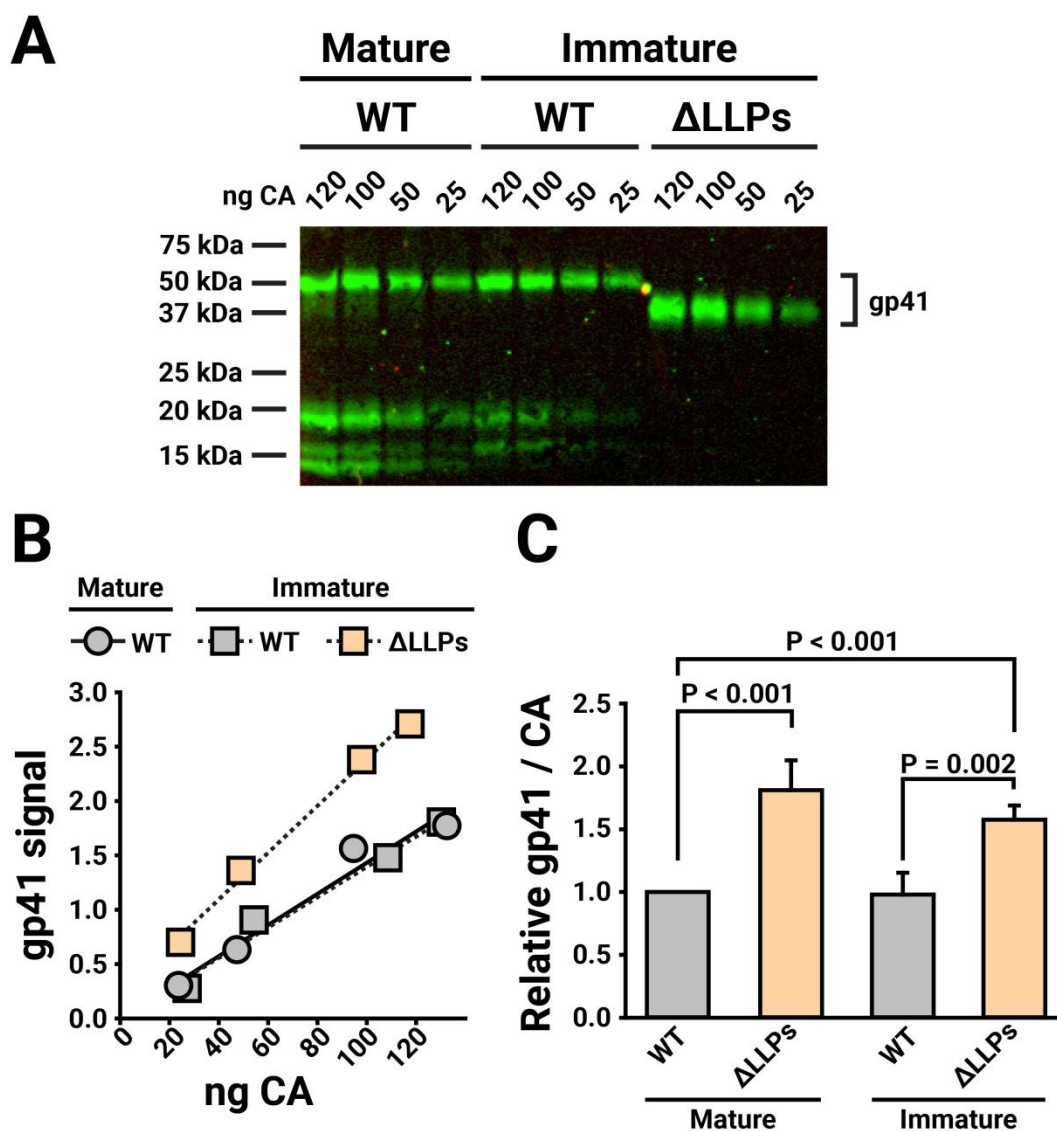


Figure 3.27 – gp41 recruitment into the virion in immature viral particles. **A** Representative Western blot of gp41 quantification. A volume of purified viral particles corresponding to 120, 100, 50 and 25 ng of CA (mature virions) or Gag equivalent (immature virions) was loaded into an SDS-PAGE for each variant. The Western blot was developed with chessie-8 anti-gp41 primary antibody, and anti-mouse IRDye800 secondary antibody (green). **B** Representative blot of gp41 signal vs ng CA or Gag equivalent. The gp41 band signal was blotted against the loaded ng of CA (mature virions) or Gag equivalent (immature virions), and the relative slopes of the linear curve fits of each variant were calculated. **C** The experiment was repeated three times and mean relative slopes were obtained for each variant. The bars represent the mean \pm SD of experiments from three independent viral purifications.

When the gp41 content of the variants is compared between mature and immature particles, and between wild type and Δ LLPs gp41 variants, the results show that the deletion of the three LLP domains (Δ LLPs variant) significantly increases the incorporation of the protein into the virion in comparable levels in both mature and immature viral particles. Similarly, no differences in wild type gp41 incorporation can be seen between mature and immature particles.

These results indicate that the mutation inhibiting the maturation of the virion does not have an effect on the gp41 incorporation into the viral particle, and that comparable to what occurs in the mature viral particles, the loss of interaction with cholesterol observed in the Δ LLPs gp41 variant (Figure 3.26) is not caused by a decrease in protein incorporation into the virion.

3.4. Discussion

The role of membrane lipids and lipid nanodomains in regulating the function of membrane proteins has long been studied. Lipid rafts, for example, have been described to be able to exclude or include proteins from certain regions of the membrane (Simons and Toomre, 2000), and lipids such as cholesterol have been shown to be tightly bound to some proteins, such as caveolins, and be necessary for their function (Smart et al., 1999). This relation between membrane lipids and proteins extends to several viral families, in which processes essential for virus replication are closely dependent on certain lipids (Lorizate and Krausslich, 2011). In the case of HIV-1, its lipid membrane has been shown to be significantly enriched when compared to the host cell plasma membrane in phosphatidylserine, hexosylceramide, or sphingomyelin, and other lipids such as cholesterol have been found to constitute almost 50% of the lipid molecules in the viral membrane (Lorizate et al., 2013). Accordingly, the general composition of the HIV-1 membrane has been described to resemble that of DRM nanodomains, which provides a strong evidence for the existence of lipid rafts in the viral membrane (Brugger et al., 2006).

Specifically, cholesterol has been described to play an important role in several steps of the HIV-1 replication cycle. Cholesterol-depleting agents such as β -cyclodextrin and statins strongly reduced HIV-1 infectivity (Campbell et al., 2002; Liao et al., 2001, 2003; Mañes et al., 2000), an effect that was also observed for cholesterol binding compounds like AME (Waheed et al., 2006). Being Env the protein responsible for the fusion between the viral and host cell membranes, a relation between this protein and the cholesterol-dependent fusion process is suggested in this thesis.

Namely, during budding of a new viral particle from the host cell, the envelope protein of HIV-1 (Env) has been shown to associate with DRMs, and this association with DRMs has been postulated to be necessary for the incorporation of Env into the virion (Bhattacharya et al., 2006). This association of Env with DRMs has been used as an indication of the possible interaction of the protein with lipids commonly associated with these membrane complexes, such as cholesterol or sphingolipids. Although the use of DRMs is of interest and has shed light in several important processes, a main drawback arises when considered carefully: studies based in DRMs rely in the use of detergents, which has been described to break certain lipid-protein interactions. Hence, although the presence of a protein in a DRM could point towards its interaction with lipids commonly associated with those structures, such as cholesterol or sphingolipids, it constitutes no absolute probe, and the absence of the protein in a DRM does not necessarily demonstrate a lack of such an interaction (Thiele et al., 2000).

In this work, the interaction of gp41 with membrane cholesterol has been studied in *in vivo* conditions by the use of photoactivatable radioactive cholesterol. The use of photoactivatable lipids presents a clear advantage over the use of DRMs, because these molecules covalently bind to any molecule closer than 3 Å after UV light irradiation (Contreras et al., 2012; Haberkant et al., 2008; Thiele et al., 2000), thus giving much more

direct information about the interaction of the lipid with a specific protein. Their radioactive labeling greatly enhances their detection, helping in the quantification of the *in vivo* protein-lipid interaction.

Using photoactivatable lipids, the results in this work demonstrate that gp41 is associated with cholesterol and sphingolipids in virus producer cells, and that this interaction is intrinsic to the protein and does not require the presence of other viral proteins (Figure 3.11), although the degree of interaction varies probably due to differences in protein expression into the plasma membrane (Figure 3.12). These results corroborate the previously published data that suggested that Env associates with DRMs, and by extension probably with cholesterol, in the cellular membrane. The results in this work have also shown that the interaction of gp41 with cholesterol is maintained in released mature viral particles (Figure 3.14A), a fact that has been long suspected but not previously demonstrated.

These results may suggest a mechanism in which the cholesterol-dependency of the fusion process described previously (Campbell et al., 2002; Liao et al., 2001, 2003; Mañes et al., 2000; Waheed et al., 2006) is based in the interaction of gp41, the protein responsible for the fusion between viral and host cell membranes, with viral membrane cholesterol. In this mechanism, alteration of cholesterol in the viral membrane (either by depletion or binding by other agents) would induce changes in the gp41 protein lipid environment, entailing an alteration of its function and the fusion between virus and host cell.

The study of the interaction of gp41 with viral membrane cholesterol in purified viral particles also generated an interesting result regarding the region responsible for the interaction: Tr-Env-CT, a protein that has been previously described and confirmed in this thesis to consist of the truncated cytoplasmic domain of gp41 (Pfeiffer et al., 2013) (Figure 3.13C), interacted with cholesterol in a level equivalent to that of the full-length gp41 (Figure 3.14B), suggesting the possibility that the cytoplasmic domain alone may be responsible for the interaction of the protein with viral membrane cholesterol. Interestingly, studies with the cholesterol binding agent Amphotericin B methyl ester, which hampers viral infectivity, found that HIV-1 strains evolved resistance to the compound by truncation of the cytoplasmic domain of gp41 (Waheed et al., 2007), further supporting that this domain is directly involved in the relation between cholesterol and infectivity.

This cytoplasmic domain of gp41 contains three highly conserved LLP (Lentiviral Lytic Peptide) sequences, which has been described to be helicoidal and membranotropic, in part due to their amphipathic nature (Abad et al., 2009). Additionally, the LLP domains have been found to be partially embedded in the membrane (Moreno et al., 2008; Murphy et al., 2017) and show cytolytic and permeabilizing properties (Miller et al., 1991, 1993). These LLP domains in the cytoplasmic domain of gp41 also regulate several processes related to the protein, including Env expression to the cell surface (Bultmann et al., 2001) and incorporation into the virion (Murakami and Freed, 2000; Piller et al., 2000), Env

stability (Lee et al., 2002) and multimerization (Lee et al., 2000), and cell-free and cell-to-cell infectivity (Durham and Chen, 2015; Kalia et al., 2003). In addition, the capacity of these domains of interacting with certain lipids or lipid nanodomains has also been studied. By tagging β -galactosidase (β -gal) with various subdomains of the gp41 cytoplasmic domain and analyzing the ability of these CT segments to target the tagged β -Gal to DRMs, other authors have shown that the LLP regions in the cytoplasmic domain of gp41 may contain lipid raft-targeting signals (Yang et al., 2010).

With the use of photoactivatable lipids, the results shown in this thesis unequivocally demonstrate for the first time that the truncation of the LLP 3 and 2 sequences of the cytoplasmic domain of gp41 significantly reduces the interaction of the protein with cholesterol (Figure 3.16). These results come in close agreement with the published data cited above in which the C-terminal two-thirds (containing the three LLPs), but not the N-terminal one-third (containing no LLP domains) of the cytoplasmic domain of gp41 was able to target β -Gal to DRMs, although the results in this work present a robust and direct demonstration of the important role of LLPs in the interaction with cholesterol, and not necessarily an association with DRMs or lipid nanodomains. Additionally, this thesis further clarifies that the LLP3 and LLP2 domains, but not the LLP1, are the regions responsible for the interaction of the gp41 with cholesterol, as the deletion of LLP1 alone has not been shown to have a measurable effect in the interaction.

In this thesis several other regions were studied as possible candidates for the interaction of gp41 with cholesterol. The MPER region of the gp41 ectodomain contains a sequence of amino acid residues conserved in several proteins known as *Cholesterol Recognition Aminoacid Consensus*, or CRAC. Peptides derived from the $_{677}\text{LWYIK}_{681}$ CRAC sequence in gp41 have been described to bind cholesterol derivatives in *in vitro* studies, an interaction that was severed by introduction of a L677I substitution (Epanand et al., 2006; Vishwanathan et al., 2008). Nevertheless, the results in this thesis challenge these findings, as they demonstrate that disruption of the CRAC sequence by introduction of the same mutation does not hamper the interaction of the full-length gp41 with viral membrane cholesterol (Figure 3.19). The study of the interaction in this thesis relies in the use of cross-linking lipids that have been demonstrated to act as endogenous lipids and be a suitable tool to study direct protein-lipid interactions (Contreras et al., 2012; Haberkant et al., 2008; Thiele et al., 2000), and the experiments in this work were carried out in *in vivo* conditions with released viral particles and a full-length gp41 protein, instead of model membranes and peptides derived from gp41 used in the works cited before. Given the above, it can be concluded that the method used in this work more closely resembles the *in vivo* situation, so while peptides composed of the CRAC sequence may interact with cholesterol derivatives *in vitro*, in the full-length gp41 protein embedded in a viral membrane, the CRAC sequence does not seem to be involved in the process.

Interestingly, the gp41 transmembrane domain or specific motifs in it were found to not be involved in the interaction with cholesterol neither. This region is the only canonically accepted membrane spanning domain, so it could be expected to be responsible for the selection of the gp41 lipid environment and the interaction with

cholesterol. Nevertheless, a complete substitution of the gp41 TMD by that of the cellular receptor CD22 in the CD22 TMD variant resulted in no alteration of the gp41 interaction with cholesterol (Figure 3.19). Additionally, the disruption of the GxxxG-motif, which is part of the transmembrane domain and has been demonstrated to be involved in cholesterol-interaction in other proteins (Barrett et al., 2012), does not have an effect in the gp41-cholesterol interaction neither. This result is not entirely surprising, as the substitution of the entire transmembrane domain did not alter cholesterol interaction, which would indicate that neither this domain nor specific sequences in it are involved in the process. Similarly, the only positively charged arginine residue in the transmembrane domain, which was suggested to be oriented close to membrane cholesterol by blind docking simulations, is not necessary for the interaction in the full-length gp41.

Finally, the role of the two most conserved arginines in the LLP2 sequence was studied. Truncation of the LLP sequences was found to reduce association of gp41 with cholesterol, but this effect does not seem to be related to the arginines in LLP2, as their substitution did not have any significant effect in cholesterol interaction (Figure 3.19), although the incorporation of the protein into the virus was heavily hampered (Figure 3.20).

These results of course do not demonstrate that the studied domains do not interact with cholesterol in any other protein structural circumstances, such as fusion intermediate or during protein trafficking to the plasma membrane. Nevertheless, although the involvement of other sequences not studied in this thesis in the interaction of gp41 with viral membrane cholesterol cannot be discarded, the LLP sequences in the cytoplasmic domain were the only regions found to be necessary for the interaction in the resting state (Figure 3.16). Additionally, in the wild type gp41 interaction studies, a protein consisting of the truncated cytoplasmic domain of gp41 with no canonical transmembrane domain sequences (Pfeiffer et al., 2013) (Figure 3.13), was found to interact with cholesterol at the same level that the full-length gp41 protein (Figure 3.14). This result further supports a direct role of the gp41 cytoplasmic domain, and specifically the LLP sequences, in the interaction with viral membrane cholesterol. This direct interaction of the LLP sequences with the lipid could be explained by several models.

The LLP domains acquire an amphipathic α -helix structure, and contain membrane targeting and perturbing properties. Additionally, they have been demonstrated to be inserted into the viral membrane in a parallel orientation with their hydrophobic residues embedded in the membrane and the hydrophilic residues protruding to the solvent (Moreno et al., 2008; Murphy et al., 2017). If their insertion into the membrane is sufficiently deep, these sequences could be directly interacting with cholesterol while maintaining their parallel orientation (Figure 3.28A).

Alternatively, several works have proposed that a region of the CT between the transmembrane domain and the LLP domains known as "Kennedy sequence" may be transiently exposed to the surface (Cleveland, 2003; Hollier and Dimmock, 2005; Lu et al., 2008), which would necessitate for gp41 to contain three membrane spanning regions.

In this alternative, the LLP3 and 2 sequences could be completely embedded in the lipid bilayer as one of the membrane spanning regions, which could facilitate a direct interaction between this region and cholesterol (Figure 3.28B).

Nevertheless, although this second direct interaction model based in the exposure of the Kennedy sequence to the extracellular region of the viral membrane deserves consideration, it is probably not the most likely model: the extracellular recognition of the Kennedy sequence by antibodies described in Env expressing cells has been suggested to not be replicated in intact released viral particles, suggesting that in virions the traditional single-transmembrane domain model more accurately reflects the conformation of gp41 (Steckbeck et al., 2010), and thus, the LLP sequences more probably interact directly with cholesterol by partially inserting into the membrane in a parallel orientation (Figure 3.28A).

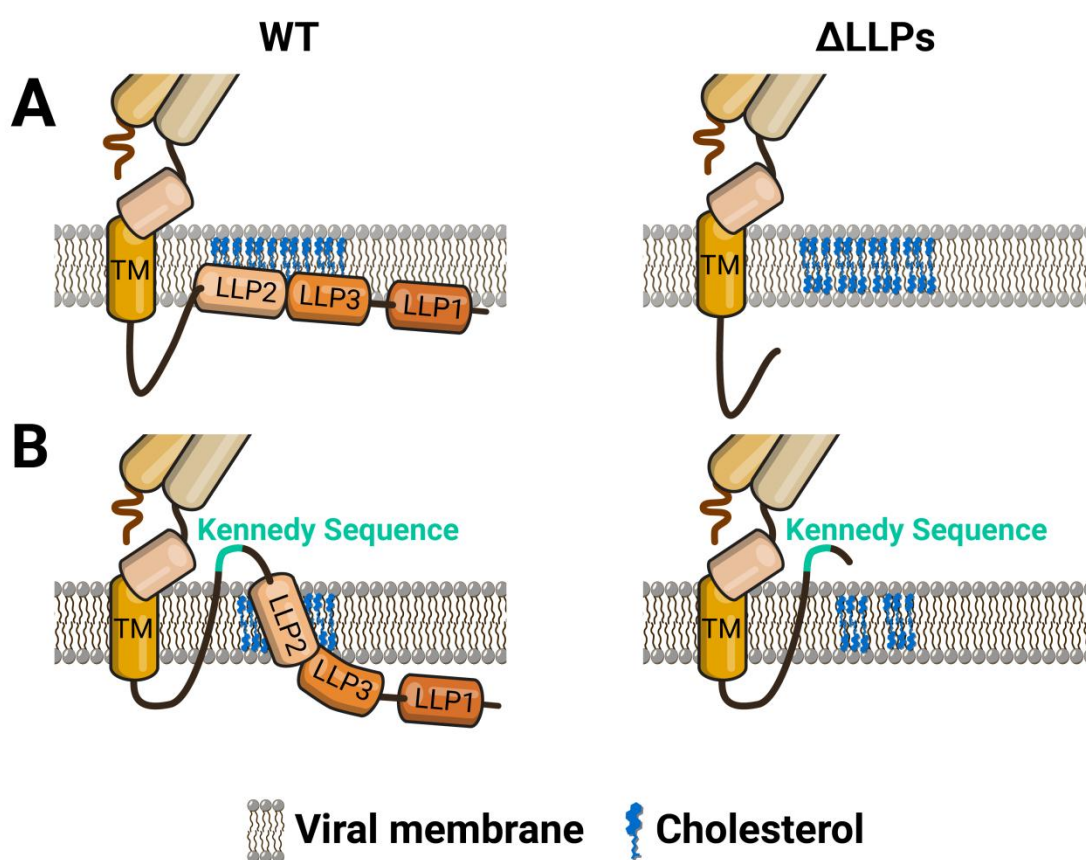


Figure 3.28 – Direct interaction models. **A|** The LLP domains may be partially embedded in the membrane, enabling a direct interaction with cholesterol. After their deletion, gp41 would lose the interaction with the lipid. **B|** To explain the transient exposure of the Kennedy sequence, the LLP sequences may be acting as a membrane spanning domain, enabling a direct interaction between this region and cholesterol. The deletion of the LLP domains would cause a direct loss of interaction.

Although the results in this thesis support a direct interaction of the LLP sequences with cholesterol, the involvement of another region not studied in this work cannot be completely discarded. It is thus possible that the regions of interaction with cholesterol

of gp41 are not the LLP sequences, but another region of the protein, and that the LLP sequences regulate the localization or conformation of the protein. On the one hand, the truncation of the three LLP domains, which constitute two-thirds of the CT of gp41, could induce a conformational change in the protein leading to the loss of interacting capacity of another region of gp41 (in the figure, the TM domain is depicted as an example, but other regions could be the ones interacting with cholesterol) (Figure 3.29A). Alternatively, although the LLP domains may not be the regions directly interacting with cholesterol, they could generate or target gp41 to a specific lipid nanodomain in the membrane and their deletion would induce a disruption of the lipid nanodomains or an exclusion of the protein from them, separating cholesterol from the protein (Figure 3.29B).

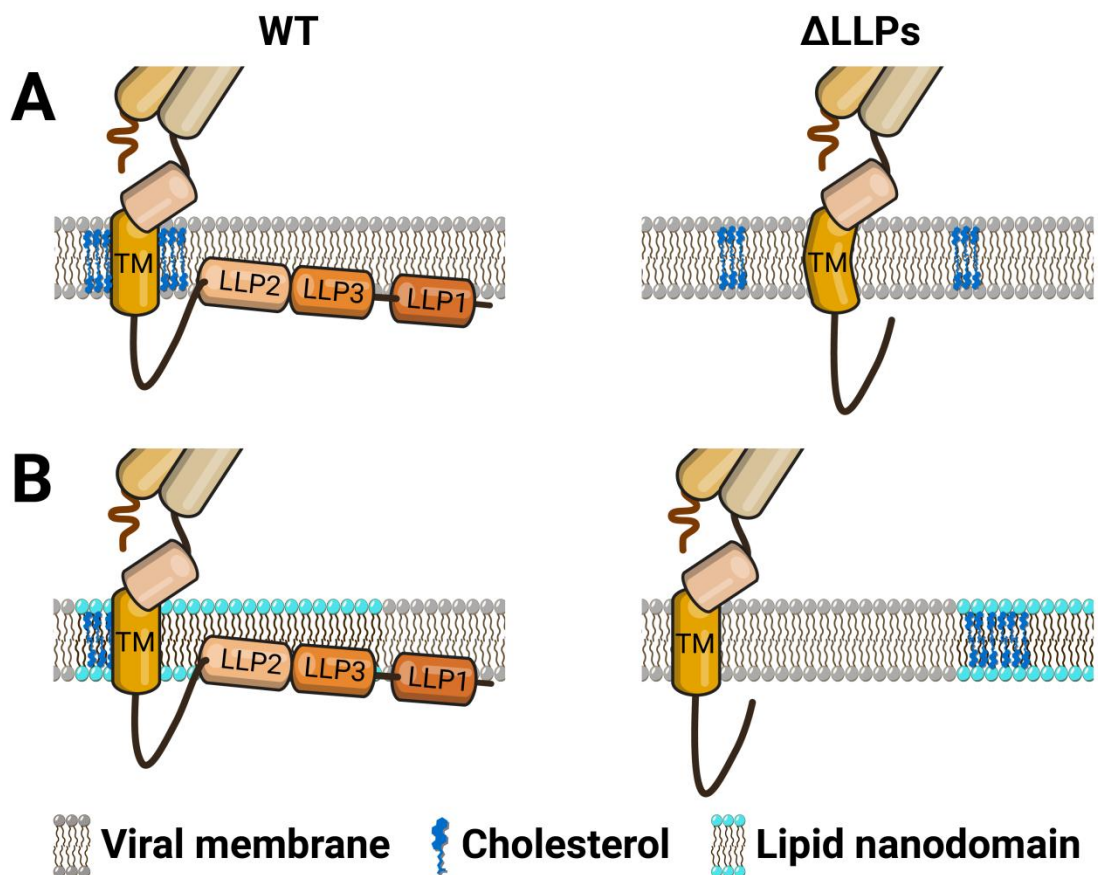


Figure 3.29 – Indirect interaction models. A) In orange shades, a gp41 monomer. Another region different to the LLP domains may interact with cholesterol (here, the TM domain is depicted as an example). After deletion of the three LLP domains, a conformational change could inhibit the interaction with the lipid. B) The LLP domains may generate or select a nanodomain, enabling another region (here, the TM domain is depicted as an example) to interact with cholesterol. After deletion of the three LLPs, gp41 would be excluded from that nanodomain, inhibiting interaction.

Nevertheless, ultimately the results in this thesis seem to support a direct model in which the LLP3 and 2 sequences interact with cholesterol by themselves by partially inserting into the membrane in a parallel orientation, as depicted in Figure 3.28A.

While studying the Env content of the mature viral particles containing the gp41 truncation variants, a role of the LLP domains in the recruitment of the protein to the virion was found in this chapter. It has long been postulated that a selection process exists in the recruitment of Env to the budding site: in cells producing viral proteins, Env has been shown to accumulate surrounding Gag assemblies, but with a lower density on the actual budding site (Muranyi et al., 2013), which seems to indicate that a recruitment mechanism coexists with a Env selection process. Similarly, recent studies suggested that Gag lattices are formed prior to Env encounter, relegating Env to the periphery of assembly sites, and limiting the amount of Env that can be incorporated (Buttler et al., 2018), although this last work is not without limitations, as it relies on the use of so-called late domain mutants, virus variants in which Gag is sequestered in a late-budding structure, which has been described to not be related with bona fide release pathways (Carlson et al., 2008).

Specifically, the cytoplasmic domain of Env has been found to regulate the recruitment of Env to budding sites, as the truncation of CT resulted in Env not accumulating in the Gag assemblies and showing a more random distribution in the membrane of producer cells (Muranyi et al., 2013). Further, other authors have reported that in the CT-dependent Env incorporation into the virion a selection/exclusion mechanism probably exists. When cells are transfected with a constant amount of Gag expression plasmid, but increasing amounts of Env expressing plasmid, the expression of the full-length Env in cells increased sequentially, while the amount of Env incorporated onto released HIV-1 particles reached a plateau. On the contrary, in an Env variant where the cytoplasmic domain was truncated, Env (Δ CT), expression in cells increased similarly, but incorporation of Env onto HIV-1 particles continued in a linear fashion without apparent saturation (Qi et al., 2013). These results, combined with the findings by (Muranyi et al., 2013), seem to indicate that the full-length Env protein is selectively accumulated around Gag assembly sites, but its localization in the budding site is regulated, as Env incorporation into the virion reaches a plateau regardless of a high expression of the protein. When the CT of gp41 is truncated, both mechanisms of accumulation around the budding site and exclusion from the actual budding site seem to be lost, as Env distributes randomly, so an increase in Env expression linearly correlates with a higher incorporation into the virion.

Although a truncation of gp41 CT entails a change in protein distribution in the cell membrane, the exact effect in protein incorporation into the virion seems to be dependent on cell type and differ from work to work: a complete deletion of the cytoplasmic domain has been shown to have no effect in Env incorporation into the virion in M8166 cells (Akari et al., 2000); to moderately reduce Env incorporation into the virion in HeLa and MT-4 producer cells and to induce a 10-fold reduction of Env incorporation in CEM and Jurkat cells (Murakami and Freed, 2000); while other authors show that the deletion of CT induces an increase in gp41 incorporation into the virion in HEK 293T cells (Wyma et al., 2004). It is important to note that these studies compared the wild type protein with a gp41 variant in which the complete CT was truncated (Δ CT), while the Δ DLLPs variant used in this work contains 47 amino acid residues remaining in the CT, which constitutes approximately a third of the tail, and thus it is not a complete

Δ CT variant. Nevertheless, they importantly demonstrate that a cell-type dependency exists in the CT regulated Env incorporation into the virion.

Interestingly, in a more detailed and comparable published study, sequential truncations of the cytoplasmic domain showed different effects in Env incorporation into the virion (Jiang and Aiken, 2007). Of special interest are the truncation of the last 42 amino acid residues of the CT (named CT42, corresponding with the Δ LLP1 variant in this thesis), which showed a reduced incorporation of gp41 into the virion, and the truncation of the last 104 amino acid residues (named CT104, corresponding with the Δ LLPs variant in this work), which showed an increased incorporation. These results come in close agreement with the findings in this thesis: the deletion of the LLP1 domain (Δ LLP1) induces a reduction of Env incorporation into the virion of ~50%, while a complete truncation of the three LLP domains (Δ LLPs) increases the incorporation of the protein to ~180% that of the wild type particles (Figure 3.18) when the virions are produced in HEK 293T cells, confirming that truncation of different regions of the CT have opposing effects in Env incorporation.

Ultimately, the results in this work show that the LLP domains play a key role in the recruitment of gp41 to the viral particle and in its interaction with cholesterol. The Δ LLPs variant of gp41 showed an increase in protein incorporation into the virion but, even so, it displayed a significant reduction in the interacting capacity with cholesterol.

Two other mutations of the gp41 protein were also found to have an effect in gp41 incorporation into the virion: substitution of the transmembrane arginine with an isoleucine (R696I variant), and substitution of the highly conserved arginines in the LLP2 domain with lysines (LLP2 R variant, R770K R778K mutation). The exchange of the positively charged arginine residue in the membrane spanning domain of gp41 resulted in a 1.5-fold increase of protein incorporation into the virion compared to the wild type protein. Previous studies concluded that this arginine was involved in the incorporation of the protein, but their studies were carried out by truncation of the cytoplasmic tail and part of the TMD which included the arginine, not by single substitutions of the residue (West et al., 2001; Yue et al., 2009). Taking into account that the results in this thesis and in previously published studies (Jiang and Aiken, 2007) demonstrate that the truncation of the cytoplasmic domain entails significant changes in protein incorporation, independent of the TMD arginine, the differences in incorporation attributed to the transmembrane domain arginine in the studies cited above are probably a mix of contributions from that specific residue and the entire cytoplasmic domain.

On the contrary, a significant decrease in Env incorporation was also observed for the LLP2 R variant. This result comes in partial agreement with previous studies, which had analyzed the effect of the substitution of the highly conserved arginines in the LLP sequences and reported a 50% decrease of incorporation into the virion (Kuhlmann et al., 2014). Although a decrease is also observed in this thesis, the results in Figure 3.20 suggest that the substitution of these arginines by lysines results in a decrease in gp41 incorporation to 175% that of wild type. Taking into account that the protein incorporation studies by Kuhlmann *et al.* were also carried out with viral particles

CHAPTER 3

obtained from HEK 293T cells, the difference in gp41 values between this work and theirs probably stems from different methods of Env quantification. Kulhmann *et al.* measured gp41 incorporation by loading a single amount of viral particles of each of the variants and staining against gp41 and CA in a Western blot. By using a single point to measure the gp41/CA ratio of the virions, this method is subject to a higher possibility of noise incorporation and errors in the measurement, as one of the protein signals measured (gp41 or CA) could not be inside the linear range of the densitometry analysis. The method used in this thesis relies on measurements in a wide range of viral concentrations, which ensures that the protein signals are within the linear range of the quantification. Additionally, by comparing the slope of the linear regression between the gp41 signal and the ng of CA loaded as detailed in the experimental techniques chapter, possible differences in protein recognition by the antibody used for the Western blot are accounted for. In summary, the gp41 quantification of the LLP2 R variant in this thesis probably better numerically represents the Env incorporation defect of the mutation.

The cytoplasmic domain of gp41, demonstrated in this thesis to be necessary for the interaction of the protein with cholesterol, has been shown to modulate fusion between the virion and the host cell (Chojnacki *et al.*, 2012; Durham and Chen, 2015; Kalia *et al.*, 2003; Murakami *et al.*, 2004; Wilk *et al.*, 1992; Wyma *et al.*, 2004). After determining that the LLP3-2 sequences are necessary for the interaction of gp41 with cholesterol, the relation between this loss of interaction and the function of the protein was studied by measuring the fusion activity of the viral particles. Our results show that the deletion of the LLP sequences hampers virus entry capacity to the host cell (Figure 3.23), which comes in agreement with previously published work (Durham and Chen, 2015; Jiang and Aiken, 2007).

When the entry assay is carried out loading the same amount of viral particles for all of the gp41 variants, the deletion of the LLP1 domain in the Δ LLP1 variant also shows an apparent entry defect. Nevertheless, contrary to the Δ LLPs variant, the Δ LLP1 mutation was shown to hamper gp41 incorporation into the virion (Figure 3.18), resulting in each virion containing approximately half the Env molecules, and thus trimers, than the wild type particle. Although the exact number of Env trimers required to interact with host cell receptors to generate a fusion between viral and cellular membranes is not yet completely defined and seems to be different between viral strains, a minimum set amount seems to exist, and viral particles containing a number of Env trimers below this minimum show a defect in entry capacity even if individual trimers function properly (Brandenberg *et al.*, 2015). Thus, the reduced entry capacity of the Δ LLP1 variant could be caused by the decrease in Env molecules in the virion and not by a loss of function of the gp41 protein caused by the truncation. When the gp41 incorporation reduction was compensated with an increased amount of virus in the entry assay, the Δ LLP1 variant promptly recovered the entry capacity to levels equivalent to the wild type particles (Figure 3.24). Instead, the Δ LLPs variant shows an increase in Env incorporation into the virion, so it can be concluded that the loss of entry capacity is not related to a reduction of the number of Env trimers in the virion.

When analyzed in combination with the previous results, the entry capacity studies suggest that the truncation of the LLP1 domain induces a defect in Env incorporation into the virion, but does not directly alter neither the fusion capacity of gp41 nor the interaction of the protein with cholesterol. On the other hand, the deletion of the three LLP domains in the Δ LLPs variant induces a clear loss of virus entry capacity, not related with a defect in Env incorporation (as this variant presents an increase of gp41 quantity in the virus), but probably related with the loss of gp41-cholesterol interaction.

The interaction between gp41 and the underlying MA lattice has been studied for a long time, and although a cross-talk between the two seems to exist and the involvement of the long cytoplasmic domain is accepted, no definitive mechanism has yet been proposed (Checkley et al., 2011).

Among other interesting published studies, both the gp41 cytoplasmic domain and the maturation of Gag have been described to have an effect in Env clustering in the viral membrane: upon virus maturation and proteolytic release of MA from Gag, wild type Env has been shown to rearrange in the membrane from a random distribution to a single cluster, while the formation of this cluster is inhibited when the gp41 CT is truncated (Chojnacki et al., 2012). Maturation of the virion has also been shown to have an effect in the mobility of Env in the viral membrane, which may be tied to its clustering, and this coupling between maturation and Env mobility is also lost when the gp41 CT is truncated (Chojnacki et al., 2017).

These results give weight to the idea that virus maturation and Env redistribution and diffusion are connected via direct or indirect interactions of gp41 CT with the underlying Gag/MA lattice. It follows then that the interaction between Gag/MA and gp41 CT, and the maturation state of the virion could also have an effect in the LLP-dependant interaction between gp41 and cholesterol. Nevertheless, when the cholesterol-interacting capacity of full-length and Δ LLPs gp41 variants was compared between mature and immature particles, the results demonstrated that the maturation state of Gag does not have an effect in the LLP3-2 dependent gp41 interaction with viral membrane cholesterol (Figure 3.26).

Thus, when compared with previously published studies, these results bring an interesting distinction between maturation, gp41 mobility and diffusion, clustering and interaction with cholesterol. In mature viral particles, if the gp41 protein contains the three LLP domains it closely interacts with viral membrane cholesterol (Figure 3.14), and this full-length gp41 is also capable of freely diffusing on the membrane (Chojnacki et al., 2017) and generating the Env clusters necessary for the fusion between the virus and the host cell (Chojnacki et al., 2012). In immature viral particles, wild type Env retains the cholesterol interacting capacity (Figure 3.26), but its diffusion and clustering is hampered. The deletion of the LLP domains in the CT induces a loss of gp41-cholesterol interaction (Figure 3.26) and this has an effect in clustering capacity, both in mature and immature viral particles, while the diffusion rate of the protein remains comparable to the wild type particles independently of the maturation state of the virus (Table 3.6).

Table 3.6 – Env diffusion, clustering, and cholesterol-interaction of gp41 variants in mature and immature viral particles.

Maturation state	Gp41 variant	Diffusion (Chojnacki et al., 2017)	Clustering (Chojnacki et al., 2012)	Cholesterol-interaction
Mature	Full-length	Positive	Positive	Positive
	Δ LLPs or Δ CT	Positive	Negative	Negative
Immature	Full-length	Negative	Negative	Positive
	Δ LLPs or Δ CT	Positive	Negative	Negative

These could indicate that the LLP3-2 dependent gp41 interaction with cholesterol is necessary or closely related with the clustering of the protein in the membrane, and thus with the fusion capacity of Env, while the diffusion of the protein relates to the steric hindrance between the long cytoplasmic domain of gp41 and the underlying rigid Gag lattice, and is not related to the interaction of the protein with cholesterol.

The hypothesis proposed in this work is that the interaction of gp41 with cholesterol is required for the coalescence of the Env molecules into a single cluster necessary for the fusion between viral and cellular membranes. In wild type HIV-1 particles, the full-length gp41 protein interacts with viral membrane cholesterol. Upon maturation and release of the Env from the rigid underlying Gag lattice, the trimers coalesce into cholesterol-rich domains, generating the cluster (Chojnacki et al., 2012) necessary for efficient fusion with the host cell (Figure 3.30A). This interaction with cholesterol is regulated, probably directly, by the LLP3-2 sequences in the cytoplasmic domain, and upon truncation of said sequences gp41 loses the cholesterol interacting capacity. After maturation, truncated Env trimers cannot coalesce into a cluster as they are excluded from the cholesterol membrane domains, which results in a random distribution (Chojnacki et al., 2012) in which Env trimers cannot work coordinately and fusion is hampered (Figure 3.30B). In immature viral particles, wild type full-length gp41 retains the interaction with cholesterol, but its diffusion and mobility is hampered by a steric hindrance between the long cytoplasmic domain of the envelope protein and the rigid underlying Gag lattice (Chojnacki et al., 2017). Because the mobility and diffusion of gp41 is restricted, even if the protein interacts with cholesterol, it cannot efficiently cluster (Chojnacki et al., 2012).

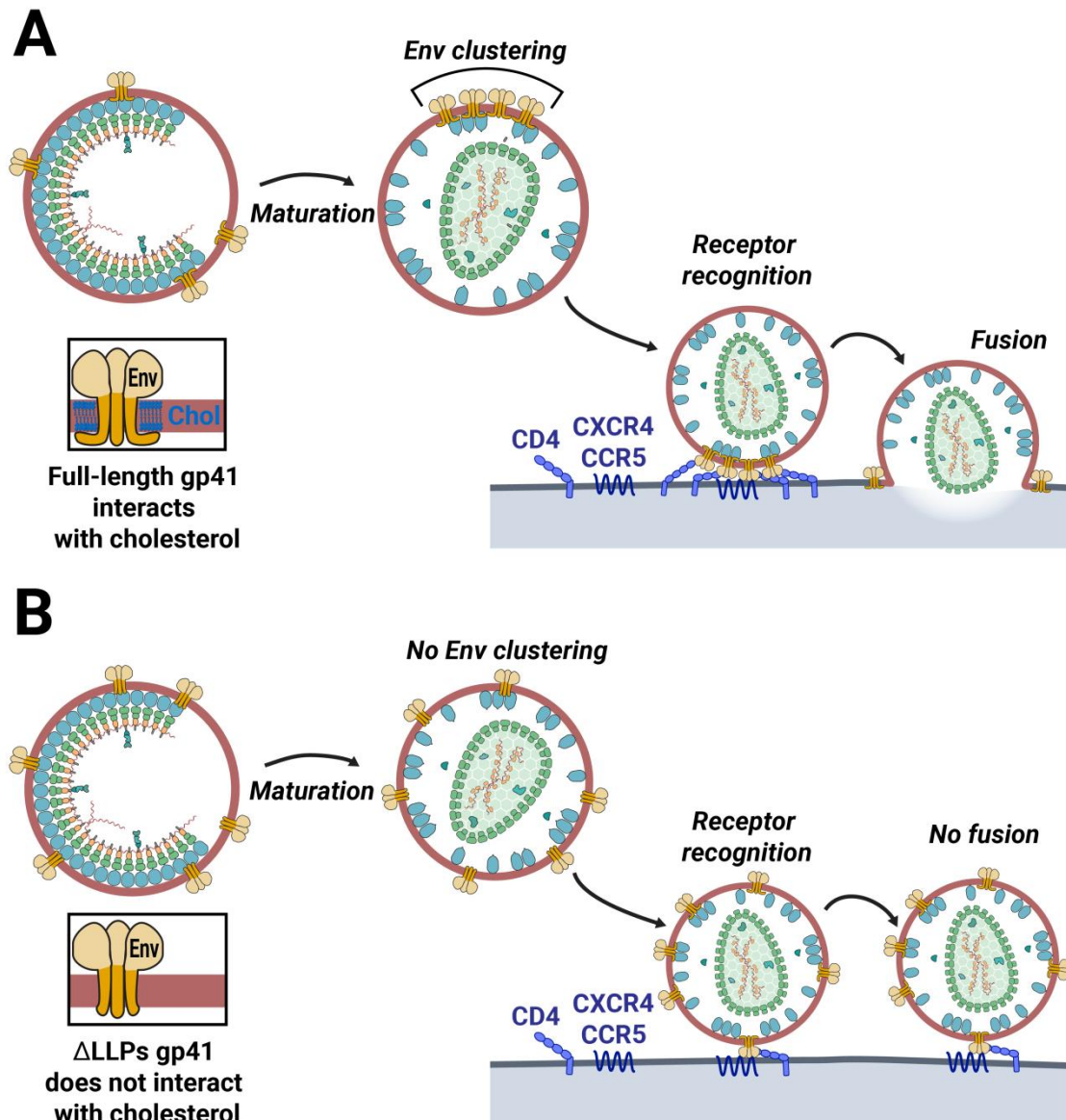


Figure 3.30 – Env clustering depends on LLP-mediated cholesterol interaction. **A** In wild type HIV-1 particles, the full-length gp41 protein interacts with viral membrane cholesterol via the LLP sequences in the cytoplasmic domain. Upon maturation, Env trimers coalesce into a single cluster mediated by their interaction with cholesterol, which enables efficient fusion with the host cell. **B** When the LLP sequences or the entire CT of gp41 are truncated, the protein loses the capacity to interact with cholesterol. Upon maturation, truncated Env trimers cannot coalesce into a single cluster as they are excluded from cholesterol-rich domains. The absence of an Env cluster results in a defect in fusion with the host cell.

In summary, this model postulates that the interaction with cholesterol mediated by the LLP sequences in the gp41 cytoplasmic domain is necessary for an efficient clustering of the Env molecules in the virion, although the diffusion of the protein, regulated by steric hindrance between the CT and Gag, also has an effect in the coalescence of Env into a single focus.

Chapter 4. Lipidomimetic Compounds as HIV-1 Entry Inhibitors

4.1. Introduction

Human immunodeficiency virus type 1 (HIV-1) is an enveloped retrovirus, which infects CD4-positive human cells. HIV-1 morphogenesis at the plasma membrane of the infected cell is driven by the viral Gag polyprotein whose N-terminal MA (matrix) domain interacts with phosphatidylinositol (4,5) biphosphate (PI(4,5)P₂) (Lorizate and Krausslich, 2011). Since retroviruses do not encode lipid-synthesizing enzymes, their lipid envelope composition depends on the membrane through which the virus buds (van Genderen et al., 1995; Griffiths and Rottier, 1992). However, viral membrane composition may differ from the donor cell membrane if virus assembly occurs at membrane subdomains or involves lipid sorting. Early studies of HIV-1 lipid composition indicated significant differences between the viral membrane and the host cell plasma membranes (Aloia et al., 1988, 1993). This observation was later confirmed by more detailed analyses of the entire viral lipidome. The HIV-1 membrane was shown to be significantly enriched in phosphatidylserine (PS), sphingomyelin, hexosylceramide and saturated phosphatidylcholine species when compared to the host cell plasma membrane (Brugger et al., 2006; Chan et al., 2008; Lorizate et al., 2013). Overall, the HIV-1 lipid composition is typical of lipid rafts (Brugger et al., 2006). Moreover, labeling HIV-1 with the order-sensing dye laurdan revealed a liquid-ordered (L_o) structure of the viral envelope (Lorizate et al., 2009).

The intrinsic properties of the viral membrane, as well as its lipid composition, have been shown to be of importance for infectivity. Cholesterol-depleting agents (β -cyclodextrin and statins) (Campbell et al., 2002; Liao et al., 2001, 2003; Mañes et al., 2000) or cholesterol-binding compounds (amphotericin B methyl ester) (Waheed et al., 2006) as well as inhibition of sphingomyelin biosynthesis (Brugger et al., 2006; Mizrachi et al., 1996; Tamma et al., 1996) strongly reduced HIV-1 infectivity, indicating an important contribution of its raft-like membrane lipid composition and/or structure to viral infection. A similar effect was observed when ceramide levels were increased in the viral membrane (Finnegan et al., 2004) or upon addition of a compound (GT11), which leads to higher dihydrosphingomyelin levels (Vieira et al., 2010), an unusual lipid enriched in the viral membrane (Brugger et al., 2006). Based on the concept of inverted cone-shaped lipids as fusion inhibitors (Chernomordik et al., 1995), synthetic rigid amphipathic fusion inhibitors (RAFIs) have been designed as potential antivirals (St.Vincent et al., 2010). These compounds insert into the viral membrane and promote positive curvature, thus increasing the energy barrier for fusion. RAFIs were shown to inhibit fusion of several unrelated enveloped viruses.

In this chapter, a screen of lipidomimetic compounds was performed, the majority of which resembling raft lipids, for their capacity to alter the membrane of HIV-1 and interfere with viral infectivity. Several compounds structurally related to cholesterol, sphingosine or aliphatic lipids with long-chain fatty acids inhibited HIV-1 infection at the stage of entry. Similar inhibition was observed when HIV-1 was pseudotyped with heterologous envelope proteins, indicating that the effect was independent of the entry

CHAPTER 4

pathway and the envelope proteins mediating it. Incorporation of the compounds into the viral membrane inhibited viral membrane fusion, induced changes in viral membrane order and subtle shifts in particle buoyant density. Thus, altering virion membrane structure by lipid-active compounds may be a promising approach for inhibiting HIV.

4.2. Experimental techniques

4.2.1. Cell culture and virus purification

HEK 293T and HeLa TZM reporter cells (Wei et al., 2002) and DFJ8 cells (Barsov et al., 2001) were kept in Dulbecco's modified Eagle's medium (DMEM), MT-4 cells (Harada et al., 1985) were kept in RPMI 1,640 medium. Both media were supplemented with 10% heat inactivated fetal calf serum (FCS), penicillin, streptomycin, 4 mM glutamine, and 10 mM HEPES. Cell cultures were maintained at 37 °C and 5% CO₂. All investigated HIV strains and constructs are listed in *Chapter 2* and in Table 4.1.

Table 4.1 – Overview of constructs and virus strains used in this chapter.

Construct and strains	Description	Reference
pCHIV	HIV-1 proviral plasmid generating non-infectious HIV-1 like particles.	(Lampe et al., 2007)
pNL4-3	HIV-1 proviral plasmid generating infectious particles.	(Adachi et al., 1986)
pMM310	Plasmid encoding the Vpr-BlaM fusion protein.	(Munk et al., 2002)
HIV-1 _{NL4-3}	Infectious HIV-1 strain, CXCR4-tropic.	(Adachi et al., 1986)
HIV-1 Vpr-BlaM	Infectious NL4-3 strain carrying Vpr-BlaM within virus particles.	(Cavrois et al., 2002)
MLV-Env	Friend ecotropic Murine Leukemia Virus glycoprotein.	(Sherer et al., 2003)
VSV-G	G glycoprotein of Vesicular Stomatitis Virus.	(Emi et al., 1991)
AAV2	Adeno-associated virus.	(Grimm, 2002)

For virus production, MT-4 cells were infected with HIV-1 strain NL4-3 (Adachi et al., 1986), and virus was harvested from cocultures of infected and uninfected cells before cytopathic effects were observed (Welker et al., 2000). HEK 293T cells were transfected with the proviral plasmid pNL4-3 (Adachi et al., 1986) or with pCHIV (Lampe et al., 2007) by calcium phosphate precipitation, as described in *Chapter 2*. For generation of pseudotyped particles, cells were co-transfected with pNL4-3 carrying a deletion of the envelope gene and a plasmid expressing either the G glycoprotein of Vesicular Stomatitis Virus (VSV) (Emi et al., 1991) or the envelope proteins of Friend ecotropic Murine Leukemia Virus (MLV) (Sherer et al., 2003) at a molar ratio of 1:2. HIV-1 purification was performed as described in section *Chapter 2*, starting with medium

harvesting, clarification, and particle concentration and purification. The particle concentration was determined by enzyme-linked immunosorbent assay (ELISA) of p24. Inactivation of infectious HIV-1 was performed by incubating the virus with 5 mM AT-2 (2,2'-dithiodipyridine; aldrithiol-2; Sigma) for 1 h at 37 °C with gentle stirring (Rossio et al., 1998). Successful inactivation was controlled by culturing inactivated samples for 10 days with highly susceptible C8166 cells. In the case of adeno-associated virus (AAV) purification, standard triple transfection, and cesium chloride (CsCl) density gradient purification procedures were used (Grimm, 2002).

4.2.2. Chemistry

The preparation of 3 β -amino-28-methoxylupene is described in (Knölker et al., 2009). J391B (3 α -amino-28-methoxylupene) was synthesized by GVK Bio (Hyderabad, India) following the identical procedure for the β -anomer. The purity was established to be > 98% by high-performance liquid chromatography (HPLC). The synthesis of J582C (Oxazolin 200) was performed as described (Zankl, 2009) with a purity of 99.2% by HPLC. IBS70 (STOCK1S-60139) and IBS95 (STOCK3S-53354) were purchased from Interbioscreen Ltd. (<http://www.ibscreen.com>).

4.2.3. Screening

Each compound was screened in duplicate, and each screen was repeated a total of two times. Compound stock solutions at 2 mM were stored in glass vials. 100 μ l of purified HIV-1_{NL4-3} (0.5-0.7 μ g/ml p24) was incubated for 30 min at 400 rpm and 37 °C on a thermomixer (Eppendorf) with the compounds at 20 μ M and 1% FCS in a 96-well glass-coated V-bottom plate (LabHut) and then diluted 1:10 into MT-4 cell suspension culture: 180 μ l MT-4 cells were seeded into 96-well plates (CORNING, Poly-D-lysine surface) at a cell density of 10⁵ cells/well and 20 μ l (25-35 ng p24) virus-compound mixture was added to the cells, mixed by pipetting and incubated at 37 °C. 18 h post-infection DNA was extracted and subjected to real-time PCR. DNA was isolated using QIAamp 96 DNA Blood Kit and vacuum extraction according to supplier's instruction. Real time PCR was performed with QuantiTect SYBR Green PCR Master Mix (Qiagen): 20 μ l reaction mix; twin.tec real-time PCR 96 well plates (skirted) and optical caps for RT-PCR; 10 μ l master mix plus primers (TIP Molbiol) at a concentration of 10 μ M each and 8.8 μ l DNA template. The program used was: 1x 15 min 95 °C, followed by 40x 15 s 95 °C 30 s 60 °C, 30 s 72 °C.

4.2.4. Compound treatment of virus particles and cells

MT-4 cells were seeded in poly-D-lysine 96-well plates (CORNING, Poly-D-lysine surface) and TZM cells were seeded in glass 96-well plates (Costar). Stocks of purified HIV-1_{NL4-3} were incubated with the different compound concentrations or DMSO as solvent control, in glass-coated plates (Costar) for 30 min at 37 °C in RPMI or DMEM medium containing 0.1% FCS. Subsequently, 50 µl virus-compound suspension was diluted into 150 µl medium containing 0.1% FCS (final p24 amounts 25-35 ng) and used to infect target cells for 2 h. Following 2 h exposure, cells were washed and cultivated for 2 more days in complete DMEM or RPMI media.

For pretreatment of cells, compounds at the indicated concentrations or DMSO as solvent control were incubated in glass-coated 96-well plates (250 µl/well) for 30 min at 37 °C in DMEM containing 0.1% FCS. Subsequently, 100 µl of each compound suspension was added to the target cells for 30 min at 37 °C followed by addition of untreated HIV-1 (25-35 ng p24) in 50 µl of medium with 0.1% FCS. Following 2 h exposure, cells were washed and cultivated for 2 more days in complete DMEM followed by infectivity readout as in section 4.2.5.

A similar procedure was done for simultaneous virus and compound addition. Cells were pre-washed with media containing 0.1% FCS, and compounds at the indicated concentrations or DMSO as solvent control were incubated in glass-coated 96-well plates (250 µl/well) for 30 min at 37 °C in DMEM containing 0.1% FCS. Afterwards 100 µl of compounds was added to the cells and immediately followed by adding untreated HIV-1 (25-35 ng p24) in 50 µl medium with 0.1% FCS for 2 h. Following a washing step, cells were cultivated for 2 more days in complete DMEM and scored for viral infectivity.

4.2.5. Infectivity and luciferase reporter assay

To determine the effect of the compounds in virus infection, intracellular capsid (CA) staining was performed. MT-4 cells were seeded in poly-D-lysine 96-well plates (CORNING, Poly-D-lysine surface). Cells were infected, as explained in section 4.2.4, with different amounts of compound-pretreated virus for 2 h, followed by cultivation in medium containing 10% FCS for 2 more days. Subsequently, cells were fixed with 4% paraformaldehyde and permeabilized for immunostaining. HIV-1 infected cells were identified by automated microscopic readout following staining with a phycoerythrin-conjugated antibody against the viral p24 CA protein (KC57-RD1; Beckman Coulter). For each well the microscope takes 16 measurements.

In case of AAV infection, TZM cells were seeded in glass 96-well plates (Costar). Afterwards virus-compound mixtures in medium containing 0.1% FCS were added to TZM cells for 2 h, followed by cultivation in medium containing 10% FCS for 2 more days. To quantify AAV-infected cells, the encoded mCherry reporter was detected by

automated microscopy 48 h after infection. Images were acquired via fluorescence microscopy and then automatically analyzed using proprietary software.

The infectivity of compound-treated HIV-1 was determined on TZM-bl reporter cells as described in section *Chapter 2*. Briefly, TZM-bl reporter cells (1.2×10^4 cells/well) were seeded one day before infection in a 96-well plate and were infected with compound-treated virus at desired concentrations as explained above. At 48 h post-infection, cells were lysed and luciferase activity was measured in the lysates as described by the manufacturer using the Promega Steady Glo kit and a microplate luminometer (Luminoskan Ascent, Thermo Labsystems). Uninfected cells were cultivated in the presence of compounds at the identical concentrations used in the infection assays, or in the presence of solvent alone (reference control). Following 2 h compound exposure, cells were washed and cultivated for 2 more days, at which time the cytotoxicity was determined by quantifying the amount for a formazan product metabolized by viable cells from the 3-(4,5-dimethylthiazol-2-yl)-2,5-diphenyltetrazolium bromide (MTT) solution (Sigma) as reported (Mosmann, 1983). Alternatively, compounds were present for 2 days before the MTT assay.

4.2.6. Entry assays

Standard HIV fusion assays were performed as described in *Chapter 2*. Briefly, HIV-1 particles carrying a Vpr-BlaM fusion protein were obtained by co-transfection of HEK 293T cells with pNL4-3 or plasmids for HIV pseudotype production and plasmid pMM310 encoding the Vpr-BlaM fusion protein (5 μ g pMM310 : 15 μ g pNL4-3). Particles were harvested, concentrated, and treated with the respective compounds as described in section 4.2.4. The virus-compound mixture was added to cells and cells were subsequently washed once, and 60 μ l of CCF2-AM β -lactamase loading solution was added and incubation was continued for 15h at room temperature. Relative fluorescence intensities of the cleaved and uncleaved substrate were recorded using a TECAN Safire instrument. After subtraction of background from unstained cells at the respective emission wavelength, the ratio of emission intensities at 447/512 nm was calculated.

4.2.7. Sucrose-density equilibrium gradient centrifugation and Western blot analysis

HIV-1_{NL4-3} or non-infectious HIV-like particles derived by transfection of pCHIV (1-3 μ g p24) were incubated with the respective compounds, solvent (DMSO; 0.35% v/v) or Triton X-100 (TX-100, 0.5% w/v). Subsequently, the particle suspensions were loaded onto a 20-60% linear sucrose gradient. After ultracentrifugation at 44,000 rpm for 16 h at 4 °C in a SW60 rotor, 20 fractions of 200 μ l each were carefully collected from top to bottom and the p24 concentration was analyzed by anti-CA Western blot as explained in *Chapter 2*.

The sucrose density of the fractions was calculated from refractive indices determined with a refractometer (Abbe, Carl Zeiss). Carefully prepared sucrose solutions were used to build the gradient and as standards in the refractometer. For this purpose a sucrose gradient was run placing loading buffer instead of particle suspension on top of the gradient. After ultracentrifugation fractionation was carried out in the same manner as above (20 fractions of 200 μ l each, from top to bottom), and the refractive index of each fraction was measured. Sucrose density in g/cm^3 was calculated from the refractive index of the standards.

For stability analysis, purified HIV-1 or HIV-like particles (3 μ g p24) were exposed to compounds or solvent (DMSO; 0.35% v/v) for 30 min at 37 $^{\circ}\text{C}$, pelleted through a 20% (w/v) sucrose cushion by ultracentrifugation (32,000 rpm, 4 $^{\circ}\text{C}$, 2 h) and re-suspended in 25 μ l SDS-PAGE sample buffer for subsequent analysis by Western blotting as described in *Chapter 2*, immunoblotted against gp41 with Chessie-8, against CA with sheep anti-CA, and MA with rabbit anti-MA, and developed with donkey anti-mouse IRDye 800, donkey anti-sheep IRDye 800, and donkey anti-rabbit IRDye 680.

4.2.8. HIV-1 laurdan staining and analysis of labeled particles

Optiprep-purified HIV-1 particles were incubated for 10 min at room temperature with 5 μ M laurdan (Molecular Probes). Labeled HIV-1 particles were subsequently purified by ultracentrifugation for 45 min through a 20% sucrose cushion in a SW60 rotor at 44,000 rpm (Lorizate et al., 2009). In the case of compound treatment, laurdan labeled HIV-1 particles were incubated with different amounts of lipidomimetics at 37 $^{\circ}\text{C}$ for 30 min under gentle stirring, followed by viral particle collection by ultracentrifugation for 2 h through a 20% cushion in a SW60 rotor at 32,000 rpm. Particles were carefully resuspended in 150 mM NaCl, 10 mM HEPES pH 7.4 and analyzed by fluorescence spectroscopy.

All fluorescence measurements were made using an SLM Aminco series 2 (Spectronic Instruments) spectrofluorimeter. Temperature was controlled during measurements, and samples were allowed to equilibrate for 5 min before measurement at each temperature. Laurdan excitation was set at 355 nm, and emission spectra were recorded. The fluorescence intensity of solvent-treated unstained HIV-1 purified in parallel was subtracted to remove the signal due to particle scattering. Furthermore, the spectrofluorometer provides an internal instrument correction, which was applied in all measurements. The program corrects any wavelength-dependent instrument response. To quantify changes in the laurdan emission spectrum, generalized polarization (GP) values were calculated:

$$GP = \frac{(I_B - I_R)}{(I_B + I_R)}$$

where I_B (at 440 nm) and I_R (at 490 nm) correspond to the intensities at the blue and red edges of the emission maxima of laurdan, respectively (Parasassi et al., 1990, 1991).

4.2.9. Lipid extraction, production of lipid vesicles and intervesicular MPER lipid mixing assay

Lipid extractions were performed according to the method of Bligh and Dyer (Bligh and Dyer, 1959). Large unilamellar vesicles (LUV) were prepared following the extrusion method (Hope et al., 1985). Laurdan-labeled LUV at a concentration of 30 μM were treated with specified amounts of lipidomimetics in PBS containing 0.1% FCS for 30 min at 37 °C under continuous stirring, followed by determination of GP profiles as in section 4.2.8. The following lipids were purchased from Avanti lipids: 1-palmitoyl-2-oleoyl-sn-glycero-3-phosphocholine (POPC); 1,2-dipalmitoyl-sn-glycero-3-phosphocholine (DPPC); 1,2-dioleoyl-sn-glycero-3-phosphate (DOPA); 1,2-dioleoyl-sn-glycero-3-phospho-L-serine (DOPS); 1,2-dioleoyl-sn-glycero-3-phosphoglycerol (DOPG); cholesterol (Chol); brain sphingomyelin (SM); 1-palmitoyl-2-hydroxy-sn-glycero-3-phosphocholine (LPC); L- α -phosphatidylethanolamine-N-(7-nitro-2-1,3-benzoxadiazol-4-yl) (N-NBD-PE); L- α -phosphatidylethanolamine-N-(lissamine rhodamine B sulfonyl) (N-Rho-PE).

Membrane lipid mixing was monitored in an SLM Aminco series 2 (Spectronic Instruments) spectrofluorimeter using a resonance energy transfer assay. The assay is based on the dilution of N-NBD-PE and N-Rho-PE (Struck et al., 1981). N-Rho-PE acts as a quencher of the N-NBD-PE fluorescence when both are present in a vesicle membrane at sufficient concentration. Upon dilution (e.g. by fusion of labeled with unlabeled vesicles), the fluorescence of N-NBD-PE is dequenched and becomes detectable (Figure 4.1). Labeled 10 μM POPC:POPS:SM:Chol (18:15:33:33 mol:mol) LUVs (NBD/Rho LUV) were incubated with different compound concentrations or LPC as fusion inhibition control for 15 min at 25 °C with continuous stirring. Afterwards, 40 μM of unlabeled LUV were added for 20 more min. Rates of fusion between vesicle mixtures were measured by following changes in fluorescence intensity at 530 nm (ex = 450 nm) as a function of time. Once the baseline signal stabilized (0% fusion), the system was considered equilibrated. Then, 0.5 μM of membrane-proximal external region (MPER) peptide was added to launch the fusion reaction and incubation continued for 15 min at 25 °C. Intervesicular lipid mixing was measured as an increase of fluorescence of N-NBD-PE caused by fusion of the labeled and unlabeled vesicle membranes. Finally, in order to obtain the 100% fusion value, 0.1% Triton X-100 was added. The fluorescence baseline before addition of MPER was defined as 0% fusion, and maximal fluorescence following final detergent addition was defined as 100% fusion.

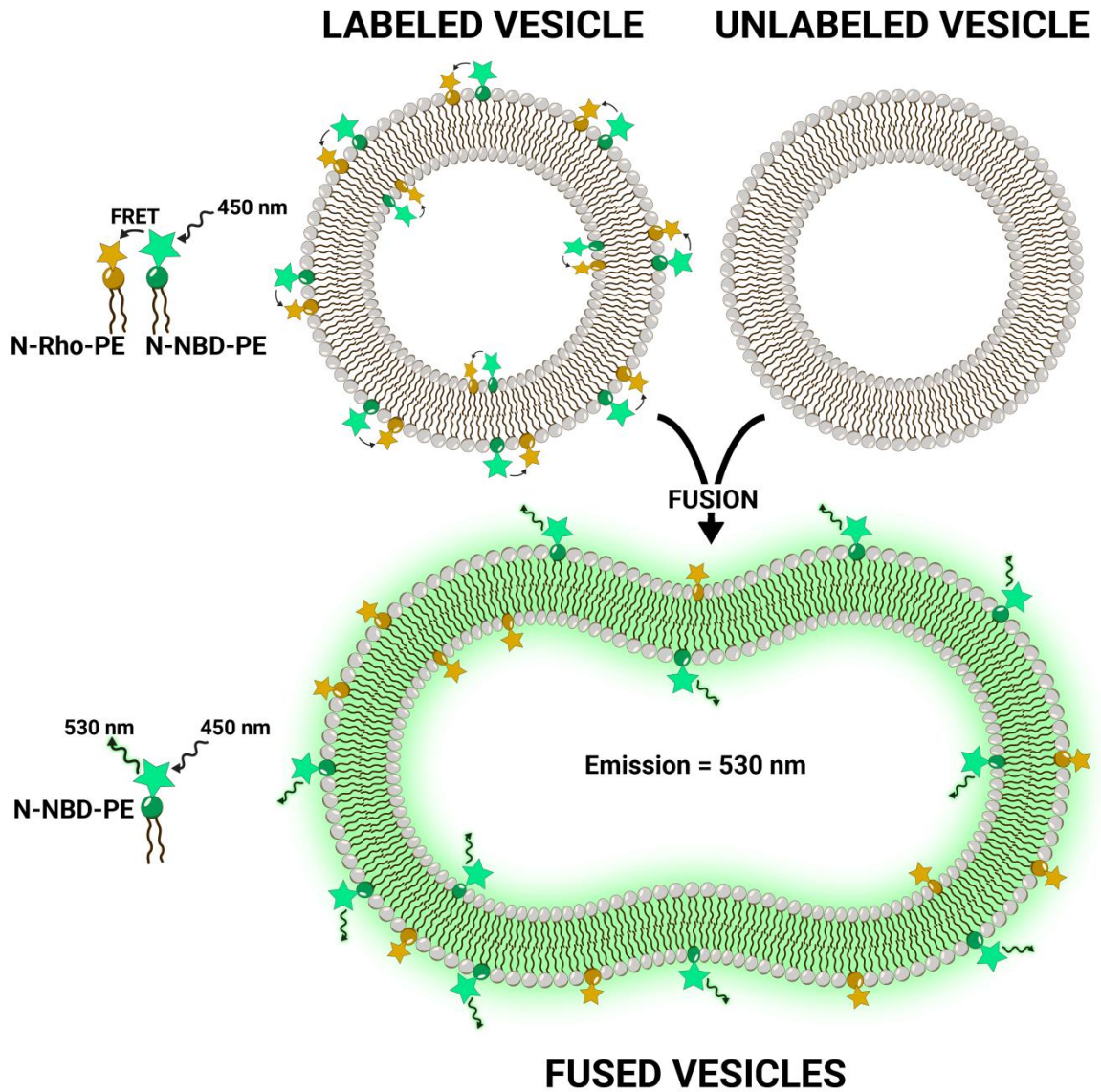


Figure 4.1 – Schematic representation of a membrane lipid measurement using N-NBD-PE and N-Rho-PE resonance energy transfer assay.

4.3. Results

4.3.1. Compound screening

Based on prior screening of hydrophobic compounds for a variety of indications where membrane raft disruption was expected to be disease-modulating (Batista et al., 2010, 2011; Rajendran et al., 2010) and taking into account published anti-HIV approaches targeting the virus envelope (St.Vincent et al., 2010; Wolf et al., 2010), 695 compounds from the proprietary JADO Technologies raft modulator library were screened, combined with selected compounds from commercial libraries of amphiphiles and lipidomimetics. The emphasis was on raft lipid-like scaffold with 30% of all compounds being sterol-derivatives, 10% ceramide and sphingosine-like molecules, and 20% long (≥ 14 C-atoms) aliphatic main chain- or fatty acid- like (alkyl) phospholipids.

Purified HIV-1 (using constructs detailed in Table 4.1) was incubated with compounds at 20 μM in the presence of 1% FCS for 30 min at 37 °C and subsequently added to target cells. The infection process was terminated after 18 h and DNA was extracted for real-time PCR analysis of viral reverse transcription products. 214 compounds inhibited infection $> 90\%$ (IC_{90}) at this concentration. After further testing of these compounds at 2 μM , 16 hits achieved $> 90\%$ inhibition. Dose-effect relations were recorded for these compounds. Three lipidomimetics were selected from the original 16 hits for mode of action studies, based on the following criteria: (1) structural diversity, i.e., distinct structural scaffolds similar to different classes of raft lipids; (2) strongest anti-HIV effect during screening and in confirmatory assays; (3) low toxicity in various preliminary assays and cell lines. Three structurally distinct compounds were chosen (Figure 4.2): a sterol derivative (J391B), a sphingosine derivative (J582C) and a long chain aliphatic lipidomimetic with an unnatural head group (IBS70). A structure that proved inactive in the screen (IBS95), while exhibiting generic characteristics of aliphatic inhibitory compounds, was selected as a negative control.

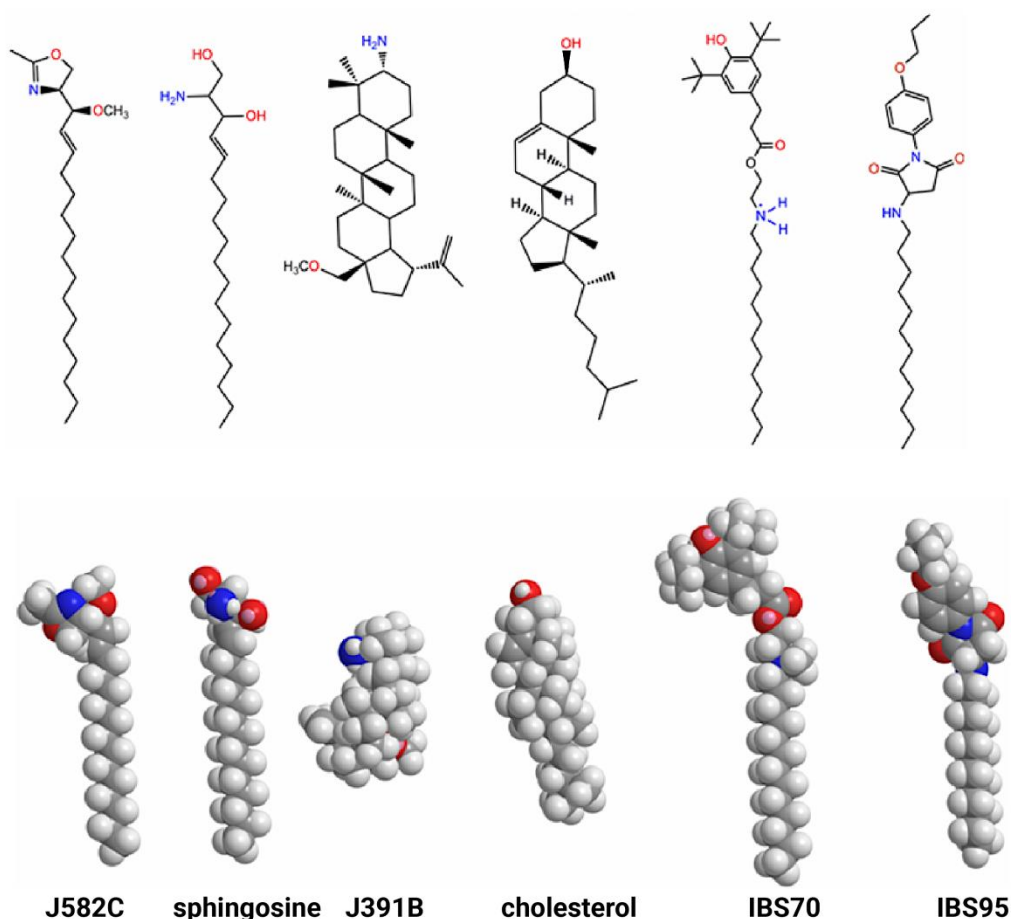


Figure 4.2 – Molecular modeling of the 3D structures of lipidomimetic compounds in comparison to natural lipids. Lowest energy structures in vacuum were computed for relevant compounds and the analogous natural lipids using CS Chem3D Ultra software employing the MM2-force field and the steepest-descent algorithm. Minimum RMS gradient was set to 0.1; minimum and maximum moved to 0.00001 and 1.0, respectively.

4.3.2. Lipidomimetics inhibit HIV-1 infection

To investigate the effects of these lipidomimetics on HIV-1 infectivity, MT-4 T-cells were infected with the prototypic CXCR4-tropic strain HIV-1_{NL4-3}, which was pretreated or not with the compounds as previously determined concentrations. Infectivity was monitored by microscopic readout after staining for the viral p24 (CA) antigen (Figure 4.3A). Immunofluorescence images randomly taken from infected MT-4 cells showed that the three active compounds at their IC₉₀s, but not the inactive control, inhibited HIV-1 infection to a similar extent as the CXCR4 co-receptor antagonist AMD3100 (at 0.5 μM, (Donzella et al., 1998)) that served as a positive control. Automated microscopic readout allowed quantitation of the inhibitory effects (Figure 4.3B), confirming inhibition of HIV-1 infection at these concentrations. Moreover, virus production was strongly reduced when cells were infected with HIV-1 that had been pretreated with the respective compounds (Figure 4.3C), demonstrating a sustained effect. Compound toxicity was examined by quantifying cell counts upon automated microscopy (Figure 4.3B) and by the standard

MTT viability assay described in section 4.2.5 (Figure An. 4.1). No toxic effects were observed at the relevant concentrations.

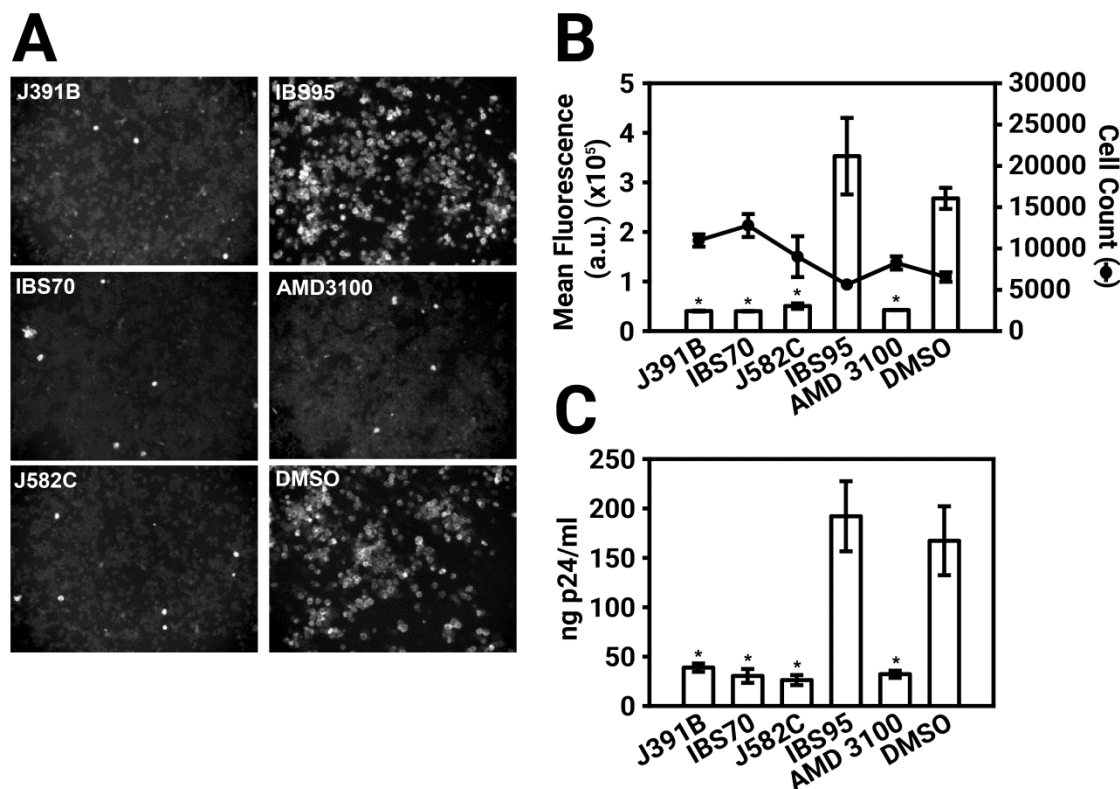


Figure 4.3 – Lipidomimetics affect HIV-1 infectivity. **A**| Immunofluorescence microscopy of intracellular p24 in infected MT-4 cells. HIV-1 was pretreated with 6 μ M J391B, 2 μ M IBS70, 20 μ M J582C, 7 μ M IBS95, 1% DMSO, or 0.5 μ M AMD3100 (as indicated in each panel) for 30 min and subsequently added to MT-4 cells for 2 h. Cells were stained 30 h post-infection. **B**| Infectivity with or without compound treatment was automatically quantified from immunofluorescence images as shown in **A** by determining the mean fluorescence of infected MT-4 cells. The effect of compound or solvent treatment on cell number was quantified in parallel (right axis). Data represent the mean \pm SD of two replicate experiments with 16 replicas each. * represent a significant ($P < 0.01$) decrease when compared to the DMSO control. **C**| Infectivity of compound-treated HIV-1 determined by quantitation of progeny virus. HIV-1 was pretreated as described in **A** and used to infect MT-4 cells. Released virus at 30 h post-infection was quantitated by p24 ELISA. Data represent the mean \pm SD of two replicate experiments with four replicas each. * represents a significant ($P < 0.01$) decrease when compared to the DMSO control.

Concentration-dependent inhibition of HIV-1 replication and potential cytotoxic effects were further investigated by titration experiments (Figure 4.4). The 50% inhibitory concentration (IC_{50}) was 2.5 μ M for J391B, 1.7 μ M for IBS70, and 4.6 μ M for J582C in TZM cells (Figure 4.4A). The maximum tolerated concentrations in TZM cells were 20 μ M for J391B, 10 μ M for IBS70 and (at least) 100 μ M for J582C, and their 50% cytotoxic concentrations (CC_{50}) were 40 μ M for J391B, 25 μ M for IBS70, and > 100 μ M for J582C (Figure 4.4B). Because the available stock solution of J582C was 10 mM concentrations above 100 μ M could not be tested. The resulting selectivity indexes were 15.8, 14.2, and > 21 for J391B, IBS70, and J582C, respectively.

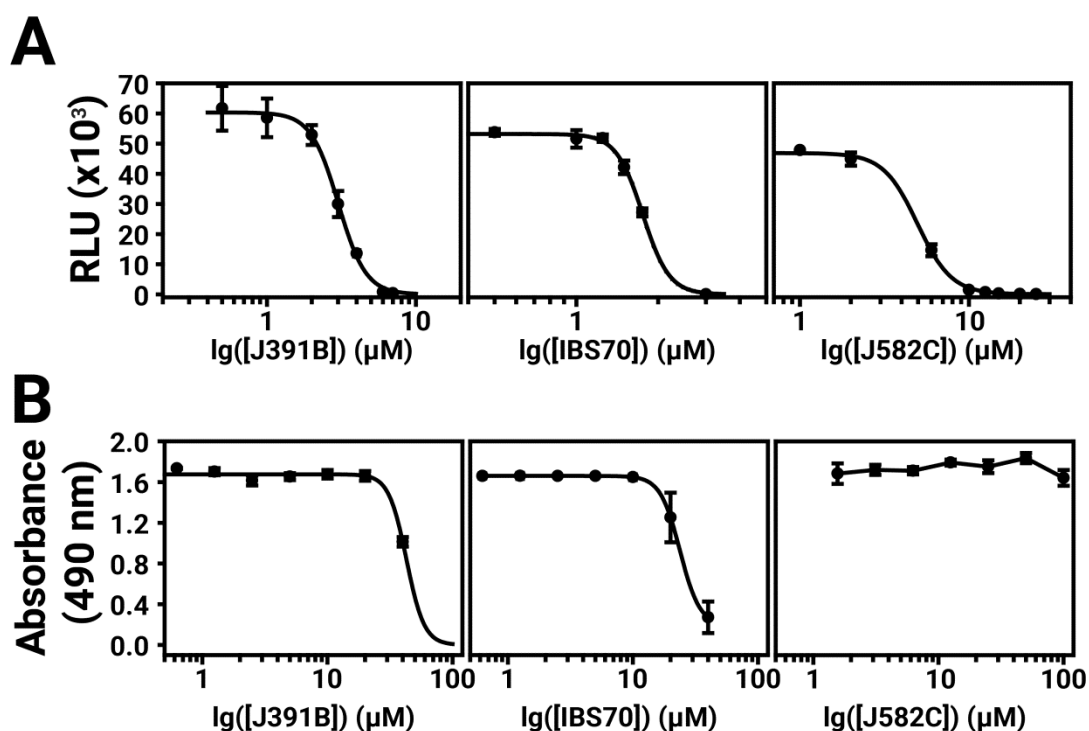


Figure 4.4 – Determination of IC_{50} and CC_{50} of each compound. **A** | Titration of inhibitory effects. HIV-1 was pretreated with compounds at different concentrations followed by infection of TZM-bl cells. TZM-bl reporter cells were harvested 42-45 h post-infection and luciferase activity induced by newly produced HIV-1 Tat was measured and is shown as relative light units (RLU). RLU values are plotted against compound concentration in a semi-logarithmic way. Data represent the mean \pm SD of four replicate experiments with nine replicas each. **B** | Determination of 50% cytotoxic concentration of lipidomimetics. TZM-bl cells were incubated for 48 h in the presence of the compounds as indicated in each panel. The CC_{50} for each compound was calculated from the dose-effect relation; mean values were 40 μM for J391B, 25 μM for IBS70 and > 100 μM for J582C. Data represent the mean \pm SD of four replicate experiments with four replicas each.

4.3.3. Lipidomimetics target the virion membrane

To study the mechanism of inhibition, it was first analyzed whether the lipidomimetic compounds acted on the virus or on the host cell. For this purpose, pretreatment of HIV-1 was compared with pretreatment of target cells prior to addition of virus, on the one hand, and to simultaneous addition of virus and compound on the other (Figure 4.5).

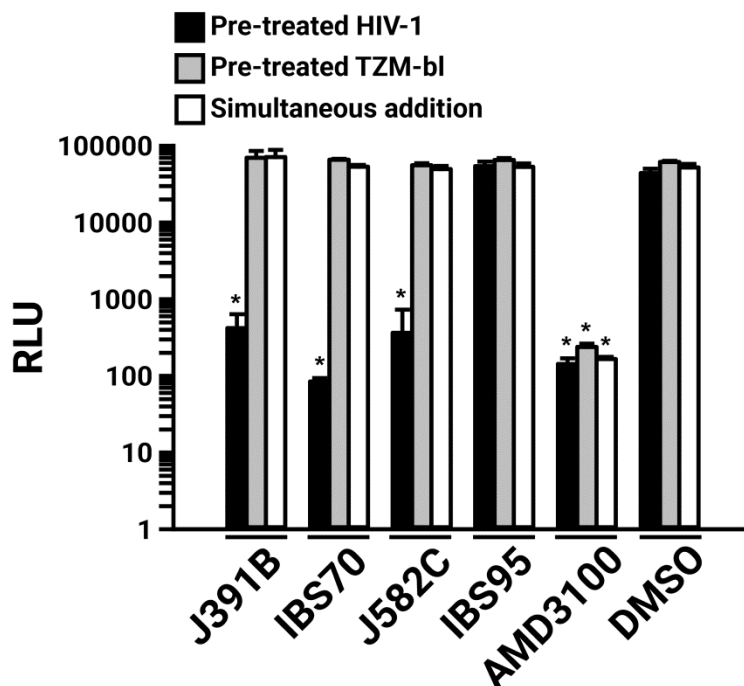


Figure 4.5 – Lipidomimetics target the virion membrane. Lipidomimetic compounds were used to either pretreat HIV-1 (black bars) or TZM-bl reporter cells (gray bars), or compounds were added to TZM-bl together with the virus (white bars). Concentrations used were 15 μ M J391B, 10 μ M IBS70, 82 μ M J582C, 20 μ M IBS95, 0.82% DMSO, and 0.5 μ M AMD3100. TZM-bl reporter cells were harvested 42-45 h post-infection and luciferase activity induced by newly produced HIV-1 Tat was measured and is shown as relative light units (RLU). Data represent the mean \pm SD of two replicate experiments with at least three replicas each. * represents a significant ($P < 0.01$) decrease when compared to the DMSO control.

All three active compounds reduced HIV-1 replication to background levels when virus was pretreated, whereas treating target cells prior to infection or simultaneously adding virus and compound had no effect on HIV-1 infectivity (Figure 4.5). To examine whether pretreatment of cells or simultaneous addition of compound and virus exhibited any antiviral effect, lipidomimetics were applied at 2-5-fold higher concentrations than required for effective pretreatment of the virus (see Figure 4.3). These concentrations were still below the maximal tolerated concentrations in TZM cells analyzed in Figure 4.4. In contrast to lipidomimetics, AMD3100, which functions by blocking the CXCR4 co-receptor essential for HIV-1 entry, inhibited viral infection irrespective of the mode of addition. AMD3100 is a hydrophilic compound ($\log P = -0.34$)² that reaches the co-receptor from the aqueous phase, whereas the lipidomimetics with $\log P > 4$ are quantitatively taken up by biological membranes and, where present, bind to lipoproteins and other hydrophobic molecules. Thus, the lipidomimetic compounds appeared to exert their effect by inactivating the virus and, therefore, had to be added prior to infection. To determine any potential non-specific effect on a non-enveloped virus, the lipidomimetic compounds were also tested against the parvovirus AAV, applying twice the effective concentrations required for HIV-1. Preincubation of AAV with any of the compounds did not affect infectivity, while heparin blocked AAV infection as expected, since it competes

² Calculated via chemicalize.com

with AAV receptor engagement (Summerford and Samulski, 1998) (Figure 4.6). These results are consistent with an effect of the lipidomimetics on the HIV-1 membrane.

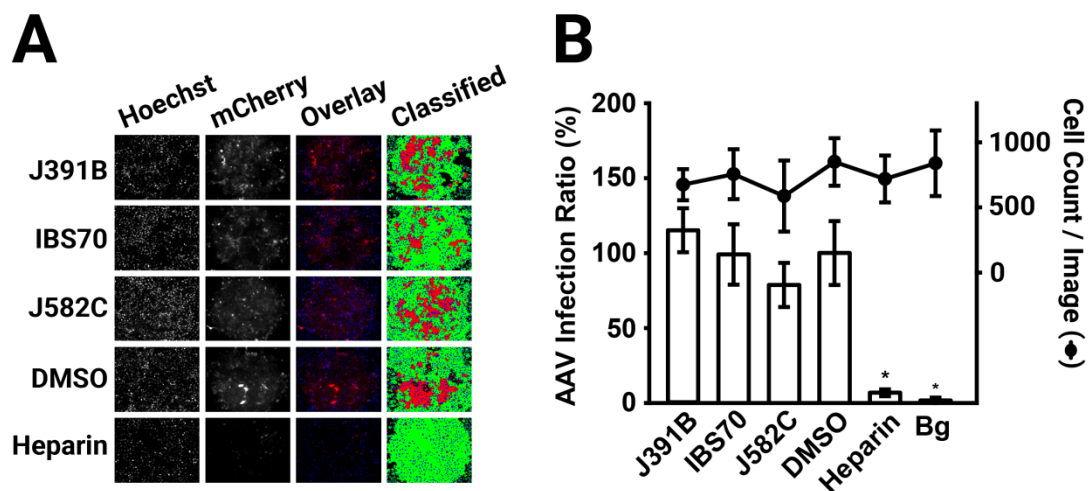


Figure 4.6 – Lipidomimetics show no effect on non-enveloped AAV. **A** Representative fluorescence images of TZM-bl cells infected with AAV expressing the reporter mCherry. AAV was pretreated with lipidomimetics at 12 μ M J391B, 4 μ M IBS70, or 40 μ M J582C. Heparin (50 μ g/ml) was used as positive entry inhibitor control, IBS95 (20 μ M) and DMSO (0.82%) as negative controls. Cell nuclei were stained by Hoechst 33342 (left panel) and AAV infection was recorded from mCherry fluorescence (second panel). The third panel shows an overlay of the two stains, and the right panel assignment of positive (red) and negative (green) cells is based on a proprietary algorithm. **B** Quantitation of automated fluorescence readout and cell counts. Fluorescent images as in **A** were automatically quantified for cell number (based on nuclear stain, right axis) and mCherry fluorescence (AAV infection ratio, left axis). Data represent the mean \pm SD of two replicate experiments with sixteen replicas each. * represents a significant ($P < 0.01$) decrease when compared to the DMSO control.

4.3.4. Lipidomimetics inhibit HIV-1 entry at the fusion step

The mode-of-addition experiments suggested that lipidomimetics act by blocking viral entry through effects on the HIV-1 membrane. To directly address this question, a quantitative HIV-1 entry assay was used, based on incorporation of a BlaM-Vpr fusion protein into replication-competent HIV-1 particles during virus production (Cavrois et al., 2002), which rationale is explained in *Chapter 2*. HIV-1 particles pre-incubated with lipidomimetics exhibited a strong reduction of virus entry in this assay, which was also observed for AMD3100, but not for the control compound IBS95 (Figure 4.7A). To ensure that the infectivity of BlaM-Vpr viruses was comparable to wild-type HIV-1 and to correlate the effects on entry with inhibition of infection, an infection experiment was performed in parallel. No significant difference in infectivity was observed between wild-type HIV-1 and BlaM-Vpr virus, and both viruses were equally affected by lipidomimetics (Figure 4.7B). Thus, inhibition of HIV-1 infection by lipidomimetics maps to the viral entry step.

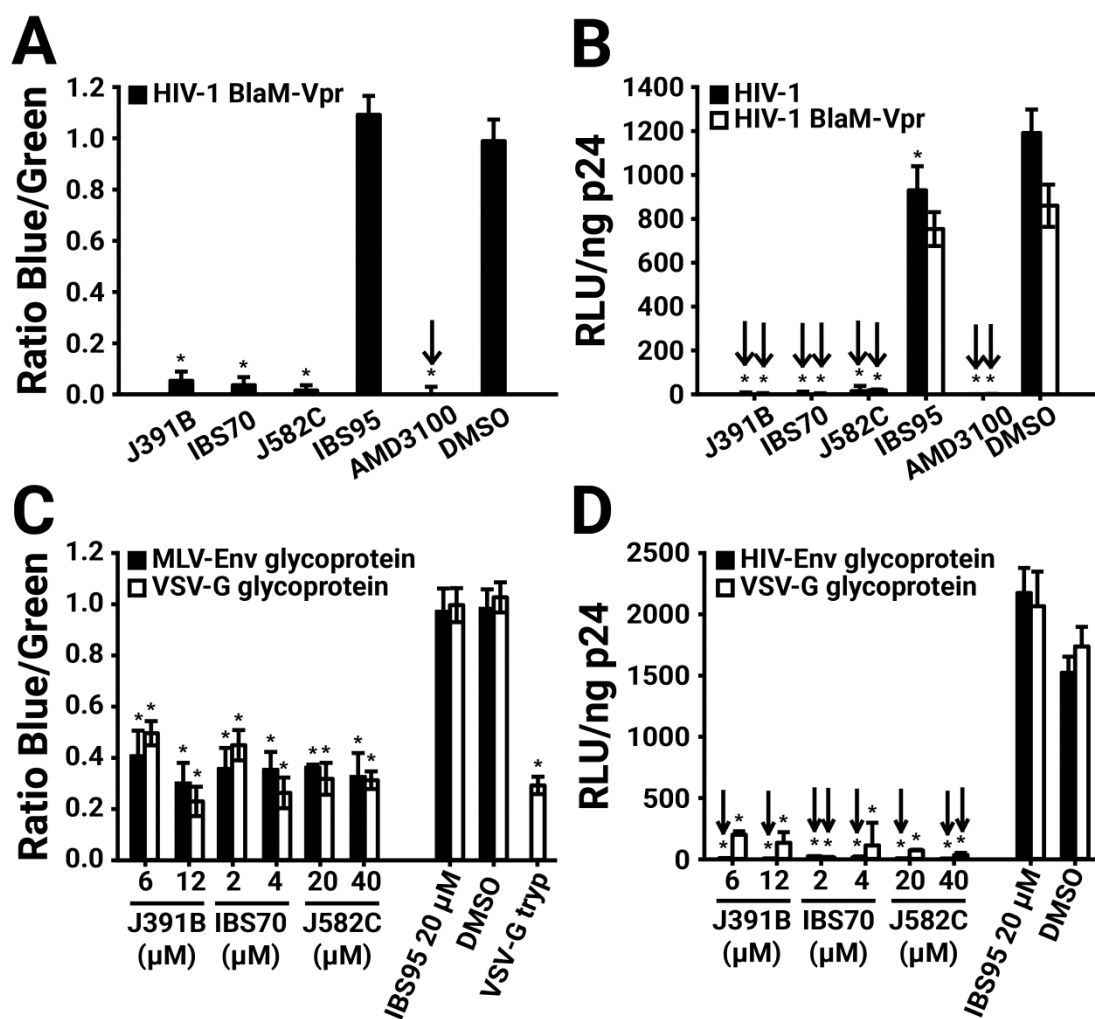


Figure 4.7 – Mapping effects of lipidomimetics to HIV-1 entry. **A** Cytoplasmic entry. HIV-1 carrying BlaM-Vpr was pretreated with 6 μ M J391B, 2 μ M IBS70, 20 μ M J582C, 20 μ M IBS95, 0.82% DMSO, or 0.5 μ M AMD3100 and added to TZM cells. Cytoplasmic entry of HIV-1 was analyzed by determining the mean fluorescence for the cleaved (blue) and uncleaved (green) CCF2 substrate after 17 h. The graph shows the ratio of the blue and green fluorescence signal normalized against the DMSO control. Data represent the mean \pm SD of three replicate experiments with nine replicas each. * represents a significant ($P < 0.01$) decrease when compared to DMSO control. **B** Comparison of BlaM-Vpr-carrying and unmodified HIV-1. HIV-1 with (white bars) or without (black bars) BlaM-Vpr was pretreated with compounds as in **A** and used to infect TZM-bl reporter cells. Relative infectivity is shown as RLU per ng of p24. Data represent the mean \pm SD of two replicate experiments with six (white bars) and nine (black bars) replicas each. * represents a significant ($P < 0.01$) decrease when compared to the DMSO control. **C** Influence of viral glycoproteins and entry route on sensitivity to compounds. HIV-1 was pseudotyped with the glycoproteins of Friend ecotropic MLV (black bars) or VSV (white bars). Pseudotyped viruses carrying BlaM-Vpr were pretreated with 6 and 12 μ M J391B, 2 and 4 μ M IBS70, 20 and 40 μ M J582C or control compounds followed by infection of TZM-bl cells (for VSV-G pseudotypes) or DFJ8 cells (for MLV pseudotypes). Cytoplasmic entry was quantified against the DMSO control as in **A**. VSV-G pseudotyped particles treated with trypsin served as an entry non-competent control. Data represent the mean \pm SD of three replicate experiments with six replicas each. * represents a significant ($P < 0.01$) decrease when compared to the DMSO control. **D** HIV-1 carrying its cognate glycoprotein (black bars) or pseudotyped with VSV-G (white bars) and containing BlaM-Vpr was pretreated with compounds as in **C** and used to infect TZM-bl cells. Relative infectivity is shown as RLU per ng of p24. Data represent the mean \pm SD of two replicate experiments with six replicas each. * represents a significant ($P < 0.01$) decrease when compared to the DMSO control.

To determine whether the effect of the lipidomimetic compounds is dependent on the HIV-1 glycoprotein or the viral entry route, experiments with HIV-1 pseudotyped with other viral glycoproteins were performed. Pseudotyping is achieved by producing virus particles lacking their cognate viral glycoproteins, but randomly incorporating heterologous glycoproteins synthesized by cotransfecting the same producer cell with an expression vector for the glycoprotein of another virus. Pseudotyping with e.g. the glycoprotein of vesicular stomatitis virus (VSV-G) also changes the viral entry route as VSV enters target cells through a pH-dependent endosomal route (Roche et al., 2008). In contrast, pseudotyping with Friend ecotropic MLV glycoproteins yields viral fusion and entry at the plasma membrane in a pH-independent manner (Meclure et al., 1990). We therefore produced HIV-1 BlaM-Vpr particles carrying the glycoproteins of either VSV or MLV and tested their capacity to enter target cells after pretreatment with lipidomimetic or control compounds. As background controls, pseudotyped HIV-1 particles were trypsin-treated prior to inoculation. Viral infectivity was determined in parallel for pseudotyped HIV-1 particles treated with lipidomimetic and control compounds as described above.

Similar to HIV-1 carrying its cognate envelope proteins, treatment with lipidomimetics efficiently and specifically inhibited cell entry by particles pseudotyped either with VSV or with MLV glycoproteins (Figure 4.7C). The effect of entry again correlated with that on virus infection (Figure 4.7D). Accordingly, the antiviral activity of the lipidomimetic compounds is not dependent on a specific envelope glycoprotein or on a particular entry pathway.

To further study the mechanism by which lipidomimetics inhibit viral entry, a liposome-based fusion inhibition assay was used (Struck et al., 1981). For this purpose, a fusogenic peptide from HIV-1, the gp41 MPER and synthetic LUVs were used (Saez-Cirion et al., 2002b; Vieira et al., 2010). As a suitable match for the lipidomimetics, LPC was chosen as a positive control compound. LPC is a well-known fusion inhibitor lipid (Chernomordik et al., 1995) with inverted cone-shaped structure, which affects membrane curvature and therefore inhibits liposomal lipid mixing. Concentration-dependent inhibition of MPER-induced fusion by lipidomimetics was studied (Figure 4.8). The extent of virus and liposome mixing correlated with the compounds' inhibition of virus infectivity (IC_{50}). IBS70 inhibited lipid mixing most efficiently, followed by J391B and J582C. Thus, lipidomimetics were capable of inhibiting viral entry at the membrane fusion step.

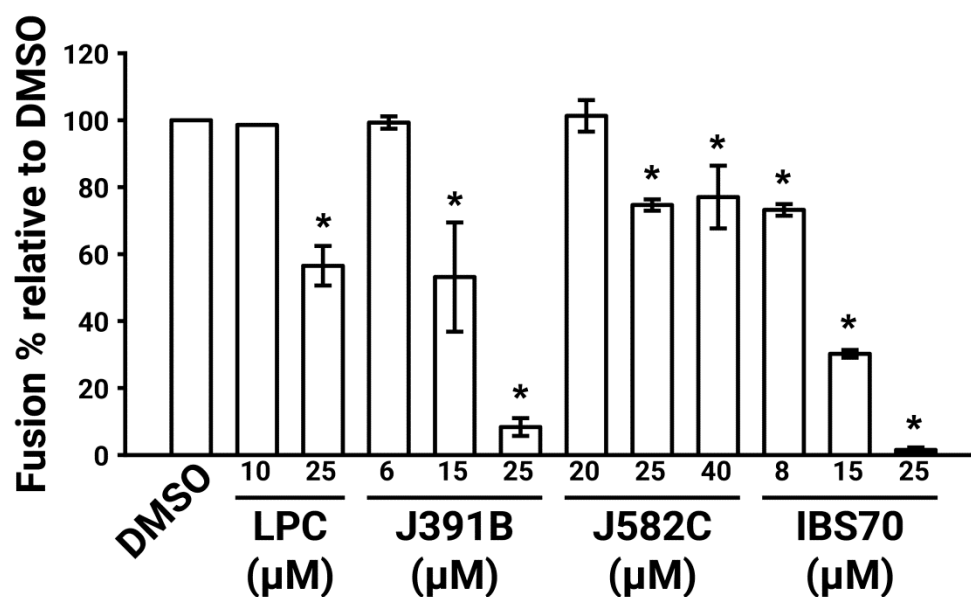


Figure 4.8 – Inhibition of fusion by lipidomimetics. LUVs were composed of POPC:POPS:SM:Chol (18:15:33:33 mol:mol) to emulate viral particle membranes. Experiments were performed at 25 °C with 0.1% FCS in 150 mM NaCl, 10 mM HEPES pH 7.4 buffer, 10 μM NBD/Rho LUV in 1 ml, incubated for 15 min with compounds or DMSO control (0.82%). Next, 40 μM of unlabeled LUV was added for 20 min. The stable background signal establishes 0% fusion. The fusion reaction was started by adding 0.5 μM MPER fusion peptide. Membrane fusion was measured as the increase of N-NBD-PE fluorescence due to intervesicular mixing and consequent dilution of the fluorophore (NBD) and quencher (Rho). Finally, Triton X-100 (0.1%) was added to establish the 100% fusion signal. Data are the mean ± SD of two replicate experiments with three replicas each. * represents a significant ($P < 0.01$) decrease when compared to the DMSO control.

4.3.5. Effects of lipidomimetics on HIV-1 stability and virion density

Detergent-like microbicides, e.g. nonoxynol, disrupt membranes non-specifically, thus inactivating HIV-1 with concomitant toxicity (Malkovsky et al., 1988). To investigate whether virus disruption plays a role in the antiviral activity of the lipidomimetic compounds, purified non-infectious HIV-1-like particles and infectious HIV-1 were treated with compounds at approximately the IC_{90} and subsequently recovered by ultracentrifugation. Western blot detecting capsid, matrix, and envelope proteins and their quantifications revealed no effect of compound treatment on virus recovery and protein composition (Figure 4.9A, B and Figure An. 4.2).

Previous studies demonstrated shifts in virion density when viral membrane composition was altered by changes in cholesterol concentration or its replacement by cholesterol analogs (Campbell et al., 2002). In order to monitor potential density shifts following treatment with lipidomimetics, both non-infectious HIV-1 like particles (Figure 4.9C) and infectious HIV-1 (Figure An. 4.2) were compound-treated and analyzed by equilibrium centrifugation on continuous sucrose gradients. HIV-1 protein distribution in gradient fractions was subsequently assayed by quantitative anti-CA Western blot or ELISA. Purified solvent-treated HIV-1 served as reference with the virus peak in fractions

10-13 at a density ranging from 1.16 to 1.2 g/cm³ (Figure An. 4.3). In contrast, virus treatment with detergent Triton X-100 led to a complete loss of the virus peak and recovery of soluble p24 antigen in the top fractions of the gradient (Figure 4.9C and Figure An. 4.2).

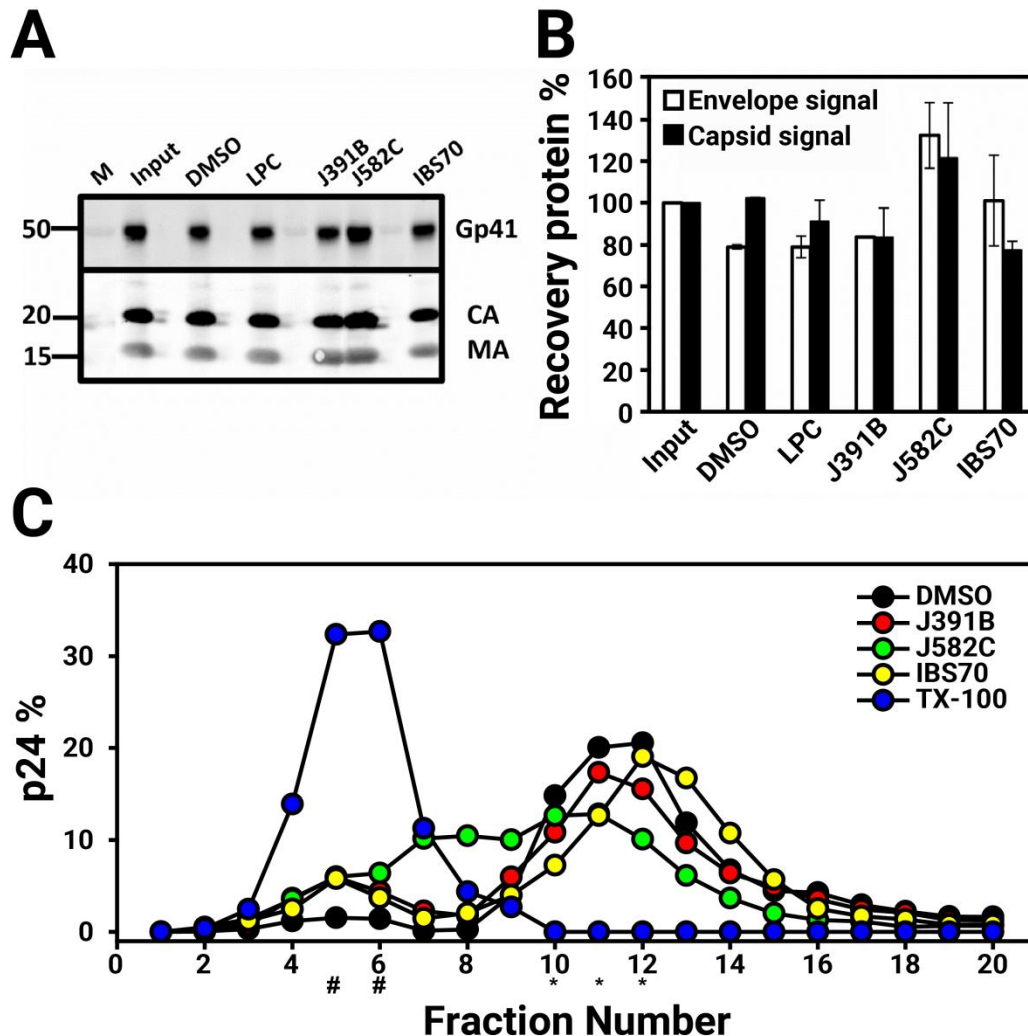


Figure 4.9 – Influence of lipidomimetics on particle stability and density. **A** Virus stability. Purified non-infectious HIV-like particles derived by transfection of pCHIV (3 µg of CA) were treated with 6 µM J391B, 8 µM IBS70, 20 µM J582C, 2.5 µM LPC, or DMSO (0.35%) for 30 min at 37 °C. Subsequently, particles were recovered by ultracentrifugation and analyzed by Western blot developed against gp41 (41 kDa), CA (24 kDa), and MA (17 kDa). Input signal refers to control virus before treatment. **B** Virus stability. Virus treated and recovered as in **A** was analyzed by quantitative Western blot, measured in LICOR quantitative system. **C** Virus buoyant density. Non-infectious HIV-like particles derived by transfection of pCHIV (3 µg of CA) were treated with 6 µM J391B, 8 µM IBS70, 20 µM J582C, 0.5% TX-100, or DMSO (0.35%) as in **A** and subsequently subjected to equilibrium density gradient ultracentrifugation. Gradient fractions were collected from the top and virus amounts were quantified by Western blot. Data represent the mean of two replicate experiments with five replicas each. # indicates sucrose density fractions where soluble p24 was expected (1.07 g/cm³) and the * the fractions where intact virus was expected (1.17-1.2 g/cm³).

Treatment of viral particles with J391B did not influence virus density and resulted in a similar virus yield detected in fractions 10-13 as observed for solvent-treated virus. However, IBS70 elicited a minor increase in virus particle density. As opposed to the other lipidomimetics, a reduction in density to 1.12-1.14 g/cm³ occurred upon exposure of HIV-1 to J582C (Figure 4.9C and Figure An. 4.2). Effects on particle density may be due to insertion of the lipidomimetic into the viral membrane. However, changes in virion density were not proportional to antiviral activity. Only a small amount of soluble p24 was released by lipidomimetic-treated virus (Figure 4.9C and Figure An. 4.2), confirming that the compounds did not act by affecting virion stability.

4.3.6. Effect of lipidomimetics on HIV-1 membrane order

Previous studies have shown that the fluorescent dye laurdan can be used to determine the degree of membrane order in virus particles (Lorizate et al., 2009), and therefore laurdan staining was applied in this work to detect potential changes in membrane order upon treatment of HIV-1 with lipidomimetics. Laurdan is homogeneously distributed within the membrane and has an emission maximum around 490 nm for fluid (liquid disordered, L_d) membranes and around 440 nm for condensed membranes (L_o , and gel phase or solid ordered, S_o). The phase state of a membrane can thus be quantified by its GP value, which is defined as the normalized intensity ratio of the two emission channels and provides a relative measure of lipid order (Bagatolli, 2006; Kaiser et al., 2009; Lorizate et al., 2009). GP values between 0.25 and 0.5 indicate L_o structure at the respective temperature, while GP values < 0.25 indicate liquid-disordered (L_d) structure (Dietrich et al., 2001).

Prior to compound treatment and laurdan staining HIV-1 was inactivated with AT-2, which covalently modifies the essential zinc fingers in the viral nucleocapsid protein (Rossio et al., 1998) without altering the membrane (Lorizate et al., 2013). Inactivated virus was treated or not with lipidomimetics or control compounds and subsequently labeled with laurdan. Particles were recovered by ultracentrifugation, re-suspended in buffer and subjected to fluorescence spectroscopy. Control experiments excluded a direct interaction of lipidomimetics with laurdan (Figure An. 4.4). Emission spectra were recorded for treated and untreated viruses at different temperatures and the corresponding GP values were calculated. The plot of GP as a function of temperature of solvent-treated particles (Figure 4.10, black circles) exhibited similar shapes and values as previously described (Lorizate et al., 2009). No transition temperature inflection was visible, as expected for membranes with high cholesterol content (Parasassi et al., 1994).

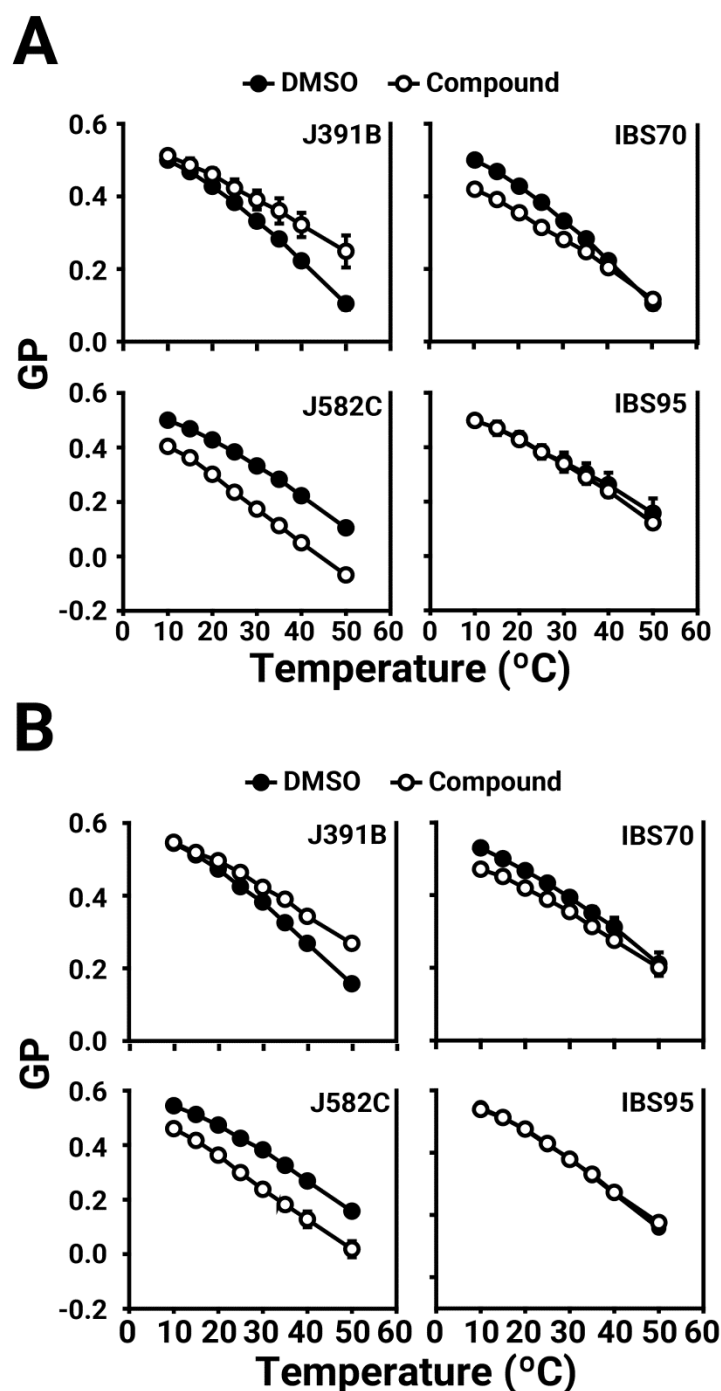


Figure 4.10 – Effect of lipidomimetics on HIV-1 membrane order. **A**| Comparison of temperature-dependent GP profiles HIV-1 with (white circles) or without (black circles) lipidomimetic treatment. Viruses were stained with 5 μ M laurdan for 20 min, treated with 6 μ M J391B, 8 μ M IBS70, 20 μ M J582C, 7 μ M IBS95, or DMSO (0.35%) for 30 min at 37 $^{\circ}$ C, and analyzed as described in experimental techniques. GP values were calculated from emission spectra recorded at each temperature. Data are the mean \pm SD of three replicate experiments. **B**| Comparison of temperature-dependent GP profiles of LUV produced from extracted viral lipids with (white circles) or without (black circles) lipidomimetic treatment. Conditions of treatment and analysis were as in **A**. Data are the mean \pm SD of three replicate experiments.

Upon treatment with J391B, J582C, and IBS70, HIV-1 particles exhibited a change in GP pattern while treatment with the inactive compound IBS95 was indistinguishable

from the solvent control, which was only subject to temperature-induced order decrease (Figure 4.10A). The cholesterol analogue J391B increased GP values of treated HIV-1 particles, generating greater membrane rigidity and counteracting the effect of temperature increase. Conversely, treatment with IBS70 and, most severely, the sphingosine-analogue J582C induced a decrease in GP values, reflecting enhanced membrane fluidity in the L_d range ($GP < 0.25$). While the reduction of membrane order by IBS70 was abated with increasing temperature, the disordering activity of J582C was constant and additive to the temperature effect (Figure 4.10A).

The proteins resident in biological membranes enforce an asymmetric distribution of lipids between the two leaflets, whereas liposomes lacking proteins exhibit a nearly symmetric lipid distribution. To determine whether the effect of the compounds on viral membrane structure is exclusively mediated by viral lipid composition, GP values were determined for LUV composed of HIV-1-derived lipids. To this end, lipids were extracted from purified HIV-1 particles and used to prepare LUV with a diameter of ~100 nm (Hope et al., 1985). These HIV-derived LUV have the lipid composition of HIV-1 but, according to their physicochemical characteristics, possess a random and presumably symmetric distribution of lipids. HIV-1 lipids-derived LUV were treated or not with the different compounds, labeled with laurdan, and GP was recorded as a function of temperature (Figure 4.10B). Similar to the results observed for wild-type HIV-1, the control compounds IBS95 did not alter LUV structure; IBS70 and J582C caused a temperature-dependent or independent decrease in membrane order, while J391B stabilized membrane order against rising temperature (Figure 4.10B). The modifications induced by all compounds in LUV were very similar to the ones observed for the complete virus, indicating that their effects were independent of viral or cellular proteins and did not require membrane asymmetry.

4.3.7. Phosphatidylserine-specific enhancement of membrane order by steroidal amine J391B

Further studies with LUVs of different membrane composition revealed an interesting lipid head group requirement for the effect of J391B on membrane order. While this compound enhanced membrane order in HIV-1 particles and LUV reconstituted from the complete set of HIV-1 lipids (Figure 4.10), a slight decrease of membrane order was observed upon J391B treatment of LUV consisting only of cholesterol, sphingomyelin, and phosphatidylcholine (the most abundant HIV-1 lipids; Figure 4.11A). Since J391B is positively charged at neutral pH (Figure 4.2), apparently the availability of negatively charged lipid head groups determined a switch between J391B reducing, maintaining or increasing membrane order.

The HIV-1 lipidome exhibits an enrichment of phosphatidylserine (PS) compared with the plasma membrane of producer cells (Lorizate et al., 2013). LUV composed of the same quaternary mixture as above but including PS substituting for part of the phosphatidylcholine exhibited increased membrane rigidity upon J391B treatment,

although the amount of saturated fatty acids had been decreased 2.5 times as a result of the higher level of unsaturated fatty acids in PS (Figure 4.11B). The effect of the compound resembled that on LUV consisting of HIV-1 extracted lipids or on complete virus (Figure 4.10).

Replacing PS with other negatively charged lipids, phosphatidylglycerol or phosphatidic acid, which hardly occur in the HIV envelope, yielded little or no effect on membrane order following J391B treatment (Figure 4.11C, D), indicative of a specific molecular interaction of J391B with PS rather than mere charge neutralization.

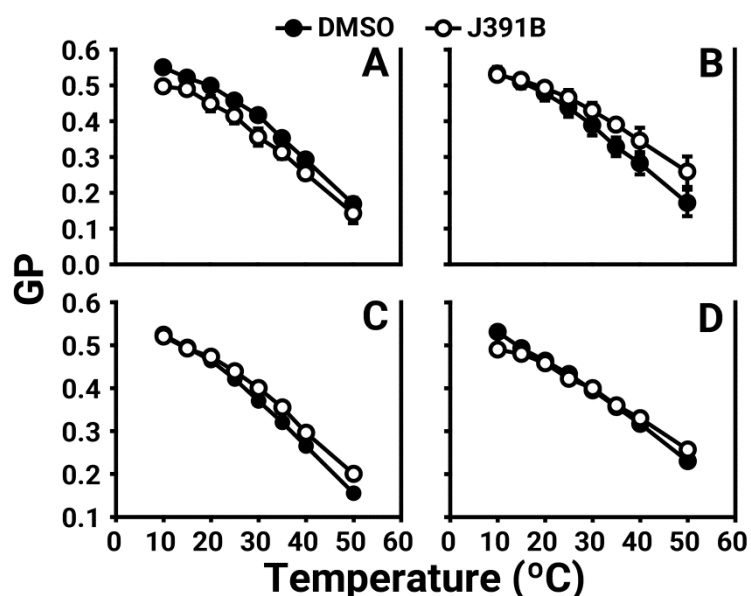


Figure 4.11 – Lipid species requirement for J391B membrane activity. Comparison of temperature-dependent GP profiles of LUVs composed of: **A**| POPC:DPPC:SM:Chol (25:16:14:45 mol:mol), **B**| POPC:DOPS:DPPC:SM:Chol (10:15:16:14:45 mol:mol), **C**| POPC:DOPG:DPPC:SM:Chol (10:15:16:14:45 mol:mol), **D**| POPC:DOPA:DPPC:SM:Chol (10:15:16:14:45 mol:mol), with (white circles) or without (black circles) treatment with 6 μ M J391B for 30 h at 37 °C. Data represent the mean \pm SD of three replicate experiments.

To explore this molecular interaction in an independent approach HeLa cells were treated with J391B for 30 min and stained with PS-specific annexin V. J391B treatment elicited exposure of PS on the outer leaflet of the plasma membrane (Figure 4.12) whereas the DMSO-treated control gave no signal. This observation indicates that J391B interaction with cell membranes induced a PS externalization without apparent signs of apoptosis.

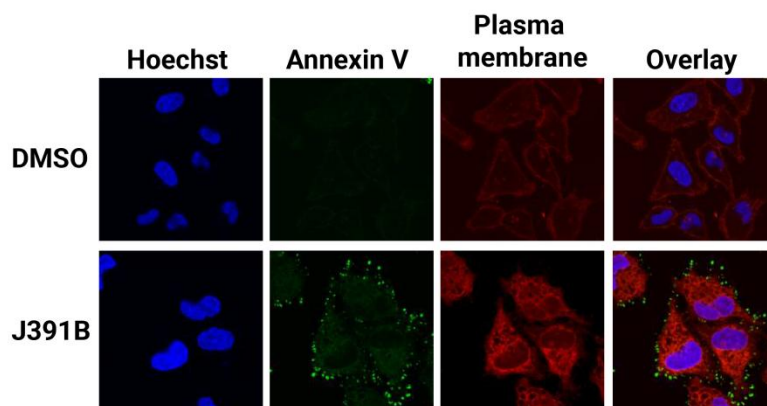


Figure 4.12 – J391B binding to the cell membrane triggers exposure of PS in the outer leaflet. HeLa cells were treated with 10 μM J391B or with 0.82% DMSO. The plasma membrane was labeled with Wheat Germ Agglutinin (red); exposed PS was detected by annexin V (green) and nuclei were stained with Hoechst 33342 (blue). The figure is a representative image of two replicate experiments.

4.3.8. J391B and J582C exhibit synergistic effects on HIV-1 infectivity

Given that J391B and J528C induced opposing effects on membrane structure, their possible antagonizing effect was studied. To study their combined effects, the two compounds were mixed at different concentrations, and the infectivity of HIV-1 treated with either compound alone or with the various mixtures was analyzed using a luciferase reporter assay (Figure 4.13A). Again, AMD3100 was employed as the positive and IBS95 as the negative control compound. Titration experiments showed that J391B had no effect on infectivity at a concentration of 1.75 μM and J582C was inactive at 3.5-4 μM . Yet a mixture of both compounds at concentrations where either compound alone was inactive strongly inhibited viral infectivity (Figure 4.13A). Thus, J391B and J582C acted synergistically. Enhanced inhibition was not due to toxicity as shown by the parallel MTT test (Figure 4.13B).

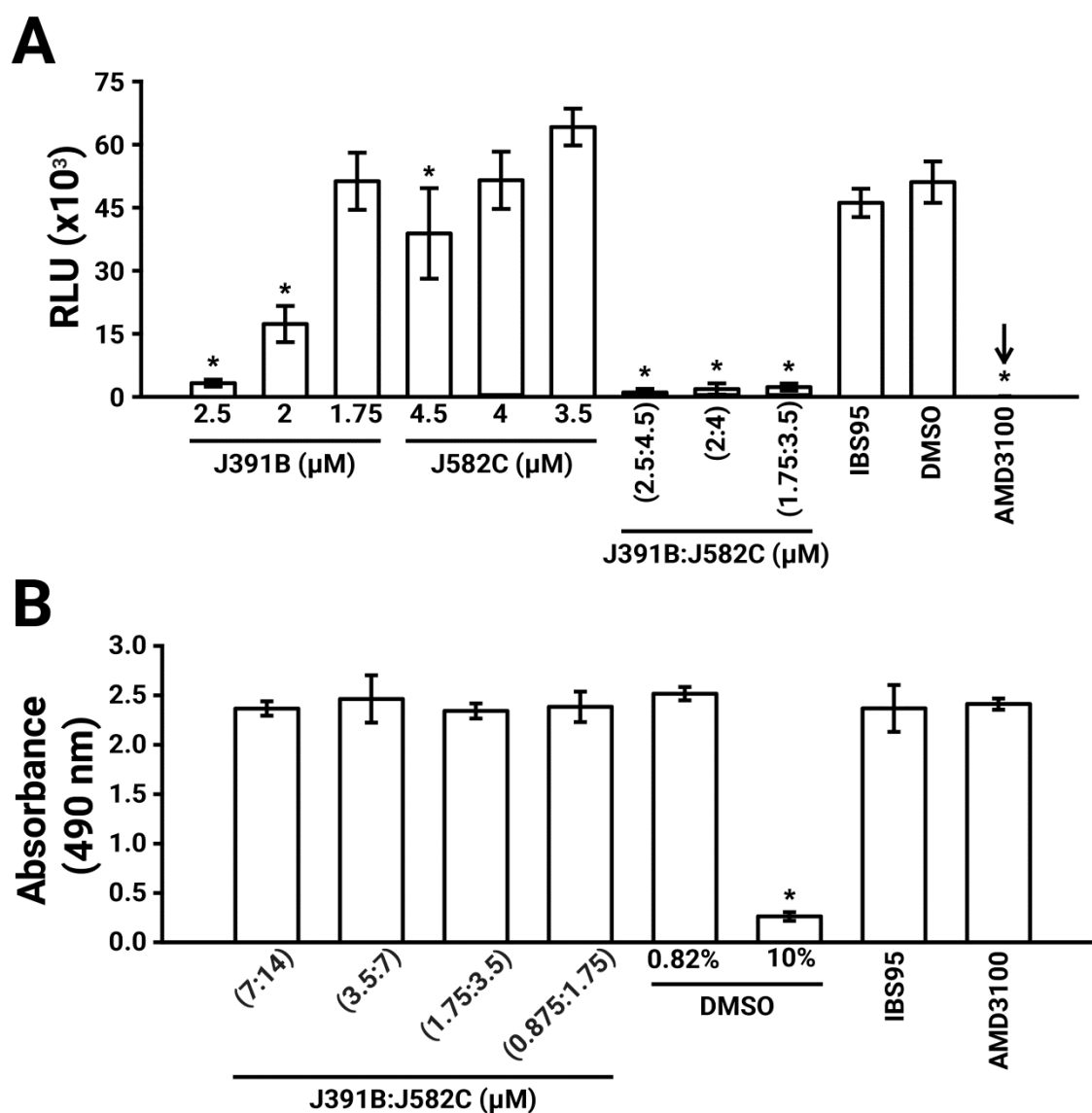


Figure 4.13 – Effect of mixtures of J391B and J582C on HIV-1 infectivity and cytotoxicity. A| HIV-1 was treated with compounds at the indicated concentrations as described in Figure 4.3 followed by infection of TZM-bl cells and luciferase assay after 24 h. Data represent the mean \pm SD of three replicate experiments with nine replicas each. * represent a significant ($P < 0.01$) decrease when compared to DMSO. **B|** MTT cytotoxicity assay for treatment with compound mixtures. The same J391B:J582C (1:2) molar ratio as in **A** at expanded concentration range was tested. DMSO (0.82%), IBS95 (7 μ M) and AMD3100 (0.5 μ M) served as controls and 10% DMSO as toxicity control. Data are the mean \pm SD of three replicate experiments with four replicas each. * represent a significant ($P < 0.01$) decrease when compared to the 0.82% DMSO control.

Next, whether the synergistic effect on viral infectivity corresponded to detectable alterations in HIV-1 membrane order was examined. HIV-1 particles and LUV composed of HIV-1 lipids were treated with individual or mixed compounds and GP profiles were recorded (Figure 4.14A). Interestingly, the compound mixture delivered a GP pattern close to that of J582C but with a temperature profile more like the one of J391B. The complex outcome at the level of membrane order was neither an antagonistic nor an additive effect (Figure 4.14B).

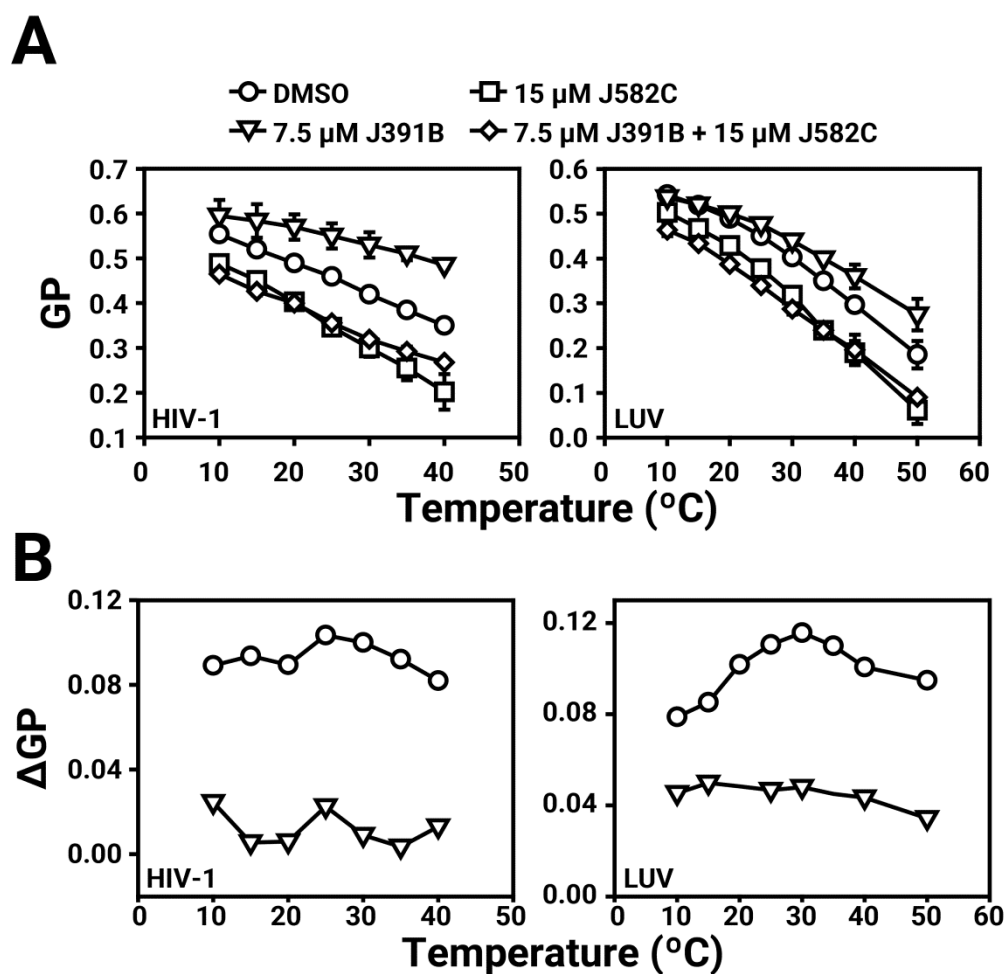


Figure 4.14 – Effect of mixtures of J391B and J582C on HIV-1 membrane structure. **A** | Comparison of temperature-dependent GP profiles of HIV-1 (left panel) and LUV composed of HIV-1 lipids (right panel). Virions or LUV were treated with 0.82% DMSO (circles), 7.5 μ M J391B (triangles), 15 μ M J582C (squares) or the mixture of 7.5 μ M J391B and 15 μ M J582C (diamonds). Data represent the mean \pm SD of three replicate experiments. **B** | Temperature-dependent GP profiles for HIV-1 (left panel) or LUV (right panel) treated with compound mixtures or individual compounds were plotted against DMSO-treated controls. Data are from the experiments shown in **A**. In order to address whether the effect of the compound mixture is additive or synergistic, the GP profile for particles treated with the mixture of J391B and J582C were plotted relative to DMSO controls (circles) or against the extrapolated additive plot for particles separately treated with both compounds (triangles).

4.4. Discussion

Targeting the lipid membrane of enveloped viruses is an attractive approach for the development of antivirals applied either systematically or on mucosal surfaces. Detergent-based structures have been developed as topical microbicides (Malkovsky et al., 1988), but shown to cause toxicity problems upon *in vivo* application (Van Damme et al., 2002; Hillier et al., 2005). Alternative approaches attempted the extraction of key lipids like cholesterol with cyclodextrin derivatives (Liao et al., 2003) or promoted alteration of membrane fusion properties by e.g., inserting inverted cone-shaped non-lipidic compounds into the viral membrane (St.Vincent et al., 2010). In this work, a screening of a library of raft lipid-like lipidomimetics as potential antiviral agents against HIV-1 was carried out, and several compounds were identified, which inhibited viral infection at the entry stage and induced structural alterations in the viral membrane.

A qualitative structure-activity analysis of antiviral vs. inactive compounds from the screen yielded the following results: the hydrophobic anchor of active sterol-like molecules often included a single oxygen atom, attenuating the hydrophobicity of the sterol-like scaffold. There was no preference for the α - or β - sterol configuration. The hydrophobic anchor of active aliphatic lipidomimetics was a single aliphatic chain ≥ 14 -18 C-atoms. Compounds with more than one aliphatic chain were inactive due to their poor diffusibility, despite the presence of serum lipoproteins. Among the inactive compounds, IBS95 was selected, which is similar to the generically active structures but has two ring moieties in its head group.

Head groups of the active compounds often encompassed OH-groups and/or a single aromatic or heterocyclic ring, and presented at least one nitrogen atom, usually positively charged or available for protonation. These observations agree with the findings of (Agarwal et al., 2013) who showed that cholesterol derivatives with positively charged head groups disrupt or augment membrane order and, in both cases, interfere with influenza virus infection. It is not unexpected that any modulation of the initial, optimal viral membrane order impairs infectivity, since all physiological processes exhibit concentration and temperature optima, often in the context of protein function. Likewise, biological membranes possess a distinct order determined by lipid species concentrations and temperature, essential for their functions (Kaiser et al., 2011). Specifically composed lateral membrane phases underlie organellar and viral membrane dynamics (fusion, budding, and fission) and trafficking (Diaz-Rohrer et al., 2014).

Lipidomimetics inhibited HIV-1 infectivity in a concentration-dependent manner with IC_{50} values in the low micromolar range. Activity required prior interaction with the viral membrane, while no effect was seen upon pre-incubation of target cells with the compounds. Given that these compounds are likely to bind to both virus and cell membranes, this suggests that their interaction with cellular membranes may not influence viral entry or/and that compounds are rapidly removed from cellular but not from viral membranes. Indeed, ATP-dependent transporters (ABC transporters, P glycoprotein) remove foreign amphiphilic compounds from cell membranes (Giacomini

et al., 2010), and may also work in this manner on the compounds studied here. Further experiments confirmed that the viral membrane is indeed the target: lipidomimetics inhibited HIV-1 entry independent of the viral envelope glycoprotein and the specific entry pathway, while no effect was observed for the non-enveloped virus AAV. It can be concluded that the described lipidomimetics directly target the viral membrane and alter its capacity to fuse with the host cell membrane. This effect suggests potential against a wider spectrum of enveloped viruses, while the lipid-dependent activity differences explored below may restrict activity to membranes with a defined lipid composition.

Studies of virus stability showed that the compounds did not disrupt particle integrity, although J592C caused a shift in buoyant density of the viral particle. Sphingosine-like (J582C) and other long acyl-chain compounds (as IBS70 or IBS95) contain a single hydrocarbon chain and have inverted cone-shape geometry like LPC, generic structures that induce positive curvature and thus inhibit membrane fusion (Chernomordik et al., 1995). While LPC itself is toxic, less toxic compounds have been shown to inhibit virus entry due to their inverted cone-shape structure (St.Vincent et al., 2010). These RAFIs consist of a nucleoside coupled to perylene and have a wide antiviral spectrum against enveloped but not naked viruses. A similar broad antiviral spectrum is exhibited by the amphiphilic fusion inhibitor, aryl methylene rhodanine derivative LJ001 (Wolf et al., 2010). Both LJ001 and RAFIs were shown to target membranes though they did not structurally resemble lipids, but the effect of LJ001 is actually mediated by photosensitization (Vigant et al., 2013), unrelated to raft modulation. More relevant, cosalane is a cholestane derivative with an oversized head group comprising disalicylmethane with activity against enveloped viruses (Zhan et al., 2010). The cholestane moiety of cosalane is reported to insert into the cell membrane and/or the viral envelope, from where the large disalicylmethane moiety protrudes and blocks the interaction between gp120 and CD4 (Cushman et al., 1994). For the activity of cosalane the membrane raft-targeting property of the lipid anchor (cholestane) appears to be important, however, the mode of action does not involve the disruption of membrane raft domains of the virus envelope. This compound would be defined as a raftophile; it is probably not a raft modulator or disrafter (Agarwal et al., 2013; Rajendran et al., 2010).

A number of lipidic HIV inhibitors were previously studied with regard to modifying both the host cell and viral membranes, their fluidity and lipid domain structure (Dumas and Haanappel, 2017). The natural compounds glycyrrhizin and fattiviracin FV-8 possess large, neutral, hydrophilic head groups, and are structurally far removed from natural raft lipids from which the lipidomimetics studied here originated. In a review of the potential relevance of membrane raft targeting by natural products as an anti-HIV strategy (Verma, 2009), a considerable body of literature on betulinic acid derivatives is cited, structurally related to the lupine derivative J391B. However, none of them carried a 3-amino group that proved decisive for the specific HIV envelope-stabilizing activity of J391B described here.

In order to study the potential effect of lipidomimetics on membrane structure, laurdan staining was used, which allows rapid determination of differences in viral membrane order (Lorizate et al., 2009). Diametrically opposed alterations in membrane

order were observed for the cholesterol analogue J391B, which increased membrane rigidity and counteracted temperature-induced melting, and the sphingosine analogue J582C, which increased membrane fluidity independent of temperature. IBS70 also increased the fluidity of the virus envelope, but its effect disappeared at higher temperatures. Membrane rigidification by the steroidal amine J391B only superficially resembled the effect of increasing the proportion of membrane cholesterol, the lipid fundamental to the existence of L_o phases (Brown and London, 2000; Simons and Ikonen, 2000). Interestingly and unlike cholesterol, the effect of J391B on membrane order required the presence of PS. This lipid dependence was not caused by an unspecific electrostatic effect as substitution of PS by either phosphatidylglycerol or phosphatidic acid at a similar concentration in the presence of J391B had little or no effect on membrane order. Surprisingly, introduction of J391B into membranes completely lacking PS and other negatively charged lipid head groups increased membrane fluidity, similar to J582C and IBS70. It can therefore be hypothesized that there is a specific electrostatic interaction of J391B with PS, and this may create more rigid membrane structures. Annexin V staining of cells treated with J391B revealed a rapid exposure of PS on the cell surface without detectable signs of apoptosis (Figure 4.12), indicating that PS flipping from the inner to the outer leaflet is trapped by the compound, which suggests a high affinity to PS. The viral membrane is highly enriched in PS compared to the producer cell plasma membrane (Lorizate et al., 2013), and this may make HIV-1 a particularly good target for J391B. As a low-molecular weight, membrane-inserting PS ligand, J391B is novel and structurally unrelated to the three hitherto described (non-lipidomimetics) PS binders (Hanshaw and Smith, 2005).

Intriguingly, upon HIV engagement of its receptors, flipping of PS to the outer leaflet of the host cell target membrane has been reported to be important for HIV fusion. Zaitseva *et al.* (Zaitseva et al., 2017) showed that HIV binding and formation of the prefusion Env-CD4-coreceptor complex leads to surface expression of PS. First, the complex triggers a Ca^{2+} signal, which in turn activates lipid scramblase TMEM16F that externalizes PS, which is then essential for the next step of fusion, gp41 restructuring and hemifusion. It will be interesting to determine if virion PS is also important for fusion and whether its function is inhibited by bound J391B. PS in the outer leaflet of the viral membrane has already been shown to be important for cell entry of other enveloped viruses (Morizono and Chen, 2014), underlining the relevance of testing J391B activity against these viruses in the future.

Treatment of HIV-1 with the sphingosine-like compound J582C led to decreased membrane order and a concomitant decrease in virus density. Laurdan directly sense the abundance of water molecules within the membrane, which inversely correlates with membrane order (Parasassi et al., 1991). Conceivably, insertion of J582C into the viral envelope may cause membrane swelling by allowing more water to penetrate. Indeed, the bulkier, uncharged head group of J582C comprises three hydrogen-bond acceptors, as opposed to the small positively charged head group of sphingosine with its three hydrogen-bond donors (Figure 4.2). Natural sphingosine has a completely different behavior compared to the uncharged compound J582C. The positive charge of sphingosine appears crucial for its membrane activity (Goñi and Alonso, 2006).

CHAPTER 4

Sphingosine rigidifies the bilayer lipid acyl chains, and as a result membrane permeabilization can occur due to the coexistence of domains of different fluidities (Contreras et al., 2006; Goñi and Alonso, 2006). On the other hand, J582C-induced positive membrane curvature in combination with water incorporation would tend to swell the membrane, explaining the observed decrease in particle density.

Based on the observed opposing effects of J391B and J582C on HIV-1 membrane order, experiments were performed with a mixture of both to investigate their potential antagonism. Counterintuitively, J391B and J582C synergistically inhibited HIV-1 infectivity, associated with an increased membrane fluidity apparently dominated by J582C, combined with a flatter temperature-dependent GP profile reminiscent of J391B alone. Dominant membrane order enhancement by the specific interaction between J391B and PS appears to be abrogated in the presence of J582C, yet the mixture of both distinct raft modulators appears to create a greater obstacle to fusion than each compound individually. Thus, in addition to the impact on global viral membrane order, as reported by the laurdan assay, membrane lipid mechanics at a smaller scale (as required for fusion) are a target of lipidomimetics, which seem to act as molecular “spanners in the works” of fusion. Further studies will be required to identify the precise mechanism of this synergistic effect.

Admittedly, efforts towards selective drug delivery are the precondition to optimizing anti-HIV lipidomimetics, since their hydrophobicity facilitates indiscriminate absorption by cell membranes, followed by either uptake into the cell or expulsion via transporters and re-loading onto lipoproteins (Giacomini et al., 2010). Selective drug delivery may, for example, target natural, highly specialized HIV infection pathways. Appropriately engineered lipidomimetic-loaded ganglioside-containing vesicles may be a promising approach of interfering with primary mucosal infection. After targeting siglec-1-expressing mature dendritic cells, which are not productively HIV-infected, the vesicles would inactivate HIV encountered in the same intracellular sac-like compartment (Izquierdo-Useros et al., 2012a, 2012b).

Very little is known about the role of membrane order and fluidity regarding virus pathogenicity and how to modulate the physicochemical properties of the virus envelope to achieve a desired inhibitory phenotype. Studying lipid-modulating compounds like the ones described here provides a glimpse of this fascinating subject and may pave the way for future studies.

4.5. Annexes

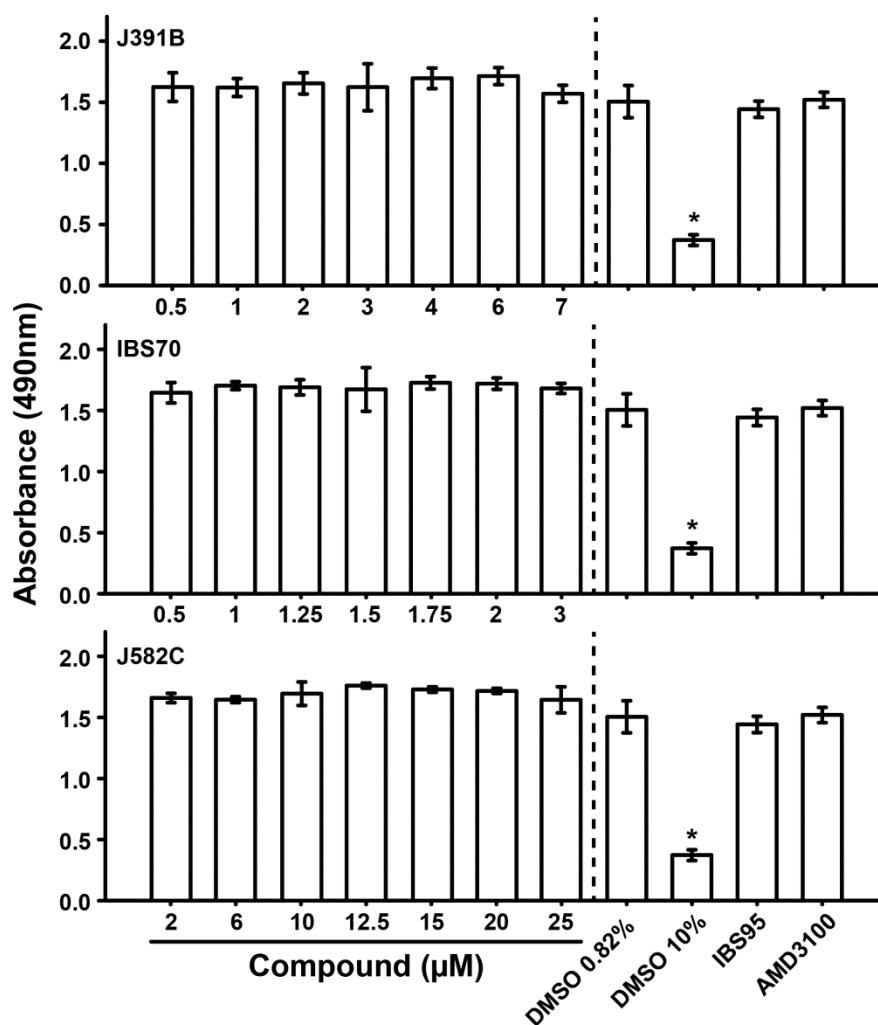


Figure An. 4.1 – MTT test for cytotoxicity of lipidomimetics at different concentrations. HeLa TZM-bl cells were incubated for 2 h in the presence of the compounds. Concentration ranges of J391B, IBS70 and J582C are depicted in each panel. DMSO (0.82%), IBS95 (7 µM) and AMD3100 (0.5 µM) served as controls and treatment with 10% DMSO served as toxicity control. Data represent the mean \pm SD of four replicates. * represents a significant ($P < 0.01$) decrease when compared to the DMSO control.

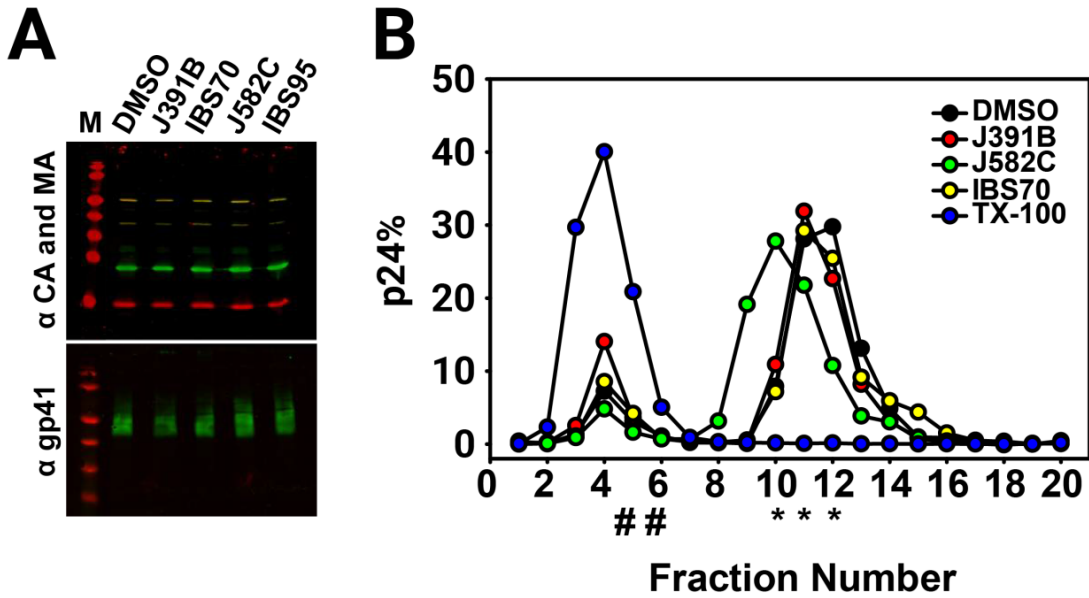


Figure An. 4.2 – Influence of lipodimetics on HIV-1 particle stability and density. **A** Virus stability. Purified HIV-1 (3 μ g of CA) was treated with 6 μ M J391B, 2 μ M IBS70, 20 μ M J582C, 7 μ M IBS95 or DMSO (0.35%) for 30 min at 37°C. Subsequently, particles were recovered by ultracentrifugation and analyzed by Western blot developed against CA (green) and MA (red) and against the HIV-1 transmembrane glycoprotein gp41. **B** Virus buoyant density. HIV-1 (1 μ g of CA) was treated with 6 μ M J391B, 2 μ M IBS70, 20 μ M J582C, 0.5% TX-100 or DMSO (0.35%) as in panel **A** and subsequently subjected to equilibrium density gradient centrifugation. Gradient fractions were collected from the top and virus amounts were quantified by p24 ELISA.

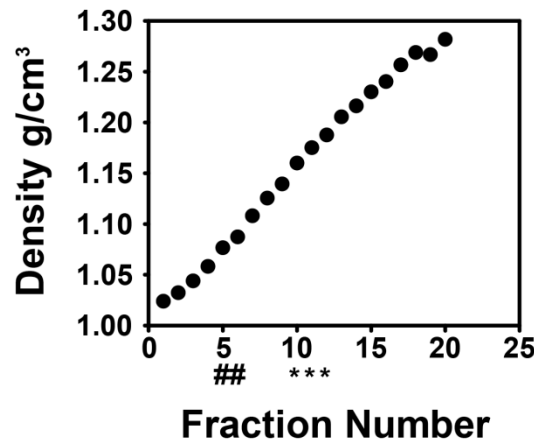


Figure An. 4.3 – Density gradient fraction-density measured by refractometer. Sucrose gradients were run and refractive index of the fractions was measured by refractometer. Fraction density was calculated. Asterisks * represent the location of virus and # the location of soluble capsid in the gradient.

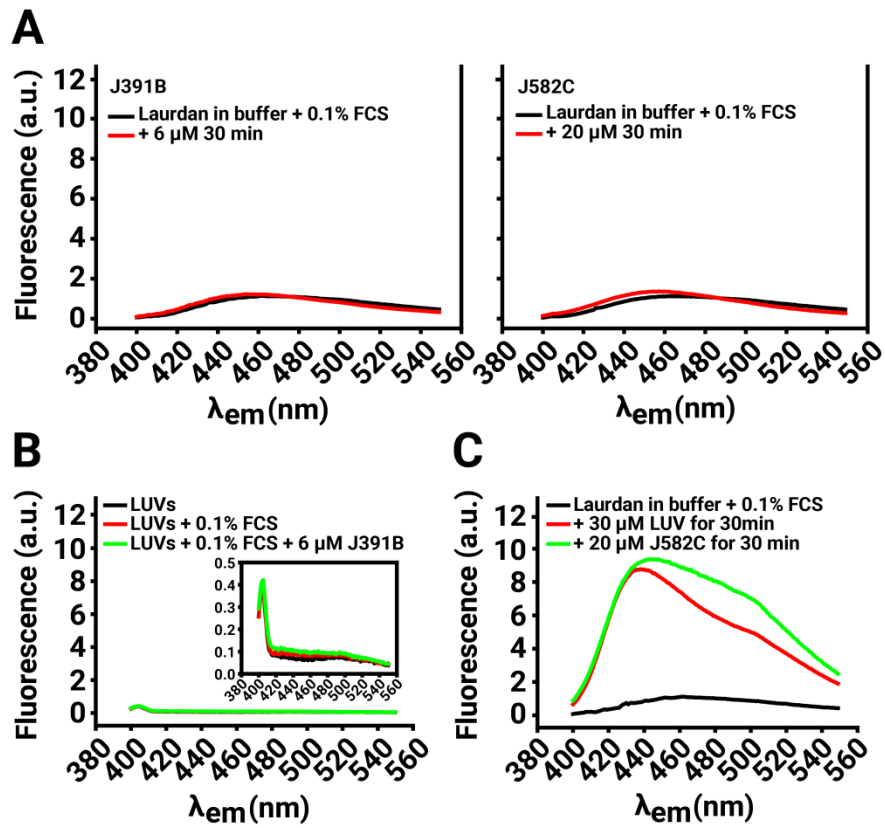


Figure An. 4.4 – Control experiments. A| J391B (left) and J582C (right) do not influence base-line laurdan fluorescence in buffer. B| LUVs in the absence of laurdan, with or without J391B produce no fluorescence signal. C| Laurdan in buffer and in the presence of J582C has no fluorescence signal, but once liposomes are added laurdan fluorescence appears, as well as the fluorescence change caused by the compound.

Chapter 5. Development of Nanoparticles for Specific Delivery of Latency Reactivation Agents

5.1. Introduction

5.1.1. Latent viral reservoirs

Antiretroviral therapy is currently capable of suppressing HIV-1 replication thanks to an approach known as “highly active antiretroviral therapy”, or HAART. The first HAART strategies were developed almost 30 years ago, and although the ease of treatment and specific drugs used have greatly evolved since then the main concept behind HAART remains unaltered: the simultaneous use of different antiretroviral drugs to suppress different steps of viral replication and hamper the progress of the virus. Nowadays, most HAART are based in the inhibition of two viral enzymes: retrotranscriptase and integrase, although protease inhibitors are also commonly used. Generally, new treatment regiments are initiated by combination of an integrase inhibitor with two different retrotranscriptase inhibitors, thus inhibiting viral gene insertion into the host cell, and consequent virus replication (Saag et al., 2018).

HAART is, in most cases, capable of controlling the spread of the virus in the host organism by suppressing virus replication, so that viral RNA levels are reduced to below the detection limits of clinical assays, and results in a prolonged lifespan and quality of life, and a lower incidence of AIDS-related illnesses (Lee et al., 2018). Nevertheless, although the improvement that HAART has brought to the life of HIV-1 infected individuals is unquestionable, it does not constitute a complete cure for HIV-1, as it does not hamper the establishment of viral reservoirs within latently infected cells. During HIV-1 infection, most of the affected CD4+ T cells die from cytophatic effects derived from virus replication. Yet, a small subset of infected cells, long-lived memory T cells and with a lower frequency other cell types such as naive CD4+ T cells (Wightman et al., 2010), tissue macrophages (Stebbing et al., 2004), astrocytes (Churchill et al., 2009) and thymocytes (Kitchen and Zack, 1997), persist indefinitely with HIV DNA integrated into their genome even in the presence of HAART (Siliciano et al., 2003). This implies that, even if no viral RNA can be detected in the blood of infected individuals under HAART, when treatment is accidentally or voluntarily suspended, latent HIV-1 is reactivated and new viral particles are produced.

Thus, elimination of latently infected cells is a requirement for the development of a cure for HIV-1. Most of the strategies followed throughout the years towards this goal are based in deliberately inducing viral reactivation by the use of latency reversing agents (LRAs) to produce latently infected cell death through cytophatic effects associated with virus production, an strategy known as “shock and kill” (Deeks et al., 2012). Unfortunately, and despite the variety of reactivation compounds available nowadays, none has proven total efficacy. Additionally, viral reactivation does not necessarily imply latently infected cell death, so viral eradication demands innovative strategies designed not only to reactivate latent viral reservoirs, but also to promote antiviral immune control and active purge of latently infected cells by the immune system. Indeed, for an effective clearance of HIV-1 reservoirs, prior antigen-specific

stimulation of CD8+ T cells has been described to be necessary to eliminate reactivated latently infected cells (Shan et al., 2012). A further complicating factor comes from the fact that the latently infected cells reside in a variety of anatomical sites scattered throughout the organism, which considerably complicates the delivery of latency reversing agents (Vanhamel et al., 2019). Thus, the development of a LRA administration route that permits specific delivery of the drugs to latently infected cells in a wide variety of tissues is key for the design of an efficient “shock and kill” HIV-1 purge strategy (Chun et al., 2015; Deeks et al., 2012).

5.1.2. *Trans-infection*

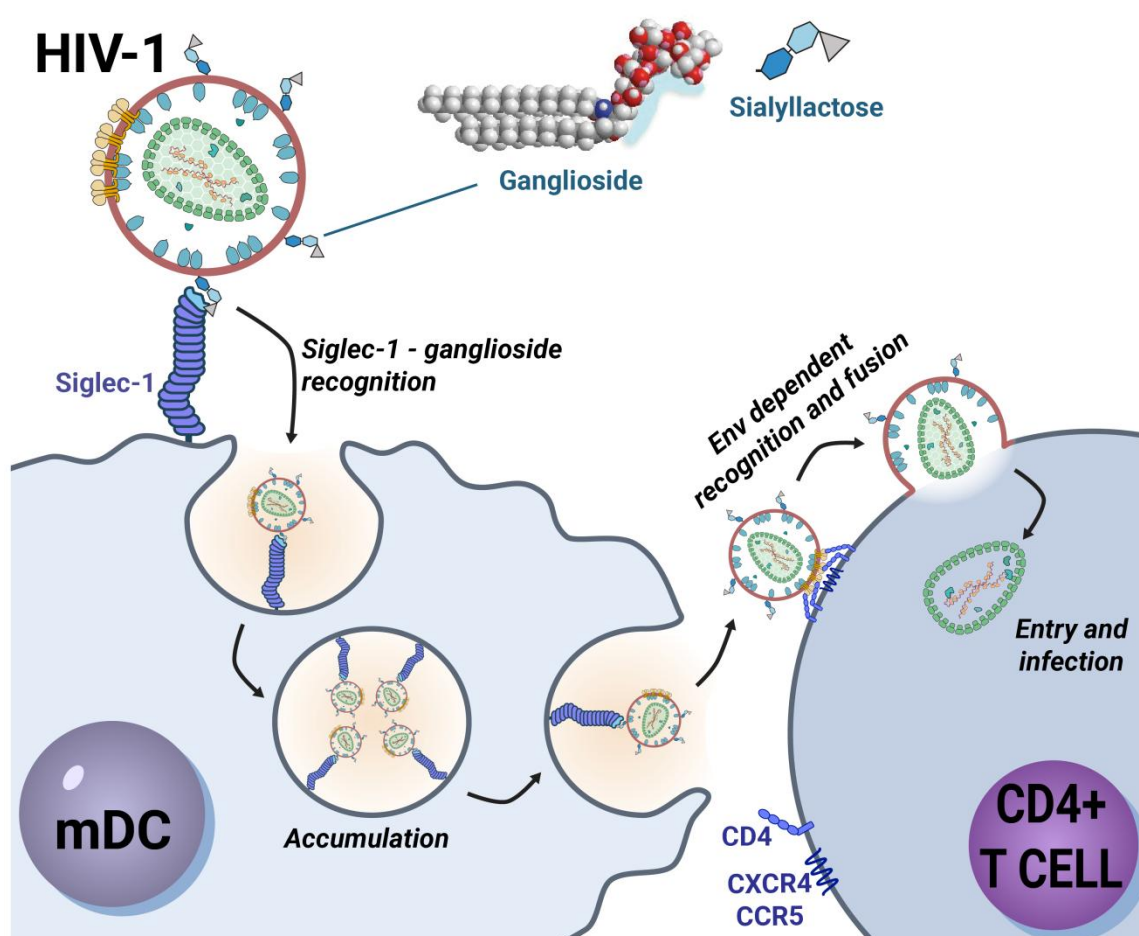


Figure 5.1 – HIV-1 trans-infection mediated by mDCs. Siglec-1 expressed in mDCs recognizes and binds sialyllactose in HIV-1 membrane gangliosides. Virions are captured by mDCs and accumulated in a sac-like compartment, and when mDCs travel to peripheral lymphoid tissues and interact with CD4+ T cells, the accumulated HIV-1 viral particles are released and infect the T cells.

Mature dendritic cells (mDCs) are potent antigen presenting cells that constantly interact with T cells to initiate immune responses. They capture antigens in peripheral tissues, transport them to lymphoid organs, and display the digested antigens to T cells.

These cells are largely resistant to infection by HIV-1 thanks to the SAMHD1 restriction factor, an antiretroviral protein that inhibits early stages of the viral replication cycle (Hrecka et al., 2011; Laguette et al., 2011). However, even if it cannot efficiently infect myeloid cells, HIV-1 has evolved strategies to subvert mDC antiviral activity and exploit these myeloid cells to promote infection of CD4⁺ T cells throughout a mechanism known as *trans*-infection. This pathway involves binding and uptake of HIV-1 by mDCs, traffic and accumulation of internalized virus and its final release allowing for productive infection of CD4⁺ T cells and other susceptible cell types (Cameron et al., 1992; Geijtenbeek et al., 2000) (Figure 5.1). In 2012 the molecular mechanism underlying the potent HIV-1 *trans*-infection capacity of mDCs was elucidated, which relies in the recognition of sialyllactose exposed on viral membrane gangliosides (Izquierdo-Useros et al., 2012a) by the receptor Siglec-1 expressed on mDCs (Izquierdo-Useros et al., 2012b), a pathway that was later confirmed to occur *in vivo* (Sewald et al., 2015). Siglec-1 is a type I transmembrane receptor with a long neck that protrudes beyond the glycocalyx of the cell, and exposes an amino-terminal V-set domain with the ability to interact with sialylated ligands. Although the affinity of Siglec-1 for sialic acid containing molecules is low, avidity for clusters of sialylated molecules is high (Crocker et al., 2007), allowing for the specific recognition of packaged gangliosides that expose sialyllactose moieties on viral membranes. Interestingly, sialyllactose recognition by Siglec-1 in mDCs was demonstrated to also occur in liposomes containing the adequate gangliosides, which were not only recognized by mDCs, but also accumulated inside the mDCs in the same sac-like compartment as the HIV-1 viral particles (Izquierdo-Useros et al., 2012a). If ganglioside-containing liposomes are captured and accumulated by mDCs through the same pathway as HIV-1, these findings point to a promising new pathway for antiretroviral drug delivery.

5.1.3. mDC mediated viral reservoir targeting

One of the main impediments for delivery of latency reversing agents is that latently infected lymphocytes are scattered throughout secondary lymphoid tissues, and targeting the drugs to this viral reservoirs has proven to be a difficult task (Deeks et al., 2012). Nevertheless, the ganglioside/Siglec-1 mediated novel pathway exploited by the virus for *trans*-infection offers in turn the unique opportunity to achieve HIV-1 eradication: by designing ganglioside-containing nanoparticles, easily accessible mDCs expressing Siglec-1 could be targeted. Nanoparticles captured by the ganglioside/Siglec-1 pathway would be accumulated in the mDCs, and natural migration of the myeloid cells to peripheral secondary lymphoid tissues which would facilitate nanoparticles transport to latently infected cells scattered throughout the organism (Steinman and Banchereau, 2007). Indeed, recently developed glycoengineering approaches have enabled targeted manipulation of the sialic acid interactions with the sialic-acid binding Siglec receptor (Büll et al., 2016), and although this has never been tested in the HIV-1 field, targeting of the ganglioside/Siglec-1 pathway shows a promising avenue to contribute to HIV-1 functional cure.

CHAPTER 5

In overview, to obtain HIV-1 eradication by reactivation of latently infected cells three main milestones must be reached: i) reactivation of latently infected cells by induction of latent HIV-1 integrated in the host cell genetic material, ii) delivery of antiretroviral drugs to render reactivated HIV-1 particles non-infectious, and iii) the specific priming of antiviral cytotoxic responses to induce purge of latently infected cells. For this purpose, different nanoparticles designed to exploit the mDC mediated ganglioside/Siglec-1 pathway for delivery the necessary agents could be used: first, nanoparticles simultaneously packaging latency reactivation agents and antiretroviral drugs (such as protease inhibitors) specifically designed to be delivered to target T cells, which would induce latency reactivation and control infection by rendering reactivated HIV-1 non-infectious (Figure 5.2). Second, nanoparticles with incorporated HIV-1 antigens (such as the viral SL9 peptide) designed to target mDCs for cross-presentation of the antigen to CD8+ T cells, stimulating the potent antiviral cytotoxic response required to eliminated reactivated HIV-1 infected CD4+ T cells (Shan et al., 2012) and purge viral reservoirs (Figure 5.2). Regarding this last point, targeting with liposomes has indeed recently proven efficacy in inducing antigen presentation *in vivo* (Kawasaki et al., 2013).

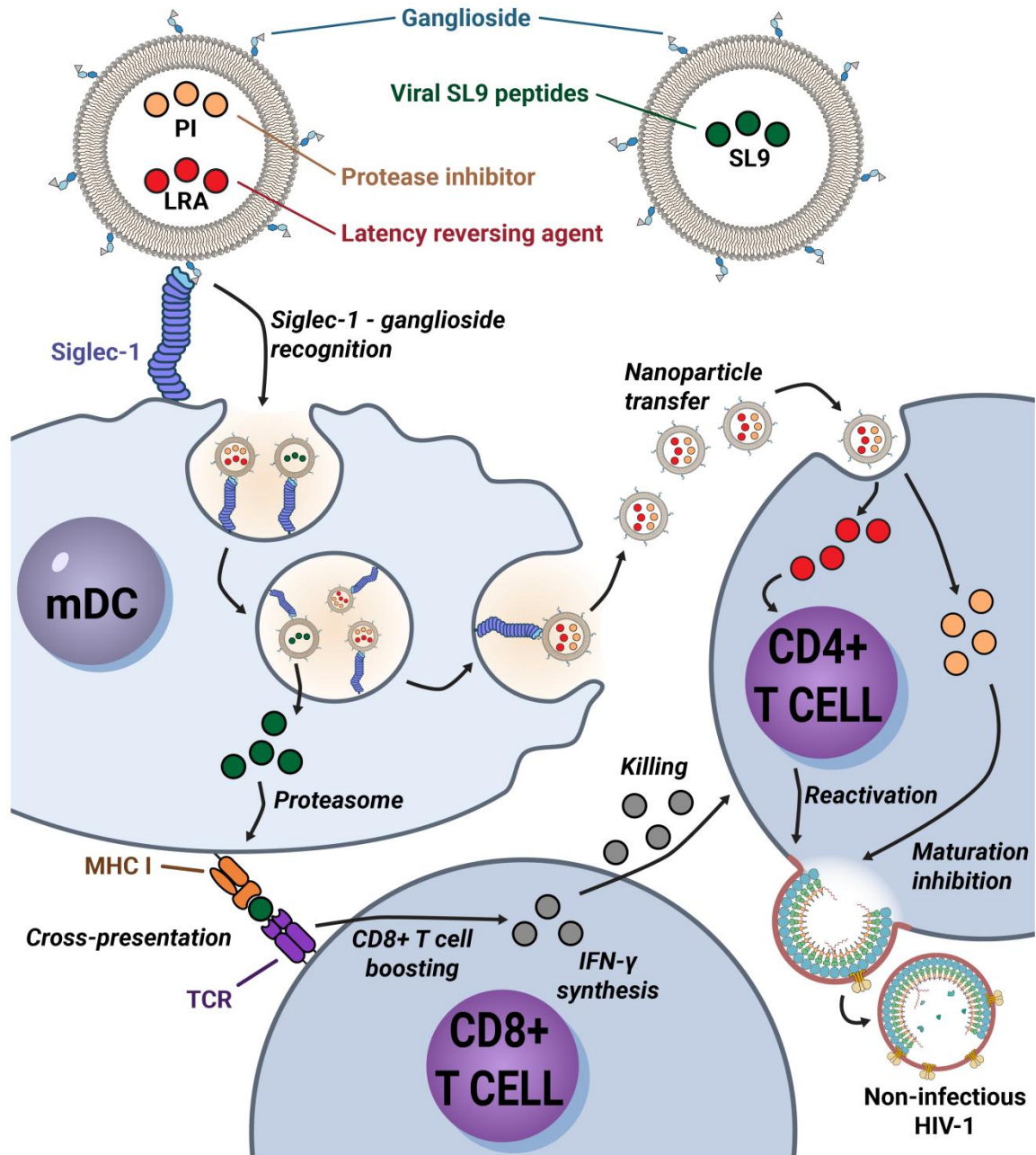


Figure 5.2 – Use of ganglioside/Siglec-1 mediated pathway for delivery of latency reversing drugs and immune boosting peptides by nanoparticles.

5.1.4. Nanoparticles for drug delivery

In addition to conferring the targeting capabilities necessary for exploitation of the ganglioside/Siglec-1 pathway, the use of nanoparticles for delivery of latency reversing and antiretroviral drugs also confer several other advantages: compound half-life is increased, drug potency is augmented up to 100,000 times as compared to free molecules, drug toxicity is reduced, solubility and stability are improved, and transport

and intracellular uptake are enhanced (Düzgüneş et al., 2005; Gunaseelan et al., 2010; Mufamadi et al., 2011; Ojewole et al., 2008; Pisal et al., 2010; Pollock et al., 2008).

In this chapter, three types of ganglioside-containing nanoparticles were used for antiretroviral drug delivery: liposomes, solid lipid nanoparticles (SLN), and lipid coated PLGA nanoparticles (Figure 5.3).

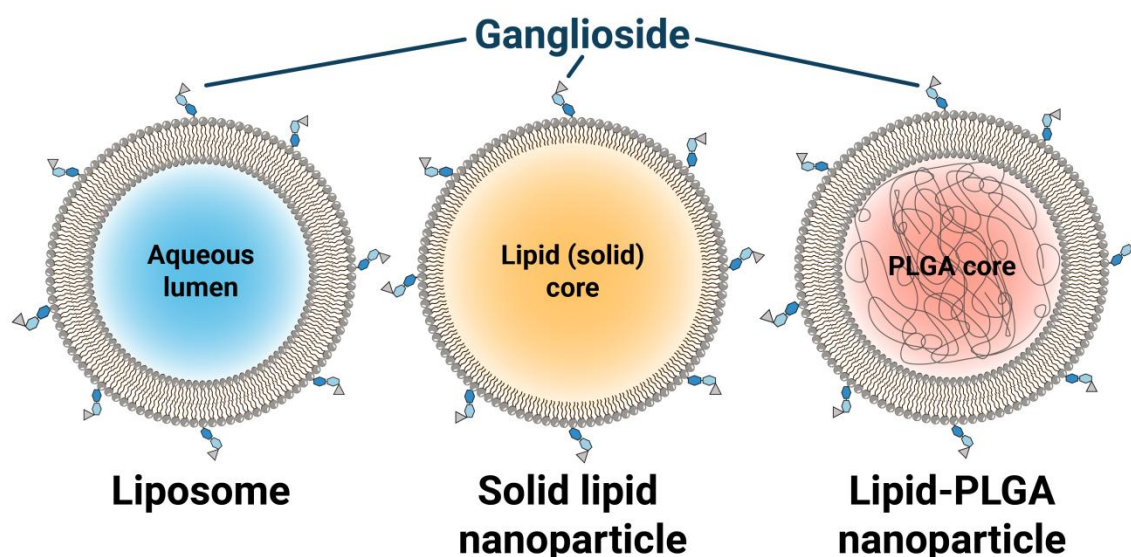


Figure 5.3 – Nanocarriers used for delivery of antiretroviral drugs.

The liposomes used in this work, large unilamellar vesicles or LUVs, are vesicles composed of a single lipid bilayer. This lipid bilayer can be engineered to confer certain properties to the particle, such as providing targeting ability, enhancing stability, allowing fluorescent labeling, or conferring pH-dependent drug delivery, all by adding specific functionalized lipids to the bilayer (Torchilin, 2005). Liposomes contain an aqueous lumen, enabling them to be used to encapsulate and deliver hydrophilic molecules to target cells. Additionally, hydrophobic drugs can also be packaged into the liposomes, as they tend to partition to the hydrophobic region of the lipid bilayer. The use of liposomes for delivery of antiretroviral drugs have long been exploited in the search of reduced toxicity issues associated with the treatments, with a wide range of approaches ranging from particles designed to reduce HIV-1 infectivity by altering lipid content of producer cells (Pollock et al., 2010), to the delivery of more traditional antiretroviral drugs (Bronstein et al., 2011; Clayton et al., 2009; Düzgüneş et al., 2005; Ramana et al., 2012). The main advantage of the liposomes relies in the ease of their production, the fact that their lipid composition can be easily chosen and adjusted, their capacity for delivering both hydrophobic and hydrophilic compounds, and augmenting the potency and life-time of the drugs in the organism (Gregoriadis and Florence, 1993).

Solid lipid nanoparticles (SLNs) contain a hydrophobic core composed of fatty acids in a solid state surrounded by a surfactant which can be composed of phospholipids (Sinha et al., 2010). Thanks to their solid lipid core they present several advantages over liposomes when hydrophobic drugs are being packaged: first, for a particle of the same size, a higher amount of hydrophobic molecules can be packaged into a solid lipid nanoparticle than into a liposome, as the volume occupied by the SLN hydrophobic core is bigger than that occupied by the liposome lipid bilayer. Second, because of the solid state of the lipids in the core drug mobility is greatly reduced, lowering undesired drug release upon nanoparticles and cell contact (Mehnert and Mäder, 2001). Additionally, the surfactant surface of solid lipid nanoparticles is composed of a phospholipids monolayer, which similarly to the liposome lipid bilayer can also be functionalized for fluorescent labeling, targeting ability, and added stability.

Finally, a third type of nanoparticles has been used in this chapter for drug delivery. Lipid covered poly(lactic-co-glycolic) (PLGA) nanoparticles are composed of two main elements: a polymeric PLGA core, capable of packaging hydrophobic drugs; and a lipid bilayer cloaking, which can also be functionalized for targeting, labeling and enhanced stability (Hu et al., 2014). In addition, recent studies have shown that PLGA cores can be coated with membranes derived from erythrocytes (Hu et al., 2011) and platelets (Hu et al., 2015), which confers a significant advantage in overcoming undesired biocompatibility issues upon patient treatment. For treatment of a HIV-1 infected patient, drug-loaded PLGA cores could be coated with erythrocyte or platelet derived membranes obtained from the same patient, thus greatly decreasing immune system response, clearance, and adverse effects from the nanoparticles.

Another advantage of lipid covered PLGA nanoparticles is that the encapsulation of the drug and the coating of the nanoparticles with functionalized lipid vesicles are carried out in two discretely separated steps: the antiretroviral drug is added to the nanoparticles during the generation of the polymeric PLGA nanoparticles, so it gets entrapped in the hydrophobic core. Drug-loaded PLGA nanoparticles are extensively washed to remove any excess free drug, so that when the PLGA nanoparticles are coated with a lipid bilayer, no free drug is present to interact with the lipid cloaking and partition to it (Hu et al., 2015). In summary, the drug is packaged in the interior of the PLGA core, clearly separated from the functionalized lipid bilayer that interacts with the targeted cells, greatly reducing undesired drug leakage upon nanoparticles and cell contact.

In this chapter targeting of nanoparticles to mDCs via the ganglioside/Siglec-1 pathway, and its suitability for delivery of LRAs to latently infected cells was studied. Additionally, delivery of immune boosting HIV-1 peptides to CD8+ T cells was investigated, to develop a complete “shock and kill” strategy for purge of viral reservoirs.

5.2. Experimental techniques

5.2.1. Reagents

For nanoparticle formation 1-palmitoyl-2-oleoyl-glycero-3-phosphocholine (POPC), and 1,2-distearoyl-sn-glycero-3-phosphoethanolamine-N-[methoxy(polyethylene glycol)-2000] (DSPE-PEG₂₀₀₀) from Avanti Polar Lipids, Asialo GM1 ganglioside (Santa Cruz Biotechnologies), GM1 ganglioside (Carbosynth), and Texas Red™ 1,2-Dihexadecanoyl-sn-Glycero-3-Phosphoethanolamine (DHPE-Texas Red) and Oregon Green™ 488 1,2-Dihexadecanoyl-sn-Glycero-3-Phosphoethanolamine (DHPE-Oregon Green) from ThermoFisher Scientific were used. For SLN formation stearic acid and sodium taurodeoxycholate were purchased from Sigma-Aldrich. Dextran Alexa Fluor 488 of 10,000 kDa of size (ThermoFisher Scientific) was used for liposome content delivery experiments. ANTS (8-Aminonaphthalene-1,3,6-Trisulfonic Acid) and DPX (p-Xylene-Bis-Pyridinium Bromide) from ThermoFisher were used for content release experiments.

5.2.2. Cells and cell culture

Cells were maintained in RPMI medium supplemented with 10% fetal bovine serum, 100 IU/ml of penicillin and 100 µg/ml of streptomycin at 37 °C and 5% (vol:vol) CO₂.

Peripheral blood mononuclear cells (PBMCs) were obtained from HIV-1-seronegative donors by Ficoll-Hypaque density gradient centrifugation (Izquierdo-Useros et al., 2012a). From these PBMCs, monocytes were isolated using CD14⁺-selection magnetic beads (Miltenyi Biotec). For obtention of dendritic cells (DCs), monocytes were cultured in the presence of 1,000 IU/ml of granulocyte-macrophage colony-stimulating factor (GM-CSF, R&D) and interleukin-4 (IL-4, R&D), obtaining immature dendritic cells (iDCs). Mature dendritic cells (mDCs) were differentiated by culturing iDCs at day five for two additional days in the presence of 100 ng/ml of lipopolysaccharide (LPS, Sigma Aldrich) or 1000 U/ml of interferon-γ (Sigma-Aldrich).

J-lat cells are a type of Jurkat-derived cells commonly used as HIV-1 latency models. They contain, under the HIV-1 promoter, a GFP reporter gene so that upon HIV-1 latency reactivation together with the viral proteins the GFP reporter fluorophore is expressed. Latency reactivation is then quantified by measurement of GFP fluorescence in J-lat cells. J-lat clone 9.2 cells were obtained through the US National Institutes of Health (NIH) AIDS Research and Reference Reagent Program.

5.2.3. Liposome preparation

Two types of liposome vesicles were used in this chapter: multilamellar vesicles (MLVs) and large unilamellar vesicles (LUVs). In both cases, liposome preparation started with the thin layer hydration method, to obtain MLVs. In the case of LUV formation, additionally an extrusion protocol was followed.

For latency drug encapsulation, romidepsin and bryostatin were dissolved in DMSO. During the initial step of liposome preparation, when lipids are mixed the organic solvent, an appropriate volume of romidepsin and bryostatin was added to the mixture. The formation of the liposomes was followed by drying, hydration and agitation, freeze and thaw cycles, and extrusion, following the protocol described before. The same rationale was followed for the SL9 peptide, which was also dissolved in DMSO and mixed with the lipids in the organic solvent prior to drying.

For encapsulation of fluorescently labeled dextran molecules in liposomes, lipids were mixed in organic solvent and dried as before. Dextran molecules covalently bound to Alexa Fluor 488 were added to the resuspension buffer at a concentration of 2 mg/ml, and this dextran-containing buffer was used for resuspension of the dried lipids. After freeze and thaw, and extrusion, non encapsulated fluorescent dextran molecules were eliminated by a size exclusion chromatography, as explained below.

5.2.3.1. Size exclusion chromatography

After molecule encapsulation into liposomes, such as dextran molecules or ANTS and DPX, separation of free non-encapsulated molecules was carried out by a size exclusion chromatography.

1. 2 g of the Sephadex G-75 (GE Healthcare) resin was hydrated in 30 ml of water and packed in a 20 cm x 1 cm glass column.
2. The column was equilibrated with 30 ml of elution buffer (HEPES 10 mM, NaCl 150 mM, pH 7.4), and the sample was loaded on top of the column.
3. Elution buffer was added on top until a turbid suspension eluded through the bottom, corresponding to the liposomes. The smaller non-encapsulated molecules remain in the column.
4. Liposome concentration was calculated by quantification of phospholipid phosphate concentration by the method already detailed (Böttcher et al., 1961).

5.2.4. ANTS/DPX leakage assay

For liposome stability studies *in vitro*, a ANTS (8-Aminonaphthalene-1,3,6-Trisulfonic Acid) and DPX (p-Xylene-Bis-Pyridinium Bromide) liberation assay was used (Ellens et al., 1985). By itself, ANTS presents a excitation maximum at 355 nm and emission maximum at 520 nm, but when both compounds are mixed at sufficiently high concentrations at a ~ 4:1 (DPX:ANTS mol:mol) ratio, ANTS fluorescence is attenuated by collisional energy transfer with DPX. When ANTS and DPX are encapsulated in a liposome at high concentrations, ANTS fluorescence is thus attenuated. Upon destabilization or rupture of the liposome membrane and leakage of its contents, ANTS and DPX dilute in the medium decreasing the quenching effect. Thus, by following the increase in fluorescent emission of ANTS, content leakage can be quantified (Figure 5.4).

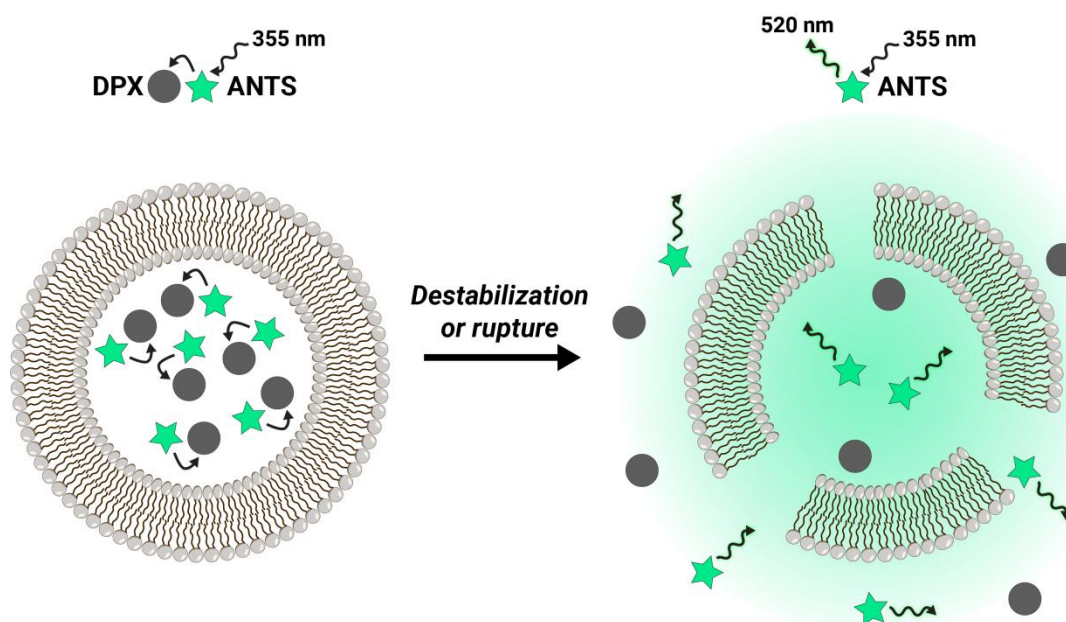


Figure 5.4 – Liposome content leakage assay using ANTS and DPX.

ANTS and DPX encapsulation into liposomes was started by resuspension of dried lipid mixtures in a HEPES 5 mM, NaCl 20 mM, pH 7.4 buffer containing ANTS and DPX at 12.5 mM and 45 mM concentrations, respectively. LUVs were generated followed the freeze/thaw and extrusion protocol already detailed, and elimination of non-encapsulated ANTS and DPX was carried out by a size exclusion chromatography as explained above (section 5.2.3.1).

For ANTS and DPX leakage quantitative analysis, initial fluorescence of the intact ANTS/DPX liposomes is taken as a 0% content leakage value. After stability analysis, 0.1% Triton X-100 is added to the sample to induce liposome rupture and complete content leakage, and the resultant fluorescent signal is taken as a 100% content leakage

value. For each time point, content leakage is calculated as a percentage using the following formula:

$$\% \text{ leakage} = \frac{(F_t - F_{0\%})}{(F_{100\%} - F_{0\%})} \times 100$$

where F_t is the ANTS fluorescence at a given time point, $F_{0\%}$ is the fluorescence of the intact liposomes, and $F_{100\%}$ is the fluorescence of the detergent-ruptured liposomes.

5.2.5. Solid lipid nanoparticles preparation

For fluorescently labeled solid lipid nanoparticles formation the warm microemulsion method was used (Arana et al., 2015; Cavalli et al., 1999; Serpe et al., 2004) (Figure 5.5). An oil/water microemulsion was formed by mixing a fatty acid that composed the hydrophobic core of the nanoparticles (stearic acid), a phospholipids mixture composing the nanoparticles surface surfactant, a co-surfactant (sodium taurodeoxycholate), and ultrapure water as a continuous phase.

1. The stearic acid (0.07 mmol) and phospholipid surfactants (0.014 mmol in total) were first melted together at 80 °C (10 °C above stearic acid melting point) under continuous stirring (1,400 rpm). As phospholipid surfactants, a mixture of POPC:DHPE-Texas Red (1:0.02 mol:mol), or POPC:GM1:DHPE-Texas Red (1:0.1:0.02 mol:mol) was used.
2. In parallel, the continuous phase (11.11 mmol) and co-surfactant (0.066 mmol) were mixed and heated to 80 °C, and added to the melted lipid mixture.
3. The mixture was stirred at 80°C until a transparent oil/water microemulsion system was formed.
4. The hot microemulsion was then dispersed into cold water (4 °C) at a 1:50 (microemulsion:water vol:vol) ratio under vigorous stirring (14,000 rpm for 10 min) with a SilentCrusher M (Heidolph Instruments) to form a SLN dispersion.
5. Samples were then washed three times using Amicon Ultra-15 centrifugal filter units (cut-off 100 kDa, Millipore).

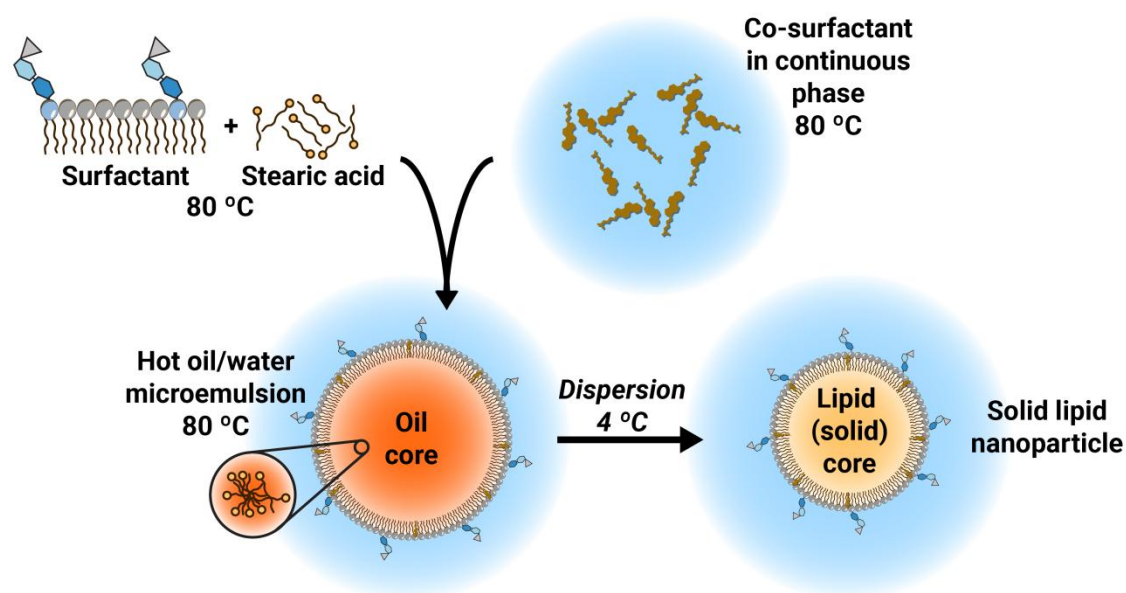


Figure 5.5 – Solid lipid nanoparticles formation by microemulsion method.

SLN with incorporated romidepsin and bryostatin were obtained by mixing the latency reversing agents dissolved in DMSO with the melted lipid mix, before adding the co-surfactant and continuous phase.

5.2.6. Lipid covered PLGA particle preparation

PLGA particles were generated by a nanoprecipitation process. A commercial lactic:glycolic acid mixture (50:50 mol:mol) (LACTEL), was used for the generation of PLGA particles (Hu et al., 2015).

1. 1ml of 10 mg/ml of lactide:glycolide 50:50 dissolved in acetone was added dropwise to 3 ml of water.
2. The mixture was stirred in open air for 1 h and placed in a vacuum for another 3 h, to ensure complete evaporation of the organic solvent.
3. The resulting nanoparticles solution was washed in water three times using Amicon Ultra-15 centrifugal filter units (cut-off 10 kDa, Millipore) and volume adjusted to 3 ml.

PLGA particles with incorporated bryostatin were obtained by mixing the latency reversing agent dissolved in DMSO with the lactide:glycolide 50:50 mixture previous to precipitation in water.

5.2.6.1. Platelet derived membranes

Platelet derived membranes were obtained from platelet rich plasma as follows:

1. Aliquots of $3 \cdot 10^9$ platelets from platelet rich plasma were pelleted at 800 g for 20 min and resuspended in 1.5 ml PBS supplemented with protease inhibitor cocktail tablets (Promega).
2. Aliquots were frozen at -80 °C and thawed at room temperature to create platelet membranes. Platelet membranes were pelleted by centrifugation at 4,000g for 3 min.
3. Platelet membranes were fluorescently marked by mixing them with 1.5 or 9% (mol:mol relative to total lipid in platelet aliquot) of DHPE-Oregon Green 488 dissolved in ethanol, adding a maximum of 1% (vol:vol) of ethanol to the platelet membrane suspension. The mixture was incubated for 120 min at room temperature and shaking.
4. Alternatively, platelet membranes were fluorescently marked by mixing them with fusogenic liposomes containing DHPE-Oregon Green 488. The fusogenic liposomes were composed of DOTAP and DOPE, and were generated by formation of MLVs followed by sonication in a bath sonicator at 39 kHz and 95 W for 15 min to generate mainly unilamellar vesicles (Kleusch et al., 2012). For platelet labeling, DOTAP:DOPE:DHPE-Oregon Green 488 (1:0.5:0.5 mol:mol) fusogenic liposomes containing 3% or 6% (mol:mol relative to total lipid in platelet aliquot) of DHPE-Oregon Green 488 were mixed with platelet membrane aliquots. The mixture was incubated for 15 min at room temperature and shaking.
5. Marked platelet membranes were then washed three times with PBS supplemented with protease inhibitors, and suspended in 1.5 ml of water.
6. The marked platelet membranes were transferred to a glass vial and sonicated in a bath sonicator at 39 kHz and 95W for 15 minutes to generate platelet membrane vesicles.

5.2.6.2. PLGA nanoparticles lipid cloaking

After particle generation, PLGA cores were coated with a lipid bilayer from either synthetic MLVs of the desired composition, or platelet derived membranes by mixing PLGA particles with the desired lipid bilayers, and sonicating (Hu et al., 2015) (Figure 5.6):

1. 10 mg of PLGA particles suspended in water were mixed with MLVs of the desired composition or platelet derived membranes.

2. The PLGA-lipid membranes mixture was sonicated with a bath sonicator at a frequency of 39 kHz and a power of 95W for 2 min. In this sonication process MLVs and platelet derived membranes are disrupted long enough to encapsulate PLGA cores, generating lipid or platelet membrane coated PLGA nanoparticles (L-PLGA or P-PLGA, respectively).
3. The resulting nanoparticles were pelleted by centrifugation to remove excess free MLVs, resuspended in PBS, and used for cell treatment.

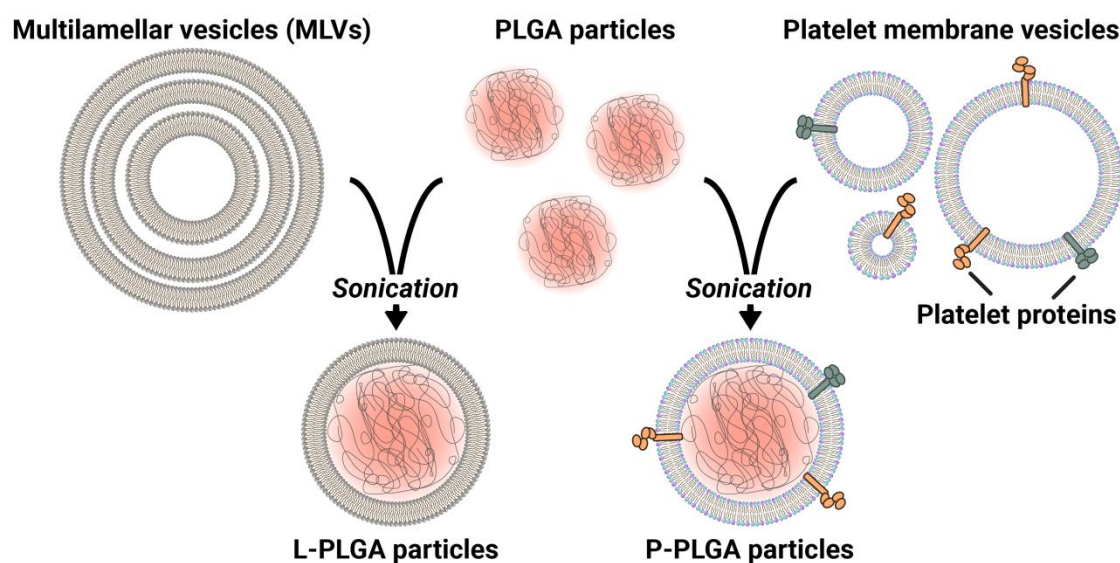


Figure 5.6 – Generation of L-PLGA and P-PLGA particles by cloaking of PLGA cores with lipid membranes.

5.2.7. Nanoparticle capture and latency reactivation quantification

Capture analysis of fluorescently labeled nanoparticles by mature dendritic cells was carried out by FACS. A culture of primary dendritic cells or monocytes was activated with IFN γ (1000 U/ml). Ganglioside/Siglec-1 dependent capture was tested by incubating fluorescently labeled nanoparticles containing, or not containing, gangliosides with activated mDCs or monocytes for 30 min at normal culture conditions. After three repeated washes with PBS, cells were collected and their fluorescence signal was measured by FACS. Nanoparticle capture was expressed either as total fluorescence signal of the measured cell population (All Geometric Mean Fluorescent Intensity or All Geo MFI), or as a percentage of fluorescently positive cells.

For nanoparticles transfer quantification from mDCs to J-lat cells, mDCs were first incubated with fluorescently labeled nanoparticles as above, and then co-cultured with J-

lat cells at 1:1 ratio for 24 h. The co-culture was then collected and the fluorescence signal of the two cell types was measured by FACS. Nanoparticle transfer from mDCs to J-lat cells was expressed either as total fluorescence signal of the measured cell population (All Geometric Mean Fluorescent Intensity or All Geo MFI), or as a percentage of fluorescently positive J-lat cells.

For latency reversing agent screening, J-lat cells cultured in normal culture conditions were incubated with different concentrations of each studied LRA dissolved in DMSO. 24 hours after addition, the percentage of reactivated cells was measured by FACS following the fluorescence of the GFP expressed upon reactivation. For mDCs mediated J-lat reactivation, mDCs previously pulsed with LRA containing nanoparticles were co-cultured with J-lat cells. 24 hours after co-culture, the cells were collected and the J-lat reactivation was quantified by measurement of the GFP signal by FACS.

5.2.8. Flow cytometry

Nanoparticle capture, J-lat reactivation, and platelet derived vesicle labeling were analyzed by flow cytometry in a FACSCalibur Flow Cytometer (BD Biosciences). For nanoparticles capture by mDCs and transfer to J-lat, and J-lat reactivation, a co-culture of mDCs and J-lat cells was loaded into the cytometer. The two cell types were differentiated by comparison of their shape and size characteristics by measuring the FSC and SSC values of the two cell populations, as explained in *Chapter 2*.

Detection of nanoparticles capture by mDCs and transfer to J-lat was carried out by measuring the fluorescent signal of the labeled nanoparticles in the cells. J-lat reactivation was measured by measuring the fluorescent signal of GFP in the cells. Labeling of platelet derived vesicles was carried out by measuring the fluorescent signal of the dye used for labeling (Table 5.1).

Table 5.1 – Excitation laser and emission detectors used in flow cytometry for measurement of different parameters.

Measured parameter	Fluorophore	Excitation laser	Emission detector
Liposome and SLN capture and transfer	PE-Texas Red	488 nm	FL4 Red
Lipid-covered PLGA capture and transfer	Oregon Green 488	488 nm	FL1 Green
	Alexa Fluor 633	635 nm	FL4 Red
J-lat reactivation	GFP	488 nm	FL1 Green
Platelet vesicle labeling	Oregon Green 488	488 nm	FL1 Green

5.2.9. Cytotoxic response quantification

The cytotoxic response of CD8⁺ T cells to the SL9 peptide was measured by quantification of the IFN γ secretion by the cells. For this purpose, a commercial anti-IFN γ enzyme-linked immune absorbent spot (ELISpot) kit was used. ELISpot plates (Milipore) were coated with monoclonal antibody to human IFN γ (1-D1K, Mabtech) overnight at 4 °C. Plates were washed six times with PBS containing 1% FCS. mDCs were pulsed with nanoparticles bearing SL9 peptide for 30 min and co-cultured with CD8⁺ T cells responsive to SL9 for 20 h in normal culture conditions. Following the manufacturers guidelines, plates were revealed with biotinylated anti-human IFN γ , streptavidin-alkaline phosphatase, and its colored substrate (Mabtech). After the revealing step, plates were disinfected by 0.05% Tween 20 (Sigma-Aldrich), washed six times with distilled water, and dried overnight at room temperature. Finally, the frequency of IFN γ secreting cells was quantified under Immuno Capture and Immuno Spot software to calculate the number of Spot Forming Cells (SFC) per well.

5.2.10. Cytokine secretion quantification

Soluble cytokines were measured by Luminex 200 (HSTCMAG-28SK kit, from MILLIPLEX® MAP Human High Sensitivity T cell Magnetic Bead Panel) using xPonent 3.1 software to evaluate collected data.

5.2.11. Confocal microscopy

For detection of nanoparticles localization after capture in myeloid cells, and determination of content release confocal microscopy imaging was used. After incubation of mDCs with nanoparticles and extensive washing, cells were fixed with 4% paraformaldehyde for 2 min and cytospun into glass slides, mounted in DAPI-containing fluorescent media and sealed with nail polish to analyze them in a Nikon TI Eclipse inverted optical microscope equipped with an Ultraview spinning disk setup (PelkinElmer), fitted with a two CCD camera (Hamamatsu).

5.3. Results

5.3.1. Ganglioside-dependent liposome capture

Fluorescent liposomes containing increasing quantities of GM1 or GM3 gangliosides were generated and used to treat activated mDCs and monocytes. In parallel, fluorescent HIV-1 viral like particles (VLPs) were incubated with the cells in the same manner, as a positive control of capture by mDCs and monocytes. Liposome and VLPs capture was measured by FACS (Figure 5.7). Liposomes containing GM1 or GM3 gangliosides specifically targeted mDCs or activated monocytes in a ganglioside-concentration dependent manner. Maximum capture was obtained with a ganglioside concentration of 10% (mol:mol) in the fluorescent POPC liposomes for both GM1 and GM3 gangliosides, comparable to the fluorescent HIV-1 VLPs. At higher concentrations (25% mol:mol), a decrease in liposome capture was observed, probably due to steric hindrance of the bulky sialyllactose head group of the gangliosides. Use of both gangliosides resulted in very similar capture yields by mDCs and monocytes, so for future studies GM1 was selected over GM3, as its bigger head group could potentially act as a hydrophilic coating helping to avoid unwanted liposome aggregation and instability.

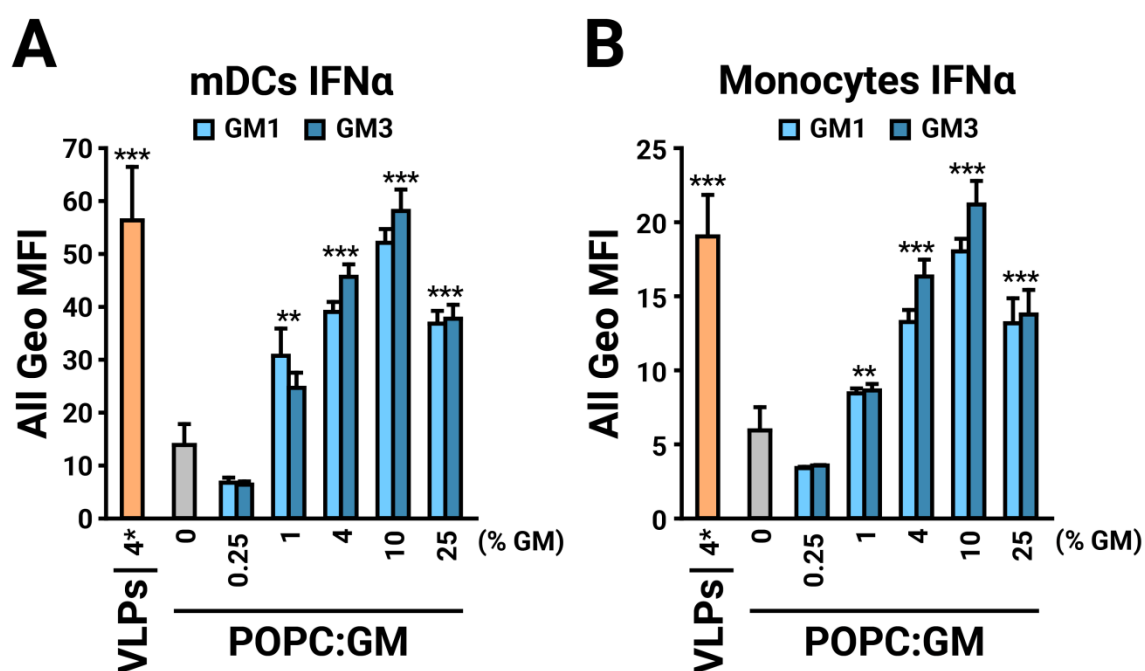


Figure 5.7 – Effect of GM in liposome capture. A| Mature dendritic cells and B| monocytes were activated with IFN α and incubated with fluorescent POPC liposomes containing different quantities of the GM1 or GM3 ganglioside. Liposome capture was measured by flow cytometry. As a control, fluorescent virus like particles were incubated with the cells in the same manner. Bars represent the mean \pm SD of three independent experiments. ** $P \leq 0.01$, *** $P \leq 0.001$ when compared to 0% GM liposomes.

To corroborate that liposome capture was specific of sialyllactose recognition by Siglec-1 expressed in mDCs, POPC:GM1 (1:0.1 mol:mol) fluorescent liposomes were incubated with mDCs and activated monocytes previously incubated with different capture inhibitors. Moreover, Siglec-1-dependent capture, 7D2 and 7-239 α -Siglec-1 antibodies were incubated with the cells at 10 mg/ml prior to liposome addition. To test ganglioside-dependent capture, free sialyllactose was added to the cells at 20 mM. As negative capture inhibition controls, an antibody of the same isotype as 7D2 and 7-239, and lactose, not recognized by Siglec-1, were used (Figure 5.8). Antibodies binding Siglec-1 efficiently inhibit liposome capture by both mDCs and activated monocytes, while an antibody of the same isotope but not recognizing Siglec-1 does not show any inhibition of capture. Addition of free sialyllactose prior to liposome incubation also inhibits capture, an effect not observed for lactose, which is not recognized by Siglec-1. These results confirm that ganglioside-containing liposome capture by mDCs and monocytes is dependent in Siglec-1 expressed in the cell surface and the sialyllactose in the head group of the gangliosides in the liposomes.

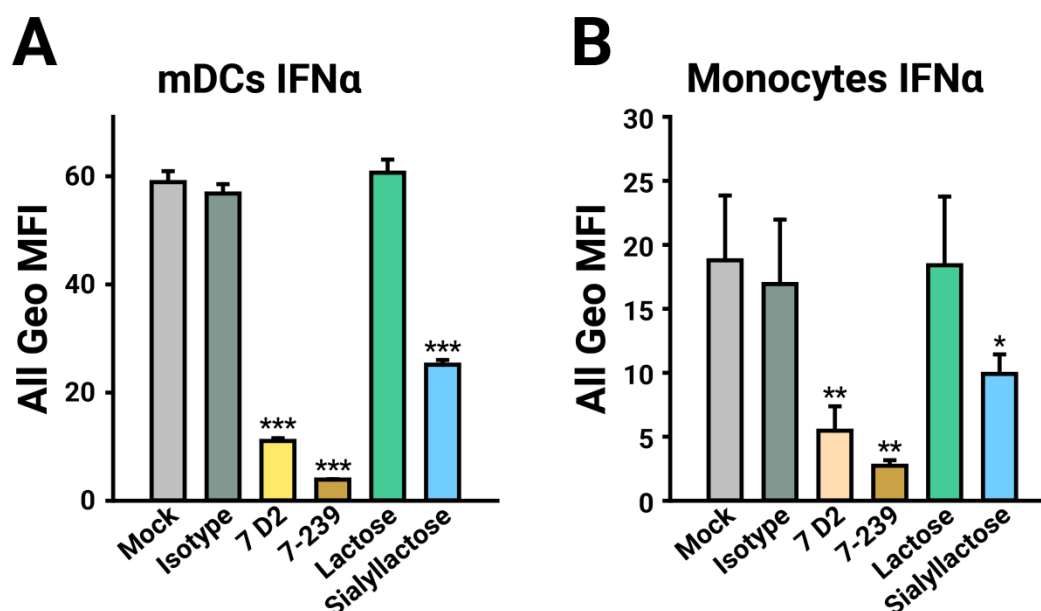


Figure 5.8 – Liposome capture is specific of Siglec-1. **A** Mature dendritic cells and **B** monocytes were treated with IFN α and incubated with different capture inhibitors (10 mg/ml of the α -Siglec-1 7D2 and 7-239 antibodies; 20 mM sialyllactose) and then incubated with 0.2 mM of fluorescent POPC liposomes containing 10% (mol:mol) of the GM1 ganglioside. Liposome capture was measured by flow cytometry. Mock treated cells were used as a control of the inhibition. Bars represent the mean \pm SD of three independent experiments. * $P \leq 0.05$, ** $P \leq 0.01$, *** $P \leq 0.001$ when compared to mock treatment.

5.3.2. Effect of PEG in liposome capture

In order to further decrease possible liposome aggregation, recognition by the immune system, and clearance by the liver in future *in vivo* studies, and to enhance stability, the addition of PEG containing lipids to the liposome was evaluated. Fluorescent POPC liposomes containing 10% GM1 (mol:mol) and increasing quantities

of PEG₂₀₀₀ covalently bound to DSPE were prepared and incubated with mDCs, and liposome capture was studied by FACS (Figure 5.9). As observed, liposome capture was inhibited by the presence of PEG₂₀₀₀ in a dose-dependent manner, possibly due to steric hindrances by the big PEG polymer that hamper the recognition of the smaller ganglioside by Siglec-1. Nevertheless, the relatively low PEG₂₀₀₀ concentration of 1.25% (mol:mol) showed a liposome capture similar to the liposomes devoid of PEG₂₀₀₀ containing lipids, so this concentration was chosen for future experiments.

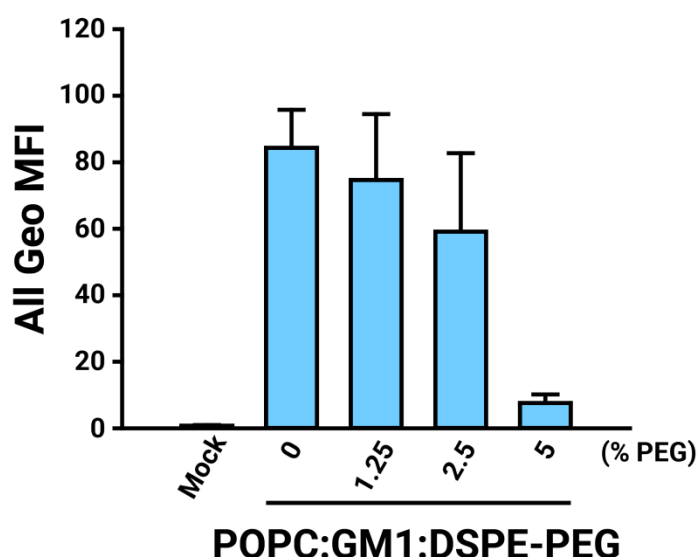


Figure 5.9 – Effect of PEG in liposome capture. Liposome capture in mDCs treated with IFN α and incubated with fluorescent POPC:GM1(10%) containing different quantities of PEG. Liposome capture was measured by flow cytometry. As a control, mock liposomes containing only POPC were incubated with the cells in the same manner. Bars represent the mean \pm SD of three independent experiments.

For *in vitro* stability studies, content leakage assays were carried out with liposomes containing 10% (mol:mol) GM1 and 1.25% (mol:mol) DSPE-PEG₂₀₀₀. For this purpose, ANTS and DPX were encapsulated in the aforementioned liposomes at concentrations in which DPX quenches the fluorescence of ANTS. Upon destabilization of the liposome membrane and leakage of its contents, ANTS and DPX dilute in the medium decreasing the quenching effect. Thus, by following the increase in fluorescent emission of ANTS, content leakage can be quantified. As a destabilizing agent for *in vitro* stability studies FCS was used, present in cell culture media, which contains albumins that commonly generate liposome aggregation and rupture (Ng et al., 2000). The ANTS fluorescent signal of ANTS/DPX containing POPC:GM1:DSPE-PEG₂₀₀₀ (88.75 : 10 : 1.25 mol:mol) liposomes was measured in a fluorimeter, and once the signal was stabilized, the system was considered equilibrated and 0% leakage was assigned to that fluorescent signal. Then, 10% and 50% (vol:vol) FCS was added to the liposomes, and they were incubated at 37 °C and constant mixing for up to 24 hours. Content leakage was measured by following changes in fluorescence intensity at 520 nm (ex = 350 nm) as a function of time. Finally, in order to obtain the 100% content leakage value, 0.1% Triton X-100 was added. For each time point the % of content leakage was calculated (Figure

5.10). After 24 hours of incubation with 50% FCS, the signal reached a plateau of 15% leakage, while the maximum value in the 10% FCS medium, the concentration normally present in cell culture media, was of 5% leakage. Thus, addition of 1.25% of DSPE-PEG₂₀₀₀ to liposomes results in a robust stability in up to 50% serum while preserving the Siglec-1 targeting ability.

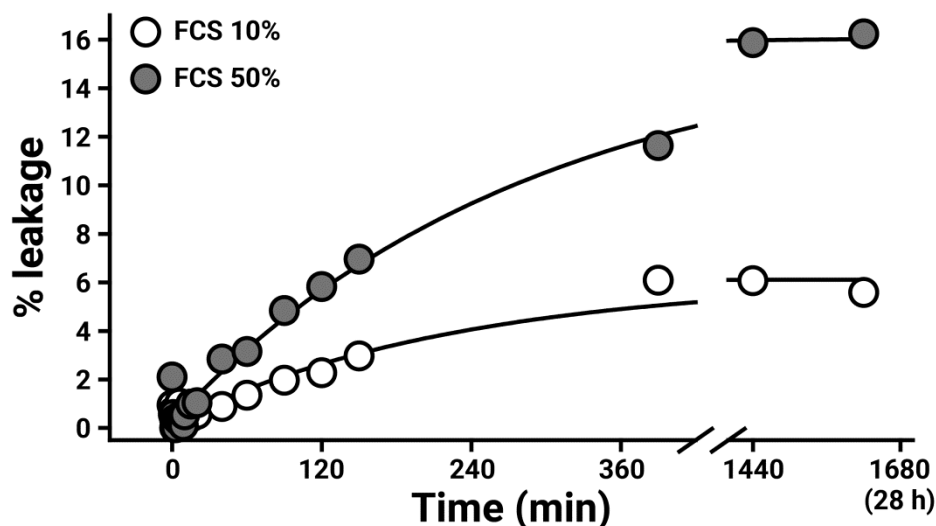


Figure 5.10 - *In vitro* stability assay. POPC:GM1(10%):DSPE-PEG₂₀₀₀(1.25%) liposomes containing encapsulated ANTS/DPX were incubated with 10% (white) or 50% (grey) FCS and their time dependent content leakage was measured with a fluorimeter.

5.3.3. Liposomes for drug delivery

Once the Siglec-1-ganglioside mediated liposome capture was corroborated, their use for CD8+ T cell activation and latency reactivation drug delivery was studied. Firstly, the proof of concept for compound delivery to mDCs via GM1/Siglec-1 was tested by the use of fluorescently labeled dextran molecules encapsulated in liposomes. For this purpose, Dextran-Alexa 488 molecules were encapsulated in fluorescently labeled liposomes with or without GM1, pulsed with mDCs to induce capture, and washed. 24 and 48 hours after incubation, fluorescent signal from the liposome and encapsulated labeled dextran molecules in the mDCs was observed via confocal microscopy (Figure 5.11).

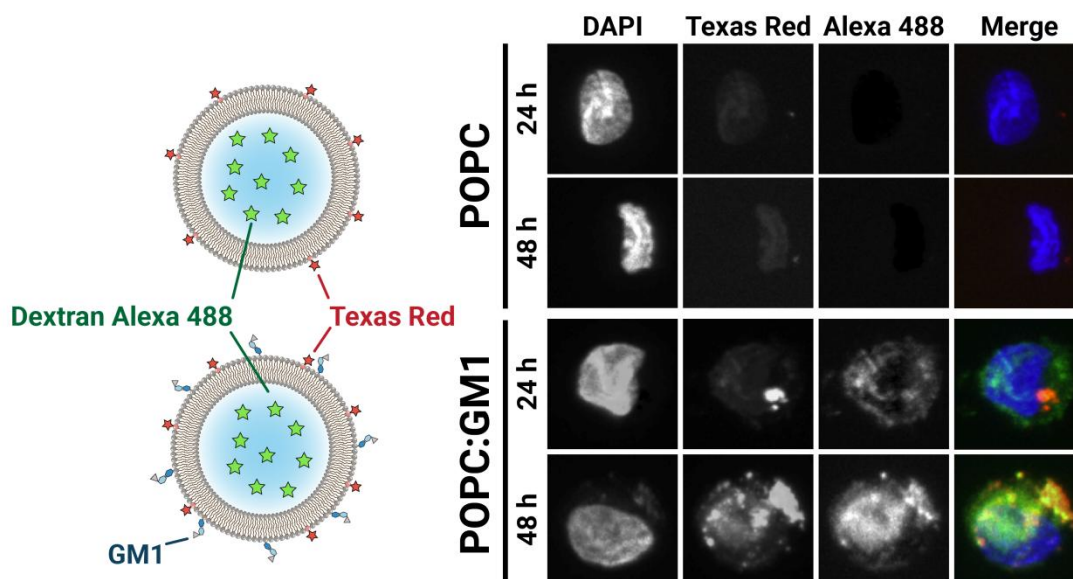


Figure 5.11 – Specific delivery to Siglec-1+ mDCs of loaded green fluorescent dextran molecules. Delivery of the encapsulated fluorescent molecules occurs only when liposomes contain gangliosides. Liposome and fluorescent molecules are retained in mDCs up to 48 h after capture. Images show a representative mature dendritic cell in each of the conditions.

Fluorescent molecules encapsulated into the lumen of liposomes are specifically delivered to the cytoplasm of Siglec-1+ cells only when they contain GM1, and they are retained inside the myeloid cells up to 48 hours after capture. This proof of concept for the delivery of compounds to myeloid cells constitutes the first step for the development of nanocarriers that exploit the GM1/Siglec-1 pathway for the delivery of latency reversing agents and cytotoxic response stimulators.

5.3.3.1. CD8+ T cell activation

To promote the killing of HIV-1 reactivated cells by boosting specific cytotoxic responses, viral SL9 peptides were incorporated into liposomes. GM1 fluorescent liposomes loaded with viral peptides were used to pulse mDCs, which were washed and co-cultured with a SL9 specific CD8+ T cell clone. IFN- γ ELISPOT was used to measure CD8+ T cell responses to peptides delivered to mDCs via liposomes (Figure 5.12, left). Noteworthy, IFN- γ production by CD8+ T cell was specific of SL9 presentation via GM1 liposomes (Figure 5.12, right).

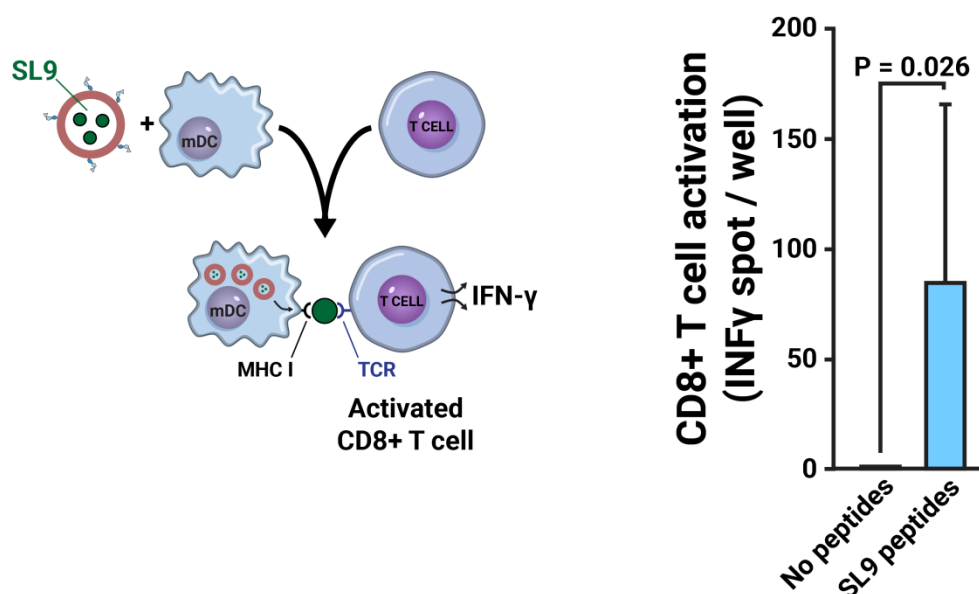


Figure 5.12 – Cytotoxic responses via SL9 viral peptide loaded liposomes on mature dendritic cells. GM1-containing liposomes loaded with viral SL9 peptide were incubated and captured by mDCs. mDCs were co-cultured with SL9-specific CD8+ T cells. Upon SL9 antigen presentation, CD8+ T cell activation was measured by secretion of INF γ via ELISpot. Bars represent the mean \pm SD of three independent experiments.

5.3.3.2. Latency reactivation

Once the Siglec-1-ganglioside mediated liposome capture was corroborated, their use for reactivation drug delivery was studied. Firstly, a screening of the reactivating capacity of several drugs was carried out in J-lat 9.2 cells, GFP-reporter Jurkat-derived HIV-1 latency models. For this purpose, different concentrations of several latency reactivating drugs dissolved in DMSO were added to the cells. 24 hours after addition, the percentage of reactivated cells was measured by FACS following the fluorescence of the GFP expressed upon reactivation (Figure 5.13). The combination of romidepsin and bryostatin at 40 and 12.5 nM respectively achieved a reactivation of more than 50% of the J-lat cells 24 hours after incubation. Interestingly, the reactivation derived from the combination of romidepsin and bryostatin is higher than the sum of the reactivations of each drug separately, which indicates a synergistic effect. For further studies, a combination of both drugs was used for reactivation assays with liposomes.

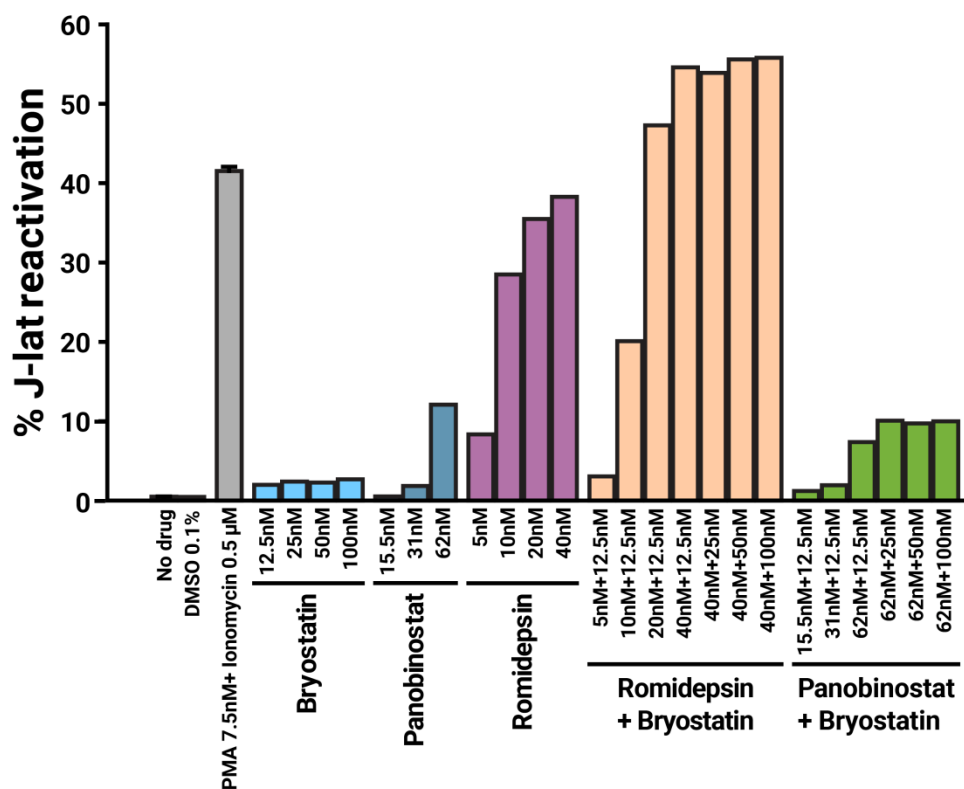


Figure 5.13 – J-lat 9.2 reactivation by several drugs and their combination. J-lat 9.2 cells were pulsed with latency reversing agents at different combinations and concentrations for 30 min, and washed. J-lat reactivation was measured 24 hours after incubation with LRA. Bars represent the mean \pm SD of three independent experiments.

For latency reactivation experiments with liposomes, romidepsin and bryostatin containing fluorescent POPC:GM1:DSPE-PEG₂₀₀₀ (88.75 : 10 : 1.25 mol:mol) were prepared. For this purpose, and taking into account the hydrophobic nature of romidepsin and bryostatin, the drugs were dissolved in DMSO and added in the organic phase of the lipid mixture in the liposome preparation protocol. The lipid and drug mixture was then dried under nitrogen flux and vacuum, and rehydrated with 10 mM HEPES, 150 mM NaCl pH 7.4, subjected to freeze and thaw cycles, and extruded to generate large unilamellar vesicles (LUVs) of 100 nm of diameter. The drugs are expected to partition to some region of the lipid bilayer of the liposome, due to their hydrophobic nature. Liposomes contained 800 nM of romidepsin and 250 nM of bryostatin so that upon addition of liposomes to the cells and consequent dilution to experiment conditions, the reactivator drugs concentrations were 40 nM and 12.5 nM, respectively.

GM1 fluorescent liposomes loaded with romidepsin and bryostatin were used to pulse mDCs, which were then washed and co-cultured with J-lat cells. Capture of liposomes by mDCs, transfer to J-lat cells and reactivation of J-lat target cells were measured by FACS. Drug loaded liposomes were captured by mDCs in a GM1/Siglec-1 dependent manner (Figure 5.14A) and transferred more efficiently to J-lat cells than liposomes

lacking GM1 (Figure 5.14B). Furthermore, J-lat reactivation took place in a liposome-dose dependent manner, and only when liposomes contained reactivation compounds (Figure 5.14C).

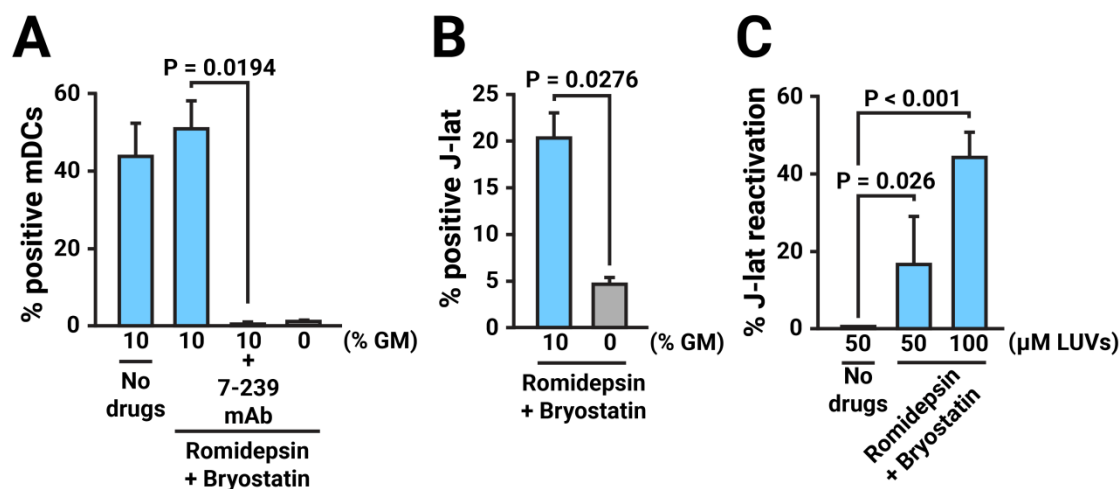


Figure 5.14 – Liposome capture, transfer, and reactivation capacity. **A** LRA loaded fluorescent liposomes were incubated with mDCs for 30 min, and capture was analyzed. mDC treatment with 10 mg/ml of the 7-239 α -Siglec-1 antibody and liposomes lacking GM1 were used to study capture specificity. **B** Liposome-containing mDCs were co-cultured with J-lat cells to study liposome transfer. **C** J-lat reactivation upon transfer of liposomes with or without LRAs was analyzed by expression of GFP. Liposome capture by mDCs and transfer to J-lat was measured by quantification of Texas Red in the liposome bilayer by FACS. J-lat reactivation was measured by quantification of GFP in the cells by FACS. Bars represent the mean \pm SD of three independent experiments.

Once capture of liposomes by mDCs and transfer to J-lat cells was corroborated to be GM1/Siglec-1 specific, and reactivation of J-lat was probed to only be observed when latency reversing agents were loaded into the liposomes, the GM1/Siglec-1 dependency of J-lat reactivation was studied. Fluorescent liposomes loaded with romidepsin and bryostatin were prepared, containing either GM1 or Asialo-GM1. Asialo-GM1 is a ganglioside derived from GM1 lacking the sialyllactose head group that is necessary for recognition of the ganglioside by the Siglec-1. Thus, Asialo-GM1 containing liposomes are not recognized by Siglec-1 and should not be specifically captured by mDCs. These liposomes were used to pulse mDCs, which were then washed and co-cultured with J-lat, after which transfer of liposomes to J-lat and J-lat reactivation were measured by FACS. Although transfer of liposomes from mDCs to J-lat was dependent on GM1 (GM1 vs Asialo-GM1) and Siglec-1 (GM1 vs GM1 + 7293 mAb), and was increased in a liposome-dose dependent manner (Figure 5.15A), a major drawback was observed in the reactivation measurement. Use of Asialo-GM1 liposomes, or blocking of GM1 liposome capture by the α -Siglec-1 7-239 mAb, resulted in J-lat reactivation levels equivalent to those obtained with GM1 liposomes (Figure 5.15B). This signifies that the reactivation of J-lat cells is not specific to capture via the ganglioside/Siglec-1 pathway, as even in the event of minimal unspecific capture of drug-loaded liposome by J-lat cells, high reactivation occurs.

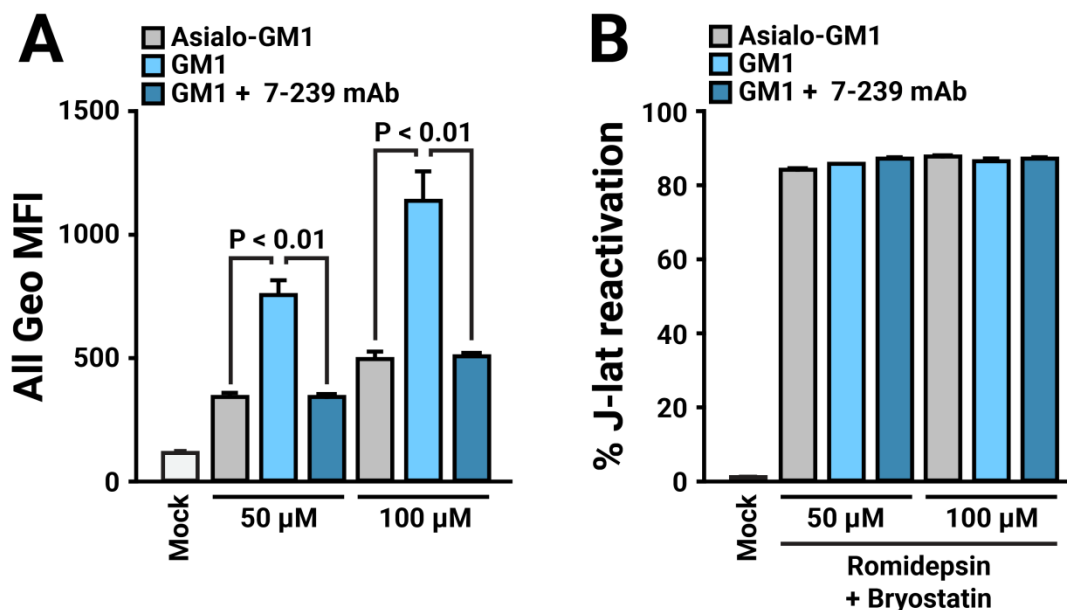


Figure 5.15 – GM1/Siglec-1 dependent liposome transfer and J-lat reactivation. **A** | mDCs were incubated with LRA loaded fluorescent liposomes for 30 min, co-cultured with J-lat cells, and liposome transfer was analyzed by FACS. mDC treatment with 10 mg/ml of the 7-239 α -Siglec-1 antibody and liposomes containing asialo-GM1 instead of GM1 were used to study initial capture and posterior transfer specificity. **B** | J-lat reactivation upon transfer of LRA loaded liposomes was analyzed by expression of GFP. Bars represent the mean \pm SD of three independent experiments.

A possible explanation of the observed results is partial leakage of the drugs. Due to the hydrophobic nature of the compounds packaged in the liposome ($\log P_{romidepsin} = 1.08$; $\log P_{bryostatatin} = 5.04$)³, they are expected to partition into the liposome membrane (instead of being transported in the aqueous lumen of the liposome), which could allow an exchange of the drug with the plasma membrane of the mDCs even if the liposomes are not captured. This capture-independent drug leakage would result in J-lat reactivation independently of liposome capture by the GM1/Siglec-1 pathway. To overcome this drug leakage, a new type of nanocarrier was designed.

5.3.4. Solid lipid nanoparticles for drug delivery

Solid lipid nanoparticles (SLN) are a type of nanocarrier composed of a hydrophobic core composed of lipid molecules in a solid state, covered by a phospholipid monolayer. The main advantage of SLN particles compared to liposomes is that hydrophobic drugs, which are not partitioned into the aqueous lumen of the liposomes, can be incorporated into the hydrophobic core of the SLN in an easier manner (Figure 5.3). By being packaged in the hydrophobic core, which is surrounded by a lipid monolayer, the unspecific drug leakage upon contact of the particle with myeloid cells is expected to be reduced.

³ Calculated via chemicalize.com

To test if these particles were capable of overcoming the unspecific leakage of reactivator drug, fluorescent SLN particles with romidepsin and bryostatin, containing 10% GM1 in the outer lipid monolayer, were prepared. Similarly to the preparation of drug-loaded liposomes, SLN particles contained 800 nM of romidepsin and 250 nM of bryostatin so that upon their addition to the cells and consequent dilution to experiment conditions, the reactivator drug concentrations were 40 nM and 12.5 nM, respectively. As for liposomes, SLN containing Asialo-GM1 instead of GM1 were used as a negative control for capture, as this ganglioside is not recognized by Siglec-1. As an additional control of capture by the GM1/Siglec-1 pathway, the recognition of GM1 by Siglec-1 was blocked by addition of the α -Siglec-1 7-239 mAb. GM1 SLN or Asialo-GM1 SLN particles were used to pulse mDCs, which were then washed, and fluorescent SLN capture was measured by FACS. Fluorescent SLN capture was shown to be dose dependent and GM1 and Siglec-1 specific. Capture only occurred when particles contained the GM1 ganglioside but not the Asialo-GM1 ganglioside, and blocking of the receptor with the α -Siglec-1 7-239 mAb inhibited GM1 containing SLN capture (Figure 5.16).

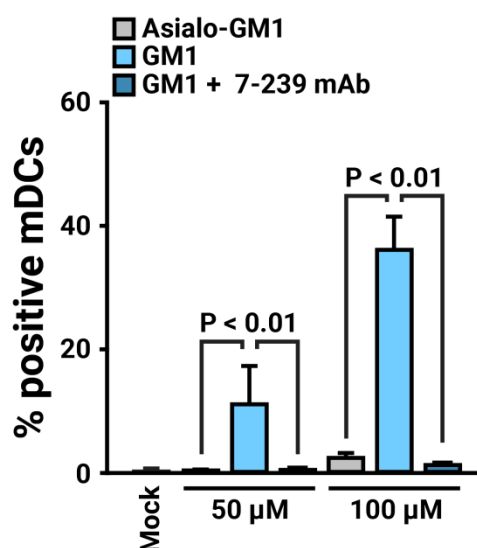


Figure 5.16 – GM1/Siglec-1 dependent SLN capture by mDCs. mDCs were incubated with SLN for 30 min and capture was measured by quantification of Texas Red in the SLN surface by FACS. mDC treatment with 10 mg/ml of the 7-239 α -Siglec-1 antibody and SLN lacking containing asialo-GM1 instead of GM1 were used to study capture specificity. Bars represent the mean \pm SD of three independent experiments.

After corroborating that GM1 containing SLN capture by mDCs was GM1/Siglec-1 pathway specific, the mDCs were co-cultured with J-lat cells, and transfer of SLN to J-lat (Figure 5.17A) and J-lat reactivation (Figure 5.17B) was measured by FACS. Although transfer of SLN from mDCs to J-lat was dependent on GM1 (GM1 vs Asialo-GM1) and Siglec-1 (GM1 vs GM1 + 7293 mAb), and was increased in a SLN-dose dependent manner (Figure 5.17A), similarly to liposomes J-lat reactivation was independent of SLN capture via the GM1/Siglec-1 pathway (Figure 5.17B).

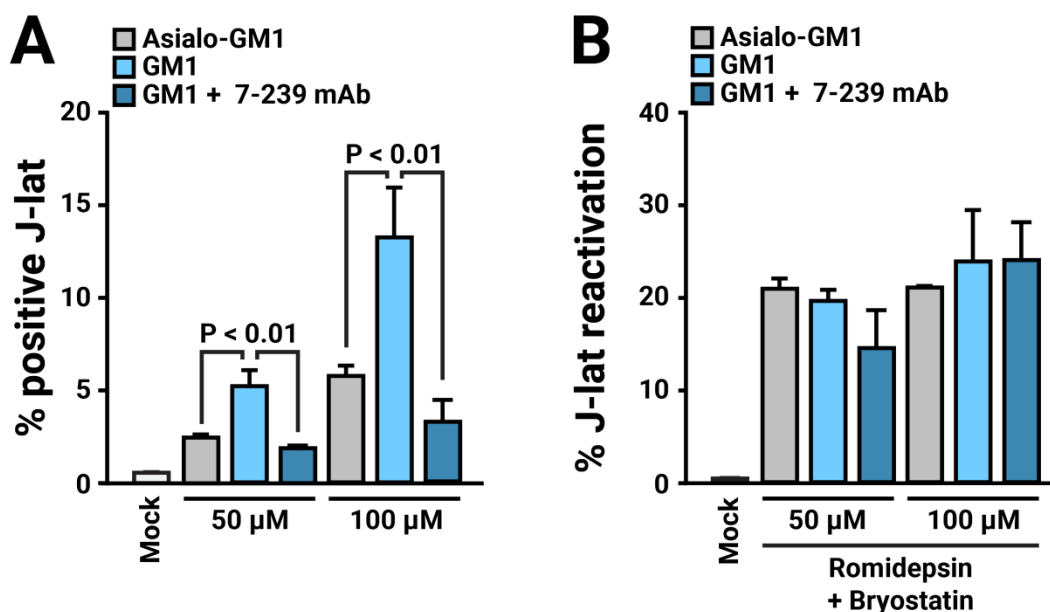


Figure 5.17 – GM1/Siglec-1 dependent SLN capture and J-lat reactivation. **A|** mDCs were incubated with LRA loaded fluorescent SLN for 30 min, co-cultured with J-lat cells, and SLN transfer was analyzed by FACS. mDC treatment with 10 mg/ml of the 7-239 α -Siglec-1 antibody and SLN containing asialo-GM1 instead of GM1 were used to study initial capture and posterior transfer specificity. **B|** J-lat reactivation upon transfer of LRA loaded SLN was analyzed by expression of GFP. Bars represent the mean \pm SD of three independent experiments.

These results seemed to indicate that even with the use of SLN, partial leakage of the drug occurred upon contact with the cells, independently of particle capture.

5.3.5. Bystander reactivation

Capture-independent reactivation had been observed for both liposome and SLN drug carriers. Although an unspecific drug leakage was suspected, the molecular mechanism of this GM1/Siglec-1 independent reactivation had yet to be discerned. The main hypothesis was that capture-independent leakage of the drugs to mDCs could induce activation of the myeloid cells, which would then initiate a GM1/Siglec-1 independent J-lat reactivation possibly by secretion of cytokines, as several cytokines which are secreted by mDCs have been described to induce latency reactivation (Spina et al., 2013; Yang et al., 2009). To test this possibility, mDCs were incubated with free bryostatin and co-cultured with J-lat cells to measure reactivation by a possible GM1/Siglec-1 independent bystander effect. In parallel, J-lat cells were incubated with bryostatin first and then co-cultured with mDCs. Additionally, J-lat cells were incubated by themselves with bryostatin to discard a direct effect of the drug in reactivation at the studied concentrations (Figure 5.18A). The results indicate that bryostatin-conditioned mDCs promote HIV-1 reactivation on co-cultured J-lat cells, while soluble bryostatin added directly to J-lat cells cultured alone has no effects on reactivation (Figure 5.18B). These

results suggest that activation of J-lat cells is not caused by a direct effect of bryostatin in the latently infected cells, but instead is related to the activation of mDCs, which in turn induce by themselves the reactivation of latency in J-lat.

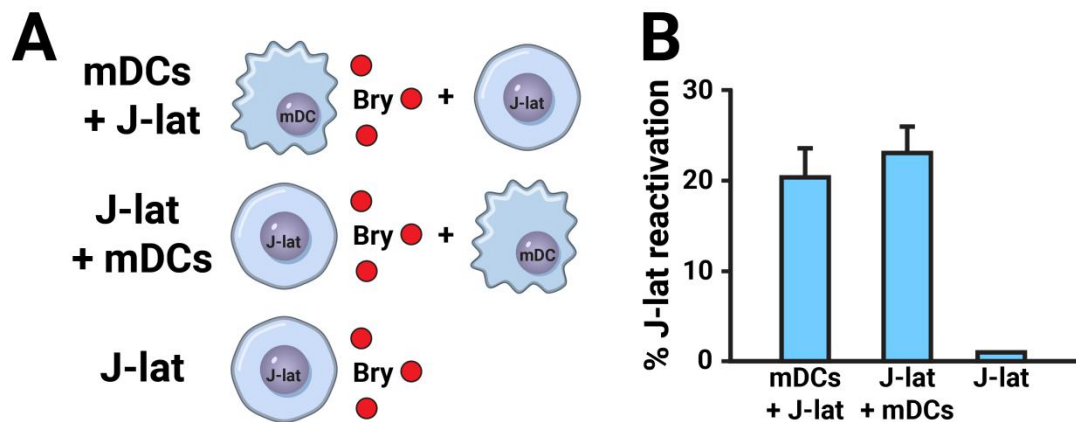


Figure 5.18 – Bystander reactivation effect. **A|** Experiment design. mDCs were incubated with free bryostatin and then co-cultured with J-lat cells (mDCs + J-lat). Alternatively, J-lat cells were incubated with bryostatin first and then co-cultured with mDCs (J-lat + mDCs). As a control, J-lat cells were incubated by themselves with bryostatin (J-lat). **B|** Reactivation of J-lat cells by a bystander effect. Reactivation of J-lat cells was measured after 24 hours of co-culture by FACS. Bars represent the mean \pm SD of three independent experiments.

Next, the molecular mechanism by which mDCs reactivate bystander J-lat cells was studied. For this purpose, mDCs were pulsed with free bryostatin at concentrations were minimal reactivation on J-lats was observed in the screening experiments (Figure 5.13), and tested for secretion of several cytokines of interest: IFN γ , IL-1b, IL-2, IL-6, IL-10, IL-12 and TNF α . Of those, only IL-6 and TNF α were detected, while the concentration of the rest of cytokines was too low for its detection, and thus are not represented in the graph (Figure 5.19A and B). When the effect of the addition of this cytokines to a J-lat culture was studied at different concentrations, only TNF α was shown to induce J-lat reactivation at the studied concentrations (Figure 5.19C). Seemingly, incubation of bryostatin-loaded liposomes and SLN with mDCs induces a secretion of TNF α even in the event of minimal capture of vesicles by the dendritic cells, which in turn, is capable of reactivating bystander J-lat cells.

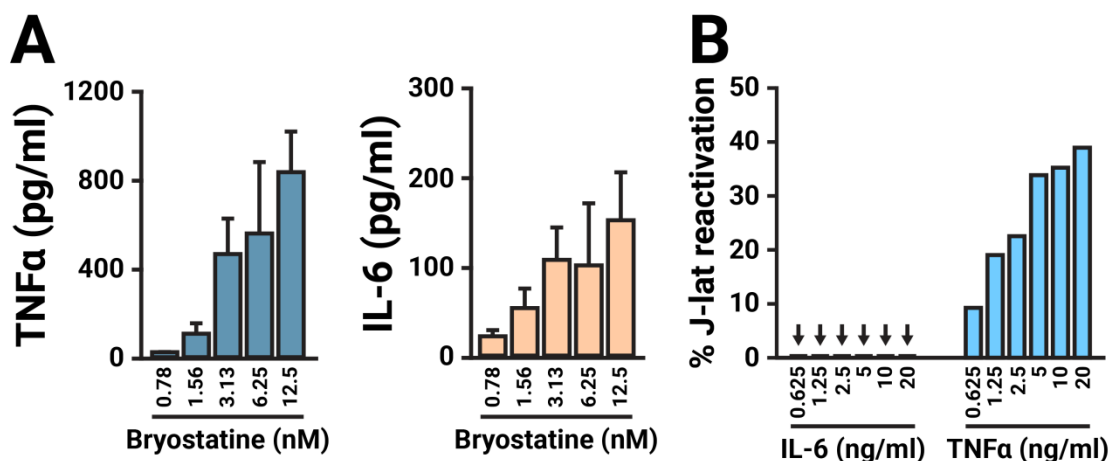


Figure 5.19 – Bryostatine induced cytokine production by mDCs and their effect in reactivation. **A** | mDCs were incubated with 12.5 mM of free bryostatin for 30 min and production of cytokines was quantified by ELISA. **B** | J-lat cells were incubated for with different concentrations of cytokines secreted by mDCs after bryostatin incubation, and J-lat reactivation was measured by GFP expression by FACS. Bars represent the mean \pm SD of three independent experiments.

Interestingly, this unexpected bystander effect provides a new approach for reactivation of latently infected cells. The original approach required the capture of drug-loaded nanoparticles by the mDCs, their retention in the myeloid cell, and finally the posterior transfer to latently infected T cells where they could act accordingly and induce the reactivation of latency. This newly discovered bystander effect could significantly simplify the drug delivery pathway and reactivation mechanism, thus holding tremendous therapeutic potential, and deserves further investigation and rational development.

Thus, a new approach was designed and tested, based on the delivery of bryostatin to mature dendritic cells in order to induce secretion of TNF α by the mDCs which, in turn, would reactivate the latently infected T cells. To adequately target the drug-loaded nanocarriers to mDCs, the GM1/Siglec-1 capture pathway will again be exploited. In the results observed up to this point, although mDCs specifically captured only liposomes and SLN containing GM1, reactivation occurred even in the event of minimal unspecific capture, probably derived from an undesired leakage of the bryostatin upon contact of the nanocarrier with the myeloid cell. This derived in unspecific reactivation of J-lat cells independent of nanocarrier capture. To overcome undesired leakage and successfully achieve the goals of this approach, a new nanoparticle system was designed and developed: a particle containing a hydrophobic core suitable for hydrophobic compound packaging that can be covered with a ganglioside-enriched lipid bilayer.

5.3.6. Lipid covered PLGA nanocarriers for drug delivery

The newly designed nanoparticle system is based in bryostatin loaded into a hydrophobic core composed of a poly(lactic-co-glycolic) (PLGA) polymer, coated with a lipid bilayer enriched in gangliosides to ensure specific capture by Siglec-1⁺ mDCs. This new nanocarrier system provides a clear advantage over the previous liposome-based system: the latency reversing agent is encapsulated in the hydrophobic core during the generation of the PLGA polymer. The drug-loaded PLGA cores are then repeatedly washed to eliminate any free drug, and covered with ganglioside-enriched lipid bilayers. By separating the drug-loading of the hydrophobic core from the lipid covering process, partition of the hydrophobic drug into the lipid bilayer is minimized, thus avoiding unspecific leakage of the drug from the particle to the mDCs upon contact. Only when the nanoparticles are specifically captured by mDCs and accumulated in the dendritic cells for a longer period of time, would the hydrophobic drug be released from the nanoparticles and induce bystander reactivation of latently infected T cell via the secretion of TNF α by mDCs.

This new nanoparticles system was designed with rapid translation into phase I clinical trials in mind, if safety and efficacy tests support the use of this technology. For this purpose, covering of the PLGA cores with clinically approved platelet-derived membranes were designed as the end goal of this approach, as they have shown superior therapeutic efficacy *in vivo* (Hu et al., 2015) and are enriched in several key sialylated gangliosides also present in the membrane of HIV-1, such as GM3 (Ferroni et al., 1997), known to specifically interact with Siglec-1 (Izquierdo-Useros et al., 2012a; Puryear et al., 2013).

Prior to use of platelet-derived membranes for PLGA covering, membranes synthesized *in vitro* using gangliosides obtained from bovine brain were used, as a proof of concept of the covering of PLGA cores with lipid bilayers, and their ganglioside/Siglec-1 specific delivery to mDCs. PLGA covering is based in the mixture of PLGA hydrophobic cores and lipid membranes and consequent sonication to induce lipid membrane rupture and PLGA encapsulation. In this first approach, lipid membranes composed of POPC and GM1 in the form of multilamellar vesicles (MLVs) were used. To easily measure PLGA covering, a double fluorescent labeling was carried out: POPC MLVs labeled with DSPE-Oregon Green 488 were used to cover Alexa Fluor 633-labeled PLGA hydrophobic cores.

To corroborate the GM1/Siglec-1 dependent capture, PLGA particles containing or not bryostatin were covered with lipid membranes with (L(GM1)-PLGA) or without (L-PLGA) gangliosides. Lipid covered PLGA particles showed a double-positive fluorescent signal from the Alexa Fluor 633 in the hydrophobic PLGA core and Oregon Green 488 in the lipid covering (AF633⁺ / OG488⁺, orange), while Alexa Fluor 633-only positive particles correspond to naked PLGA cores (AF633⁺ / OG488⁻, red), and Oregon Green 488-only positive particles correspond to empty lipid vesicles (AF633⁻ / OG488⁺, green) (Figure 5.20A).

After PLGA-vesicle mixture at adequate ratios and posterior sonication resulting nanoparticles were centrifuged to remove excess free lipid vesicles, washed, and incubated with either mDCs (Figure 5.20B), or mDCs previously treated with the α -Siglec-1 7-239 mAb as explained before (Figure 5.20C). In both cases, as additional positive control of capture fluorescently labeled VLPs and MLVs containing GM1 were used. Bryostatin containing PLGA cores not covered with lipids (PLGA-Bry) were also used to test unspecific PLGA core capture. After nanoparticle capture, the fluorescence signal of the cells was measured by FACS.

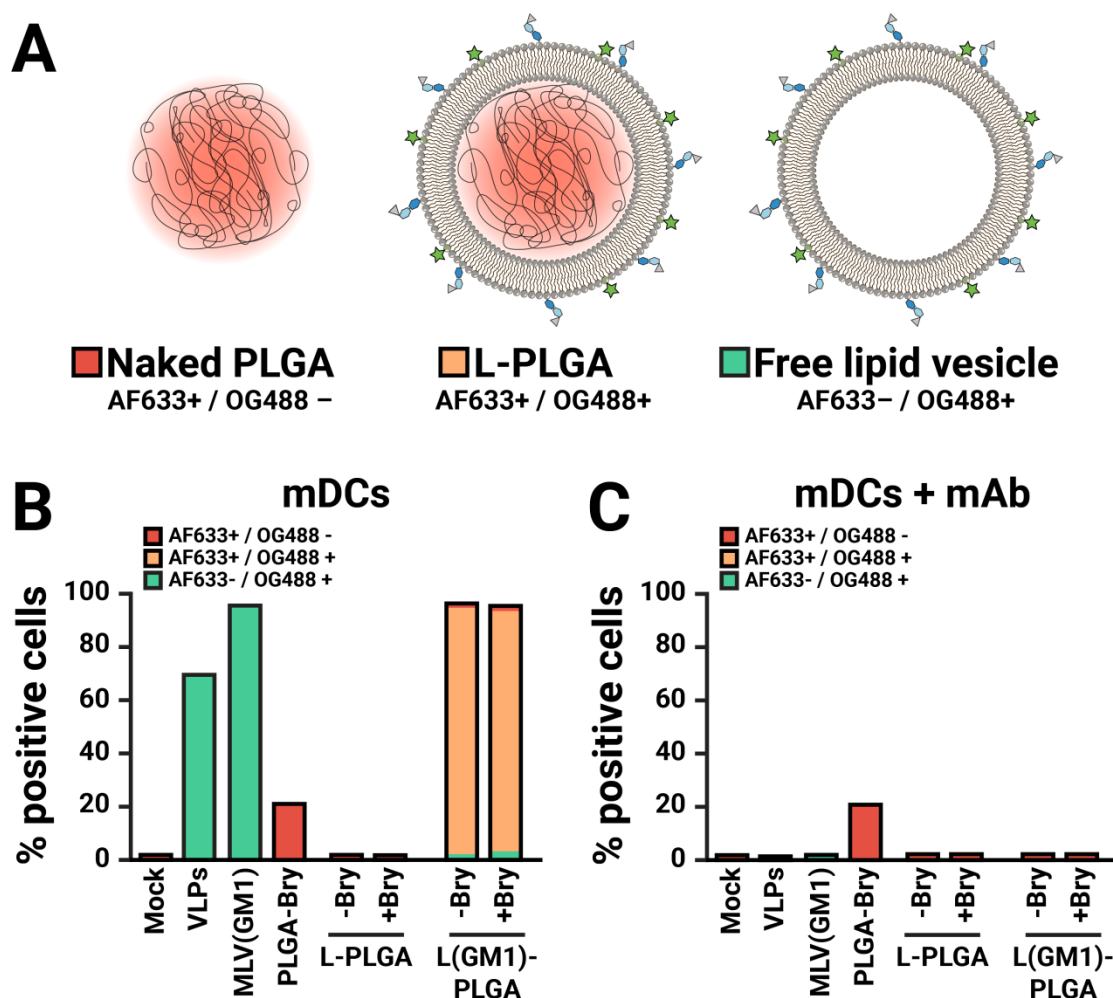


Figure 5.20 – Lipid covered PLGA nanoparticles capture by mDC cells. **A** Three particle populations may exist after PLGA covering with lipid vesicles, differentiable by their fluorescence signals. **B** Siglec-1 expressing mDCs and **C** mDCs previously treated with 10 mg/ml of α -Siglec-1 7-239 mAb were incubated with double-labeled nanoparticles. As a negative control mock treated cells were used. As a positive capture control, labeled VLPs and MLVs containing GM1 were incubated with the cells. Nanoparticle capture was measured by FACS. Bars represent the mean \pm SD of experiments with mDCs from two different donors.

The nanoparticle capture results in Figure 5.20 demonstrate that lipid-covered PLGA particles are specifically captured via Siglec-1 only when GM1 ganglioside is present in the lipid cover. Double-positive PLGA particles covered with GM1-containing lipid vesicles are readily incorporated by \sim 90% of the Siglec-1 expressing mDCs (Figure

5.20B), while minimal unspecific incorporation is observed in mDCs treated with an α -Siglec-1 mAb (Figure 5.20C). Although double-positive mDC cells could, admittedly, result from independent capture of free AF633+ PLGA cores and OG488+ naked lipid vesicles, the absence of free AF633+ PLGA core capture by Siglec-1-blocked mDCs (Figure 5.20C) rules out this possibility. Additionally, the presence of bryostatin in the PLGA cores did not have an effect in specific nanoparticles capture by mDCs.

After demonstrating specific capture of PLGA cores coated with ganglioside-containing lipid vesicles, their ability to induce secretion of TNF α by mDCs was tested. For this purpose, the same nanoparticles as above were incubated with mDCs for 2 h, after which cells were washed and incubated for an additional 18 h to allow cytokine secretion as stated in the experimental techniques section. Then, mDC secreted TNF α concentration in the medium was measured (Figure 5.21). A considerable increase was observed in TNF α secretion by mDCs with bryostatin-loaded nanoparticles containing GM1 (L(GM1)-PLGA) when compared to naked nanoparticles (PLGA-Bry) or nanoparticles coated with vesicles lacking GM1 (L-PLGA). This demonstrates that specific nanoparticles capture via GM1/Siglec-1 favours secretion of TNF α by mDCs, conferring to this delivery system the desired specificity.

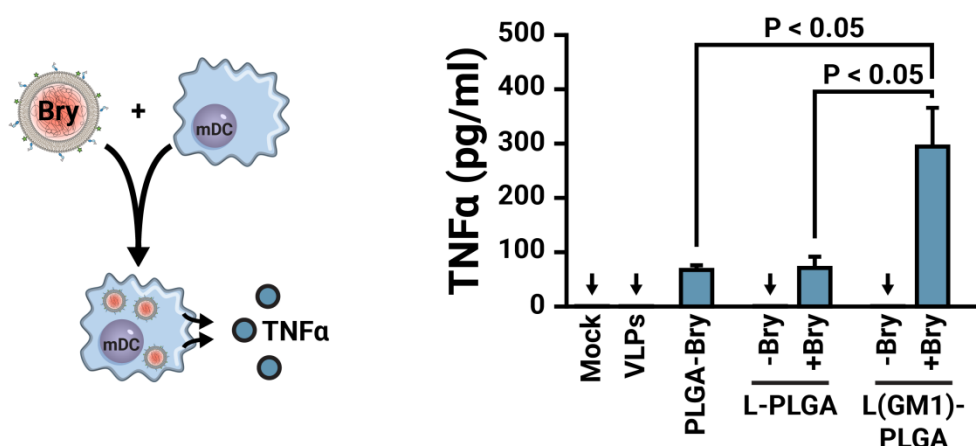


Figure 5.21 – TNF α secretion by mDCs after incubation with bryostatin loaded L-PLGA nanoparticles. PLGA cores loaded or not with bryostatin were coated with lipid vesicles with or without GM1 and incubated with mDCs for 2h, and cells were washed. 18h after incubation TNF α secretion by mDCs was measured by ELISA. Bars represent the mean \pm SD of experiments with mDCs from two different donors.

Next, PLGA nanoparticles were covered with membranes derived from platelets. Prior to PLGA cloaking, platelet derived membranes were labeled with DHPE-Oregon Green 488 for their fluorescence detection. For this purpose, two alternative labeling approaches were used: in one hand, DHPE-Oregon Green 488 was dissolved in ethanol and incubated with platelet membranes. Two concentrations of DHPE-Oregon Green 488 were used: 1.5% or 9% (mol:mol) in relation to the total lipid content of the platelet membrane aliquot, added in ethanol at a final ethanol concentration of 1% (v/v). On the other hand, fusogenic liposomes composed of DOTAP:DOPE:DHPE-Oregon Green 488 (1:0.5:0.5 mol:mol) were prepared at two different concentrations of DHPE-Oregon Green

488, 3% and 6% (mol:mol) in relation to the total lipid content of the platelet membrane aliquot. After labeling, platelet membranes were washed three times with PBS and their fluorescent labeling was measured by FACS (Figure 5.22).

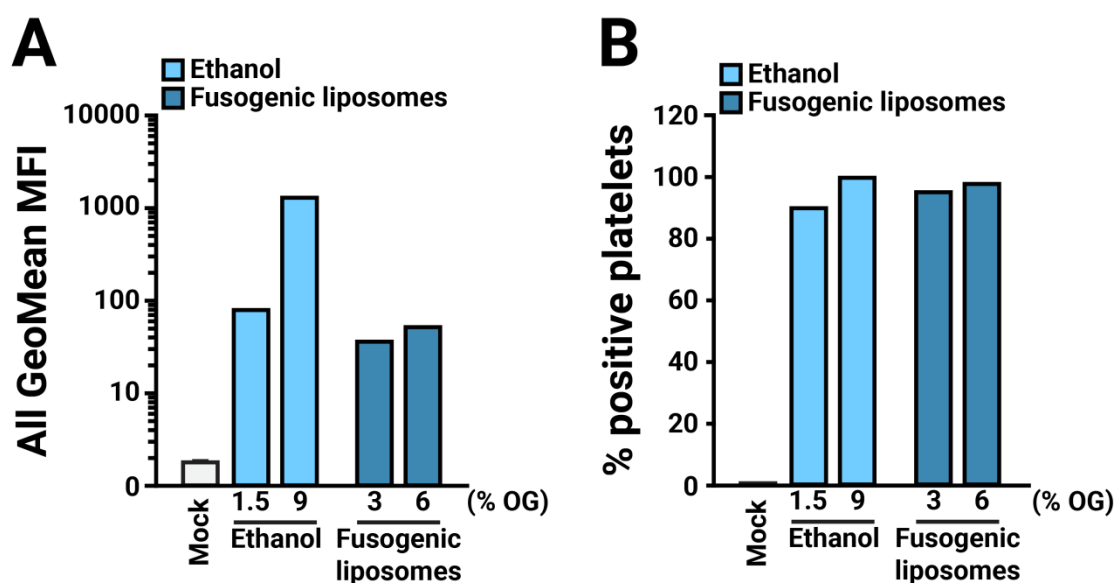


Figure 5.22 – Platelet membrane labeling with DHPE-Oregon Green 488. **A|** Platelets were labeled by incubation with fluorescent dye dissolved in ethanol or integrated in fusogenic liposomes. Platelet labeling was quantified by FACS. 100,000 platelets were measured in each condition. Mock treated platelets were used as a control. Geometric mean fluorescence intensity data is represented logarithmically. **B|** Percentage of platelets positive for Oregon Green 488 fluorescence. 100,000 platelets were measured in each condition. Mock treated platelets were used as a control. Positive fluorescence was established as samples with a higher fluorescent signal than mock treated platelets.

All of the conditions tested resulted in a similar percentage of positively labeled platelets (Figure 5.22B), but labeling by dissolving 9% (mol:mol relative to total lipid content of platelets) DHPE-Oregon Green 488 in ethanol rendered the highest fluorescent signal of all of the samples 10-fold to 100-fold higher than for the rest of conditions (Figure 5.22A).

Subsequently, PLGA core coating with labeled platelet derived vesicles was tested by mixing of the two components and sonication. After purification of the platelet derived vesicles coated PLGA (P-PLGA) particles by centrifugation, coating efficiency was studied by transmission electron cryomicroscopy (CryoTEM) (Figure 5.23).

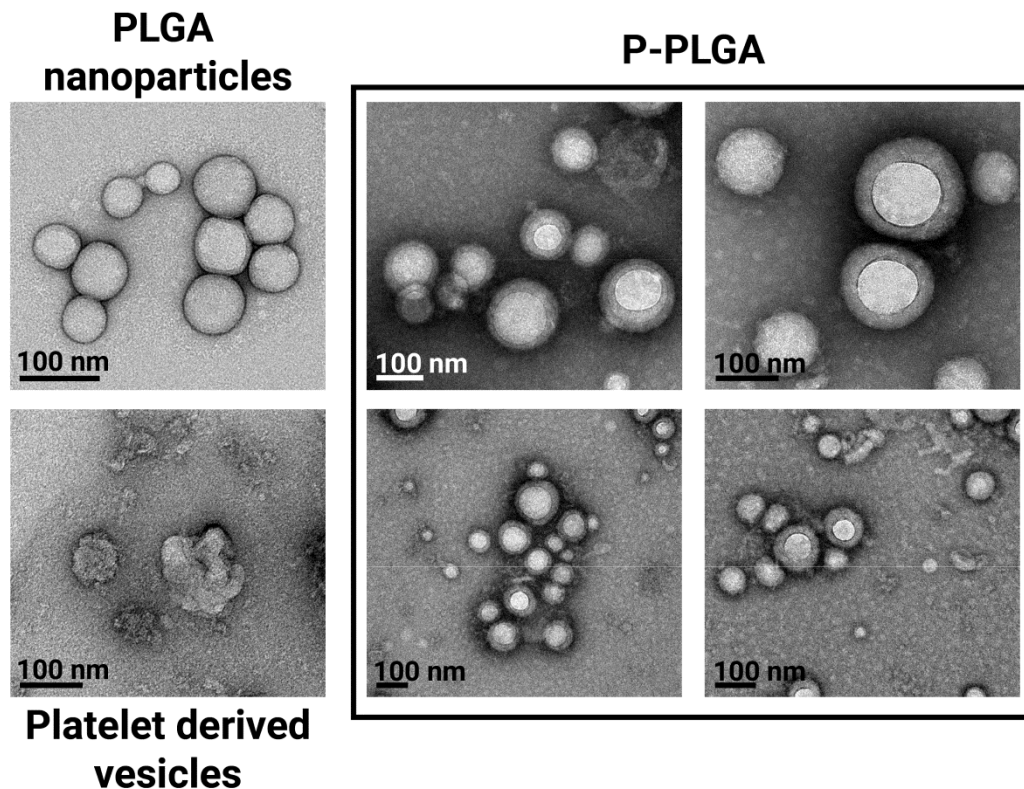


Figure 5.23 – CryoTEM images of PLGA coated with platelet derived vesicles. PLGA nanoparticles (upper left), platelet derived vesicles (lower left), and PLGA cores coated with platelet derived vesicles (right) were imaged with transmission electron cryomicroscopy.

These TEM images clearly show that PLGA cores are readily coated with platelet derived vesicles after sonication. These results open the door for the development of lipid coated PLGA nanoparticles for LRA delivery with the added advantage of allowing the use of platelets derived from the same patient in *in vivo* experiments or treatments, considerably increasing biocompatibility.

5.4. Discussion

Current antiretroviral therapy is capable of suppressing HIV-1 in the blood of the infected patient to undetectable levels. Nevertheless, if antiretroviral therapy is interrupted, in as early as two weeks a viral rebound occurs and virus replication and spread initiates again. This phenomenon is the result of the generation of viral reservoirs in very early stages of patient infection by HIV-1.

During the HIV-1 replication cycle, the virus integrates its genetic material into the host cell. This genetic material may lay dormant for long periods of time establishing a non-productive infection of cells, a process regulated by mechanisms not yet completely understood (Siliciano et al., 2003). These cells are called “latently infected cells”, and are scattered throughout the body in different anatomical sites, constituting a wide variety of viral reservoirs or sanctuaries (Vanhamel et al., 2019). When a patient infected by HIV-1 is administered the highly effective combinatory anti-retroviral therapy known as HAART, replication of new viral particles is inhibited in most of the cases, and infection of new cells and consequent viral spread and development of AIDS gets hampered. Nevertheless, HAART does not target the non-productively infected cells and thus it is incapable of purging viral reservoirs. Until a prophylactic vaccine against HIV-1 is developed which avoids any initial infection by the virus, the establishment of viral reservoirs very early on the infection phase constitutes one of the main milestones in the development of an HIV-1 cure.

Most of the current therapeutical approaches designed to purge viral reservoirs are based in a strategy known as “shock and kill” (Archin et al., 2012). This strategy is based in the delivery of latency reversing agents (LRAs) to latently infected cells, to induce expression of viral proteins and production of new viral particles. The cytopathic effect derived from production of high amounts of HIV-1 is expected to kill the latently infected cell, purging the viral reservoirs. As a supplementary aid, the administration of LRAs can be complemented with viral peptides designed to boost the immune system for the specific killing of reactivated cells newly presenting those antigens. Several studies have developed therapeutical approaches based in the “shock and kill” strategy, but up until now some optimization is needed (Thorlund et al., 2017). Additionally, one of the main handicaps of the *in vivo* application of the “shock and kill” therapy is the delivery of LRAs to viral reservoirs spread throughout the body in a wide variety of anatomical sites.

The work presented in this thesis demonstrates a new approach for the delivery of LRAs to latently infected cells, looking to overcome the difficulties of targeting several cell types accumulated in different tissues or organs, which includes viral reservoirs separated from the bloodstream by the hematoencephalic barrier. The approach followed in this work is based in the HIV-1 *trans*-infection that the virus naturally follows in the organism.

The *trans*-infection pathway is primarily mediated by mature dendritic cells (mDCs), one of the most important types of antigen-presenting cells in the organism. The Siglec-1

receptor on the surface of mDCs (Izquierdo-Useros et al., 2012b) recognizes sialyllactose-containing gangliosides in the viral lipid envelope (Izquierdo-Useros et al., 2012a), resulting in HIV-1 capture by mDCs and accumulation in a sac-like compartment. During their normal antigen-presenting function, HIV-1 loaded mDCs interact with susceptible CD4+ T cells, moment in which the viral particles are released from the mDCs and productively infect the T cells (Izquierdo-Useros et al., 2014). This virus accumulation in mDCs mediated by recognition of gangliosides in the viral lipid by the Siglec-1 receptor offers the unique opportunity to accelerate HIV-1 eradication by glycoengineering nanoparticles that mimic HIV-1 membranes and also target Siglec-1 expressing activated myeloid cells. This way, mDCs could be used as “Trojan horses” for the delivery of LRA or immune-boosting peptide loaded nanoparticles to key anatomical sites where latently infected cells reside, helping increase specific targeting of the nanoparticles and considerably increasing their bioavailability by avoiding clearance by the liver or spleen.

Firstly, LRAs delivery to latently infected cells by the mDC mediated ganglioside/Siglec-1 pathway was tested using liposomes. Liposomes are composed of a lipid monolayer composed in this case of phospholipids, and contain an aqueous interior lumen. The first step was to corroborate the ganglioside-dependent capture of liposomes by mDCs expressing Siglec-1. Liposomes containing gangliosides with a sialyllactose group (GM1 and GM3 gangliosides) were captured by mDCs in a ganglioside dose-dependent manner (Figure 5.7A). Presence of 10% (mol:mol) of ganglioside in the liposome resulted in particle capture equivalent to fluorescently labeled viral-like particles (VLPs), demonstrating that capture levels equivalent to HIV-1 can be obtained by addition of gangliosides to liposomes. Interestingly, activated monocytes also captured liposomes in a ganglioside-dependent manner (Figure 5.7B). Although monocytes do not seem to be the primary force involved in the *trans*-infection pathway *in vivo* (Geijtenbeek et al., 2000; Izquierdo-Useros et al., 2014), Siglec-1 is also expressed in this cell types (van der Kuyl et al., 2007; Rempel et al., 2008), entailing that monocytes could also participate in the delivery of LRA-loaded liposomes to viral reservoirs. Additionally, the targeting of ganglioside-containing liposomes to activated monocytes demonstrated in this work opens a door to the development of new therapies looking to treat the wide variety of diseases involving monocytes. Capture of ganglioside containing liposomes was also confirmed to be specific of sialyllactose and Siglec-1 (Figure 5.8). Because capture of GM1 and GM3 containing liposomes was quantitatively equivalent, GM1 was selected over GM3 as its bigger hydrophilic head group has been described to confer certain stabilizing properties to the nanoparticles (Taira et al., 2004). Additionally, for following experiments 10% (mol:mol) ganglioside quantity was selected, as it presented the highest capture by both mDCs and monocytes.

Use of liposomes for *in vivo* treatment of diseases presents several handicaps regarding their stability and bioavailability. Albumins in the blood commonly induce liposome aggregation and rupture, and their bioavailability is significantly reduced by their clearance from the organism by the liver or the spleen. The hydrophilic head group of gangliosides has been described to confer some stabilizing properties to the liposomes and GM1 in particular has been found to increase liposome circulation half-

life (Taira et al., 2004). To additionally increase liposome stability in drug delivery assays polyethylene glycol was added to the particles, in the form of DHPE-PEG₂₀₀₀. The PEG molecule generates a hydrophilic barrier surrounding the liposome which significantly increases its stability and bioavailability upon administration *in vivo* (Liu et al., 2011; Torchilin, 2005), and reduce unspecific internalization of nanoparticles (Arana et al., 2019). Prior to stability studies, the effect of addition of PEG-containing phospholipids to ganglioside-dependent liposome capture was tested, as the big polymeric PEG molecule in DHPE-PEG₂₀₀₀ could hamper ganglioside recognition by Siglec-1. As expected, increasing amounts of DHPE-PEG₂₀₀₀ in GM1-containing liposomes resulted in a dose-dependent inhibition of capture by mDCs (Figure 5.9), probably due to steric hindrances from the big PEG polymer. Nevertheless, the presence of 1.25% (mol:mol) of PEG in the liposomes resulted in only an anecdotal decrease in capture, and small concentrations of PEG have been described to be enough for exertion of the stabilizing properties (Liu et al., 2011; Torchilin, 2005). For this reason, liposomes with 1.25% (mol:mol) of DHPE-PEG₂₀₀₀ were prepared and their stability *in vitro* was tested with a ANTS/DPX leakage assay. As a destabilizing agent fetal calf serum (FCS) at two different concentrations, 10% and 50% (vol:vol), was used. Liposomes containing 1.25% (mol:mol) PEG suffered a maximum content leakage of 15% after 24 hours of incubation with 50% serum, and only a 6% of leakage when incubated with 10% serum. These results indicate that addition of DHPE-PEG₂₀₀₀ to liposomes results in sustained stability in up to 50% serum while maintaining the Siglec-1 targeting ability.

The *in vivo* delivery of drugs to viral reservoirs mediated by mDCs proposed in this work requires capture and accumulation of nanocarriers by the myeloid cells and their posterior transport to key anatomical sites. Thus, nanoparticles must remain accumulated inside the mDCs for some period of time before they can be transferred to latently infected cells and exert their function. As a proof of concept, liposomes loaded with fluorescently labeled dextran molecules were incubated with mDCs to test their retaining over time, and they were found to be accumulated inside the mDCs up to 48 hours after incubation (Figure 5.11). This result fulfills one of the milestones for the development of an efficient mDC-mediated delivery system of drug loaded nanoparticles to viral reservoirs.

The purge of viral reservoirs likely necessitates prior boosting of the immune system to promote specific responses against HIV-1-peptide expressing CD4+ T cells, to ensure a complete purge of latently infected cells if the cytopathic effects of HIV-1 reactivation do not prove to be sufficient (Shan et al., 2012). Interestingly, immune boosting with targeted liposomes has already proven efficacy (Kawasaki et al., 2013), and although this study delivered lipid antigens, it constitutes a solid proof-of-concept for the use of nanoparticles to induce antigen presentation and immune activation. In this thesis, immune boosting of CD8+ T cells with liposomes was tested by loading HIV-1 derived SL9 peptides into the ganglioside-containing particles. The liposomes were incubated with mDCs to induce Siglec-1 dependent capture and, after extensive washing, myeloid cells were co-cultured with CD8+ T cells specific for the SL9 peptide (Figure 5.12). Delivery of SL9 peptide to mDCs resulted in specific cytotoxic responses from CD8+ T cells (measured as secretion of IFN γ), demonstrating that antigen presentation and

immune boosting can be induced by delivery of HIV-1 derived peptides via the ganglioside/Siglec-1 pathway. This result fulfills another of the preliminary milestones necessary for the development of a therapeutic purge of HIV-1.

The main strategy behind the “shock and kill” approach relies on the reactivation of latently infected cells. Several latency reversal agents have been described throughout the years, including cytokines such as interleukin 2 (IL-2) (Lafeuillade et al., 2001; Prins et al., 1999), Protein Kinase C agonists such as prostatin (Korin et al., 2002; Kulkosky et al., 2001) and bryostatins (Mehla et al., 2010). One of the main drawbacks of the use of these molecules for reactivation of latent HIV-1 is that the concentrations at which significant reactivation is observed are generally toxic (Thorlund et al., 2017), which limits their use as free molecules to induce reactivation. Nevertheless, one of the main advantages of the use of targeted liposomes or other nanoparticles for delivery of drugs is that drug potency can be augmented up to 100,000 times compared to the free drug, which decreases drug cytotoxic effects and toxicity (Pollock et al., 2008).

Thus, a combination of LRAs that resulted in a synergistic high reactivation in a screening experiment when administered as free drugs (Figure 5.13), romidepsin and bryostatins, was used to load ganglioside-containing liposomes, and test their reactivating ability. Transfer of LRA-loaded liposomes to the latently infected cell model J-lat cells was found to be dependent on initial liposome capture, and reactivation occurred only when LRAs were loaded into the liposomes (Figure 5.14). Nevertheless, reactivation of J-lat cells was also observed in the case of minimal unspecific liposome capture (Figure 5.15). Romidepsin and bryostatins are both hydrophobic molecules with o/w partition coefficient values of $\log P = 1.08$ and $\log P = 5.04$, respectively. As such, they are expected to partition to the liposome lipid bilayer, and not the interior aqueous lumen, which could facilitate leakage of the LRAs upon unspecific contact between liposomes and mDCs, explaining the capture-independent reactivation of J-lat cells.

To overcome this drawback a new type of nanoparticles was developed, Solid Lipid Nanoparticles (SLNs). In addition to the process used for their formation, the main difference between SLNs and liposomes resides in the nature of their interior. While liposomes contain an aqueous lumen, suitable for encapsulation of hydrophilic drugs, SLNs contain a hydrophobic core composed of fatty acids in a solid state. This lipid core presents two main advantages: it greatly enhances the hydrophobic molecule loading capacity of the nanoparticles when compared to liposomes and, more interestingly, due to the solid state of the fatty acids in the core, the mobility of the drugs is greatly reduced (Mehnert and Mäder, 2001). This later property, combined with the fact that the hydrophobic core is surrounded by a phospholipid monolayer acting as a barrier, was expected to aid in the reduction of the unspecific LRA leakage suspected with the use of liposomes.

SLN with a surface phospholipid monolayer containing GM1 gangliosides were loaded with romidepsin and bryostatins and used to reactivate J-lat cells via the ganglioside/Siglec-1 pathway mediated by mDCs. Unfortunately, although the hydrophobic LRAs probably partition mainly in the solid lipid core of the SLN, or the

interface between the core and fatty acid chains of the phospholipid monolayer, the same unspecific reactivation of latently infected cells was observed (Figure 5.17). Loading of SLN with hydrophobic drugs is carried out by adding the lipophilic molecules to the initial lipid mixture, prior to microemulsion and particle generation. Because the generation of the solid lipid core and the surface monolayer occur in the same microemulsion step, the hydrophobic drugs could partition close to the surface and not necessarily in the core, which could facilitate LRA leakage.

The main hypothesis behind the capture-independent J-lat reactivation observed with liposomes and SLNs is a so-called bystander reactivation. The LRAs loaded in the nanoparticles, instead of inducing their effect directly in the latently infected cells, could induce activation of the bystander myeloid cells, which in turn would activate J-lat cells. This hypothesis is based in the fact that several cytokines secreted by mDCs have been described to be able to induce latency reactivation (Spina et al., 2013; Yang et al., 2009). Indeed, mDCs pulsed with free bryostatin and then co-cultured with J-lat cells were found to induce latency reactivation, while incubation of bryostatin with J-lat cells alone did not have an effect (Figure 5.18). When secretion of cytokines by mDCs was tested, bryostatin was found to induce the secretion of TNF α and IL-6 by the myeloid cells, and of the two, TNF α alone was demonstrated to induce a strong reactivation of J-lat cells (Figure 5.19). In summary, unspecific leakage of bryostatin from the LRA loaded liposomes or SLNs upon contact with mDCs seem to induce production of TNF α by the myeloid cells, which in turn induces reactivation of latently infected bystander cells.

Interestingly, the discovery of the bystander reactivation offers a new approach for the development of a “shock and kill” therapy. In the initial design, LRA loaded nanoparticles had to be captured by mDCs, accumulated, and delivered to latently infected cells so the drug could directly induce reactivation. The existence of a bystander reactivation by mDCs, in turn, facilitates the design of a new less complex delivery system in which delivery of bryostatin to mDCs induces a bystander reactivation of latently infected cells. This new approach still requires the elimination of unspecific leakage of bryostatin upon contact with cells, in order to minimize the secondary effects that this drug could have in the organism. As such, bryostatin-loaded nanoparticles have to be specifically captured via the ganglioside/Siglec-1 pathway for an efficient specific delivery to mDCs and monocytes, and drug leakage must be eliminated.

For this purpose, a new type of delivery system was engineered based in the use of lipid covered poly(lactic-co-glycolic) (PLGA) polymeric particles. Hydrophobic molecules are readily incorporated into the hydrophobic core of the PLGA particle, facilitating delivery of bryostatin. Interestingly, drug-loaded PLGA cores can be coated with lipid membranes, synthetic or natural, allowing surface functionalization and ganglioside-dependent targeting to Siglec-1 expressing mDCs (Hu et al., 2011, 2015). The main advantage of this particle resides in their production method: the hydrophobic drug is loaded during the generation of the PLGA core, so that it gets entrapped in the inside. After purification of the drug-loaded PLGA particle and extensive washing to ensure no free drug exists, PLGA cores are coated with lipid vesicles. The separation of the drug loading and lipid coating processes in two discrete steps greatly minimizes the partition

of the hydrophobic drug to the surface lipid bilayer coating, thus reducing drug leakage upon contact with the cells. Interestingly, PLGA cores can be coated with platelet derived membranes (Hu et al., 2015), which have been described to be enriched in gangliosides (Ferroni et al., 1997). The use of platelet derived membranes enriched in gangliosides to coat PLGA cores assures a rapid translation into clinical trials, as both biomaterials are clinically approved by the Food and Drug Administration (FDA) (Hu et al., 2015).

Prior to using platelet derived membranes, PLGA core coating with lipid vesicles and posterior specific capture was tested using synthetic lipid bilayers containing GM1 ganglioside. Fluorescent multilamellar vesicles (MLVs) were used to coat PLGA cores labeled with Alexa fluorophores by sonication. The resulting lipid-coated PLGA (L-PLGA) nanoparticles were found to be specifically captured by the ganglioside/Siglec-1 pathway, and minimal unspecific incorporation of non-coated PLGA cores was observed (Figure 5.20). These results demonstrate that PLGA cores coated with ganglioside-containing lipid vesicles are specifically captured by Siglec-1 expressing cells, fulfilling the first requirements. Additionally, secretion of TNF α by mDCs was favoured when bryostatin loaded nanoparticles were captured via the GM1/Siglec-1 pathway (Figure 5.21), conferring to the delivery system the desired specificity.

Additionally, preliminary experiments testing the use of platelet derived lipid vesicles were also carried out. Labeling of platelets with fluorophores covalently bound to phospholipids was demonstrated (Figure 5.22), and PLGA cores were found to be efficiently coated with labeled platelet derived membranes upon sonication (Figure 5.23). Future experiments will study the delivery of bryostatin to mDCs with the use of lipid coated PLGA nanoparticles, and their effect in reactivation of latently infected cell models such as J-lat. If successful, induction of latency reactivation by the development of lipid coated PLGA nanoparticles for the delivery of bryostatin to mDCs via the specific ganglioside/Siglec-1 pathway could lay the basis for prospect clinical trials that could induce reactivation of latently infected cells in viral reservoirs, and their concomitant purge. This could impact the quality of life of HIV-1 infected individuals, reducing the side effects linked to antiretroviral regimens and improving the life expectancy and overall wellbeing of thousands of people.

Chapter 6. General conclusions

Viral membrane cholesterol has repeatedly been found to be necessary for efficient viral and host cell membrane fusion and subsequent viral entry. The gp41 subunit of the HIV-1 envelope protein has been suggested to interact with lipid raft nanodomains. With the use of radioactively labeled photoactivatable cholesterol, a tool which offers the possibility of easily detecting and quantifying *in vivo* interactions of viral membrane proteins with cholesterol, this thesis demonstrates that gp41 directly interacts with cellular and viral membrane cholesterol. Even more, the LLP 2 and 3 sequences, but not LLP1, in the gp41 cytoplasmic domain are necessary for this interaction. Mutational analysis of several other regions and domains of gp41 that presumably could be involved in said interaction seem to indicate that they are not directly related to the interaction with cholesterol.

The specific structure of the membrane envelope of retroviruses has also been demonstrated to be of crucial importance for infectivity. Alterations in membrane fluidity and lipid curvature, and disruption of lipid nanodomains have been found to increase the energy barrier necessary for viral and cellular membrane fusion, inhibiting entry. In this regard, the use of lipid-like molecules as anti-retroviral agents has been explored in this thesis. These raftophilic lipodomimetics were found to partition into the viral membrane and alter its structure changing the lipid lateral packing and resulting in an inhibition of fusion between the viral and host cell membranes. Interestingly, although different lipodomimetic compounds induced diagonally opposed alterations in the structure of the membrane, either rigidifying or fluidifying it, all resulted in inhibition of viral infectivity at entry level. Surprisingly, combination of lipodomimetics with opposing effects in membrane structure resulted in a synergistic inhibition of infectivity. Thus, alteration of membrane structure, and not only lipid composition, is a viable target for the development of antiretroviral therapies. These lipodomimetics act as infectivity inhibitors at low micromolar range, and their usage could be translated to different enveloped viruses or pathogens, for which more studies based in the selected lipodomimetics should be carried out.

The main milestone for the development of a sterilizing cure against HIV-1 is the purge of latently infected cells in viral reservoirs scattered through the organism. In this regard, one of the main drawbacks for elimination of viral reservoirs is the delivery of latency reversing agents to a wide variety of anatomical sanctuaries in which latently infected cells reside, many of which are difficult to access. In this thesis a new pathway for the delivery of latency reversing agents was developed, based on the capture by the Siglec-1 receptor in myeloid cells of nanoparticles functionalized with sialyllactose-containing gangliosides. The developed nanoparticles were specifically captured via the ganglioside/Siglec-1 pathway, accumulated in mDCs up to 48 hours, and were able to induce reactivation in latently infected cells. Nevertheless, an unspecific leakage of the latency reversing agent upon contact with mDCs induced secretion of cytokines by the myeloid cells which in turn reactivated bystander latent cells. New types of nanoparticles, solid lipid nanoparticles and lipid covered PLGA nanoparticles, were developed to try to overcome the unspecific drug leakage, and exploit the reactivation of bystander latently infected cells by inducing secretion of TNF α by mDCs following the specific ganglioside/Siglec-1 pathway.

CHAPTER 6

According to the results obtained in this thesis, the following general conclusions are proposed:

HIV-1 gp41 specifically interacts with cholesterol

- The gp41 subunit of the HIV-1 Env protein specifically interacts with cholesterol in the cellular and viral membranes.
- The cholesterol interaction region is located in the gp41 cytoplasmic domain, but it does not involve the LLP1 sequence.
- None of the other domains of gp41 usually considered to interact with cholesterol were found to be involved in the process.
- Virus maturation does not have an effect in gp41 interaction with cholesterol.
- Viral entry capacity is hampered when gp41 interaction with cholesterol is lost.

Lipidomimetics altering the viral membrane structure and order inhibit viral infectivity at entry step

- Synthetic raft lipid-like lipidomimetic compounds are a promising anti-retroviral tool as they inhibit viral infection at the fusion stage with IC_{50} values in the low micromolar range.
- Lipidomimetic compounds specifically target the viral membrane and exert their entry inhibition effect by altering membrane structure.
- The cholesterol derivative J391B compound required phosphatidylserine for its membrane restructuring activity.
- Compounds J391B and J582C with antagonistic effects on membrane order, inhibited virus infectivity synergistically.

Development of latency reactivation strategies

- Nanoparticles (i.e. liposomes, SLN, lipid coated PLGA) with sialyllactose-containing gangliosides are specifically captured by the cellular Siglec-1 receptor in mature dendritic cells and monocytes, and transferred to J-lat cells.

- Viral peptides can be loaded into liposomes for mDC-mediated presentation to CD8+ T cells and activation of the anti-HIV cytotoxic responses necessary for purge of viral reservoirs.
- Bryostatin encapsulated in liposomes and SLN induces secretion of TNF α by mDCs, which in turn induces reactivation of J-lat cells.
- PLGA nanoparticles can be effectively coated with fluorescently labeled platelet derived vesicles for an increased biocompatibility.

Chapter 7. References

Abacioglu, Y.H., Fouts, T.R., Laman, J.D., Claassen, E., Pincus, S.H., Moore, J.P., Roby, C.A., Kamin-Lewis, R., and Lewis, G.K. (1994). Epitope Mapping and Topology of Baculovirus-Expressed HIV-1 gp160 Determined with a Panel of Murine Monoclonal Antibodies. *AIDS Res. Hum. Retroviruses* 10, 371–381.

Abad, C., Martínez-Gil, L., Tamborero, S., and Mingarro, I. (2009). Membrane topology of gp41 and amyloid precursor protein: interfering transmembrane interactions as potential targets for HIV and Alzheimer treatment. *Biochim. Biophys. Acta* 1788, 2132–2141.

Adachi, A., Gendelman, H.E., Koenig, S., Folks, T., Willey, R., Rabson, A., and Martin, M.A. (1986). Production of acquired immunodeficiency syndrome-associated retrovirus in human and nonhuman cells transfected with an infectious molecular clone. *J. Virol.* 59, 284–291.

Agarwal, S., Schroeder, C., Schlechtingen, G., Braxmeier, T., Jennings, G., and Knölker, H.-J. (2013). Evaluation of steroidal amines as lipid raft modulators and potential anti-influenza agents. *Bioorg. Med. Chem. Lett.* 23, 5165–5169.

Akari, H., Fukumori, T., and Adachi, A. (2000). Cell-Dependent Requirement of Human Immunodeficiency Virus Type 1 gp41 Cytoplasmic Tail for Env Incorporation into Virions. *J. Virol.* 74, 4891–4893.

Aloia, R.C., Jensen, F.C., Curtain, C.C., Mobley, P.W., and Gordon, L.M. (1988). Lipid composition and fluidity of the human immunodeficiency virus. *Proc. Natl. Acad. Sci. U. S. A.* 85, 900–904.

Aloia, R.C., Tian, H., and Jensen, F.C. (1993). Lipid composition and fluidity of the human immunodeficiency virus envelope and host cell plasma membranes. *Proc. Natl. Acad. Sci. U. S. A.* 90, 5181–5185.

Apellániz, B., Rujas, E., Serrano, S., Morante, K., Tsumoto, K., Caaveiro, J.M.M., Jiménez, M.Á., and Nieva, J.L. (2015). The Atomic Structure of the HIV-1 gp41 Transmembrane Domain and Its Connection to the Immunogenic Membrane-proximal External Region. *J. Biol. Chem.* 290, 12999–13015.

Arana, L., Salado, C., Vega, S., Aizpurua-Olaizola, O., Arada, I. de la, Suarez, T., Usobiaga, A., Arrondo, J.L.R., Alonso, A., Goñi, F.M., et al. (2015). Solid lipid nanoparticles for delivery of *Calendula officinalis* extract. *Colloids Surfaces B Biointerfaces* 135, 18–26.

Arana, L., Bayón-Cordero, L., Sarasola, L., Berasategi, M., Ruiz, S., and Alkorta, I. (2019). Solid Lipid Nanoparticles Surface Modification Modulates Cell Internalization and Improves Chemotoxic Treatment in an Oral Carcinoma Cell Line. *Nanomaterials* 9, 464.

Archin, N.M., Liberty, A.L., Kashuba, A.D., Choudhary, S.K., Kuruc, J.D., Crooks, A.M., Parker, D.C., Anderson, E.M., Kearney, M.F., Strain, M.C., et al. (2012). Administration of vorinostat disrupts HIV-1 latency in patients on antiretroviral therapy. *Nature* 487, 482–485.

Bagatolli, L.A. (2006). To see or not to see: Lateral organization of biological membranes and fluorescence microscopy. *Biochim. Biophys. Acta - Biomembr.* 1758, 1541–1556.

Baker, M.K. (2014). Molecular simulations and modeling of HIV-1 gp41 membrane spanning domain (MSD) in a model viral bilayer. Drexel University.

Baker, M.K., Gangupomu, V.K., and Abrams, C.F. (2014). Characterization of the water defect at the HIV-1 gp41 membrane spanning domain in bilayers with and without cholesterol using molecular simulations. *Biochim. Biophys. Acta - Biomembr.* 1838, 1396–1405.

Barre-Sinoussi, F., Chermann, J.C., Rey, F., Nugeyre, M.T., Chamaret, S., Gruest, J., Dautet, C., Axler-Blin, C., Vezinet-Brun, F., Rouzioux, C., et al. (1983). Isolation of a T-lymphotropic retrovirus from a patient at risk for acquired immune deficiency syndrome (AIDS). *Science* 220, 868–871.

Barrett, P.J., Song, Y., Van Horn, W.D., Hustedt, E.J., Schafer, J.M., Hadziselimovic, A., Beel, A.J., and Sanders, C.R. (2012). The Amyloid Precursor Protein Has a Flexible Transmembrane Domain and Binds Cholesterol. *Science* 336, 1168–1171.

Barsov, E. V, Payne, W.S., and Hughes, S.H. (2001). Adaptation of Chimeric Retroviruses In Vitro and In Vivo: Isolation of Avian Retroviral Vectors with Extended Host Range. *J. Virol.* 75, 4973–4983.

Barton, K., Winckelmann, A., and Palmer, S. (2016). HIV-1 Reservoirs During Suppressive Therapy. *Trends Microbiol.* 24, 345–355.

Batista, J., Friedrichson, T., Schlechtingen, G., Braxmeier, T., Jennings, G., and Bajorath, J. (2010). Computational screening for membrane-directed inhibitors of mast cell activation. *Eur. J. Med. Chem.* 45, 2700–2704.

Batista, J., Schlechtingen, G., Friedrichson, T., Braxmeier, T., and Bajorath, J. (2011). Lipid-like sulfoxides and amine oxides as inhibitors of mast cell activation. *Eur. J. Med. Chem.* 46, 2147–2151.

Bhattacharya, J., Repik, A., and Clapham, P.R. (2006). Gag Regulates Association of Human Immunodeficiency Virus Type 1 Envelope with Detergent-Resistant Membranes. *J. Virol.* 80, 5292–5300.

Bligh, E.G., and Dyer, W.J. (1959). A rapid method of total lipid extraction and purification. *Can. J. Biochem. Physiol.* 37, 911–917.

Böttcher, C.J.F., Van Gent, C., and Pries, C. (1961). A rapid and sensitive sub-micro phosphorus determination. *Anal Chim Acta* 24, 203–204.

Brandenberg, O.F., Magnus, C., Rusert, P., Regoes, R.R., and Trkola, A. (2015). Different Infectivity of HIV-1 Strains Is Linked to Number of Envelope Trimers Required for Entry. *PLoS Pathog.* 11, e1004595.

Briggs, J.A.G., Simon, M.N., Gross, I., Kräusslich, H.-G., Fuller, S.D., Vogt, V.M., and Johnson, M.C. (2004). The stoichiometry of Gag protein in HIV-1. *Nat. Struct. Mol. Biol.* 11, 672–675.

Bronshtein, T., Toledano, N., Danino, D., Pollack, S., and Machluf, M. (2011). Cell derived liposomes expressing CCR5 as a new targeted drug-delivery system for HIV infected cells. *J. Control. Release* 151, 139–148.

Brown, D. a, and London, E. (1997). Structure of detergent-resistant membrane domains: does phase separation occur in biological membranes? *Biochem. Biophys. Res. Commun.* 240, 1–7.

Brown, D.A., and London, E. (2000). Structure and Function of Sphingolipid- and Cholesterol-rich Membrane Rafts. *J. Biol. Chem.* 275, 17221–17224.

Brown, D.A., and Rose, J.K. (1992). Sorting of GPI-anchored proteins to glycolipid-enriched membrane subdomains during transport to the apical cell surface. *Cell* 68, 533–544.

Brugger, B., Glass, B., Haberkant, P., Leibrecht, I., Wieland, F.T., and Krausslich, H.-G. (2006). The HIV lipidome: A raft with an unusual composition. *Proc. Natl. Acad. Sci.* 103, 2641–2646.

Büll, C., Heise, T., Adema, G.J., and Boltje, T.J. (2016). Sialic Acid Mimetics to Target the Sialic Acid–Siglec Axis. *Trends Biochem. Sci.* 41, 519–531.

Bultmann, A., Muranyi, W., Seed, B., and Haas, J. (2001). Identification of Two Sequences in the Cytoplasmic Tail of the Human Immunodeficiency Virus Type 1 Envelope Glycoprotein That Inhibit Cell Surface Expression. *J. Virol.* 75, 5263–5276.

Burnie, J., and Guzzo, C. (2019). The Incorporation of Host Proteins into the External HIV-1 Envelope. *Viruses* 11, 85.

Buttler, C.A., Pezeshkian, N., Fernandez, M. V., Aaron, J., Norman, S., Freed, E.O., and van Engelenburg, S.B. (2018). Single molecule fate of HIV-1 envelope reveals late-stage viral lattice incorporation. *Nat. Commun.* 9, 1861.

Cameron, P., Freudenthal, P., Barker, J., Gezelter, S., Inaba, K., and Steinman, R. (1992). Dendritic cells exposed to human immunodeficiency virus type-1 transmit a vigorous cytopathic infection to CD4+ T cells. *Science* 257, 383–387.

Campbell, S., Gaus, K., Bittman, R., Jessup, W., Crowe, S., and Mak, J. (2004). The Raft-Promoting Property of Virion-Associated Cholesterol, but Not the Presence of Virion-Associated Brij 98 Rafts, Is a Determinant of Human Immunodeficiency Virus Type 1 Infectivity. *J. Virol.* 78, 10556–10565.

Campbell, S.M., Crowe, S.M., and Mak, J. (2002). Virion-associated cholesterol is critical for the maintenance of HIV-1 structure and infectivity. *AIDS* 16, 2253–2261.

Carlson, L., Briggs, J.A.G., Glass, B., Riches, J.D., Simon, M.N., Johnson, M.C., Müller, B., Grünewald, K., and Kräusslich, H.-G. (2008). Three-Dimensional Analysis of Budding Sites and Released Virus Suggests a Revised Model for HIV-1 Morphogenesis. *Cell Host Microbe* 4, 592–599.

Cavalli, R., Peira, E., Caputo, O., and Gasco, M.R. (1999). Solid lipid nanoparticles as carriers of hydrocortisone and progesterone complexes with β -cyclodextrins. *Int. J. Pharm.* 182, 59–69.

Cavrois, M., de Noronha, C., and Greene, W.C. (2002). A sensitive and specific enzyme-based assay detecting HIV-1 virion fusion in primary T lymphocytes. *Nat. Biotechnol.* 20, 1151–1154.

Chan, R., Uchil, P.D., Jin, J., Shui, G., Ott, D.E., Mothes, W., and Wenk, M.R. (2008). Retroviruses Human Immunodeficiency Virus and Murine Leukemia Virus Are Enriched in Phosphoinositides. *J. Virol.* 82, 11228–11238.

Checkley, M.A., Lutge, B.G., and Freed, E.O. (2011). HIV-1 Envelope Glycoprotein Biosynthesis, Trafficking, and Incorporation. *J. Mol. Biol.* 410, 582–608.

Chen, S.S.-L., Yang, P., Ke, P.-Y., Li, H.-F., Chan, W., Chang, D., Chuang, C., Tsai, Y., and Huang, S. (2009). Identification of the LWYIK motif located in the human immunodeficiency virus type 1 transmembrane gp41 protein as a distinct determinant for viral infection. *J. Virol.* 83, 870–883.

Chernomordik, L., Chanturiya, A., Green, J., and Zimmerberg, J. (1995). The hemifusion intermediate and its conversion to complete fusion: regulation by membrane composition. *Biophys. J.* 69, 922–929.

Chertova, E., Bess, J.W.J., Crise, B.J., Sowder II, R.C., Schaden, T.M., Hilburn, J.M., Hoxie, J.A., Benveniste, R.E., Lifson, J.D., Henderson, L.E., et al. (2002). Envelope glycoprotein incorporation, not shedding of surface envelope glycoprotein (gp120/SU), is the primary determinant of SU content of purified human immunodeficiency virus type 1 and simian immunodeficiency virus. *J. Virol.* 76, 5315–5325.

Chevallet, M., Luche, S., and Rabilloud, T. (2006). Silver staining of proteins in polyacrylamide gels. *Nat. Protoc.* 1, 1852–1858.

Chojnacki, J., Staudt, T., Glass, B., Bingen, P., Engelhardt, J., Anders, M., Schneider, J., Muller, B., Hell, S.W., and Krausslich, H.-G. (2012). Maturation-Dependent HIV-1 Surface Protein Redistribution Revealed by Fluorescence Nanoscopy. *Science* 338, 524–528.

Chojnacki, J., Waithe, D., Carravilla, P., Huarte, N., Galiani, S., Enderlein, J., and Eggeling, C. (2017). Envelope glycoprotein mobility on HIV-1 particles depends on the virus maturation state. *Nat. Commun.* 8, 545.

Chun, T.-W., Justement, J.S., Murray, D., Hallahan, C.W., Maenza, J., Collier, A.C., Sheth, P.M., Kaul, R., Ostrowski, M., Moir, S., et al. (2010). Rebound of plasma viremia following cessation of antiretroviral therapy despite profoundly low levels of HIV reservoir: implications for eradication. *AIDS* 24, 2803–2808.

Chun, T.-W., Moir, S., and Fauci, A.S. (2015). HIV reservoirs as obstacles and opportunities for an HIV cure. *Nat. Immunol.* 16, 584–589.

Churchill, M.J., Wesselingh, S.L., Cowley, D., Pardo, C.A., McArthur, J.C., Brew, B.J., and Gorry, P.R. (2009). Extensive astrocyte infection is prominent in human immunodeficiency virus-associated dementia. *Ann. Neurol.* 66, 253–258.

Cihlar, T., and Ray, A.S. (2010). Nucleoside and nucleotide HIV reverse transcriptase inhibitors: 25 years after zidovudine. *Antiviral Res.* 85, 39–58.

Clayton, R., Ohagen, A., Nicol, F., Del Vecchio, A.M., Jonckers, T.H.M.M., Goethals, O., Van Loock, M., Michiels, L., Grigsby, J., Xu, Z., et al. (2009). Sustained and specific in vitro

inhibition of HIV-1 replication by a protease inhibitor encapsulated in gp120-targeted liposomes. *Antiviral Res.* **84**, 142–149.

Cleveland, S.M. (2003). A region of the C-terminal tail of the gp41 envelope glycoprotein of human immunodeficiency virus type 1 contains a neutralizing epitope: evidence for its exposure on the surface of the virion. *J. Gen. Virol.* **84**, 591–602.

Cohen, S.N., Chang, A.C.Y., and Hsu, L. (1972). Nonchromosomal Antibiotic Resistance in Bacteria: Genetic Transformation of *Escherichia coli* by R-Factor DNA. *Proc. Natl. Acad. Sci.* **69**, 2110–2114.

Contreras, F.-X., Sot, J., Alonso, A., and Goñi, F.M. (2006). Sphingosine Increases the Permeability of Model and Cell Membranes. *Biophys. J.* **90**, 4085–4092.

Contreras, F.-X., Ernst, A.M., Haberkant, P., Björkholm, P., Lindahl, E., Gönen, B., Tischer, C., Elofsson, A., von Heijne, G., Thiele, C., et al. (2012). Molecular recognition of a single sphingolipid species by a protein's transmembrane domain. *Nature* **481**, 525–529.

Crocker, P.R., Paulson, J.C., and Varki, A. (2007). Siglecs and their roles in the immune system. *Nat. Rev. Immunol.* **7**, 255–266.

Cushman, M., Golebiewski, W.M., McMahon, J.B., Buckheit, R.W., Clanton, D.J., Weislow, O., Haugwitz, R.D., Bader, J.P., Graham, L., and Rice, W.G. (1994). Design, synthesis, and biological evaluation of cosalane, a novel anti-HIV agent which inhibits multiple features of virus reproduction. *J. Med. Chem.* **37**, 3040–3050.

Van Damme, L., Ramjee, G., Alary, M., Vuylsteke, B., Chandeying, V., Rees, H., Sirivongrangson, P., Mukenge-Tshibaka, L., Ettiègne-Traoré, V., Uaheowitchai, C., et al. (2002). Effectiveness of COL-1492, a nonoxynol-9 vaginal gel, on HIV-1 transmission in female sex workers: a randomised controlled trial. *Lancet (London, England)* **360**, 971–977.

Deeks, S.G., Autran, B., Berkhout, B., Benkirane, M., Cairns, S., Chomont, N., Chun, T.-W., Churchill, M., Di Mascio, M., Katlama, C., et al. (2012). Towards an HIV cure: a global scientific strategy. *Nat. Rev. Immunol.* **12**, 607–614.

Derdeyn, C.A., Decker, J.M., Sfakianos, J.N., Wu, X., O'Brien, W.A., Ratner, L.E.E., Kappes, J.C., Shaw, G.M., Hunter, E., Brien, W.A.O., et al. (2000). Sensitivity of Human Immunodeficiency Virus Type 1 to the Fusion Inhibitor T-20 Is Modulated by Coreceptor Specificity Defined by the V3 Loop of gp120. *J. Virol.* **74**, 8358–8367.

Dettenhofer, M., and Yu, X.F. (1999). Highly purified human immunodeficiency virus type 1 reveals a virtual absence of Vif in virions. *J. Virol.* **73**, 1460–1467.

Diaz-Rohrer, B., Levental, K.R., and Levental, I. (2014). Rafting through traffic: Membrane domains in cellular logistics. *Biochim. Biophys. Acta - Biomembr.* **1838**, 3003–3013.

Dietrich, C., Bagatolli, L.A., Volovyk, Z.N., Thompson, N.L., Levi, M., Jacobson, K., and Gratton, E. (2001). Lipid Rafts Reconstituted in Model Membranes. *Biophys. J.* **80**, 1417–1428.

Domanska, M.K., Dunning, R.A., Dryden, K.A., Zawada, K.E., Yeager, M., and Kasson, P.M. (2015). Hemagglutinin Spatial Distribution Shifts in Response to Cholesterol in the

Influenza Viral Envelope. *Biophys. J.* 109, 1917–1924.

Donzella, G.A., Schols, D., Lin, S.W., Esté, J.A., Nagashima, K.A., Maddon, P.J., Allaway, G.P., Sakmar, T.P., Henson, G., DeClercq, E., et al. (1998). AMD3100, a small molecule inhibitor of HIV-1 entry via the CXCR4 co-receptor. *Nat. Med.* 4, 72–77.

Dumas, F., and Haanappel, E. (2017). Lipids in infectious diseases – The case of AIDS and tuberculosis. *Biochim. Biophys. Acta - Biomembr.* 1859, 1636–1647.

Durham, N.D., and Chen, B.K. (2015). HIV-1 Cell-Free and Cell-to-Cell Infections Are Differentially Regulated by Distinct Determinants in the Env gp41 Cytoplasmic Tail. *J. Virol.* 89, 9324–9337.

Düzgüneş, N., Simões, S., Slepushkin, V., Pretzer, E., Flasher, D., Salem, I.I., Steffan, G., Konopka, K., and Pedrosa de Lima, M.C. (2005). Delivery of antiviral agents in liposomes. *Methods Enzymol.* 391, 351–373.

Ellens, H., Bentz, J., and Szoka, F.C. (1985). H⁺- and Ca²⁺-induced fusion and destabilization of liposomes. *Biochemistry* 24, 3099–3106.

Emi, N., Friedmann, T., and Yee, J.K. (1991). Pseudotype formation of murine leukemia virus with the G protein of vesicular stomatitis virus. *J. Virol.* 65, 1202–1207.

Epand, R.F., Thomas, A., Bresseur, R., Vishwanathan, S.A., Hunter, E., and Epand, R.M. (2006). Juxtamembrane protein segments that contribute to recruitment of cholesterol into domains. *Biochemistry* 45, 6105–6114.

Ferroni, P., Lenti, L., Martini, F., Ciatti, F., Pontieri, G.M., and Gazzaniga, P.P. (1997). Ganglioside content of human platelets—differences in resting and activated platelets. *Thromb. Haemost.* 77, 548–554.

Finnegan, C.M., Rawat, S.S., Puri, A., Wang, J.M., Ruscetti, F.W., and Blumenthal, R. (2004). Ceramide, a target for antiretroviral therapy. *Proc. Natl. Acad. Sci.* 101, 15452–15457.

Fiske, C., and Subbarow, Y. (1925). The Colorimetric Determination of Phosphorus. *J. Biol. Chem* 66, 375–400.

Freed, E.O. (2015). HIV-1 assembly, release and maturation. *Nat. Rev. Microbiol.* 13, 484–496.

Gahbauer, S., and Böckmann, R.A. (2016). Membrane-Mediated Oligomerization of G Protein Coupled Receptors and Its Implications for GPCR Function. *Front. Physiol.* 7, 1–17.

Gallo, R.C., Sarin, P.S., Gelmann, E.P., Robert-Guroff, M., Richardson, E., Kalyanaraman, V.S., Mann, D., Sidhu, G.D., Stahl, R.E., Zolla-Pazner, S., et al. (1983). Isolation of human T-cell leukemia virus in acquired immune deficiency syndrome (AIDS). *Science* 220, 865–867.

Gangupomu, V.K., and Abrams, C.F. (2010). All-Atom Models of the Membrane-Spanning Domain of HIV-1 gp41 from Metadynamics. *Biophys. J.* 99, 3438–3444.

Gao, F., Bailes, E., Robertson, D.L., Chen, Y., Rodenburg, C.M., Michael, S.F., Cummins,

L.B., Arthur, L.O., Peeters, M., Shaw, G.M., et al. (1999). Origin of HIV-1 in the chimpanzee *Pan troglodytes troglodytes*. *Nature* 397, 436–441.

Gaschen, B. (2002). Diversity Considerations in HIV-1 Vaccine Selection. *Science* 296, 2354–2360.

Geijtenbeek, T.B.H., Kwon, D.S., Torensma, R., van Vliet, S.J., van Duijnhoven, G.C., Middel, J., Cornelissen, I.L.M.H.A., Nottet, H.S.L.M., KewalRamani, V.N., Littman, D.R., et al. (2000). DC-SIGN, a Dendritic Cell-Specific HIV-1-Binding Protein that Enhances trans-Infection of T Cells. *Cell* 100, 587–597.

van Genderen, I.L., Godeke, G.J., Rottier, P.J., and van Meer, G. (1995). The phospholipid composition of enveloped viruses depends on the intracellular membrane through which they bud. *Biochem. Soc. Trans.* 23, 523–526.

Giacomini, K.M., Huang, S.-M., Tweedie, D.J., Benet, L.Z., Brouwer, K.L.R., Chu, X., Dahlin, A., Evers, R., Fischer, V., Hillgren, K.M., et al. (2010). Membrane transporters in drug development. *Nat. Rev. Drug Discov.* 9, 215–236.

Goñi, F.M., and Alonso, A. (2006). Biophysics of sphingolipids I. Membrane properties of sphingosine, ceramides and other simple sphingolipids. *Biochim. Biophys. Acta - Biomembr.* 1758, 1902–1921.

Gregoriadis, G., and Florence, A.T. (1993). Liposomes in Drug Delivery. *Drugs* 45, 15–28.

Griffiths, G., and Rottier, P. (1992). Cell biology of viruses that assemble along the biosynthetic pathway. *Semin. Cell Biol.* 3, 367–381.

Grimm, D. (2002). Production methods for gene transfer vectors based on adeno-associated virus serotypes. *Methods* 28, 146–157.

Gunaseelan, S., Gunaseelan, K., Deshmukh, M., Zhang, X., and Sinko, P.J. (2010). Surface modifications of nanocarriers for effective intracellular delivery of anti-HIV drugs. *Adv. Drug Deliv. Rev.* 62, 518–531.

Gupta, R.K., Abdul-jawad, S., McCoy, L.E., Mok, H.P., Peppas, D., Salgado, M., Martinez-Picado, J., Nijhuis, M., Wensing, A.M.J., Lee, H., et al. (2019). HIV-1 remission following CCR5 Δ 32/ Δ 32 haematopoietic stem-cell transplantation. *Nature*.

Haberkant, P., Schmitt, O., Contreras, F.-X.F.-X., Thiele, C., Hanada, K., Sprong, H., Reinhard, C., Wieland, F.T., Brügger, B., and Bru, B. (2008). Protein-sphingolipid interactions within cellular membranes. *J. Lipid Res.* 49, 251–262.

Hanshaw, R.G., and Smith, B.D. (2005). New reagents for phosphatidylserine recognition and detection of apoptosis. *Bioorg. Med. Chem.* 13, 5035–5042.

Haqqani, A.A., and Tilton, J.C. (2013). Entry inhibitors and their use in the treatment of HIV-1 infection. *Antiviral Res.* 98, 158–170.

Harada, S. (2005). The broad anti-viral agent glycyrrhizin directly modulates the fluidity of plasma membrane and HIV-1 envelope. *Biochem. J.* 392, 191–199.

Harada, S., Koyanagi, Y., and Yamamoto, N. (1985). Infection of HTLV-III/LAV in HTLV-

I-carrying cells MT-2 and MT-4 and application in a plaque assay. *Science* 229, 563–566.

Harada, S., Yokomizo, K., Monde, K., Maeda, Y., and Yusa, K. (2007). A broad antiviral neutral glycolipid, fattiviracin FV-8, is a membrane fluidity modulator. *Cell. Microbiol.* 9, 196–203.

Hawkes, D., Jones, K.L., Smyth, R.P., Pereira, C.F., Bittman, R., Jaworowski, A., and Mak, J. (2015). Properties of HIV-1 associated cholesterol in addition to raft formation are important for virus infection. *Virus Res.* 210, 18–21.

Henrich, T.J., Hatano, H., Bacon, O., Hogan, L.E., Rutishauser, R., Hill, A., Kearney, M.F., Anderson, E.M., Buchbinder, S.P., Cohen, S.E., et al. (2017). HIV-1 persistence following extremely early initiation of antiretroviral therapy (ART) during acute HIV-1 infection: An observational study. *PLOS Med.* 14, e1002417.

Henriksson, P., and Bosch, V. (1998). Inhibition of Cellular Glycoprotein Incorporation into Human Immunodeficiency Virus-like Particles by Coexpression of Additional Cellular Interaction Partner. *Virology* 251, 16–21.

Hillier, S.L., Moench, T., Shattock, R., Black, R., Reichelderfer, P., and Veronese, F. (2005). In vitro and in vivo: the story of nonoxynol 9. *J. Acquir. Immune Defic. Syndr.* 39, 1–8.

Hogue, I.B., Grover, J.R., Soheilian, F., Nagashima, K., and Ono, A. (2011). Gag Induces the Coalescence of Clustered Lipid Rafts and Tetraspanin-Enriched Microdomains at HIV-1 Assembly Sites on the Plasma Membrane. *J. Virol.* 85, 9749–9766.

Hollier, M.J., and Dimmock, N.J. (2005). The C-terminal tail of the gp41 transmembrane envelope glycoprotein of HIV-1 clades A, B, C, and D may exist in two conformations: an analysis of sequence, structure, and function. *Virology* 337, 284–296.

Hope, M.J., Bally, M.B., Webb, G., and Cullis, P.R. (1985). Production of large unilamellar vesicles by a rapid extrusion procedure. Characterization of size distribution, trapped volume and ability to maintain a membrane potential. *Biochim. Biophys. Acta - Biomembr.* 812, 55–65.

Hrecka, K., Hao, C., Gierszewska, M., Swanson, S.K., Kesik-Brodacka, M., Srivastava, S., Florens, L., Washburn, M.P., and Skowronski, J. (2011). Vpx relieves inhibition of HIV-1 infection of macrophages mediated by the SAMHD1 protein. *Nature* 474, 658–661.

Hu, C.-M.J., Zhang, L., Aryal, S., Cheung, C., Fang, R.H., and Zhang, L. (2011). Erythrocyte membrane-camouflaged polymeric nanoparticles as a biomimetic delivery platform. *Proc. Natl. Acad. Sci.* 108, 10980–10985.

Hu, C.J., Fang, R.H., Wang, K., Luk, B.T., Thamphiwatana, S., Dehaini, D., Nguyen, P., Angsantikul, P., Wen, C.H., Kroll, A. V, et al. (2015). Nanoparticle biointerfacing by platelet membrane cloaking. *Nature* 526, 118–121.

Hu, Y., Ehrich, M., Fuhrman, K., and Zhang, C. (2014). In vitro performance of lipid-PLGA hybrid nanoparticles as an antigen delivery system: lipid composition matters. *Nanoscale Res. Lett.* 9, 434.

Huang, J., Ofek, G., Laub, L., Louder, M.K., Doria-Rose, N.A., Longo, N.S., Imamichi, H., Bailer, R.T., Chakrabarti, B., Sharma, S.K., et al. (2012). Broad and potent neutralization of

HIV-1 by a gp41-specific human antibody. *Nature* 491, 406–412.

Hütter, G., Nowak, D., Mossner, M., Ganepola, S., Müßig, A., Allers, K., Schneider, T., Hofmann, J., Kücherer, C., Blau, O., et al. (2009). Long-Term Control of HIV by CCR5 Delta32/Delta32 Stem-Cell Transplantation. *N. Engl. J. Med.* 360, 692–698.

Izquierdo-Useros, N., Lorizate, M., Contreras, F.-X., Rodriguez-Plata, M.T., Glass, B., Erkizia, I., Prado, J.G., Casas, J., Fabriàs, G., Kräusslich, H.-G., et al. (2012a). Sialyllactose in Viral Membrane Gangliosides Is a Novel Molecular Recognition Pattern for Mature Dendritic Cell Capture of HIV-1. *PLoS Biol.* 10, e1001315.

Izquierdo-Useros, N., Lorizate, M., Puertas, M.C., Rodriguez-Plata, M.T., Zangger, N., Erikson, E., Pino, M., Erkizia, I., Glass, B., Clotet, B., et al. (2012b). Siglec-1 Is a Novel Dendritic Cell Receptor That Mediates HIV-1 Trans-Infection Through Recognition of Viral Membrane Gangliosides. *PLoS Biol.* 10, e1001448.

Izquierdo-Useros, N., Lorizate, M., McLaren, P.J., Telenti, A., Kräusslich, H.-G., and Martinez-Picado, J. (2014). HIV-1 Capture and Transmission by Dendritic Cells: The Role of Viral Glycolipids and the Cellular Receptor Siglec-1. *PLoS Pathog.* 10, e1004146.

Jiang, J., and Aiken, C. (2007). Maturation-Dependent Human Immunodeficiency Virus Type 1 Particle Fusion Requires a Carboxyl-Terminal Region of the gp41 Cytoplasmic Tail. *J. Virol.* 81, 9999–10008.

Kaiser, H.-J., Lingwood, D., Levental, I., Sampaio, J.L., Kalvodova, L., Rajendran, L., and Simons, K. (2009). Order of lipid phases in model and plasma membranes. *Proc. Natl. Acad. Sci.* 106, 16645–16650.

Kaiser, H.-J., Surma, M.A., Mayer, F., Levental, I., Grzybek, M., Klemm, R.W., Da Cruz, S., Meisinger, C., Müller, V., Simons, K., et al. (2011). Molecular Convergence of Bacterial and Eukaryotic Surface Order. *J. Biol. Chem.* 286, 40631–40637.

Kalia, V., Sarkar, S., Gupta, P., and Montelaro, R.C. (2003). Rational site-directed mutations of the LLP-1 and LLP-2 lentivirus lytic peptide domains in the intracytoplasmic tail of human immunodeficiency virus type 1 gp41 indicate common functions in cell-cell fusion but distinct roles in virion envelope incorpora. *J. Virol.* 77, 3634–3646.

Kawasaki, N., Vela, J.L., Nycholat, C.M., Rademacher, C., Khurana, A., van Rooijen, N., Crocker, P.R., Kronenberg, M., and Paulson, J.C. (2013). Targeted delivery of lipid antigen to macrophages via the CD169/sialoadhesin endocytic pathway induces robust invariant natural killer T cell activation. *Proc. Natl. Acad. Sci.* 110, 7826–7831.

Kitchen, S.G., and Zack, J.A. (1997). CXCR4 expression during lymphoiesis: implications for HIV-1 infection of the thymus. *J. Virol.* 71, 6928–6934.

Klein, F., Mouquet, H., Dosenovic, P., Scheid, J.F., Scharf, L., and Nussenzweig, M.C. (2013). Antibodies in HIV-1 Vaccine Development and Therapy. *Science* 341, 1199–1204.

Kleusch, C., Hersch, N., Hoffmann, B., Merkel, R., and Csiszár, A. (2012). Fluorescent Lipids: Functional Parts of Fusogenic Liposomes and Tools for Cell Membrane Labeling and Visualization. *Molecules* 17, 1055–1073.

Kliger, Y., and Shai, Y. (1997). A Leucine Zipper-Like Sequence from the Cytoplasmic Tail of the HIV-1 Envelope Glycoprotein Binds and Perturbs Lipid Bilayers †. *Biochemistry*

36, 5157–5169.

Kliger, Y., and Shai, Y. (2000). Inhibition of HIV-1 entry before gp41 folds into its fusion-active conformation. *J. Mol. Biol.* 295, 163–168.

Klug, Y.A., Rotem, E., Schwarzer, R., and Shai, Y. (2017). Mapping out the intricate relationship of the HIV envelope protein and the membrane environment. *Biochim. Biophys. Acta - Biomembr.* 1859, 550–560.

Knölker, H.-J., Agarwal, S., Schlechtingen, G., Braxmeier, T., Schroeder, C., and Jennings, G. (2009). Steroid sapogenin, androstane and triterpenoid sapogenin derivatives for the treatment and prevention of infectious diseases (VOSSIUS & PARTNER).

Korin, Y.D., Brooks, D.G., Brown, S., Korotzer, A., and Zack, J.A. (2002). Effects of prostratin on T-cell activation and human immunodeficiency virus latency. *J. Virol.* 76, 8118–8123.

Kuhlmann, A., Steckbeck, J.D., Sturgeon, T.J., Craigo, J.K., and Montelaro, R.C. (2014). Unique Functional Properties of Conserved Arginine Residues in the Lentivirus Lytic Peptide Domains of the C-terminal Tail of HIV-1 gp41. *J. Biol. Chem.* 289, 7630–7640.

Kulkosky, J., Culnan, D.M., Roman, J., Dornadula, G., Schnell, M., Boyd, M.R., and Pomerantz, R.J. (2001). Prostratin: activation of latent HIV-1 expression suggests a potential inductive adjuvant therapy for HAART. *Blood* 98, 3006–3015.

Kulpa, D.A., and Chomont, N. (2015). HIV persistence in the setting of antiretroviral therapy: when, where and how does HIV hide? *J. Virus Erad.* 1, 59–66.

van der Kuyl, A.C., van den Burg, R., Zorgdrager, F., Groot, F., Berkhout, B., and Cornelissen, M. (2007). Sialoadhesin (CD169) Expression in CD14+ Cells Is Upregulated Early after HIV-1 Infection and Increases during Disease Progression. *PLoS One* 2, e257.

Kwon, B., Lee, M., Waring, A.J., and Hong, M. (2018). Oligomeric Structure and Three-Dimensional Fold of the HIV gp41 Membrane-Proximal External Region and Transmembrane Domain in Phospholipid Bilayers. *J. Am. Chem. Soc.* 140, 8246–8259.

Lafeuillade, A., Poggi, C., Chadapaud, S., Hittinger, G., Chouraqui, M., Pisapia, M., and Delbeke, E. (2001). Pilot study of a combination of highly active antiretroviral therapy and cytokines to induce HIV-1 remission. *J. Acquir. Immune Defic. Syndr.* 26, 44–55.

Laguet, N., Sobhian, B., Casartelli, N., Ringeard, M., Chable-Bessia, C., Ségéral, E., Yatim, A., Emiliani, S., Schwartz, O., and Benkirane, M. (2011). SAMHD1 is the dendritic- and myeloid-cell-specific HIV-1 restriction factor counteracted by Vpx. *Nature* 474, 654–657.

Lampe, M., Briggs, J.A.G., Endress, T., Glass, B., Riegelsberger, S., Kräusslich, H., Lamb, D.C., Bräuchle, C., and Müller, B. (2007). Double-labelled HIV-1 particles for study of virus–cell interaction. *Virology* 360, 92–104.

Lee, J.H., Ozorowski, G., and Ward, A.B. (2016). Cryo-EM structure of a native, fully glycosylated, cleaved HIV-1 envelope trimer. *Science* 351, 1043–1048.

Lee, J.S., Cole, S.R., Achenbach, C.J., Dittmer, D.P., Richardson, D.B., Miller, W.C.,

Mathews, C., Althoff, K.N., Moore, R.D., and Eron, J.J. (2018). Cancer risk in HIV patients with incomplete viral suppression after initiation of antiretroviral therapy. *PLoS One* 13, e0197665.

Lee, S., Ko, C., Wang, C.-T., and Chen, S.S.-L. (2002). Effect of Point Mutations in the N Terminus of the Lentivirus Lytic Peptide-1 Sequence of Human Immunodeficiency Virus Type 1 Transmembrane Protein gp41 on Env Stability. *J. Biol. Chem.* 277, 15363–15375.

Lee, S.F., Wang, C.T., Liang, J.Y.P., Hong, S.L., Huang, C.C., and Chen, S.S.L. (2000). Multimerization potential of the cytoplasmic domain of the human immunodeficiency virus type 1 transmembrane glycoprotein gp41. *J. Biol. Chem.* 275, 15809–15819.

Lemey, P., Pybus, O.G., Wang, B., Saksena, N.K., Salemi, M., and Vandamme, A.-M. (2003). Tracing the origin and history of the HIV-2 epidemic. *Proc. Natl. Acad. Sci. U. S. A.* 100, 6588–6592.

Lev, N., Fridmann-Sirkis, Y., Blank, L., Bitler, A., Epand, R.F., Epand, R.M., and Shai, Y. (2009). Conformational Stability and Membrane Interaction of the Full-Length Ectodomain of HIV-1 gp41: Implication for Mode of Action †. *Biochemistry* 48, 3166–3175.

Liao, Z., Cimasky, L.M., Hampton, R., Nguyen, D.H., and Hildreth, J.E.K. (2001). Lipid Rafts and HIV Pathogenesis: Host Membrane Cholesterol Is Required for Infection by HIV Type 1. *AIDS Res. Hum. Retroviruses* 17, 1009–1019.

Liao, Z., Graham, D.R., and Hildreth, J.E.K. (2003). Lipid Rafts and HIV Pathogenesis: Virion-Associated Cholesterol Is Required for Fusion and Infection of Susceptible Cells. *AIDS Res. Hum. Retroviruses* 19, 675–687.

Liu, S., Levine, S., and Winn, H. (2011). Targeting ischemic penumbra Part II: selective drug delivery using liposome technologies. *J. Exp. Stroke ...* 4, 16–23.

Lorizate, M., and Krausslich, H.-G. (2011). Role of Lipids in Virus Replication. *Cold Spring Harb. Perspect. Biol.* 3, a004820–a004820.

Lorizate, M., Huarte, N., Sáez-Ciri3n, A., and Nieva, J.L. (2008). Interfacial pre-transmembrane domains in viral proteins promoting membrane fusion and fission. *Biochim. Biophys. Acta* 1778, 1624–1639.

Lorizate, M., Brügger, B., Akiyama, H., Glass, B., Müller, B., Anderlüh, G., Wieland, F.T., Kräusslich, H.-G., Brugger, B., Akiyama, H., et al. (2009). Probing HIV-1 Membrane Liquid Order by Laurdan Staining Reveals Producer Cell-dependent Differences. *J. Biol. Chem.* 284, 22238–22247.

Lorizate, M., Sachsenheimer, T., Glass, B., Habermann, A., Gerl, M.J., Kräusslich, H.-G., and Brügger, B. (2013). Comparative lipidomics analysis of HIV-1 particles and their producer cell membrane in different cell lines. *Cell. Microbiol.* 15, 292–304.

Lu, L., Zhu, Y., Huang, J., Chen, X., Yang, H., Jiang, S., and Chen, Y. (2008). Surface Exposure of the HIV-1 Env Cytoplasmic Tail LLP2 Domain during the Membrane Fusion Process. *J. Biol. Chem.* 283, 16723–16731.

Magee, A.I., and Parmryd, I. (2003). Detergent-resistant membranes and the protein composition of lipid rafts. *Genome Biol.* 4.

Malikov, V., da Silva, E.S., Jovasevic, V., Bennett, G., de Souza Aranha Vieira, D.A., Schulte, B., Diaz-Griffero, F., Walsh, D., and Naghavi, M.H. (2015). HIV-1 capsids bind and exploit the kinesin-1 adaptor FEZ1 for inward movement to the nucleus. *Nat. Commun.* 6, 6660.

Malkovsky, M., Newell, A., and Dalgleish, A.G. (1988). Inactivation of HIV by nonoxynol-9. *Lancet (London, England)* 1, 645.

Mañes, S., del Real, G., Lacalle, R.A., Lucas, P., Gómez-Moutón, C., Sánchez-Palomino, S., Delgado, R., Alcamí, J., Mira, E., and Martínez-A, C. (2000). Membrane raft microdomains mediate lateral assemblies required for HIV-1 infection. *EMBO Rep.* 1, 190–196.

Meclure, M.O., Sommerfelt, M.A., Marsh, M., Weiss, R.A., McClure, M.O., Sommerfelt, M.A., Marsh, M., and Weiss, R.A. (1990). The pH independence of mammalian retrovirus infection. *J. Gen. Virol.* 71, 767–773.

Megha, and London, E. (2004). Ceramide Selectively Displaces Cholesterol from Ordered Lipid Domains (Rafts). *J. Biol. Chem.* 279, 9997–10004.

Mehla, R., Bivalkar-Mehla, S., Zhang, R., Handy, I., Albrecht, H., Giri, S., Nagarkatti, P., Nagarkatti, M., and Chauhan, A. (2010). Bryostatins modulates latent HIV-1 infection via PKC and AMPK signaling but inhibits acute infection in a receptor independent manner. *PLoS One* 5, e11160.

Mehnert, W., and Mäder, K. (2001). Solid lipid nanoparticles: production, characterization and applications. *Adv. Drug Deliv. Rev.* 47, 165–196.

Miller, M.A., Garry, R.F., Jaynes, J.M., and Montelaro, R.C. (1991). A structural correlation between lentivirus transmembrane proteins and natural cytolytic peptides. *AIDS Res. Hum. Retroviruses* 7, 511–519.

Miller, M.A., Cloyd, M.W., Liebmann, J., Rinaldo, C.R., Islam, K.R., Wang, S.Z.S., Mietzner, T.A., and Montelaro, R.C. (1993). Alterations in Cell Membrane Permeability by the Lentivirus Lytic Peptide (LLP-1) of HIV-1 Transmembrane Protein. *Virology* 196, 89–100.

Mizrachi, Y., Lev, M., Harish, Z., Sundaram, S.K., and Rubinstein, A. (1996). L-cycloserine, an inhibitor of sphingolipid biosynthesis, inhibits HIV-1 cytopathic effects, replication, and infectivity. *J. Acquir. Immune Defic. Syndr. Hum. Retrovirol.* 11, 137–141.

Molinos-Albert, L.M., Bilbao, E., Agulló, L., Marfil, S., García, E., Concepción, M.L.R.D. La, Izquierdo-Useros, N., Vilaplana, C., Nieto-Garai, J.A., Contreras, F.-X., et al. (2017). Proteoliposomal formulations of an HIV-1 gp41-based miniprotein elicit a lipid-dependent immunodominant response overlapping the 2F5 binding motif. *Sci. Rep.* 7, 40800.

Moore, M.D., and Hu, W.S. (2011). HIV-1 RNA dimerization: It takes two to tango. *AIDS Rev.* 11, 91–102.

Moreno, M.R., Pérez-Berná, A.J., Guillén, J., and Villalaín, J. (2008). Biophysical characterization and membrane interaction of the most membranotropic region of the HIV-1 gp41 endodomain. *Biochim. Biophys. Acta - Biomembr.* 1778, 1298–1307.

Morizono, K., and Chen, I.S.Y. (2014). Role of Phosphatidylserine Receptors in Enveloped Virus Infection. *J. Virol.* 88, 4275–4290.

Mosmann, T. (1983). Rapid colorimetric assay for cellular growth and survival: application to proliferation and cytotoxicity assays. *J. Immunol. Methods* 65, 55–63.

Mücksch, F., Laketa, V., Müller, B., Schultz, C., and Kräusslich, H.-G. (2017). Synchronized HIV assembly by tunable PIP2 changes reveals PIP2 requirement for stable Gag anchoring. *Elife* 6, 1–26.

Mufamadi, M.S., Pillay, V., Choonara, Y.E., Du Toit, L.C., Modi, G., Naidoo, D., and Ndesendo, V.M.K. (2011). A Review on Composite Liposomal Technologies for Specialized Drug Delivery. *J. Drug Deliv.* 2011, 1–19.

Muller, B., Tessmer, U., Schubert, U., and Krausslich, H.G. (2000). Human immunodeficiency virus type 1 Vpr protein is incorporated into the virion in significantly smaller amounts than gag and is phosphorylated in infected cells. *J. Virol.* 74, 9727–9731.

Muller, B., Daecke, J., Fackler, O.T., Dittmar, M.T., Zentgraf, H., Krausslich, H.-G., Mu, B., Daecke, J., Fackler, O.T., Dittmar, M.T., et al. (2004). Construction and Characterization of a Fluorescently Labeled Infectious Human Immunodeficiency Virus Type 1 Derivative. *J. Virol.* 78, 10803–10813.

Munk, C., Brandt, S.M., Lucero, G., and Landau, N.R. (2002). A dominant block to HIV-1 replication at reverse transcription in simian cells. *Proc. Natl. Acad. Sci.* 99, 13843–13848.

Murakami, T., and Freed, E.O. (2000). The long cytoplasmic tail of gp41 is required in a cell type-dependent manner for HIV-1 envelope glycoprotein incorporation into virions. *Proc. Natl. Acad. Sci.* 97, 343–348.

Murakami, T., Ablan, S., Freed, E.O., and Tanaka, Y. (2004). Regulation of Human Immunodeficiency Virus Type 1 Env-Mediated Membrane Fusion by Viral Protease Activity. *J. Virol.* 78, 1026–1031.

Muranyi, W., Malkusch, S., Müller, B., Heilemann, M., and Kräusslich, H.-G. (2013). Super-Resolution Microscopy Reveals Specific Recruitment of HIV-1 Envelope Proteins to Viral Assembly Sites Dependent on the Envelope C-Terminal Tail. *PLoS Pathog.* 9, e1003198.

Murphy, R.E., Samal, A.B., Vlach, J., and Saad, J.S. (2017). Solution Structure and Membrane Interaction of the Cytoplasmic Tail of HIV-1 gp41 Protein. *Structure* 25, 1708–1718.e5.

Ng, K., Zhao, L., Liu, Y., and Mahapatro, M. (2000). The effects of polyethyleneglycol (PEG)-derived lipid on the activity of target-sensitive immunoliposome. *Int. J. Pharm.* 193, 157–166.

Nieto-Garai, J.A., Glass, B., Bunn, C., Giese, M., Jennings, G., Brankatschk, B., Agarwal, S., Börner, K., Contreras, F.X., Knölker, H.-J., et al. (2018). Lipidomimetic Compounds Act as HIV-1 Entry Inhibitors by Altering Viral Membrane Structure. *Front. Immunol.* 9, 1–18.

Nieva, J.L., Apellaniz, B., Huarte, N., and Lorizate, M. (2011). A new paradigm in

molecular recognition? specific antibody binding to membrane-inserted HIV-1 epitopes. *J. Mol. Recognit.* 24, 642–646.

Ojewole, E., Mackraj, I., Naidoo, P., and Govender, T. (2008). Exploring the use of novel drug delivery systems for antiretroviral drugs. *Eur. J. Pharm. Biopharm.* 70, 697–710.

Ono, A., and Freed, E.O. (2001). Plasma membrane rafts play a critical role in HIV-1 assembly and release. *Proc. Natl. Acad. Sci.* 98, 13925–13930.

Ozorowski, G., Pallesen, J., de Val, N., Lyumkis, D., Cottrell, C.A., Torres, J.L., Copps, J., Stanfield, R.L., Cupo, A., Pugach, P., et al. (2017). Open and closed structures reveal allostery and pliability in the HIV-1 envelope spike. *Nature* 547, 360.

Parasassi, T., De Stasio, G., D'Ubaldo, A., Gratton, E., Stasio, G. De, Ubaldo, A., and Grattong, E. (1990). Phase fluctuation in phospholipid membranes revealed by Laurdan fluorescence. *Biophys. J.* 57, 1179–1186.

Parasassi, T., De Stasio, G., Ravagnan, G., Rusch, R.M., and Gratton, E. (1991). Quantitation of lipid phases in phospholipid vesicles by the generalized polarization of Laurdan fluorescence. *Biophys. J.* 60, 179–189.

Parasassi, T., Di Stefano, M., Loiero, M., Ravagnan, G., and Gratton, E. (1994). Influence of cholesterol on phospholipid bilayers phase domains as detected by Laurdan fluorescence. *Biophys. J.* 66, 120–132.

Perrin, J., Bary, A., Vernay, A., and Cosson, P. (2018). Role of the HIV-1 envelope transmembrane domain in intracellular sorting. *BMC Cell Biol.* 19, 3.

Pfeiffer, T., Ruppert, T., Schaal, H., and Bosch, V. (2013). Detection and initial characterization of protein entities consisting of the HIV glycoprotein cytoplasmic C-terminal domain alone. *Virology* 441, 85–94.

Piller, S.C., Dubay, J.W., Derdeyn, C.A., and Hunter, E. (2000). Mutational analysis of conserved domains within the cytoplasmic tail of gp41 from human immunodeficiency virus type 1: effects on glycoprotein incorporation and infectivity. *J. Virol.* 74, 11717–11723.

Pisal, D.S., Kosloski, M.P., and Balu-Iyer, S. V (2010). Delivery of Therapeutic Proteins. *J. Pharm. Sci.* 99, 2557–2575.

Pollock, S., Dwek, R.A., Burton, D.R., and Zitzmann, N. (2008). N-Butyldeoxynojirimycin is a broadly effective anti-HIV therapy significantly enhanced by targeted liposome delivery. *AIDS* 22, 1961–1969.

Pollock, S., Nichita, N.B., Bohmer, A., Radulescu, C., Dwek, R.A., and Zitzmann, N. (2010). Polyunsaturated liposomes are antiviral against hepatitis B and C viruses and HIV by decreasing cholesterol levels in infected cells. *Proc. Natl. Acad. Sci.* 107, 17176–17181.

Prins, J.M., Jurriaans, S., van Praag, R.M., Blaak, H., van Rij, R., Schellekens, P.T., ten Berge, I.J., Yong, S.L., Fox, C.H., Roos, M.T., et al. (1999). Immuno-activation with anti-CD3 and recombinant human IL-2 in HIV-1-infected patients on potent antiretroviral therapy. *AIDS* 13, 2405–2410.

Puryear, W.B., Akiyama, H., Geer, S.D., Ramirez, N.P., Yu, X., Reinhard, B.M., and Gummuluru, S. (2013). Interferon-inducible mechanism of dendritic cell-mediated HIV-1 dissemination is dependent on Siglec-1/CD169. *PLoS Pathog.* 9, e1003291.

Qi, M., Williams, J.A., Chu, H., Chen, X., Wang, J.-J., Ding, L., Akhirome, E., Wen, X., Lapierre, L.A., Goldenring, J.R., et al. (2013). Rab11-FIP1C and Rab14 Direct Plasma Membrane Sorting and Particle Incorporation of the HIV-1 Envelope Glycoprotein Complex. *PLoS Pathog.* 9, e1003278.

Rajendran, L., Knölker, H.-J., and Simons, K. (2010). Subcellular targeting strategies for drug design and delivery. *Nat. Rev. Drug Discov.* 9, 29–42.

Ramana, L.N., Sharma, S., Sethuraman, S., Ranga, U., and Krishnan, U.M. (2012). Investigation on the stability of saquinavir loaded liposomes: implication on stealth, release characteristics and cytotoxicity. *Int. J. Pharm.* 431, 120–129.

Rempel, H., Calosing, C., Sun, B., and Pulliam, L. (2008). Sialoadhesin Expressed on IFN-Induced Monocytes Binds HIV-1 and Enhances Infectivity. *PLoS One* 3, e1967.

Roberts, J.D., Bebenek, K., and Kunkel, T.A. (1988). The accuracy of reverse transcriptase from HIV-1. *Science* 242, 1171–1173.

Roche, S., Albertini, A.A. V, Lepault, J., Bressanelli, S., and Gaudin, Y. (2008). Structures of vesicular stomatitis virus glycoprotein: membrane fusion revisited. *Cell. Mol. Life Sci.* 65, 1716–1728.

Rodger, A., Cambiano, V., Bruun, T., Vernazza, P., Collins, S., Corbelli, G.M., Degen, O., Estrada, V., Geretti, A.M., and Beloukas, A. (2018). Risk of HIV transmission through condomless sex in MSM couples with suppressive ART: The PARTNER2 Study extended results in gay men. In *Journal of the International AIDS Society*, p. 163.

Rodger, A.J., Cambiano, V., Bruun, T., Vernazza, P., Collins, S., van Lunzen, J., Corbelli, G.M., Estrada, V., Geretti, A.M., Beloukas, A., et al. (2016). Sexual Activity Without Condoms and Risk of HIV Transmission in Serodifferent Couples When the HIV-Positive Partner Is Using Suppressive Antiretroviral Therapy. *JAMA* 316, 171.

Rossio, J.L., Esser, M.T., Suryanarayana, K., Schneider, D.K., Bess, J.W., Vasquez, G.M., Wiltrout, T.A., Chertova, E., Grimes, M.K., Sattentau, Q., et al. (1998). Inactivation of human immunodeficiency virus type 1 infectivity with preservation of conformational and functional integrity of virion surface proteins. *J. Virol.* 72, 7992–8001.

Rousso, I., Mixon, M.B., Chen, B.K., and Kim, P.S. (2000). Palmitoylation of the HIV-1 envelope glycoprotein is critical for viral infectivity. *Proc. Natl. Acad. Sci.* 97, 13523–13525.

Saag, M.S., Benson, C.A., Gandhi, R.T., Hoy, J.F., Landovitz, R.J., Mugavero, M.J., Sax, P.E., Smith, D.M., Thompson, M.A., Buchbinder, S.P., et al. (2018). Antiretroviral Drugs for Treatment and Prevention of HIV Infection in Adults. *JAMA* 320, 379.

Saez-Cirion, A., Nir, S., Lorizate, M., Agirre, A., Cruz, A., Perez-Gil, J., and Nieva, J.L. (2002a). Sphingomyelin and cholesterol promote HIV-1 gp41 pretransmembrane sequence surface aggregation and membrane restructuring. *J. Biol. Chem.* 277, 21776–21785.

Saez-Cirion, A., Nir, S., Lorizate, M., Agirre, A., Cruz, A., Perez-Gil, J., Nieva, J.L.J.L., Sáez-Ciri6n, A., Nir, S., Lorizate, M., et al. (2002b). Sphingomyelin and cholesterol promote HIV-1 gp41 pretransmembrane sequence surface aggregation and membrane restructuring. *J. Biol. Chem.* *277*, 21776–21785.

Schaffner, C.P., Plescia, O.J., Pontani, D., Sun, D., Thornton, A., Pandey, R.C., and Sarin, P.S. (1986). Anti-viral activity of amphotericin B methyl ester: inhibition of HTLV-III replication in cell culture. *Biochem. Pharmacol.* *35*, 4110–4113.

Schibli, D.J., Montelaro, R.C., and Vogel, H.J. (2001). The membrane-proximal tryptophan-rich region of the HIV glycoprotein, gp41, forms a well-defined helix in dodecylphosphocholine micelles. *Biochemistry* *40*, 9570–9578.

Sengupta, P., Seo, A.Y., Pasolli, H.A., Song, Y.E., Johnson, M., and Lippincott-Schwartz, J. (2019). A lipid-based partitioning mechanism for selective incorporation of proteins into membranes of HIV particles. *Nat. Cell Biol.* *21*, 452–461.

Serpe, L., Catalano, M.G., Cavalli, R., Ugazio, E., Bosco, O., Canaparo, R., Muntoni, E., Frairia, R., Gasco, M.R., Eandi, M., et al. (2004). Cytotoxicity of anticancer drugs incorporated in solid lipid nanoparticles on HT-29 colorectal cancer cell line. *Eur. J. Pharm. Biopharm.* *58*, 673–680.

Sewald, X., Ladinsky, M.S., Uchil, P.D., Beloor, J., Pi, R., Herrmann, C., Motamedi, N., Murooka, T.T., Brehm, M.A., Greiner, D.L., et al. (2015). Retroviruses use CD169-mediated trans-infection of permissive lymphocytes to establish infection. *Science* *350*, 563–567.

Shan, L., Deng, K., Shroff, N.S., Durand, C.M., Rabi, S.A., Yang, H.-C., Zhang, H., Margolick, J.B., Blankson, J.N., and Siliciano, R.F. (2012). Stimulation of HIV-1-Specific Cytolytic T Lymphocytes Facilitates Elimination of Latent Viral Reservoir after Virus Reactivation. *Immunity* *36*, 491–501.

Sherer, N.M., Lehmann, M.J., Jimenez-Soto, L.F., Ingmundson, A., Horner, S.M., Cicchetti, G., Allen, P.G., Pypaert, M., Cunningham, J.M., Mothes, W., et al. (2003). Visualization of Retroviral Replication in Living Cells Reveals Budding into Multivesicular Bodies. *Traffic* *4*, 785–801.

Siliciano, J.D., Kajdas, J., Finzi, D., Quinn, T.C., Chadwick, K., Margolick, J.B., Kovacs, C., Gange, S.J., and Siliciano, R.F. (2003). Long-term follow-up studies confirm the stability of the latent reservoir for HIV-1 in resting CD4+T cells. *Nat. Med.* *9*, 727–728.

Simons, K., and Ikonen, E. (1997). Functional rafts in cell membranes. *Nature* *387*, 569–572.

Simons, K., and Ikonen, E. (2000). How cells handle cholesterol. *Science* *290*, 1721–1726.

Simons, K., and Sampaio, J.L. (2011). Membrane Organization and Lipid Rafts. *Cold Spring Harb. Perspect. Biol.* *3*, a004697–a004697.

Simons, K., and Toomre, D. (2000). Lipid rafts and signal transduction. *Nat. Rev. Mol. Cell Biol.* *1*, 31–39.

Sinha, V.R., Srivastava, S., Goel, H., and Jindal, V. (2010). Solid Lipid Nanoparticles (SLN ' S) – Trends and Implications in Drug Targeting. *Int. J. Adv. Pharm. Sci.* *1*, 212–

Smart, E.J., Graf, G.A., McNiven, M.A., Sessa, W.C., Engelman, J.A., Scherer, P.E., Okamoto, T., and Lisanti, M.P. (1999). Caveolins, Liquid-Ordered Domains, and Signal Transduction. *Mol. Cell. Biol.* *19*, 7289–7304.

Sot, J., Collado, M.I., Arrondo, J.L.R., Alonso, A., and Goñi, F.M. (2002). Triton X-100-Resistant Bilayers: Effect of Lipid Composition and Relevance to the Raft Phenomenon. *Langmuir* *18*, 2828–2835.

Spina, C.A., Anderson, J., Archin, N.M., Bosque, A., Chan, J., Famiglietti, M., Greene, W.C., Kashuba, A., Lewin, S.R., Margolis, D.M., et al. (2013). An In-Depth Comparison of Latent HIV-1 Reactivation in Multiple Cell Model Systems and Resting CD4+ T Cells from Aviremic Patients. *PLoS Pathog.* *9*, e1003834.

Srinivas, S.K., Srinivas, R. V., Anantharamaiah, G.M., Segrest, J.P., Compans, R.W., and Compansll, R.W. (1992). Membrane interactions of synthetic peptides corresponding to amphipathic helical segments of the human immunodeficiency virus type-1 envelope glycoprotein. *J. Biol. Chem.* *267*, 7121–7127.

St.Vincent, M.R., Colpitts, C.C., Ustinov, A. V, Muqadas, M., Joyce, M.A., Barsby, N.L., Epand, R.F., Epand, R.M., Khramyshev, S.A., Valueva, O.A., et al. (2010). Rigid amphipathic fusion inhibitors, small molecule antiviral compounds against enveloped viruses. *Proc. Natl. Acad. Sci.* *107*, 17339–17344.

Stebbing, J., Gazzard, B., and Douek, D.C. (2004). Where Does HIV Live? *N. Engl. J. Med.* *350*, 1872–1880.

Steckbeck, J.D., Sun, C., Sturgeon, T.J., and Montelaro, R.C. (2010). Topology of the C-Terminal Tail of HIV-1 gp41: Differential Exposure of the Kennedy Epitope on Cell and Viral Membranes. *PLoS One* *5*, e15261.

Steinman, R.M., and Banchereau, J. (2007). Taking dendritic cells into medicine. *Nature* *449*, 419.

Stiegler, G., Kunert, R., Purtscher, M., Wolbank, S., Voglauer, R., Steindl, F., and Katinger, H. (2001). A potent cross-clade neutralizing human monoclonal antibody against a novel epitope on gp41 of human immunodeficiency virus type 1. *AIDS Res. Hum. Retroviruses* *17*, 1757–1765.

Struck, D.K., Hoekstra, D., and Pagano, R.E. (1981). Use of resonance energy transfer to monitor membrane fusion. *Biochemistry* *20*, 4093–4099.

Suarez, T., Gallaher, W.R., Agirre, A., Goni, F.M., and Nieva, J.L. (2000b). Membrane interface-interacting sequences within the ectodomain of the human immunodeficiency virus type 1 envelope glycoprotein: putative role during viral fusion. *J. Virol.* *74*, 8038–8047.

Suarez, T., Nir, S., Goni, F.M., Saez-Cirion, A., and Nieva, J.L. (2000a). The pre-transmembrane region of the human immunodeficiency virus type-1 glycoprotein: a novel fusogenic sequence. *FEBS Lett.* *477*, 145–149.

Summerford, C., and Samulski, R.J. (1998). Membrane-associated heparan sulfate proteoglycan is a receptor for adeno-associated virus type 2 virions. *J. Virol.* *72*, 1438–

1445.

Taira, M.C., Chiaramoni, N.S., Pecuch, K.M., and Alonso-Romanowski, S. (2004). Stability of Liposomal Formulations in Physiological Conditions for Oral Drug Delivery. *Drug Deliv.* 11, 123–128.

Tamma, S.L., Sundaram, S.K., Lev, M., and Coico, R.F. (1996). Inhibition of Sphingolipid Synthesis Down-Modulates CD4 Expression by Peripheral Blood T Lymphocytes and T Lymphoma Cells. *Biochem. Biophys. Res. Commun.* 220, 916–921.

Thiele, C., Hannah, M.J., Fahrenholz, F., and Huttner, W.B. (2000). Cholesterol binds to synaptophysin and is required for biogenesis of synaptic vesicles. *Nat. Cell Biol.* 2, 42–49.

Thorlund, K., Horwitz, M.S., Fife, B.T., Lester, R., and Cameron, D.W. (2017). Landscape review of current HIV 'kick and kill' cure research - some kicking, not enough killing. *BMC Infect. Dis.* 17, 595.

Torchilin, V.P. (2005). Recent advances with liposomes as pharmaceutical carriers. *Nat. Rev. Drug Discov.* 4, 145–160.

Vanhamel, J., Bruggemans, A., and Debyser, Z. (2019). Establishment of latent HIV-1 reservoirs : what do we really know ? 3–9.

Verma, S. (2009). HIV: A Raft-Targeting Approach for Prevention and Therapy Using Plant-Derived Compounds (Review). *Curr. Drug Targets* 10, 51–59.

Vieira, C.R., Munoz-Olaya, J.M., Sot, J., Jiménez-Baranda, S., Izquierdo-Useros, N., Abad, J.L., Apellániz, B., Delgado, R., Martínez-Picado, J., Alonso, A., et al. (2010). Dihydrospingomyelin Impairs HIV-1 Infection by Rigidifying Liquid-Ordered Membrane Domains. *Chem. Biol.* 17, 766–775.

Vigant, F., Lee, J., Hollmann, A., Tanner, L.B., Akyol Ataman, Z., Yun, T., Shui, G., Aguilar, H.C., Zhang, D., Meriwether, D., et al. (2013). A Mechanistic Paradigm for Broad-Spectrum Antivirals that Target Virus-Cell Fusion. *PLoS Pathog.* 9, e1003297.

Vincent, N., Genin, C., and Malvoisin, E. (2002). Identification of a conserved domain of the HIV-1 transmembrane protein gp41 which interacts with cholesteryl groups. *Biochim. Biophys. Acta - Biomembr.* 1567, 157–164.

Vishwanathan, S.A., Thomas, A., Brasseur, R., Epanand, R.F.R.M., Hunter, E., and Epanand, R.F.R.M. (2008). Large changes in the CRAC segment of gp41 of HIV do not destroy fusion activity if the segment interacts with cholesterol. *Biochemistry* 47, 11869–11876.

Waheed, A.A., Ablan, S.D., Mankowski, M.K., Cummins, J.E., Ptak, R.G., Schaffner, C.P., and Freed, E.O. (2006). Inhibition of HIV-1 Replication by Amphotericin B Methyl Ester. *J. Biol. Chem.* 281, 28699–28711.

Waheed, A.A., Ablan, S.D., Roser, J.D., Sowder, R.C., Schaffner, C.P., Chertova, E., and Freed, E.O. (2007). HIV-1 escape from the entry-inhibiting effects of a cholesterol-binding compound via cleavage of gp41 by the viral protease. *Proc. Natl. Acad. Sci.* 104, 8467–8471.

Waheed, A.A., Ablan, S.D., Soheilian, F., Nagashima, K., Ono, A., Schaffner, C.P., and

Freed, E.O. (2008). Inhibition of Human Immunodeficiency Virus Type 1 Assembly and Release by the Cholesterol-Binding Compound Amphotericin B Methyl Ester: Evidence for Vpu Dependence. *J. Virol.* 82, 9776–9781.

Wang, Y., Lv, Z., and Chu, Y. (2015). HIV protease inhibitors: a review of molecular selectivity and toxicity. *HIV/AIDS - Res. Palliat. Care* 95.

Wei, X., Decker, J.M., Liu, H., Zhang, Z., Arani, R.B., Kilby, J.M., Saag, M.S., Wu, X., Shaw, G.M., and Kappes, J.C. (2002). Emergence of resistant human immunodeficiency virus type 1 in patients receiving fusion inhibitor (T-20) monotherapy. *Antimicrob. Agents Chemother.* 46, 1896–1905.

Weiss, R.A., and Wrangham, R.W. (1999). From Pan to pandemic. *Nature* 397, 385–386.

Weiss, A., Wiskocil, R.L., and Stobo, J.D. (1984). The role of T3 surface molecules in the activation of human T cells: a two-stimulus requirement for IL 2 production reflects events occurring at a pre-translational level. *J. Immunol.* 133, 123–128.

Welker, R., Kottler, H., Kalbitzer, H.R., and Kräusslich, H.G. (1996). Human immunodeficiency virus type 1 Nef protein is incorporated into virus particles and specifically cleaved by the viral proteinase. *Virology* 219, 228–236.

Welker, R., Hohenberg, H., Tessmer, U.W.E., Huckhagel, C., Kräusslich, H.G., and Krausslich, H.G. (2000). Biochemical and structural analysis of isolated mature cores of human immunodeficiency virus type 1. *J. Virol.* 74, 1168–1177.

West, J.T., Johnston, P.B., Dubay, S.R., and Hunter, E. (2001). Mutations within the Putative Membrane-Spanning Domain of the Simian Immunodeficiency Virus Transmembrane Glycoprotein Define the Minimal Requirements for Fusion, Incorporation, and Infectivity. *J. Virol.* 75, 9601–9612.

Wightman, F., Solomon, A., Khoury, G., Green, J.A., Gray, L., Gorry, P.R., Ho, Y.S., Saksena, N.K., Hoy, J., Crowe, S.M., et al. (2010). Both CD31 + and CD31 - Naive CD4 + T Cells Are Persistent HIV Type 1-Infected Reservoirs in Individuals Receiving Antiretroviral Therapy. *J. Infect. Dis.* 202, 1738–1748.

Wilk, T., Pfeiffer, T., and Bosch, V. (1992). Retained in vitro infectivity and cytopathogenicity of HIV-1 despite truncation of the C-terminal tail of the env gene product. *Virology* 189, 167–177.

Wilk, T., Pfeiffer, T., Bukovsky, A., Moldenhauer, G., and Bosch, V. (1996). Glycoprotein Incorporation and HIV-1 Infectivity Despite Exchange of the gp160 Membrane-Spanning Domain. *Virology* 218, 269–274.

Wolf, M.C., Freiberg, A.N., Zhang, T., Akyol-Ataman, Z., Grock, A., Hong, P.W., Li, J., Watson, N.F., Fang, A.Q., Aguilar, H.C., et al. (2010). A broad-spectrum antiviral targeting entry of enveloped viruses. *Proc. Natl. Acad. Sci.* 107, 3157–3162.

Wyma, D.J., Jiang, J., Shi, J., Zhou, J., Lineberger, J.E., Miller, M.D., and Aiken, C. (2004). Coupling of Human Immunodeficiency Virus Type 1 Fusion to Virion Maturation: a Novel Role of the gp41 Cytoplasmic Tail. *J. Virol.* 78, 3429–3435.

Yang, C., Spies, C.P., and Compans, R.W. (1995). The human and simian

immunodeficiency virus envelope glycoprotein transmembrane subunits are palmitoylated. *Proc. Natl. Acad. Sci.* 92, 9871–9875.

Yang, H., Xing, S., Shan, L., O'Connell, K., Dinoso, J., Shen, A., Zhou, Y., Shrum, C.K., Han, Y., Liu, J.O., et al. (2009). Small-molecule screening using a human primary cell model of HIV latency identifies compounds that reverse latency without cellular activation. *J. Clin. Invest.* 119.

Yang, P., Ai, L.-S., Huang, S.-C., Li, H.-F., Chan, W.-E., Chang, C.-W., Ko, C.-Y., and Chen, S.S.-L. (2010). The Cytoplasmic Domain of Human Immunodeficiency Virus Type 1 Transmembrane Protein gp41 Harbors Lipid Raft Association Determinants. *J. Virol.* 84, 59–75.

Yu, D., Ding, X., Liu, Z., Wu, X., Zhu, Y., Wei, H., Chong, H., Cui, S., and He, Y. (2018). Molecular mechanism of HIV-1 resistance to sifuvirtide, a clinical trial–approved membrane fusion inhibitor. *J. Biol. Chem.* 293, 12703–12718.

Yue, L., Shang, L., and Hunter, E. (2009). Truncation of the membrane-spanning domain of human immunodeficiency virus type 1 envelope glycoprotein defines elements required for fusion, incorporation, and infectivity. *J. Virol.* 83, 11588–11598.

Zaitseva, E., Zaitsev, E., Melikov, K., Arakelyan, A., Marin, M., Villasmil, R., Margolis, L.B., Melikyan, G.B., and Chernomordik, L. V. (2017). Fusion Stage of HIV-1 Entry Depends on Virus-Induced Cell Surface Exposure of Phosphatidylserine. *Cell Host Microbe* 22, 99–110.e7.

Zankl, C. (2009). Stereoselektive Synthese von Sphingolipiden zur Inhibierung der Degranulation von Mastzellen (Dresden).

Zhan, P., Li, Z., and Liu, X. (2010). Cosalane and its analogues: a unique class of anti-HIV agents. *Mini Rev. Med. Chem.* 10, 966–976.

Zhu, T., Korber, B.T., Nahmias, A.J., Hooper, E., Sharp, P.M., and Ho, D.D. (1998). An African HIV-1 sequence from 1959 and implications for the origin of the epidemic. *Nature* 391, 594–597.

Zolopa, A.R., Berger, D.S., Lampiris, H., Zhong, L., Chuck, S.L., Enejosa, J. V., Kearney, B.P., and Cheng, A.K. (2010). Activity of Elvitegravir, a Once-Daily Integrase Inhibitor, against Resistant HIV Type 1: Results of a Phase 2, Randomized, Controlled, Dose-Ranging Clinical Trial. *J. Infect. Dis.* 201, 814–822.